

# Sheffield Hallam University

*Properties of biomass fly ash concrete*

ELBUAISHI, Eman Elhadi

Available from the Sheffield Hallam University Research Archive (SHURA) at:

<http://shura.shu.ac.uk/28475/>

## A Sheffield Hallam University thesis

This thesis is protected by copyright which belongs to the author.

The content must not be changed in any way or sold commercially in any format or medium without the formal permission of the author.

When referring to this work, full bibliographic details including the author, title, awarding institution and date of the thesis must be given.

Please visit <http://shura.shu.ac.uk/28475/> and <http://shura.shu.ac.uk/information.html> for further details about copyright and re-use permissions.

# **Properties of Biomass Fly Ash Concrete**

**Eman Elhadi Elbuaishi**

**A thesis submitted in partial fulfilment of the requirement of  
Sheffield Hallam University for the degree of Doctor of Philosophy**

**January 2020**

## *Declaration*

I hereby declare that:

1. I have not been enrolled for another award of the University, or other academic or professional organisation, whilst undertaking my research degree.
2. None of the material contained in the thesis has been used in any other submission for an academic award.
3. I am aware of and understand the University's policy on plagiarism and certify that this thesis is my own work. The use of all published or other sources of material consulted have been properly and fully acknowledged.
4. The work undertaken towards the thesis has been conducted in accordance with the SHU Principles of Integrity in Research and the SHU Research Ethics Policy.
5. The word count of the thesis is 50,075.

Name	Eman Elhadi Elbuaishi
Award	PhD
Date of Submission	January 2020
Faculty	Material and Engineering Research Institute. Faculty of Science, Technology and Arts
Director(s) of Studies	Professor. Pal Mangat and Professor. Fin O'Flaherty

## *Dedication*

This research work is dedicated to:

My parents, who have raised me to be the person I am today. None of this would have been possible without your unending love, support and encouragement, which have served as a foundation for me during the best and worst of times.

To my husband Adel, I honestly say that without your help and support this work would not exist. So thank you for being with me.

My lovely kids Mohammad and Mohab, your kind support, sacrifices and good wishes were more worthy than you could imagine.

To my siblings, thank you for your love and the ongoing encouragement over the years.

## *Acknowledgements*

The author would like to thank various people, where this work would never have been possible without their support and guidance.

First and foremost, I would like to express my sincere gratitude to the director of my study professor Pal Mangat for his inspiring guidance and support throughout my time here at Sheffield Hallam University. You have always encouraged me to follow my own path and to constantly strive to become a better researcher. I am fortunate to have you as my mentor.

I would also like to express my appreciation to Prof Fin O'Flaherty, Dr Vincenzo Starinieri, Dr Olalekan Ojedokun and Dr Shahriar Abubakri of the Centre for Infrastructure Management, Sheffield Hallam University for their assistance and support throughout this research project.

Special thanks should also be given to MERI staff (Gail, Rachael, Clare, Amy and Jane) and my PhD colleagues at MERI for their kind support whenever required. My appreciation also for the assistance given by the technical staff of the Construction Materials Laboratory.

Last but not least, I am grateful for the funding provided by The Ministry of Higher Education and Scientific Research, Libya and to Libyan cultural affairs in London who supported me during my study.

## *Abstract*

The environmental concerns of carbon emissions by the energy industry have led to a change in the way energy is generated as the UK moves to a low carbon future. While biomass combustion is gaining attraction as the most available renewable energy source, the resulting ash is most often landfilled and is still not accepted in the concrete industry as in the case of coal fly ash. This is mainly because of the limited knowledge of the in-service life of concrete made with this fly ash. This research investigates the use of two types of wood biomass fly ash, obtained from two power plants in the UK, in cement and concrete production to provide a performance-based database for evaluating its utilization in the concrete industry.

The study comprises of three parts, the first part deals with determining the chemical, mineralogical and physical properties of these two fly ashes enhanced biomass ash (EBA) and virgin wood biomass ash (WBA). The results show that EBA has a chemical composition more similar to coal fly ash (CFA) than WBA and EBA satisfies the BS EN 450-1 requirements for the main oxides and other chemical components. The mineralogical structure of both ashes is mainly amorphous; EBA particles are mainly spherical whereas the morphology of WBA particles is fibrous irregular in shape and size. WBA has a higher surface area than both EBA and CFA while its pozzolanic reactivity is less. The mechanical and durability properties investigated in parts 2 and 3 are related to these characteristics (e.g., chemical compositions, pozzolanic reactivity and particle size) and also to pore properties investigated in part 2.

Part 2 of this study is concerned with the effect of both ashes on the fresh and hardened properties of concrete compared to coal fly ash. Blended fly ash pastes and mortars substituting the cement at 10, 20 and 30% were produced and numerous tests were performed. The results show that the incorporation of EBA reduces the water demand and improves the workability similar to the effect of coal fly ash while the behavior of WBA is the opposite. The coarse and high surface area of WBA particles contributes to its higher water demand. The early age hydration behavior of EBA is quite similar to CFA. The CFA and EBA mixes release considerably higher heat than WBA mixes, indicating a higher rate of hydration. The compressive and flexural strength decreases gradually as the percentage of both EBA and WBA in the mix increases. The compressive strength of CFA mixes is higher than EBA mixes

while WBA mixes give the lowest strength. The incorporation of EBA and WBA increases the total porosity of cement pastes.

Part 3 investigates the durability properties of enhanced biomass fly ash concrete by exposing it to long-term sulphate, chloride and carbon dioxide environments which are substances that cause deterioration and damage to concrete structures. Durability properties were tested under laboratory conditions over a period of one year and control samples of ordinary OPC concrete and coal fly ash concrete were produced for comparison. Generally, enhanced biomass fly ash concrete shows better durability properties than OPC concrete except for the carbonation resistance. The depth of carbonation of enhanced biomass fly ash concrete is higher than OPC concrete but less than coal fly ash concrete which shows the highest carbonation depth. The results also show that the incorporation of enhanced biomass fly ash improves the sulphate resistance compared to control OPC, however, it is still less effective than coal fly ash in resisting sulphate attack. The chemically and physically bound chloride of enhanced biomass fly ash concrete is lower than OPC concrete but it is higher than coal fly ash concrete. The efficiency of both enhanced biomass fly ash and virgin wood biomass ash in mitigating alkali-silica reaction was also examined based on the accelerated mortar bar test. The results show that enhanced biomass fly ash reduced the expansion caused by ASR to the low-risk level of deterioration according to ASTM C1260/1576 standards whereas the reduction of expansion in the case of virgin wood biomass ash was not sufficient to reduce the risk from potentially deleterious level to low risk.

## *Table of Contents*

CHAPTER 1 INTRODUCTION.....	1
1.1. Project Background and Motivations.....	1
1.2. Aim and Objectives.....	4
1.3. Research layout.....	6
1.4. References.....	9
CHAPTER 2 LITERATURE REVIEW.....	12
2.1. Introduction.....	12
2.2. Ash classification.....	12
2.2.1. Coal fly ash.....	12
2.2.2. Biomass fly ash.....	14
2.2.3. Co-combustion coal and biomass fly ash.....	16
2.3. Current Standards for Fly Ash Use in Concrete.....	17
2.4. Cement Hydration and the Effect of Fly Ash in Cementitious Systems.....	19
2.4.1. Cement Hydration.....	19
2.4.2. Effect of Fly Ash in Cementitious Systems (Pozzolanic Properties of Fly Ash).....	19
2.5. Coal, Biomass and Co-combustion Fly Ash Usage in Concrete.....	20
2.5.1. Effect of Fly Ashes on Fresh Properties.....	21
2.5.1.1. Workability (flow) and water demand.....	21
2.5.1.2. Setting time.....	22
2.5.1.3. Heat of hydration.....	23
2.5.2. Effect of Fly Ashes on Hardened and durability Properties.....	25
2.5.2.1. Compressive and flexural strength.....	25
2.5.2.2. Microstructure and hydrated phase development.....	26
2.5.2.3. Durability of Concrete.....	28
2.5.2.3.1 Carbonation.....	28
2.5.2.3.2 Sulphate Attack.....	33
2.5.2.3.3 Chloride Ingress in Concrete.....	36

2.5.2.3.4 Alkali silica reaction (ASR).....	45
2.6. References .....	50
CHAPTER 3 CHARACTERIZATION OF BIOMASS FLY ASHES.....	64
3.1. Introduction.....	64
3.2. Experimental Techniques.....	64
3.2.1. Chemical Characterization.....	64
3.2.2. Mineralogical Characterization.....	65
3.2.3. Physical Characterization.....	65
3.2.3.1. Particle Size Distribution .....	65
3.2.3.2. Specific Surface Area.....	66
3.2.3.3. Morphology.....	66
3.2.3.4. Pozzolanic Activity Index (PAI).....	68
3.3. Results and Discussion.....	69
3.3.1. Chemical Characterization.....	69
3.3.2. Mineralogical Characterization.....	71
3.3.3. Physical Characterization.....	74
3.3.3.1. Particle Size Distribution .....	74
3.3.3.2. Specific Surface Area (SSA).....	77
3.3.3.3. Morphology.....	77
3.3.3.4. Pozzolanic Activity Index .....	82
3.4. Conclusions.....	83
3.5. References .....	85
CHAPTER 4 PROPERTIES OF BIOMASS FLY ASH PASTES AND MORTARS.....	87
4.1. Introduction.....	87
4.2. Test Programme .....	87
4.2.1. Materials.....	88
4.2.1.1. Cement .....	88
4.2.1.2. Fly Ash.....	88
4.2.1.3. Aggregates .....	88
4.2.1.4. Superplasticizer.....	90
4.2.1.5. Water.....	90

4.2.2.	Mix Proportion .....	90
4.3.	Experimental Methods .....	91
4.3.1.	Fresh Properties.....	91
4.3.1.1.	Water Demand and Setting Times .....	91
4.3.1.2.	Consistency (workability) of Cement Mortars.....	92
4.3.1.3.	Heat of Hydration.....	94
4.3.2.	Hardened Properties .....	95
4.3.3.	Microstructure Analyses .....	95
4.3.4.	Phase Analyses.....	97
4.4.	Results and Discussion.....	98
4.4.1.	Fresh Property .....	98
4.4.1.1.	Water Demand and Setting Time.....	98
4.4.1.2.	Consistency (flow) of Cement Mortars.....	101
4.4.1.3.	Heat of Hydration.....	102
4.4.2.	Hardened Properties .....	104
4.4.2.1.	Compressive Strength .....	104
4.4.2.2.	Flexural Strength.....	108
4.4.3.	Microstructure Development .....	110
4.4.3.1.	Total Porosity .....	110
4.4.3.1.1.	Effect of curing age.....	111
4.4.3.1.2.	Effect of fly ash content .....	111
4.4.3.2.	Pore Structure of Fly Ash Blended Cement Paste .....	112
4.4.3.2.1.	Volume of small pores < 0.1µm. ....	113
4.4.3.2.2.	Volume of large pores > 0.1 µm .....	113
4.4.4.	Hydrated Phases .....	121
4.5.	Conclusion .....	127
4.6.	References .....	130

CHAPTER 5	CARBONATION OF ENHANCED BIOMASS FLY ASH CONCRETE.....	133
5.1.	Introduction.....	133
5.2.	Experimental Programme .....	134

5.2.1.	Materials.....	134
5.2.2.	Mix Design and Proportions .....	135
5.2.3.	Mixing.....	135
5.2.4.	Sample Preparation .....	136
5.2.4.1.	Carbonation Depth Specimens.....	136
5.2.4.2.	Carbonation and Drying Shrinkage Specimens .....	137
5.2.5.	Experimental Procedures .....	138
5.2.5.1.	Carbonation Depth Measurement .....	138
5.2.5.2.	Carbonation Shrinkage Measurement.....	139
5.3.	Results and Discussion.....	141
5.3.1.	Carbonation Depth .....	141
5.3.2.	Rate of Carbonation .....	143
5.3.3.	Shrinkage of EBA, CFA and OPC Concrete .....	145
5.3.3.1.	Carbonation Shrinkage.....	145
5.3.3.2.	Drying Shrinkage .....	146
5.3.3.3.	Carbonation and Drying Shrinkage.....	148
5.4.	Conclusions.....	149
5.5.	References.....	151
 CHAPTER 6 SULPHATE ATTACK AND ALKALI-SILICA REACTION OF BIOMASS FLY ASH MORTARS.....		 154
6.1.	Sulphate Attack.....	154
6.1.1.	Experimental Programme .....	155
6.1.1.1.	Materials.....	155
6.1.1.2.	Mix Proportions for Sulphate Attack Test .....	155
6.1.1.3.	Mixing.....	156
6.1.1.4.	Casting .....	156
6.1.1.5.	Curing.....	157
6.1.1.6.	Testing.....	157
6.1.2.	Results.....	159
6.1.2.1.	Effect of Coal Fly Ash (CFA).....	160
6.1.2.2.	Effect of Enhanced Biomass Ash (EBA).....	162
6.1.2.3.	Weight Change.....	164
6.1.2.4.	SEM/EDX Examination.....	165

6.1.3.	Discussion .....	169
6.1.3.1.	Effect of Chemical and Mineralogical Compositions .....	170
6.1.3.2.	Effect of Pore Structure .....	175
6.1.3.3.	Weight Change .....	176
6.1.3.4.	Correlation between SEM, Expansion and Visual Observation Results .....	177
6.2.	Alkali-silica Reaction (ASR) .....	178
6.2.1.	Experimental Programme .....	178
6.2.1.1.	Materials .....	179
6.2.1.2.	Mix proportions for ASR Test .....	179
6.2.1.3.	Sample Preparation and Testing .....	180
6.2.2.	Results and Discussion .....	183
6.3.	Conclusions .....	187
6.3.1.	Sulphate Attack .....	187
6.3.2.	Alkali-silica Reaction .....	188
6.4.	References .....	190
CHAPTER 7 CHLORIDE DIFFUSION IN ENHANCED BIOMASS FLY ASH CONCRETE .....		194
7.1.	Introduction .....	194
7.2.	Experimental Programme .....	195
7.2.1.	Materials .....	195
7.2.2.	Mix Proportions .....	196
7.2.3.	Mixing, Casting, and Curing .....	196
7.2.4.	Sample Preparation and Powder Collection .....	197
7.2.5.	Testing Procedure .....	200
7.2.5.1.	Acid-soluble Chloride Analyses .....	200
7.2.5.2.	Water-soluble Chloride Analyses .....	201
7.3.	Results and Discussion .....	202
7.3.1.	Introduction .....	202
7.3.2.	Chloride Diffusion Profiles .....	203
7.3.2.1.	Acid-soluble Chloride .....	203
7.3.2.2.	Water-soluble Chloride .....	207
7.3.3.	Chloride Diffusion Parameters ( $C_0$ , $D_c$ ) .....	209

7.3.3.1. Surface Chloride Concentration $C_0$ .....	210
7.3.3.2. Chloride Diffusion Coefficient $D_c$ .....	212
7.3.4. Long-term Prediction of Chloride Diffusion Coefficient .....	217
7.4. Conclusions .....	219
7.5. References .....	221
CHAPTER 8 CONCLUSIONS AND FUTURE WORK .....	224
8.1 Conclusions .....	224
8.2 Future Work .....	225
APPENDIX I.....	227

## *List of Tables*

Table 1.1 Research programme.....	5
Table 2.1 The chemical compositions of coal fly ash according to Vassilev et.al [7].....	14
Table 2.2 The chemical compositions of wood biomass and co-combustion wood ashes according to Vassilev et.al[8, 12].....	16
Table 2.3 Chemical requirements for fly ash in ASTM C618 and BS EN 450-1 standards.....	18
Table 2.4 Chloride transport mechanisms for various marine exposure conditions[103].....	40
Table 2.5 Chloride diffusion coefficient $D_c$ values as Published in literature.....	44
Table 3.1 The chemical analyses of CFA, EBA and WBA fly ashes .....	71
Table 3.2 Particle size distribution by laser diffraction.....	74
Table 3.3 Specific surface area of fly ashes.....	77
Table 3.4 Compressive strength and pozzolanic activity index .....	82
Table 4.1 Test programme .....	87
Table 4.2 Chemical composition of CEM I 52.5 N .....	88
Table 4.3 The chemical analyses of fly ashes .....	89
Table 4.4 Details of paste and mortar mixes.....	91
Table 4.5 Total heat evolved during hydration of OPC and fly ash mixtures .....	104
Table 4.6 Comparison of compressive strength at various curing ages.....	107
Table 4.7 The influence of CFA, EBA and WBA fly ashes on the pore structure of blended cement pastes.....	114
Table 4.8 The amorphous and CH contents of all paste samples at 90 days .....	121
Table 4.9 Main crystalline phases of the pastes .....	122
Table 5.1 Mix proportions.....	135
Table 6.1 The proportion of evaluated mixes for sulphate attack test .....	156

Table 6.2 The chemical composition of cement, CFA and EBA.....	<b>171</b>
Table 6.3 R-Factor limits as proposed by Dunstan [9].....	<b>172</b>
Table 6.4 Comparison between the practical and expected behaviour according to R values.....	<b>174</b>
Table 6.5 Total porosity and pore size distribution of OPC and blended fly ash (CFA and EBA) samples.....	<b>175</b>
Table 6.6 The proportion of evaluated mixes for ASR test.....	<b>180</b>
Table 6.7 Grading requirements in ASTM C 1567 and grading for CEN sand.....	<b>180</b>
Table 6.8 The important chemical elements leading to ASR expansion.....	<b>185</b>
Table 7.1 Mix proportions.....	<b>196</b>
Table 7.2 Acid and water -soluble chloride concentration parameters ( $C_0$ , $D_c$ ).....	<b>209</b>
Table 7.3 Chloride diffusion coefficient $D_c$ values as Published in literature.....	<b>216</b>
Table 7.4 $m$ values as Published in literature .....	<b>218</b>
Table 7.5 Predicted chloride diffusion coefficient at 10 and 20 years of exposure.....	<b>218</b>

## *List of Figures*

Figure 2.1 Portland cement hydration stages as a function of time given by isothermal calorimetry measurements.....	23
Figure 2.2 Factors controlling the carbonation of cementitious materials, according to the classification of Fernández-Bertos et al.[57].....	29
Figure 2.3 The presence of chloride in Concrete.....	36
Figure 2.4 The fitting curve of the solution of Fick's second law on chloride penetration profile in concrete with a W/B ratio of 0.65 at 7-year exposure [111]...	43
Figure 3.1 Malvern Mastersizer 3000 analyser.....	66
Figure 3.2 Micromeritics ASAP 2020 volumetric adsorption BET analyser. ....	67
Figure 3.3 Nova- Nano 200 SEM analyser .....	67
Figure 3.4 Three-point bending and equivalent cube compressive strength tests.....	69
Figure 3.5 XRD patterns of EBA .....	72
Figure 3.6 XRD patterns of CFA .....	73
Figure 3.7 XRD patterns of WBA .....	73
Figure 3.8 Particle size distribution (PSD) of EBA, CFA and WBA .....	75
Figure 3.9 Manual sieve analyses of WBA.....	76
Figure 3.10 Particle size distribution of WBA by manual sieving .....	76
Figure 3.11 The appearance of EBA, WBA and CFA.....	78
Figure 3.12 SEM images of CFA.....	79
Figure 3.13 SEM images of EBA .....	80
Figure 3.14 SEM images of WBA .....	81
Figure 4.1 Grading curve of sand by manual sieving.....	89
Figure 4.2 Grading curve for 10 mm gravel.....	90
Figure 4.3 Initial and final setting time measurements.....	92
Figure 4.4 Mixing and flow measurements.....	93
Figure 4.5 Heat of hydration measurements.....	94
Figure 4.6 Pascal 140/240 mercury intrusion porosimetry device used for analyses ...	96
.....	96
Figure 4.7 XRD samples stored in self-sealing bags.....	98

Figure 4.8 water demand for normal consistency for OPC, CFA, EBA and WBA pastes.....	<b>99</b>
Figure 4.9 Initial and final setting times for EBA, CFA, WBA and OPC pastes....	<b>100</b>
Figure 4.10 Mortar flow for EBA, CFA, WBA and OPC mixes.....	<b>101</b>
Figure 4.11 Calorimetric curves of OPC and fly ash mixtures measured at 25°C... <b>103</b>	
Figure 4.12 Compressive strength development in OPC, EBA and WBA blended mortars.....	<b>106</b>
Figure 4.13 Flexural strength development in OPC, EBA and WBA blended mortars.....	<b>109</b>
Figure 4.14 Flexural-compressive strength relationship for OPC, EBA, WBA and CFA mortars.....	<b>110</b>
Figure 4.15 The total porosity of control OPC paste and blended fly ash pastes at 28 and 90 days age.....	<b>111</b>
Figure 4.16 The differential and cumulative pore volume curves of OPC and EBA cement pastes at 28 days of curing.....	<b>115</b>
Figure 4.17 The differential and cumulative pore volume curves of OPC and EBA cement pastes at 90 days of curing.....	<b>116</b>
Figure 4.18 The differential and cumulative pore volume curves of OPC and CFA cement pastes at 28 days of curing.....	<b>117</b>
Figure 4.19 The differential and cumulative pore volume curves of OPC and CFA cement pastes at 90 days of curing.....	<b>118</b>
Figure 4.20 The differential and cumulative pore volume curves of OPC and WBA cement pastes at 28 days of curing.....	<b>119</b>
Figure 4.21 The differential and cumulative pore volume curves of OPC and WBA cement pastes at 90days of curing.....	<b>120</b>
Figure 4.22 XRD of OPC paste at 28, 90 days of curing.....	<b>123</b>
Figure 4.23 XRD of OPC, 10, 20, 30 CFA at 90 days of curing.....	<b>124</b>
Figure 4.24 XRD of OPC, 10, 20, 30 EBA at 90 days of curing.....	<b>125</b>
Figure 4.25 XRD of OPC, 10, 20 WBA at 90 days of curing.....	<b>126</b>
Figure 5.1 Four faces coated with bitumen paint and the remaining two side longitudinal faces left uncoated.....	<b>137</b>
Figure 5.2 The samples exposed to 3- 4% CO <sub>2</sub> inside the carbonation chamber....	<b>137</b>
Figure 5.3 Steel demec points attached along the two parallel longitudinal aces....	<b>138</b>

Figure 5.4 Phenolphthalein indicator applied to the freshly cut faces.....	<b>140</b>
Figure 5.5 Carbonation depth measurements at different locations.....	<b>141</b>
Figure 5.6 The split surface of the samples resealed with bitumen paint.....	<b>141</b>
Figure 5.7 Carbonation depth of control OPC, CFA and EBA.....	<b>143</b>
Figure 5.8 Rate of carbonation for EBA, CFA and OPC concrete.....	<b>144</b>
Figure 5.9 The coefficient of carbonation for CFA, EBA and OPC concrete.....	<b>145</b>
Figure 5.10 Carbonation shrinkage of CFA, EBA and OPC concrete.....	<b>146</b>
Figure 5.11 Drying shrinkage of EBA, CFA and OPC concrete.....	<b>147</b>
Figure 5.12 Carbonation and drying shrinkage of CFA, EBA and OPC concrete.....	<b>148</b>
Figure 6.1 Samples preparation for sulphate resistance test.....	<b>158</b>
Figure 6.2 QUANTA 650 SEM equipped with EDX spectrums.....	<b>159</b>
Figure 6.3 The effect of coal fly ash on sulphate resistance of mortars.....	<b>160</b>
Figure 6.4 The appearance of OPC and blended coal fly ash mortar samples after 150 days of immersion in 5% Na <sub>2</sub> SO <sub>4</sub> solution.....	<b>161</b>
Figure 6.5 The appearance of OPC and blended coal fly ash mortars after 420 days of immersion in 5% Na <sub>2</sub> SO <sub>4</sub> solution.....	<b>162</b>
Figure 6.6 The effect of enhanced biomass ash on sulphate resistance of mortars..... .....	<b>163</b>
Figure 6.7 The appearance of OPC and enhanced biomass ash blended mortar samples after 420 days of immersion in 5% Na <sub>2</sub> SO <sub>4</sub> solution.....	<b>164</b>
Figure 6.8 The weight change of the mortars after 420 days of immersion in 5% Na <sub>2</sub> SO <sub>4</sub> solution.....	<b>165</b>
Figure 6.9 SEM micrograph on OPC mortar after 420 days of immersion in Na <sub>2</sub> SO <sub>4</sub> solution.....	<b>166</b>
Figure 6.10 SEM micrograph on 10% EBA mortar after 450 days of immersion in Na <sub>2</sub> SO <sub>4</sub> solution.....	<b>167</b>
Figure 6.11 SEM micrograph on 30% EBA mortar after 450 days of immersion in Na <sub>2</sub> SO <sub>4</sub> solution.....	<b>168</b>
Figure 6.12 Comparison of sulphate resistance of OPC, CFA and EBA mortar samples.....	<b>169</b>
Figure 6.13 Effect of small pores on the expansion caused by sulphate attack.....	<b>176</b>
Figure 6.14 ASR test procedures.....	<b>182</b>

Figure 6.15 The expansion of OPC, CFA, EBA and WBA due to ASR.....	<b>184</b>
Figure 6.16 The effect of alkali (equivalent) content of fly ash on the expansion of mortar bars.....	<b>185</b>
Figure 7.1 Sample preparation for chemical analyses .....	<b>197</b>
Figure 7.2 Sample dimensions .....	<b>199</b>
Figure 7.3 Water-soluble chloride analyses .....	<b>201</b>
Figure 7.4 Acid-soluble chloride curves of EBA concrete at 90, 210, 300 and 400 days of exposure to 4% NaCl solution.....	<b>203</b>
Figure 7.5 Acid-soluble chloride curves of CFA concrete at 90, 210, 300 and 400 days of exposure to 4% NaCl solution.....	<b>204</b>
Figure 7.6 Acid-soluble chloride curves of OPC, EBA and CFA concrete at 90 and 300 days of exposure to 4% NaCl solution.....	<b>204</b>
Figure 7.7 Acid-soluble chloride concentration for EBA and CFA concrete at the depths 8, 15, 25mm .....	<b>206</b>
Figure 7.8 Water-soluble chloride curves of EBA concrete at 90, 210, 300 and 400 days of exposure to 4% NaCl solution.....	<b>207</b>
Figure 7.9 Water-soluble chloride of EBA, CFA and OPC concretes at 210 and 400 days of exposure to 4% NaCl solution.....	<b>208</b>
Figure 7.10 Relationship between the acid-soluble surface chloride concentration, $(C_0)_{as}$ , and chloride exposure period. ....	<b>210</b>
Figure 7.11 Relationship between the water-soluble surface chloride concentration, $(C_0)_{as}$ , and exposure period. ....	<b>211</b>
Figure 7.12 Acid-soluble and water-soluble surface chloride concentration of EBA and CFA concrete at 210 and 400 days of exposure and 180 days for OPC concrete [17]......	<b>212</b>
Figure 7.13 Relationship between the surface chloride concentration and the volume of large pores.....	<b>213</b>
Figure 7.14 Relationship between the chloride diffusion coefficient and the volume of large pores.....	<b>214</b>
Figure 7.15 Relationship of acid-soluble chloride diffusion coefficient with chloride exposure period for EBA and CFA concrete. ....	<b>217</b>

## ***LIST OF ABBREVIATIONS***

ACI	American Concrete Institute
AMBT	Accelerated Mortar Bar Test
ASR	Alkali- silica reaction
ASTM	American Society for Testing and Materials
BET	Brunauer-Emmett-Teller
BS	British Standard
CFA	Coal Fly Ash
DOE	Department of Environment
EBA	Enhanced Biomass Ash
EDX	Energy-dispersive X-ray spectroscopy
EN	European Standard
GGBS	Ground granulated blast furnace slag
LOI	Loss on Ignition
MIP	Mercury Intrusion Porosimetry
OPC	Ordinary Portland Cement
PSD	Particle size distribution
QXRD	Quantitative X-ray diffraction
RCPT	Rapid chloride permeability test
RH	Relative humidity
SAI	Strength activity index
SCMs	Supplementary cementitious materials
SEM	Scanning electron microscope
SSA	Specific surface area
TGA	Thermal - gravimetric analysis
WBA	Wood Biomass Ash
w/b	water to binder ratio
w/c	Water to cement ratio
XRD	X-ray diffraction
XRF	X-ray fluorescence spectrometry

## ***LIST OF SYMBOLS***

$\text{Al}_2\text{O}_3 \cdot 2\text{SiO}_2$	Mullite
$\text{C}_3\text{A}$	Tricalcium aluminate
$\text{C}_2\text{S}$	Dicalcium silicate
$\text{C}_3\text{S}$	Tricalcium silicate
$\text{C}_4\text{AF}$	Tetracalcium aluminoferrite
C-Al-H	Calcium aluminate hydrates
C-S-H	Calcium silicate hydrates
CaO	Calcium oxide
$\text{CaCO}_3$	Calcium carbonate (Calcite)
$\text{Ca}(\text{OH})_2$ or CH	Calcium hydroxide (Portlandite)
$\text{CO}_2$	Carbon dioxide
$C_0$	Surface chloride concentration (%)
$C_{\text{as}}$	Acide-soluble chloride concentration (%)
$C_{\text{ws}}$	Water-soluble chloride concentration (%)
$\text{CaSO}_4 \cdot 2\text{H}_2\text{O}$	Gypsum
Cs	Compressive strength (Mpa)
Dc	Diffusion coefficient ( $\text{m}^2/\text{s}$ )
d	Depth of carbonation (mm)
Fc	Maximum load at fracture (N)
$\text{Fe}_2\text{O}_3$	Iron oxide (hematite)
$F_s$	Flexural strength (Mpa)
GF	Gauge factor of the extensometer
k	Coefficient of carbonation ( $\text{mm}/\text{year}$ ) <sup>0.5</sup>
m	Age factor
NaCl	Sodium chloride
$\text{NaSO}_4$	Sodium sulphate
P	Applied pressure (Pa)
R	Dunstan's factor
$\text{SiO}_2$	Quartz
r	Radius of pores ( $\mu\text{m}$ )
t	Period of exposure (year)

$W$	Weight change (%)
$\delta$	Surface tension of mercury
$\epsilon$	Shrinkage strain ( $\mu\text{m}$ )

# CHAPTER 1 INTRODUCTION

## 1.1. Project Background and Motivations

Portland cement concrete is the most widely used construction material. Its success is mainly due to the availability, low cost of its main ingredients and its high mechanical properties [1–3]. However, the manufacture of the Cement is high-energy demanding and responsible for producing 5-7% of worldwide CO<sub>2</sub> emissions. It is estimated that every ton of cement emits approximately 0.87 ton of carbon dioxide [4–6]. Moreover, the manufacturing of Portland cement consumes approximately 2–3% of the global primary energy [4]. With increasing concern about CO<sub>2</sub> emissions, there has been a move to specify sustainable, high performance and environmentally friendly (through manufacturing and operational process) binders with reasonable cost to reduce the environmental impact and energy consumed by cement [4, 7, 8]. One of those solutions is to use less cement by partial replacement with other reactive industrial by-products such as ground granulated blast furnace slag (GGBS) and fly ash. The use of by-products also reduces the amount of material that would usually be disposed of at landfill and provides protection to the environment. It has been estimated that 18% replacement of Portland cement would result in a 17% reduction of CO<sub>2</sub> emissions [9].

Fly ash released from coal combustion in electric power stations has been effectively used to replace a portion of cement in concrete production to reduce the environmental footprint of cement production and produce durable concrete. However, a quantity of CO<sub>2</sub> is released to the atmosphere during the coal burning process [10]. Therefore, there has been a move to change the way energy is generated by employing innovative techniques to generate renewable energy. The move towards biomass combustion instead of coal combustion as a fuel source for the energy industry is currently the global trend. Combustion of biomass and co-combustion of coal with biomass are considered the most promising technology for producing power using renewable energy sources [11–13]. Biomass as a forestry and agricultural waste is considered a low cost and CO<sub>2</sub> neutral source of renewable energy due to its CO<sub>2</sub> consumption while growing being the same as that released by

burning [14, 15]. The global growth of biomass is estimated between 112 and 220 billion tonnes per year [16]. Currently, biomass contributes between 8-15% of the world energy supplies for heat and electricity and is expected to reach 33-50% of the world's primary energy consumption by 2050 [16–18]. The UK government have supported biomass electricity more than any other renewable energy sources to meet the renewable energy target to provide 15% renewable energy by 2020. Biomass power station projects which could burn over 23 million tonnes per year have been already approved. Some power stations with a capacity of 6 million tonnes per year, such as Lynemouth, have already opened [19].

The term "biomass" generally describes solid organic materials used to generate energy such as wood, grass, and straw; therefore, similar characteristics cannot be expected from the biomass fly ash generated from different sources of biomass and from different plants [20–22]. Consequently, the growing use of this technology in power generation releases a huge amount of a new class of fly ash that differs from the coal combustion fly ash in its quality, chemistry, and mineralogy. The characteristics of biomass fly ash differ due to a variety of its sources and depend on combustion conditions (fixed or fluidized beds), biomass sources (wood, herbaceous, rice husk, etc.) and the location where the ash is collected after combustion (fly ash or bottom ash) [14, 20, 23]. Generally, wood-based biomass burning is the main source of electricity in Europe which is considered the largest importer and consumer of wood in the world whereas the UK is by far the biggest wood consumer in Europe. The converted coal-fired power stations to biomass, such as Drax and Lynemouth (the suppliers of the biomass fly ash used in the current investigation), only use high-quality wood pellets. It has been reported that about 15 million tonnes per year of wood were burnt in the UK and Drax power station is the biggest which burns the majority of biomass. For instance, in 2014/2015 it burnt around 9 million tonnes of wood and in 2015 more than 20% of global wood pellet supply was burnt at Drax [19, 24].

Currently, the majority (approximately 70%) of the biomass ash is disposed of in landfills without any control and needs an adequate management system as an industrial waste [14, 20, 25]. Incorporation of biomass ash as a supplementary

cementitious material (SSMs) could be one strategy to produce sustainable concrete. From an environmental point of view, utilization of biomass in cement-based materials adds beneficial effects by reducing CO<sub>2</sub> emission, preserves the natural resources and reduces the energy used in cement production. In addition, it can be a solution to the environmental problem related to ash disposal and the rising cost of landfill disposal [20, 26].

Various types of biomass ash such as rice husk ash, palm oil fuel ash can have a similar pozzolanic property to coal fly ash with a high amount of silica in an amorphous form which has the potential to be used as a pozzolanic material to replace a portion of cement in concrete [9, 27]. However, most of the international standards such as ASTM C618 and EN450-1 that specify requirements for utilization of fly ash in concrete only accept the use of fly ash released from coal combustion and precludes the use of any material not derived from coal combustion from their use as cement components. Recently, EN 450-1 approved the use of fly ash obtained from co-combustion biomass up to 20% of the total fuel [28, 29] whereas pure biomass is still not included in this standard.

Unlike coal fly ash, limited research has been conducted on the use of biomass fly ash in the concrete industry; however, most of the research has been focused on co-combustion fly ashes with less focus on pure biomass ash. It has been reported in the literature that utilization of coal fly ash as a partial replacement of cement not only prevents it from disposal in landfill, but it also improves long term strength and durability properties of concrete. This raises the expectation of biomass ashes providing similar benefits by their use in concrete. Therefore, co-combustion and biomass ash require similar evaluation by research before they can be widely accepted for use in concrete construction.

The compositions of biomass and co-combustion ashes can be more variable than coal fly ash. Therefore, comprehensive research on different types of biomass produced at different power stations is required to develop guidelines for their use in concrete production and subsequent introduction in standards and codes of practice. Although there have been a number of studies on the chemical and mineralogical compositions of biomass ashes, little research has been done to investigate their

durability properties in concrete and their applicability to alkali-activated technology. The structural integrity of any cementitious material is compromised by the ingress of chloride, carbon dioxide and sulphates from the environment. Understanding the resistance of biomass fly ash concrete when exposed to such aggressive environments is critical to predicting how the material will behave in service.

## **1.2. Aims and Objectives**

The aim of this work is to investigate the use of two types of wood biomass fly ash in cement and concrete production and to provide a performance-based database for evaluating their utilization in concrete for its potential application. Also, to determine the relationship between the compositions of biomass ashes and the properties of concrete made with these fly ashes.

An intensive programme of research was prepared as summarized in Table 1.1 in order to achieve the following objectives:

1. Carry out a critical review on the state of art of fly ash classification and the extent of research on the effect of biomass fly ashes on the performance of concrete in order to identify areas requiring new research.
2. Determine the chemical, mineralogical and physical properties of two types of biomass fly ashes produced in the UK by using different testing techniques.
3. Investigate the effect of biomass fly ashes on the properties of fresh and hardened concrete, including microstructure and hydrated phase development.
4. Investigate the depth, rate of carbonation and carbonation shrinkage of biomass fly ash concretes over a long period of exposure to accelerated carbonation process.
5. Investigate the sulphate resistance of biomass fly ash mortars when exposed to 5% sodium sulphate solution over one year.
6. Investigate the efficiency of the biomass fly ashes in mitigating ASR when exposed to high alkali hydroxide solution for 28 days.
7. Investigate the chloride diffusion parameters of biomass fly ash concrete when exposed to 4% sodium chloride solution over a period of 400 days.

8. Analyse and evaluate the data of biomass ash concrete and both the control coal fly ash concrete and Portland cement-based concrete in order to develop conclusions for the use of biomass fly ashes in concrete construction.

**Table 1.1 Research programme**

<b>Test</b>	<b>Property</b>	<b>Test method</b>	<b>Standard</b>
<b>Fly ash characterization</b>	Chemical composition	X-ray Fluorescence (XRF)	none
	Mineralogical composition	X-ray Diffraction XRD	none
	Particle size distribution	Laser diffraction	none
	Specific surface area	BET	none
	Morphology	SEM	none
	Pozzolanic activity	Strength activity index	BS EN 450-1
<b>Fresh properties</b>	Setting time	Vicat needle	BS EN 196-3
	Consistency	Mortar flow	EN 1015-3
	Heat of hydration	Isothermal calorimetry	ASTM C1702
<b>Hardened and durability property</b>	Compressive & flexure strength	Mortar strength	BS EN 196-1
	Microstructure	Mercury intrusion porosimetry (MIP)	none
	Hydrated phases	Quantitative x-ray diffraction (QXRD)	none
	Carbonation	Accelerated carbonation method for carbonation resistance	BS 1881-210
	Sulphate attack resistance	Mortar bar expansion test	ASTM C1012
	Alkali-silica reaction (ASR)	Accelerated mortar bar test	ASTM C1260/C1567
	Chloride diffusion	Accelerated diffusion tests	Nord Test 443 & CEN, TS 12390

### 1.3. Research layout

The thesis is divided into eight chapters and a brief overview of each chapter is presented below:

**Chapter 1** provides a brief description of the study background and gives the motivation for undertaking of the research. The aim, objectives, strategy and layout of the research plan are also presented in this chapter.

**Chapter 2** a literature study has been performed on the state-of-the-art of the ash classification in terms of origin (the source from which it has been derived), the combustion technology and the chemical composition. The literature on the use and the effect of biomass combustion on the properties of fly ashes and on the performance of concrete using these ashes are also discussed in this chapter. A brief review of the durability properties of concrete is given in this chapter to provide the background for discussion relating to the durability properties of biomass ash concrete.

**Chapter 3** presents the techniques used to characterize two types of wood biomass fly ashes available in the UK, namely the Enhanced Pozzolanic Biomass Ash (EBA) generated from Drax power station and virgin wood biomass fly ash (WBA) produced in Lynemouth power station. The chemical and physical properties (particle size distribution, specific surface area and morphology) of these ashes are investigated. The chemical compositions were evaluated against the requirements specified in BS EN 450-1 and ASTM C618-12 for coal fly ash. The strength activity index method was used as an indirect method of evaluating the pozzolanic reactivity of the two ashes.

**Chapter 4** examines the influence of these ashes on early-age hydration properties (water demand, setting time, heat of hydration and workability), strength, microstructure properties and hydrated phase development of mortar. Blended fly ash cement pastes and mortars were prepared at cement replacement levels 10, 20 and 30% by weight of the total binder. A parallel investigation was also conducted on coal fly ash (CFA) blended cement mortars by using the same cement

replacement levels together with control specimens of mortar made with 100% OPC cement for comparison.

**Chapter 5** investigates the carbonation resistance of enhanced biomass ash (EBA) concrete by the accelerated carbonation method. A total of 9 concrete prisms of size (75 x 75 x 300) mm were cast for each mix to determine the depth of carbonation, carbonation shrinkage and drying shrinkage. The carbonation depth samples were cured in water for 28 days after demoulding before exposure to 3- 4% CO<sub>2</sub> at 20 ± 2 °C and 50-70% RH in a carbonation chamber up to one year. The carbonation and drying shrinkage specimens were cured in water for 7 days and then they were cured in the laboratory air (20 ± 2 °C, 50% RH). The carbonation shrinkage specimens were put inside the carbonation chamber at 45 days age together with the carbonation depth samples. The depth of carbonation, carbonation and drying shrinkage were determined at regular intervals and compared to coal fly ash concrete and control OPC concrete designed for similar strength. A discussion of the results is given followed by the major outcomes of the investigation.

**Chapter 6** comprises of two parts. The first part examines the sulphate resistance of enhanced biomass fly ash mortars. The mortars were prepared at cement replacement levels 10, 20 and 30% by weight of the total binder. All samples were cured in water at 20°C until 28 days age to develop sufficient strength and then immersed in 5% sodium sulphate solution for 420 days. The degree of sulphate attack was evaluated by measuring the expansion of the mortars, the final weight change, visual observation and the morphology. The second part of this chapter investigates the influence of biomass fly ash on the expansion caused due to alkali-silica reaction (ASR). Blended fly ash cement mortars containing 20% replacement of cement by enhanced biomass fly ash (EBA) and wood biomass ash (EBA) were examined. The samples were preconditioned in water maintained at 80 °C inside an oven for 24 h. They were subsequently transferred to a plastic container filled with 4% sodium hydroxide solution (NaOH) maintained at 80°C inside the oven. The length change of mortar bars was periodically measured over 28 days of exposure.

A parallel investigation on coal fly ash (CFA) blended cement mortars by using the same cement replacement levels and control specimens of mortar made with 100%

OPC cement was also conducted for comparison. The results are discussed and relevant conclusions are given.

**Chapter 7** investigates the physically and chemically bound chloride diffusion properties for three concrete mixtures (20% EBA, 20% CFA and OPC). A total of 10 slabs for each mix were cast in 250 x 250 x 75mm dimension polystyrene moulds and cured in water for 28 days before long term periods of exposure to 4% sodium chloride solution. Accelerated chloride diffusion (bulk diffusion) test procedures were used to provide rapid chloride ingress. The tests for physically and chemically bound chlorides were conducted on 2 slabs of each concrete mix at 90, 210, 300 and 400 days of exposure to the chloride solution. Chemical analyses were performed on the concrete powder collected at 8, 15, 25, 35, 50 and 65mm depths from the surface exposed to the chloride solution. The remaining faces of the slab specimens were sealed with bitumen paint to provide unidirectional chloride diffusion. Chloride diffusion characteristics including the chloride diffusion profiles, the equilibrium surface chloride concentration ( $C_0$ ), and diffusion coefficient ( $D_c$ ) for acid-soluble and water-soluble chloride concentrations were determined by applying Fick's second law of diffusion and performing a regression analysis of the experimental data. The results are then discussed in relation to the current and previous work and relevant conclusions are given.

**Chapter 8** provides the overall conclusions derived from this study and gives recommendations for future work.

## 1.4. References

1. Pacheco-Torgal F (2015) Introduction to Handbook of Alkali-activated Cements, Mortars and Concretes. Woodhead Publishing Limited. <http://linkinghub.elsevier.com/retrieve/pii/B9781782422761500010>
2. Juenger MCG, Winnefeld F, Provis JL, Ideker JH (2011) Advances in alternative cementitious binders. *Cem Concr Res* 41:1232–1243 . <https://doi.org/10.1016/j.cemconres.2010.11.012>
3. Fernández-jiménez AM, Palomo A, López-hombrados C (2006) Engineering Properties of Alkali-Activated Fly Ash Concrete. *ACI Mater J* 103:15–17
4. Garcia-Lodeiro I., Palomo A. F-JA (2015) An overview of the chemistry of alkali activated cement based binders. Woodhead Publishing Limited. <http://dx.doi.org/10.1533/9781782422884.1.19>
5. Temuujin J, Minjigmaa A, Bayarzul U, Zolzaya T, Davaabal B, Amgalan J (2014) Fundamentals of Geopolymers and Related Alkali Activated Materials. *Mater Sci Forum* 803:144–147 . <https://doi.org/10.4028/www.scientific.net/MSF.803.144>
6. Gastaldi D, Canonico F, Capelli L, Buzzi L, Boccaleri E, Irico S (2015) An investigation on the recycling of hydrated cement from concrete demolition waste. *Cem Concr Compos* 61:29–35 . <https://doi.org/10.1016/j.cemconcomp.2015.04.010>
7. Allahverdi A, N E (2013) Use of construction and demolition waste for alkali-activated or geopolymer cement.pdf. Woodhead Publishing Limited. <http://dx.doi.org/10.1533/9780857096906.3.439>
8. Zhang Z, Provis JL, Reid A, Wang H (2014) Geopolymer foam concrete: An emerging material for sustainable construction. *Constr Build Mater* 56:113–127 . <https://doi.org/10.1016/j.conbuildmat.2014.01.081>
9. Demis S, Tapali JG, Papadakis VG (2014) An investigation of the effectiveness of the utilization of biomass ashes as pozzolanic materials. *Constr Build Mater* 68:291–300 . <https://doi.org/10.1016/j.conbuildmat.2014.06.071>
10. Tkaczewska E, Małolepszy J (2009) Hydration of coal – biomass fly ash cement. *Constr Build Mater* 23:2694–2700 . <https://doi.org/10.1016/>

j.conbuildmat. 2008.12.018

11. Shearer CR, Kurtis KE (2015) Use of Biomass and Co-Fired Fly Ash in Concrete. *ACI Mater Journal*, V 112 209–218 . <https://doi.org/10.14359/51686827>
12. Wang S, Baxter L (2007) Comprehensive study of biomass fly ash in concrete: Strength, microscopy, kinetics and durability. *Fuel Process Technol* 88:1165–1170 . <https://doi.org/10.1016/j.fuproc.2007.06.016>
13. Barbosa R, Lapa N, Dias D, Mendes B (2013) Concretes containing biomass ashes: Mechanical, chemical, and ecotoxic performances. *Constr Build Mater* 48:457–463 . <https://doi.org/10.1016/j.conbuildmat.2013.07.031>
14. Cheah Chee Ban MRS (2011) The incorporation of wood waste ash as a partial cement replacement material for making structural grade concrete: An overview. *Resour Conserv Recycl* 55:669–685 . <https://doi.org/10.1016/j.asej.2014.11.005>
15. Carević I, Štirmer N, Banjad Pečur I, Milovanović B, Rukavina Jelčić M (2017) Potential of use wood biomass ash in the cement composites. *Proceedings 1st Int Conf Constr Mater Sustain Futur Zadar, Croat* 19 - 21 April 2017 109–114
16. Vassilev S V., Baxter D, Andersen LK, Vassileva CG (2013) An overview of the composition and application of biomass ash. Part 1. Phase-mineral and chemical composition and classification. *Fuel* 105:40–76 . <https://doi.org/10.1016/j.fuel.2012.09.041>
17. Williams A, Jones JM, Ma L, Pourkashanian M (2012) Pollutants from the combustion of solid biomass fuels. *Prog Energy Combust Sci* 38:113–137 . <https://doi.org/10.1016/j.pecs.2011.10.001>
18. Demirbaş A (2001) Biomass resource facilities and biomass conversion processing for fuels and chemicals. *Energy Convers Manag* 42:1357–1378 . [https://doi.org/10.1016/S0196-8904\(00\)00137-0](https://doi.org/10.1016/S0196-8904(00)00137-0)
19. Biofuelwatch (2016) Biomass FAQ. 1–14 . <https://doi.org/https://www.biofuelwatch.org.uk/2013/biomass-faq-2/>
20. Rajamma R, Ball RJ, Tarelho LAC, Allen GC, Labrincha JA, Ferreira VM (2009) Characterisation and use of biomass fly ash in cement-based materials.

- J Hazard Mater 172:1049–1060. <https://doi.org/10.1016/j.jhazmat.2009.07.109>
21. Lowe R (2012) Pozzolanic Properties of Biomass Fly Ash, Master of Science Thesis. Clemson University. doi: 10.1186/s12866-014-0223-5
  22. Shearer CR, Provis JL, Bernal SA, Kurtis KE (2016) Alkali-activation potential of biomass-coal co-fired fly ash. *Cem Concr Compos* 73:62–74 . <https://doi.org/10.1016/j.cemconcomp.2016.06.014>
  23. Berra M, Mangialardi T, Paolini AE (2015) Reuse of woody biomass fly ash in cement-based materials. *Constr Build Mater* 76:286–296 . <https://doi.org/10.1016/j.conbuildmat.2014.11.052>
  24. Flach B, Lieberz S, Rondon M, Williams B, Wilson C (2016) EU-28 Biofuels Annual 2016. *Glob Agric Inf Netw* 42 . <https://doi.org/NL6021>
  25. Ukrainczyk N, Vrbos N, Koenders EAB (2016) Reuse of Woody Biomass Ash Waste in Cementitious Materials. 30:137–148 . <https://doi.org/10.15255/CABEQ.2015.2231>
  26. Maschio S, Tonello G, Piani L, Furlani E (2011) Fly and bottom ashes from biomass combustion as cement replacing components in mortars production: Rheological behaviour of the pastes and materials compression strength. *Chemosphere* 85:666–671 . <https://doi.org/10.1016/j.chemosphere.2011.06.070>
  27. Wang S, Miller A, Llamazos E, Fonseca F, Baxter L (2008) Biomass fly ash in concrete : Mixture proportioning and mechanical properties. *Fuel* 87:365–371 . <https://doi.org/10.1016/j.fuel.2007.05.026>
  28. Esteves TC, Rajamma R, Soares D, Silva AS, Ferreira VM, Labrincha JA (2011) Use of biomass fly ash for mitigation of alkali-silica reaction of cement mortars. *Constr Build Mater* 1–7 . <https://doi.org/10.1016/j.conbuildmat.2011.06.075>
  29. BS EN 450 (2012) Fly ash for concrete Part 1 : Definition , specifications and conformity criteria. BS EN Stand

## **CHAPTER 2 LITERATURE REVIEW**

### **2.1. Introduction**

This chapter presents a review on the characteristics and properties of coal, biomass and co-combustion fly ashes and their application in cement and concrete industries including their impact on early-age properties, strength and durability. A brief literature review on the aspects which are relevant to the durability properties investigated in this study is also presented in this chapter.

### **2.2. Ash classification**

Fly ash is generally classified by its chemical composition, the source from which it has been derived, the combustion technology and the place from where it has been collected. It consists of a complex mixture of finely divided particles that differ in their chemical compositions and physical characteristics. The chemical and mineral compositions of fly ash change its colour depending on the content of unburnt carbon.

#### **2.2.1. Coal fly ash**

Coal fly ash is a fine powder resulting from coal combustion in power stations. It is defined by the American concrete institute (ACI) as "the finely divided residue that results from the combustion of ground or powdered coal that is transported by flue gasses from the combustion zone to the particle removal system"[1]. During the coal combustion, two types of ashes can be obtained according to the zone from where they are collected. About 20% of the ash is collected at the bottom of the furnace as bottom ash whereas 80% is captured from utility boilers and is called fly ash. The classification and properties of coal fly ash depend on the type of coal burnt (bituminous, sub-bituminous, lignite), however, bituminous coal is the most commonly used for energy production [2, 3].

ASTM C 618 [1] standard classifies coal ash, based on its chemical and physical properties, into Class C and Class F. Class C (high calcium fly ash) contains a high amount of calcium oxide (CaO) and is normally produced from burning sub-bituminous or lignite coal. This class has cementitious and pozzolanic properties. Class F (low calcium fly ash), which has a high level of silica and alumina compounds, is produced from bituminous coal burning [1]. The main difference between Class F and Class C fly ash is in their calcium, silica, alumina and iron content. In addition, the amount of alkalis (equivalent sodium and potassium) is relatively higher in Class C than Class F [2].

Generally, coal fly ash particles have predominantly spherical shape either solid or hollow spheres which allow fly ash to flow and blend easily in a concrete mix [4]. The particle sizes of fly ash vary from less than 1 $\mu$ m to more than 100  $\mu$ m with a typical range of 74  $\mu$ m to 5  $\mu$ m. The spherical shape of fly ash particles and their extreme fineness have a beneficial effect on the workability of concrete [3–5]. Its surface area ranges from about 200 m<sup>2</sup>/kg to 500 m<sup>2</sup>/kg, and the relative density ranges between 1.9 and 2.8 [4, 6]. It consists of a heterogeneous mix of crystalline phases such as quartz (SiO<sub>2</sub>), mullite (3Al<sub>2</sub>O<sub>3</sub>·2SiO<sub>2</sub>) and hematite (Fe<sub>2</sub>O<sub>3</sub>) and amorphous (glassy) phases which account for over 50% of coal fly ash. Many elements which exist in fly ash are usually expressed as the equivalent oxides. These are primarily silica, alumina, iron, and calcium with minor constituents being magnesium, sulphur, sodium, potassium, and carbon [3, 4]. The silica and alumina are mainly derived from quartz and clay minerals while calcium is mostly from calcium carbonate and calcium sulphates in coal [5].

The chemical compositions of 37 different types of coal fly ash previously analysed in literature [7, 8] are listed in Table 2.1. It is clear that lignite and sub-bituminous coal which produce Class C fly ash contain higher amount of calcium oxide and sulphate than bituminous coal fly ash.

**Table 2.1 The chemical compositions of coal fly ash according to Vassilev et.al [7]**

Element	Range	Type of ash		
		Bituminous (Av) Class F	Sub-bituminous(Av) Class C	Lignite (Av) Class C
SiO <sub>2</sub>	32- 68	56.1	54.7	44.9
Al <sub>2</sub> O <sub>3</sub>	11- 35	24.8	22.9	17.1
Fe <sub>2</sub> O <sub>3</sub>	0.8- 16	7.6	5.3	10.8
CaO	0.4- 28	4.9	7.1	13.1
MgO	0.3- 4	1.6	2.1	2.5
K <sub>2</sub> O	0.3- 4	1.6	1.7	1.5
Na <sub>2</sub> O	0.09- 3	0.8	1.1	0.5
SO <sub>3</sub>	0.3- 14	2.2	4.1	8.6
P <sub>2</sub> O <sub>5</sub>	0.1- 2	0.2	0.1	0.2
TiO <sub>2</sub>	0.6- 2	1.2	1.0	0.8

### 2.2.2. Biomass fly ash

The term biomass is the name given to all living matter on earth. As a class, biomass ash differs from coal ashes in their chemistry and mineralogy. Generally, biomass ash is classified according to the origin of the ash-forming matter in the biomass, which includes materials of vegetable, animal or industrial origin. For instance, biomass-based on vegetable origin is divided into wood biomass such as wood pellets and waste wood, agricultural biomass representing residues from food processing such as olive and rice husks [9]. Qualitatively, the basic element composition of biomass and coal is similar but differences can be found in the content of individual elements and chemical compounds in these materials [10]. The chemical composition of biomass ash based on vegetable origin is based on the chemical elements which are required for the plant to grow such as Carbon(C), Hydrogen (H), Oxygen (O) and Nitrogen (N), which comes essentially from air and water, in addition to some elements which come from soil during plant growth such

as Silicon (Si). Some agricultural waste or herbaceous biomass fuels such as rice husk ash have high silicon content (Si) while some have high alkali metal content such as wood ash [2].

Wood-based biomass is the only suitable source which can be fired in the large scale pulverized coal boilers. Therefore, it is the primary type that is burnt for electricity generation in the world generally and in the UK specifically because the existing coal power plants can be easily converted to either biomass or co-combustion plants. Thus, wood ash is the focus of this section.

Biomass firing temperatures are typically lower than coal firing temperatures because biomass materials can have comparatively lower ash melting and fusion temperatures depending on their composition [10]. Combustion temperature of wood inside the furnace governs both the content and chemical composition of the resulting ash [11]. The combustion of wood at higher temperatures beyond 1000°C produces a lower amount of wood ash (1-2%) and depends on many factors such as the harvesting method and the contamination with soil. The main components are Ca, K and Mg. Vassilev et al. [8, 12] summarized the chemical compositions of wood ash from literature (Table 2.2). It shows that biomass ash has a wide range of chemical composition compared to the range of coal fly ash shown in Table 2.1. The bulk of wood ash consists mainly of CaO, SiO<sub>2</sub> and K<sub>2</sub>O which account for about 75-80% of it, whereas the alumina content is low [5, 13]. The presence of alkali (potassium, sodium) and chlorine metals in the biomass can adversely affect its quality and cause slagging during combustion due to ash agglomeration [14, 15]. The combustion processes control the alkali concentration in the biomass ash, higher combustion temperatures can lead to a decrease of alkalis while the other major elements remain almost constant or increase [16].

The combustion technology used in the thermal plant has a significant effect on the physical properties of the resulting ash. Wood biomass ash particles are commonly irregular in shape with large average particle size and high surface area due to their porous structure [3]. The density of wood ash decreases with increasing the carbon

content [2]. The average particle size is 230  $\mu\text{m}$ , pH values are between 9 and 13.5 and specific gravity varies between 2260 and 2600  $\text{kg/m}^3$  [17].

**Table 2.2 The chemical compositions of wood biomass and co-combustion wood ashes according to Vassilev et al. [8, 12]**

Element	Wood biomass		Co-combustion coal and wood biomass	
	Range %	Wood ash (Av)%	Range %	Co-combustion wood (Av)%
SiO <sub>2</sub>	2-68	22.2	18-80	49.2
Al <sub>2</sub> O <sub>3</sub>	0.1-15	5.1	6-33	23.3
Fe <sub>2</sub> O <sub>3</sub>	0.4-10	3.4	3-11	7.1
CaO	3-83	43	1-51	11.5
MgO	1-15	6.1	1-19	2.2
K <sub>2</sub> O	2-32	10.8	1-5	1.9
Na <sub>2</sub> O	0.1-30	2.9	0.1-8	1.5
SO <sub>3</sub>	0.4-12	2.8	0.02-6	1.9
P <sub>2</sub> O <sub>5</sub>	0.7-13	3.5	0.002-6	1.5
TiO <sub>2</sub>	0.06-1	0.3	0.1-2	1.1

### 2.2.3. Co-combustion coal and biomass fly ash

Co-combustion (co-firing) is the burning of more than one type of fuel simultaneously. Co-firing coal and biomass can be a low-cost option for converting biomass energy to electricity efficiently by adding biomass as a partial substitute fuel in high-efficiency coal boilers. This option offers several environmental benefits such as reduced emissions of carbon dioxide. The suitability of biomass for co-firing with coal is because both biomass and coal are solid fuels and the equipment designed to burn coal is able to use biomass as well [9]. The diversity and variable amount of biomass burnt with coal in industrial processes affect the characteristics of the ash produced [10]. The effect of co-firing biomass with coal on the resulting ash composition and its properties is less understood compared to coal fly ash alone.

The co-firing temperatures are lower than coal combustion alone (<1600°C) due to the high moisture contents of some biomass fuels. The lower firing temperatures might affect the composition of the ash derived from the coal fraction during co-firing compared to coal-only combustion [5]. Co-fired fly ash particles are a mixture of individual biomass fly ash particles and coal fly ash particles, however, its chemical and physical properties depend on the content of biomass fuel that is burnt with coal [18]. It has been reported that with up to 50% wood as a fuel, the resulting co-combustion ash is slightly influenced and can meet the limiting values of European standard BS EN450 [19] for coal fly ash while combustion of above 50% wood with coal leads to more variation in the chemical composition of the resulting co-combustion ash which might fail to satisfy the limits allowed for coal fly ash [13]. The content of several components such as phosphor, potassium and calcium in the fly ash will change under co-combustion compared to standard coal fly ash.

The chemical compositions of 29 co-fired ashes, which were derived from co-combustion of wood with coal at 3 to 66% of the total fuel weight, as reported in the literature [5, 8, 12], are compared with the chemical composition of biomass ash derived from wood-burning only in Table 2.3. It is clear that the chemical composition of co-fired wood ash differs from wood biomass ash and is highly affected by the higher co-fired percentage of coal compared to biomass. Co-combustion fly ashes have a wide range of Na<sub>2</sub>O, K<sub>2</sub>O and P<sub>2</sub>O<sub>5</sub> contents; however, they are less variable than biomass fly ash.

### **2.3. Current Standards for Fly Ash Use in Concrete**

The American standard ASTM C 618 [1] and European Standard BS EN450-1 [19] provide the specification for coal fly ash and raw or calcined natural pozzolans for use in concrete. The use of biomass fly ash in cement and concrete production is prohibited under ASTM C618 standard, which defines fly ash as “The finely divided residue that results from the combustion of ground or powdered coal and that is transported by flue gasses”. The European Standard BS EN 450-1 currently approves the use of fly ash obtained by burning pulverized coal with co-combustion materials

up to 20% of the total fuel, however, pure biomass is still not included in this standard.

The main chemical requirements for coal fly ash specified in the ASTM C 618 [1] and BS EN450-1 [19] for construction purpose are presented in Table 2.3. The chemical requirements stipulated by BS EN 450-1 include additional limits for co-combustion fly ash compared to ASTM C 618. These additional requirements include maximum chloride, free calcium oxide contents, maximum amount of alkalis equivalent (Na<sub>2</sub>O)<sub>eq</sub> and total phosphate.

There are no standards for co-combustion and biomass fly ash, however, some co-combustion and biomass ashes can potentially satisfy the BS EN 450-1 specification as will be discussed in chapter 3 (section 3.3.1).

**Table 2.3 Chemical requirements for fly ash in ASTM C618 and BS EN 450-1 standards**

Properties	ASTM C 618		BS EN 450-1
	Class C	Class F	
$\Sigma(\text{SiO}_2 + \text{Al}_2\text{O}_3 + \text{Fe}_2\text{O}_3) \%$	50	70	$\geq 70$
Max % SO <sub>3</sub>	5	5	$\leq 3$
Max % Moisture content	3	3	-
Max % Loss of ignition (LOI)	6	6	9
Max % (Na <sub>2</sub> O) <sub>eq</sub>	-	-	<5
Max % free CaO	-	-	$\leq 10$
Max % Total P <sub>2</sub> O <sub>5</sub>	-	-	$\leq 5$
Max % (Cl <sup>-</sup> )	-	-	$\leq 0.1$

## 2.4. Cement Hydration and the Effect of Fly Ash in Cementitious Systems

### 2.4.1. Cement Hydration

The hydration reactions of the primary compounds of Portland cement, tricalcium silicate ( $C_3S$ ) and dicalcium silicate ( $C_2S$ ), produce calcium silicate hydrates gel (C-S-H) and calcium hydroxide (CH) as shown in equations 2.1 and 2.2.



The two reactions are very similar but the  $C_2S$  reaction proceeds much more slowly and the quantity of CH produced by  $C_2S$  is less than  $C_3S$ . Calcium silicate hydrate (C-S-H) is the main hydration product that accounts for most of the volume of the hydrated paste and is responsible for strength development. Calcium hydroxide (CH) is the second most reaction product which occupies about 20-25% of the paste volume, however, the strength contribution of CH is much less than C-S-H due to its lower surface area. The other compounds of Portland cement, tricalcium aluminate ( $C_3A$ ) and tetracalcium aluminoferrite ( $C_4AF$ ) also contribute to the hydration reactions as follows:



However, the rate of reaction for all compounds is different,  $C_3S$  hydrates rapidly relative to the other cement compounds and is primarily responsible for the initial concrete setting and strength development [20].

### 2.4.2. Effect of Fly Ash in Cementitious Systems (Pozzolanic Properties of Fly Ash)

Fly ash is a pozzolanic material and its primary phase is amorphous alumina-silicate with varying amounts of calcium. Its success as a raw material in the cement and

concrete industry is mainly due to its pozzolanic properties. When mixed with Portland cement and water, the amorphous alumina-silicate in fly ash reacts chemically with free lime, calcium hydroxide (CH), released by the hydration of cement, to produce additional calcium-silicate hydrates (C-S-H) and calcium-aluminate hydrates (C-AI-H) gels.

Some fly ashes which have higher amounts of calcium (i.e. Class C) are able to react with water to produce hydrates in the absence of a source of calcium hydroxide which is provided by cement hydration. These pozzolanic reactions increase the quantity of the cementitious binder phase (C-S-H) which is responsible for most of the compressive strength [21]. The pozzolanic reaction is slow at early- age but over time it improves the long- term strength and permeability. The rate of pozzolanic reaction depends on the chemical and physical properties of the fly ash. The summation of primary oxide content ( $\text{SiO}_2 + \text{Al}_2\text{O}_3 + \text{Fe}_2\text{O}_3$ ), Fineness, amorphous (glass) content and surface area are important factors affecting the pozzolanic reaction rate [22]. The pozzolanic reaction of fly ash becomes effective at around 90 days and beyond when the mechanical and durability properties of the concrete show improvement [4, 23, 24].

The pozzolanic behaviour of fly ash in mortar and concrete can be determined by using different methods. A direct method of quantifying the pozzolanic behaviour is to measure the consumption of calcium hydroxide,  $\text{Ca}(\text{OH})_2$ , while indirect methods measure the influence of the pozzolanic behaviour on the physical properties such as compressive strength (activity index) or electrical conductivity of mortar or concrete [25].

## **2.5. Coal, Biomass and Co-combustion Fly Ash Usage in Concrete**

Coal fly ash has been effectively used to replace a portion of cement in concrete production to reduce the environmental footprint of cement production and produce durable concrete whereas the majority (approximately 70%) of the biomass fly ash is disposed of in landfills. A limited amount is used as a soil supplement to improve the

alkalinity of soil or in highways as filler material in road pavements [11, 26]. Recent research [2, 5, 27–30] was performed to investigate the use of co-combustion and biomass fly ashes as a partial cement replacement material for concrete production.

### **2.5.1. Effect of Fly Ashes on Fresh Properties**

#### **2.5.1.1. Workability (flow) and water demand**

It's well known that the physical properties of coal fly ash provide a great advantage in working with fresh concrete, where the spherical shape of fly ash particles and their extreme fineness have a beneficial effect on the workability of concrete. The greater the percentage of fly ash, the better the flow of concrete due to the “ball bearing effect” of the fly ash particles [4, 5, 20]. A water reduction of 5% to 15% in blended fly ash mixes compared to OPC mixes is achieved for the same workability [31]. The high fineness and low carbon content of coal fly ash reduce the water demand of concrete and improve the cohesiveness of concrete [4]. In contrast, biomass fly ash has a negative impact on rheology as its physical properties differ from coal fly ash. Some studies have shown that the inclusion of wood biomass fly ash as a partial cement replacement resulted in high water demand to achieve a standard level of cement consistency. The workability, measured by either slump or mortar flow, was reduced [2, 5, 27, 30, 32]. The water demand increases with increasing level of cement replacement due to the high specific area of the irregular shape and porous particles of wood biomass ash. For instance, Udoeyo et al. [27] investigated the effect of wood waste fly ash on the workability of concrete containing varying percentages of wood waste fly ash compared to control OPC concrete of the same water content. The replacement levels were from 5% to 30% with a regular increment of 5% by weight of OPC. The slump reduced from 62mm for OPC concrete to 8 mm at 5% wood waste ash, 2.5 mm at 15% wood waste ash and zero slump when the replacement level exceeded 20%. Shearer [5] examined the influence of co-combustion coal biomass and pure biomass fly ashes on the flow of blended mortars. The test results showed that mortar mixes with co-combustion and biomass fly ashes had less flow compared to control OPC mortar.

Biomass fly ashes can reduce the workability much more than co-combustion fly ashes due to their high water demand and irregular shape particles morphology.

#### **2.5.1.2. Setting time**

The effect of coal fly ash on the setting time is well documented. It is generally agreed that class F fly ashes delay setting time whereas Class C fly ashes have mixed effects on setting time depending on their composition, amount and the reactivity of the glassy phase [33]. Similar behaviour was observed for co-combustion and biomass fly ashes from different sources, which delayed the setting time compared to plain cement [3, 27, 29]. The delay in setting time becomes more significant by increasing the cement replacement levels [11]. The inclusion of wood waste ash delays setting time due to the dilution effect (less cement content) which results in retardation of hydration as the wood fly ash is less reactive than cement. On the other hand, Rajamma et al. [2, 34] have investigated the effect of two types of waste wood biomass ash on fresh properties, including setting time, of blended mixes. He observed that the inclusion of 10% wood waste ash had increased the setting time compared to control OPC mix but when substitution dosage of ash increases above 20%, the setting time was shortened. These apparent accelerated setting times at high dosage can be due to drying (stiffening) of the mortar mixture rather than initial setting due to chemical reaction. This is due to the water adsorption by the wood biomass fly ash and its high carbon content which lead to greater absorption of the mixing water leading to fast drying.

Shearer [5] has also reported an acceleration (decrease) in initial setting time by more than 2.5 hrs than the control OPC at 25% replacement by wood biomass fly ash in a blended cement paste. In contrast, he observed a delay (increase) in setting time in co-combustion biomass fly ash blended paste at the same level of cement replacement. The co-combustion fly ash particles are a mixture of individual biomass fly ash particles and coal fly ash particles, however, the resulting co-combustion ash is only slightly influenced when the content of biomass in the fuel is < 50% of the total fuel. Therefore, co-combustion fly ash behaves similarly to coal fly ash on its influence on setting time.

### 2.5.1.3. Heat of hydration

Portland cement hydration is divided into four stages, as shown in Figure 2.1 [22, 35]. The first stage is dissolution period ( $C_3S$  dissolution) which starts directly after adding water and only takes few minutes producing a high amount of heat followed by a slow reaction or induction period (dormant stage) as illustrated by stage 2 in figure 2.1. At the end of dormant period, the rate of hydration increases rapidly due to the higher rate of  $C_3S$  dissolution. This stage is known as acceleration period (stage 3, figure 2.1) and the initial setting of cement mostly occurs on the lower side of this stage whereas the final setting occurs after reaching the maximum peak (upper side of stage 3). The last stage is deceleration period which starts when the reaction slows down after the maximum peak is reached. After 24 hours, the rate of reaction becomes slow and continues until all free water is consumed [36]. High heat of hydration can indicate high early strength but sometimes results in decreased durability performance whereas, lower heat of hydration reduces early strength and improves long-term durability [5, 37].

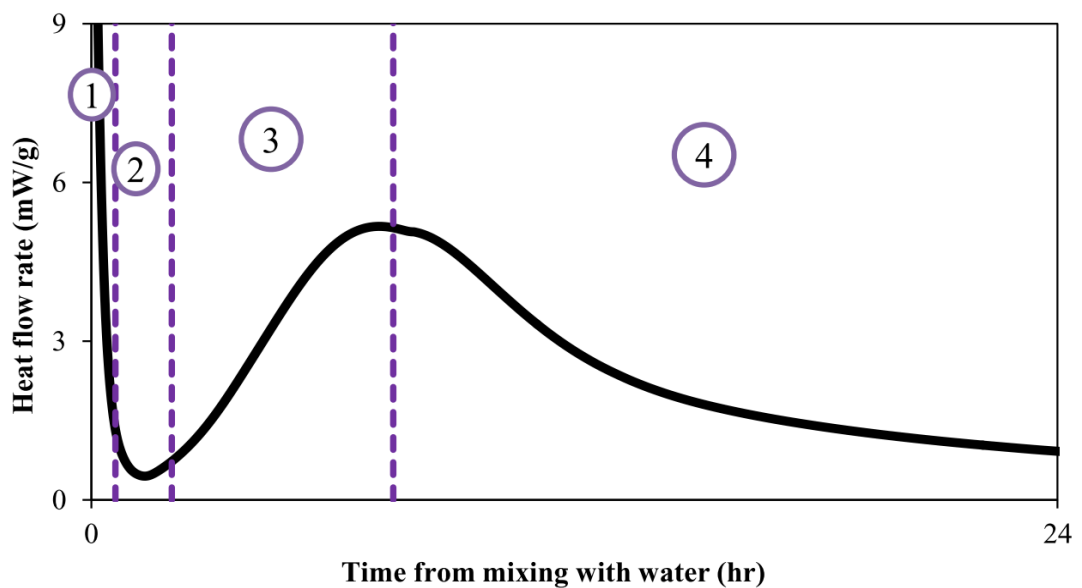


Figure 2.1 Portland cement hydration stages as a function of time given by isothermal calorimetry measurements.

Stages 1 and 2, a slowdown in dissolution and induction period, stage 3 acceleration period and stage 4 deceleration period.

Measurement of hydration heat can give an indication of the reactions which occur in the early age of cement hydration. Several methods have been used to measure the heat of hydration, however, calorimeter test methods (isothermal, adiabatic and semi-adiabatic) are the most common.

The addition of supplementary cementitious materials such as fly ash normally result in slow hydration and low heat of hydration [38–40]. Replacement of cement with coal fly ash reduces the hydration heat due to the dilution effect of fly ash as its pozzolanic reaction is very slow at early age. This occurs when less cement is available for hydration due to its partial replacement with fly ash. Limited research has been conducted to investigate the impact of biomass ash and co-combustion coal and biomass fly ash on the heat of hydration. Rajamma et al. [2, 32] found that the hydration peak reduced and accelerated slightly by incorporating two types of wood waste biomass ash at cement replacement levels 10, 20 and 30% compared to control OPC mix. The peak acceleration was attributed to the high alkali and chloride content of wood biomass fly ashes. However, the high water demand and specific surface area of biomass fly ashes is also the likely reason, as will be discussed in chapter 4 (section 4.4.1.3).

Tkaczewska et al. [41, 42] investigated the effect of co-combustion wood biomass fly ash on the heat of hydration and found that the blended co-combustion biomass fly ash mixes retarded hydration of cement compared to coal fly ash. Similar behaviour was reported by Shearer [5] for mixes containing 25% cement replacement by wood waste biomass and co-combustion biomass fly ashes. The variation between the results of biomass and co-combustion fly ashes could be due to the differences in their physical and chemical composition. However, early-age hydration kinetics involve many simultaneous complex processes of hydration in the different compounds of cement (e.g.  $C_3A$ ,  $C_3S$ ) making it difficult to correlate the hydration results with the chemical and physical properties of the ashes. Therefore, more research is needed to better understand the impact of biomass fly ash on the early-age hydration of cementitious systems due to its physical and chemical properties.

## **2.5.2. Effect of Fly Ashes on Hardened and Durability Properties**

### **2.5.2.1. Compressive and flexural strength**

Compressive strength is the most important property of concrete which is directly related to the degree of hydration and the structure of the hardened material. Structural design and specifications generally refer to 28 days compressive strength. Generally, the replacement of cement with fly ash reduces the early age strength up to 28 days when the pozzolanic reaction is slow and improves the long-term strength [43, 44]. The pozzolanic reaction increases the quantity of C-S-H phase which is responsible for most of the compressive strength. However, Class C fly ash, due to its high CaO content, has more rapid strength gain at early age than Class F whereas the latter contributes more to long term strength [4].

The chemical and physical properties of biomass fly ash differ from coal fly ash and its pozzolanic reactivity can be significantly less than coal fly ash depending on its SiO<sub>2</sub> and Al<sub>2</sub>O<sub>3</sub> contents. Several studies have investigated the compressive and flexural strength of wood biomass fly ash mortar and concrete [5, 20, 27, 29, 32]. There is a general agreement that the use of wood waste ash, as a partial cement replacement, reduces both compressive and flexural strength relative to control OPC. Udoeyo et al. [27] determined the compressive and flexural strength of concrete made with waste wood ash from 5 to 30% cement replacement. He found that the strength increases with age but decreases with the increase in the wood ash content. However, the rate of flexural strength gain is slower than compressive strength rate. Some studies have shown that 10% substitution of cement with wood ash exhibited similar or higher 28 days compressive strength than the control OPC mix whereas at replacement levels higher than 10%, the compressive strength reduced [2, 30]. On the other hand, Abdullahi [45] reported the compressive strength results at 28 and 60 days age of wood ash concrete at replacement percentages 10, 20, 30, and 40% compared to control OPC concrete. The results showed that the OPC concrete had the highest compressive strength. The mixture containing 20% wood ash had higher strength than that containing 10% wood ash at 28 and 60 days. An increase in wood ash content beyond 20% resulted in a reduction in strength at 28 and 60 days. He

explained that the silica provided by 10% wood ash was inadequate to react with the calcium hydroxide provided by the hydration of cement but when substitution dosage of ash increased above 20%, the silica present in the mix was in excess of the amount required to combine with the calcium hydroxide.

Co-combustion biomass fly ash has shown mixed behaviour with regard to strength gain. Wang et al. [28], Johnson et al. [46] and Saraber [13] indicated that co-combustion biomass fly ashes produced from wood pellets, switchgrass behave similarly to coal fly ash, which improves long-term strength compared to control OPC. In contrast, Tkacewska et al. [41, 42] found mixed results, one type of co-combustion fly ash from wood biomass had a compressive strength less than class F coal fly ash mix and another type of co-combustion fly ash (also from wood) had higher strength compared to class F fly ash and the control OPC at later age. The variation in the combustion process and conditions such as furnace temperature or the type of coal which was used as a fuel in the co-combustion process could be the reason for this outcome.

#### **2.5.2.2. Microstructure and hydrated phase development**

The pore structure of cement-based materials is one of the most important factors that influence their physical, mechanical and durability properties. The porosity and pore size distribution are the main parameters characterizing the pore structure of hydrated cement paste. Many experimental methods have been used to study the microstructure and phase development of cement-based materials such as Mercury intrusion porosimetry (MIP), Thermal analysis (TGA) and X-ray diffraction (XRD). MIP is the most widely used method to measure the porosity and pore structure whereas TGA and XRD techniques are used to estimate the calcium hydroxide (CH) content which indicates the amount of C-S-H gel produced.

The influence of coal fly ash on the porosity and pore structure of blended cement paste is well documented [47–51]. The addition of fly ash generally results in an increase in early porosity compared to traditional OPC concrete and improve the long-term transport properties of concrete [50, 52, 53]. The C-S-H gels produced by

the pozzolanic reaction of fly ash with calcium hydroxide fill in and refine the pore structure of cement paste [49, 54].

Compared to the extensive results available on the hydration mechanisms and microstructure of coal fly ash cement pastes and concrete, few studies have investigated the effect of biomass fly ash on the microstructure and hydrated phase development of cement pastes. Shearer [5] conducted microstructural analyses to investigate the effect of co-combustion fly ash, produced by combustion of coal and wood biomass, and pure wood biomass fly ash on the microstructure development of blended cement mixes compared to coal fly ash and control OPC at 7 and 90 days. TGA data revealed a steady increase in calcium hydroxide (CH) content between 1 and 7 days for both co-combustion and wood biomass fly ash samples compared to the significant increase observed by OPC control. This indicates that co-combustion and wood biomass fly ash particles have not contributed to hydration reaction at this age. At 90 days, the co-combustion fly ash underwent a late-age pozzolanic reaction similar to coal fly ash and consumed a significant amount of calcium hydroxide (CH) relative to the plain control cement. In contrast, the wood biomass ash remained unreacted even at late-ages and ultimately inhibited strength gain due to the lack of pozzolanic reactivity.

MIP analyses were performed by Rajamma [2] on two types of waste wood fly ash blended cement pastes at cement replacement levels 10, 20 and 30% of total weight. The results showed that the total porosity of all blended wood fly ash samples is higher than the control OPC. Although total porosity increases with increasing fly ash replacement, the median pore diameter decreases. In addition, the TGA curves of the same samples show that the intensity peaks of the calcium hydroxide (CH) in the blended fly ash pastes were less than to that of control OPC cement paste.

It is unclear from those studies whether the inclusion of biomass fly ash contributes to the refining of pore structure of cement paste similar to coal fly ashes or whether there is no visible contribution from the biomass fly ash in terms of accelerating the hydration process except that it acts more like a filler than as a binder. Therefore, more research is needed on this aspect.

### 2.5.2.3. Durability of Concrete

The design of concrete structures is generally based on the required strength while the durability performance does not always receive similar attention at the design stage. Low permeability and shrinkage are two performance characteristics that can prolong the service life of concrete structures when subjected to severe exposure conditions. The ingress of ions, water and various deleterious materials, which are the origin of many forms of attack on concrete, decreases when the permeability of concrete is low. Fly ash can result in pore refinement due to the pozzolanic reaction products, which can considerably reduce the permeability, thereby decreasing the ingress of moisture, oxygen, CO<sub>2</sub>, chlorides and other harmful agents that affect the durability of concrete.

#### 2.5.2.3.1. Carbonation

Carbonation has been recognized as one of the main causes of concrete deterioration and reinforcement corrosion. It occurs due to the diffusion of atmospheric CO<sub>2</sub> through its pore system dissolved in the pore solution and forming HCO<sub>3</sub> ion. In the presence of moisture, this ion reacts with calcium hydroxide, Ca(OH)<sub>2</sub>, which is the main product of cement hydration to form calcium carbonate, CaCO<sub>3</sub>, according to the following equation [55, 56]:



The calcium silicate hydrate gel C-S-H and the unreacted components C<sub>3</sub>S and C<sub>2</sub>S can also react with CO<sub>2</sub> and produce calcium carbonate and silica gel according to the following reactions [57]:



The reaction of C-S-H takes place in a similar way as carbonation of Ca(OH)<sub>2</sub> but at a slower rate because it is more dependent on Ca/Si ratio and the permeability of

concrete. Therefore the reaction of  $\text{Ca}(\text{OH})_2$  is more crucial to the carbonation process [56, 58]. The C-S-H dissolves faster leading to a higher rate of carbonation when supplementary cementitious materials (SSMs) are incorporated into concrete.

There are several factors that control the propagation of carbonation into concrete, however, the main parameters are those controlling the diffusivity and the reactivity of  $\text{CO}_2$  with the binding paste as summarised in Figure 2.2. The amount and type of the hydration products of the binder influence their reaction products with  $\text{CO}_2$ . The diffusivity of  $\text{CO}_2$  into concrete depends on the saturation level of its pores and exposure conditions such as the concentration of  $\text{CO}_2$ , relative humidity and temperature. For instance, the pores will be filled with water at very high relative humidity thereby prohibiting the diffusion of  $\text{CO}_2$ . On the other hand, insufficient water will be available at low humidity to dissolve  $\text{CO}_2$  and support the carbonation reaction. The highest rate of carbonation reaction is achieved within the range of 50-70% relative humidity [55, 59, 60]. In addition, the carbonation rate is affected by the concentration of  $\text{CO}_2$  in the atmosphere. The carbonation process is too slow under the ambient conditions as the  $\text{CO}_2$  concentration in the atmosphere is approximately 0.04% whereas under accelerated carbonation conditions (accelerated tests) the  $\text{CO}_2$  concentration exceeds 5%.

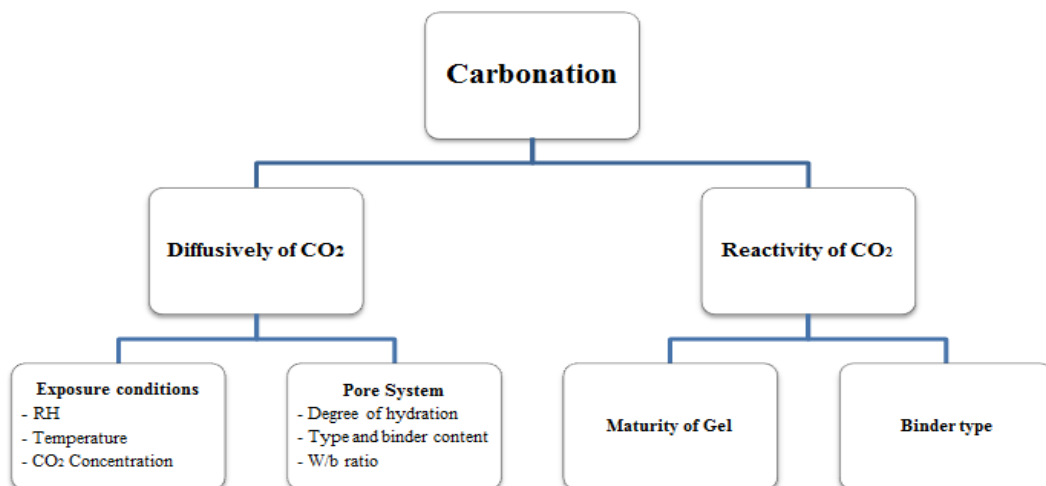


Figure 2.2 Factors controlling the carbonation of cementitious materials, according to the classification of Fernández-Bertos et al.[55].

The pore system of concrete depends upon the degree of hydration, water to binder ratio and the type and content of binder. The depth of carbonation decreases when the binder content in the concrete mix increases as the carbonation occurs only in the binder gel. In addition, the depth of carbonation increases as the water to binder ratio increases since higher water content leads to an increase in porosity [57, 61]. However, carbonation in concrete is a complex process which can not easily be described due to the variation in its rate at different sections within the same concrete structure.

The phenolphthalein indicator method is the most popular method for measuring the depth of carbonation of concrete which involves spraying of the solution on the concrete surface to show a change in colour when the pH becomes non-alkaline [57].

- **Carbonation Shrinkage**

When hardened cement or concrete are exposed to the atmosphere, drying and carbonation occur simultaneously, resulting in combined volume change. However, the mechanisms of drying and carbonation shrinkage are different. While drying shrinkage is the volume change of hardened cement paste due to moisture loss, carbonation shrinkage is the irreversible volume change due to the chemical reaction with the carbon dioxide,  $\text{CO}_2$ , in the atmosphere [62]. Carbonation reaction results in shrinkage and cracking on the surface of concrete due to stresses induced in the cementitious matrix. When calcium carbonate is formed, the total porosity in the carbonated zone is reduced causing differential shrinkage between the carbonated and uncarbonated zones. Unlike drying shrinkage, the mechanism of carbonation shrinkage is still poorly understood as the carbonation shrinkage results in mass gain rather than mass loss due to the formation of calcium carbonate,  $\text{CaCO}_3$ . Chen et al. [59, 63] suggested that carbonation shrinkage is a special case of decalcification shrinkage that occurs when the Ca/Si ratio of the C-S-H gel is reduced below 1.2. On the other hand, Swenson and Sereda [63] suggested that carbonation shrinkage occurs due to a gradient of moisture content within the calcium carbonate,  $\text{CaCO}_3$ , passivation layer which forms around carbonated calcium hydroxide  $\text{Ca}(\text{OH})_2$ .

However, the magnitude of carbonation shrinkage in concrete is small compared to long term drying shrinkage.

- **Effect of Fly Ash on Carbonation Resistance**

The incorporation of supplementary cementitious materials (SSMs) including fly ash in concrete improves properties such as strength (long-term) and shrinkage. However, the influence of fly ash on carbonation is controversial. In OPC concrete,  $\text{Ca(OH)}_2$  is the main product of cement hydration and the depth of carbonation is limited by the quantity of  $\text{Ca(OH)}_2$  available to react with  $\text{CO}_2$ . The quantity of  $\text{Ca(OH)}_2$  will decrease in blended fly ash concrete due to the lower amount of cement and its pozzolanic reaction with fly ash which reduces its resistance against carbonation [60, 64]. The consumption of free lime  $\text{Ca(OH)}_2$  is highly influenced by the pozzolanic activity of fly ash.

Studies focusing on the influence of fly ash on carbonation resistance are limited in comparison with the extensive research that has been conducted on the carbonation of OPC concrete. There is no general agreement between researchers whether incorporation of fly ash in concrete reduces its carbonation rate. Papadakis [61] investigated the effect of high and low calcium fly ashes on the carbonation behaviour of fly ash concrete at replacement level of 10, 20 and 30% by weight of the binder. He found that the carbonation depth increases with increasing cement replacement by both ashes, but when the fly ash was used as a fine aggregate replacement, the carbonation depth decreased because the binder content increased. Other studies report contradictory results with regard to the carbonation of concrete made with fly ash. Hussain et al. [56] have conducted a comparative study of accelerated carbonation of plain cement and fly ash concrete with various dosages of fly ash from 10% to 70% replacement by weight. They found that fly ash concrete shows similar resistance against carbonation as the control OPC concrete when designed for the same water/binder ratio. Atis [65] also reported that fly ash concrete, made with 50% cement replacement and lower water/binder ratio than OPC concrete, showed lower or comparable carbonation depth as OPC concrete. According to Venkat and Meena [57], the carbonation depth of high volume fly ash concrete is similar to the carbonation depth of control OPC concrete after 90 days of  $\text{CO}_2$

exposure. Literature survey [60] reviewed the studies which have been undertaken since 1968 on the effect of fly ash on carbonation of concrete. They found 65% of the studies reported that fly ash reduces the carbonation resistance of concrete compared to OPC concrete mainly due to the lower content of  $\text{Ca}(\text{OH})_2$  resulting from the pozzolanic reaction which consumes  $\text{Ca}(\text{OH})_2$ . In contrast, 4% of the studies recorded lower carbonation rate of fly ash concrete which was attributed to its denser hardened structure, 5% reported no change, 13% reported varying results (increase and decrease) and 13% of these studies there is no reference OPC mix to compare. The variation in the test conditions in terms of temperature, relative humidity and  $\text{CO}_2$  concentration (natural or accelerated) in addition to the mix design, curing duration and fly ash content are the main factors responsible for these outcomes. From earlier studies, it was shown that the strength of concrete, curing period and  $\text{CO}_2$  content have direct influence on carbonation. The curing period has direct impact on permeability, strength of concrete and consequently depth of carbonation. The increase in curing period increases strength of concrete and decreases depth of carbonation. Furthermore, it was observed that carbonation depth is increased when the  $\text{CO}_2$  concentration is high. In addition, it has been reported that low-strength fly ash concrete carbonates more than conventional OPC concrete of similar strength whereas high-strength fly ash concrete shows similar rate of carbonation to OPC concrete designed for the same strength [57].

These observations suggest that incorporating fly ash as a cement replacement requires careful consideration in the design of concrete mixes and proper curing in order to produce fly ash concrete of similar carbonation resistance to OPC concrete.

There has been little research on the carbonation of biomass or co-combustion biomass fly ash based concrete. Ramos et al. [66] have investigated the carbonation resistance of mortar samples containing 10% and 20% wood waste ash compared to control OPC sample. The specimens were water cured for 14 days ( $20^\circ\text{C} \pm 2^\circ\text{C}$  and  $\text{RH} = 100\%$ ) and then transferred to a chamber at  $20^\circ\text{C} \pm 2^\circ\text{C}$  and  $50\% \pm 5\%$  RH until 28 days to reach moisture equilibrium. Specimens were then exposed to  $5\% \pm 0.1\%$  carbon dioxide,  $\text{RH} = 60\% \pm 5\%$  and temperature  $23^\circ\text{C} \pm 3^\circ\text{C}$ , in an accelerated carbonation chamber for 30 days. The results showed that the

carbonation depth for blended wood waste ash-cement mixtures was greater than for the control OPC mixture. It was found that the depth of carbonation increases along with the increase in wood waste fly ash content. The increase in carbonation depth could be due to the reduction of  $\text{Ca}(\text{OH})_2$  caused by the pozzolanic reaction, however, the duration of carbonation process (30days) is too short to provide a clear picture of the effect of biomass ash on carbonation.

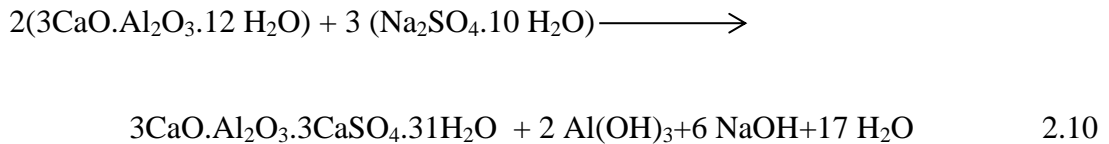
Chee and Ramli [67] investigated the effect of partial replacement of cement with high calcium wood ash (HCWA) on the carbonation resistance of concrete. They indicate that inclusion of 5% of HCWA in blended cement mortar reduced the carbonation depth compared to control OPC while it increased at replacement level from 10 to 25%. No previous research has examined the impact of co-combustion biomass fly ash on carbonation resistance. Therefore, research is needed to determine if these types of fly ashes can be used to improve the carbonation resistance of concrete.

#### **2.5.2.3.2. Sulphate Attack**

Sulphate attack on concrete occurs when environmental sulphate (from water, soil or seawater) penetrates the concrete structure. Sodium, potassium and magnesium are the main sources of sulphate ions in the soil while calcium sulphates are the main sulphate ions in groundwater. Solid sulphate salts are harmless to concrete unless they are present in solution. Sulphate damage manifests itself in several ways depending on which of the following chemical processes occur and are dominant. Sulphates can combine with soluble calcium hydroxide and calcium silicate hydrate in the presence of water to form gypsum ( $\text{CaSO}_4$ ) and/or react with calcium aluminate hydrate to form ettringite ( $\text{C}_3\text{A}.3\text{CaSO}_4.32\text{H}_2\text{O}$ ). The volume of resulting gypsum and ettringite is higher than the volume of its initial components, therefore, their formation causes large expansion which may lead to cracking, spalling and loss of strength [31, 68–70]. However, not all sulphates react with all cement-based materials' phases. For instance, sodium sulphate reacts only with calcium hydroxide and calcium aluminate hydrate whereas magnesium sulphate can directly attack calcium silicate hydrate (C-S-H) in addition to calcium hydroxide ( $\text{Ca}(\text{OH})_2$ ) and calcium aluminate hydrate (C-Al-H). Therefore, magnesium sulphate attack is more

severe than any other type of sulphates as it causes loss of strength and adhesion of cement paste due to decalcification of calcium silicate hydrate [31].

The reaction of sodium sulphate with calcium hydroxide and calcium aluminate hydrate can be expressed as follows[71]:



The reaction of magnesium sulphate with calcium silicate hydrate is shown in the following formula:



It is generally agreed that the type of cement, reflected by the content of components that contribute to sulphate reactions ( $\text{C}_3\text{A}$  and  $\text{CaO}$ ), permeability of concrete and the concentration of sulphate solution are the main factors affecting the rate of sulphate attack. Higher  $\text{C}_3\text{A}$  and  $\text{CaO}$  contents in cement lead to more sulphate reaction [72]. Moreover, the more permeable the concrete, the more sulphate ions can penetrate leading to higher rate of sulphate attack. In addition, sulphate attack depends upon the concentration and type of sulphate solution (i.e. sodium, magnesium) to which the concrete is exposed. Park et al. [73] found that the expansion of OPC mortar samples exposed to 10% sodium sulphate was about 75% higher than the expansion of samples immersed in magnesium sulphate with the same concentration as sodium sulphate. In contrast, the samples immersed in magnesium sulphate suffered a large strength loss accompanied by a significant reduction in weight compared to the samples immersed in sodium sulphate. This indicates that the mode of attack is different between sodium and magnesium sulphate exposure which suggest that the type and the concentration of sulphate ions play an important role in controlling the sulphate attack.

- **Influence of Fly Ash on Sulphate Resistance**

It is recognized that incorporation of pozzolanic materials such as fly ash, silica fume and blast furnace slag in concrete production improves sulphate resistance either by lowering C<sub>3</sub>A and CaO content in the blended binder or reducing the permeability. Early work conducted by Dimic and Droljc [72] reported that the sulphate resistance of concrete is highly affected by the amount of tricalcium aluminate(C<sub>3</sub>A).

Fly ash is generally known to be effective in reducing sulphate attack on concrete due to the pozzolanic reaction which consumes Ca(OH)<sub>2</sub>, however, high calcium fly ash has shown to be less effective in resisting sulphate attack compared to low calcium fly ash. Tikalsky and Carrasquillo [74] reported that concrete with fly ash of calcium oxide (CaO) content greater than 20% was more susceptible to sulphate attack than fly ash with less than 10% calcium oxide. Dunstan [75] has reported that the resistance of fly ash concrete to sulphate attack (up to 25% replacement level) is a function of calcium and iron content of the fly ash and can be identified by using simple resistance factor "R" given in the following equation.

$$R = \frac{CaO-5}{Fe_2O_3} \quad 2.12$$

Dunstan found that values of  $R < 1.5$  increase sulphate resistance whereas values  $>3$  decrease the sulphate resistance. However, other studies [70, 71] argued that this factor was insufficient to determine the sulphate resistance of fly ash concrete and only the actual fly ash content could improve the sulphate resistance. The validity of factor R to concretes made with biomass fly ash requires investigation and it will be discussed in chapter 6 (section 6.1.3.1).

Compared to coal fly ash on which significant research has been done, there has been little research on sulphate resistance of concrete made with biomass or co-fired biomass fly ash and their effect is still unclear. One study found that mortars made with co-combustion bituminous coal and biomass fly ash exhibited lower resistance to sulphate attack than the mortars made with coal fly ash [76]. Rajamma [2] reported work on the sulphate resistance of mortars made with two types of wood waste biomass fly ashes at various cement replacement levels, exposed to a

combination of 5% magnesium sulphate and 5% sodium sulphate solution up to one year. The two ashes have different chemical composition and provide different porosity of the mortars. He found that the expansion due to sulphate attack increases with increasing content of both biomass fly ashes. He attributed that to the higher porosity of both biomass fly ash mortars compared to control OPC mortar. The results also indicated that higher carbon content and high porosity of the fly ash leads to a higher rate of deterioration. Shearer [5] also reported that biomass fly ash is ineffective in mitigating the expansion caused by sulphate attack due to a lack of pozzolanicity (low content of silica and alumina). However, the current literature of biomass fly ash provides inconclusive information on the sulphate resistance of biomass ash mortar or concrete and, therefore, more research is needed on this subject.

### 2.5.2.3.3. Chloride Ingress in Concrete

The highly alkaline environment of concrete provides a passive layer on the surface of steel bars which protects the steel reinforcement from corrosion. However, chloride ions can diffuse into concrete through its pore water and attack this passive layer. When chloride ions penetrate into concrete from an environmental solution, they can be either captured by the hydration products (physically and chemically bound chloride) or stay free in the pore solution (free chloride). The summation of bound chloride and free chloride gives the total chloride as shown in Figure 2.3.

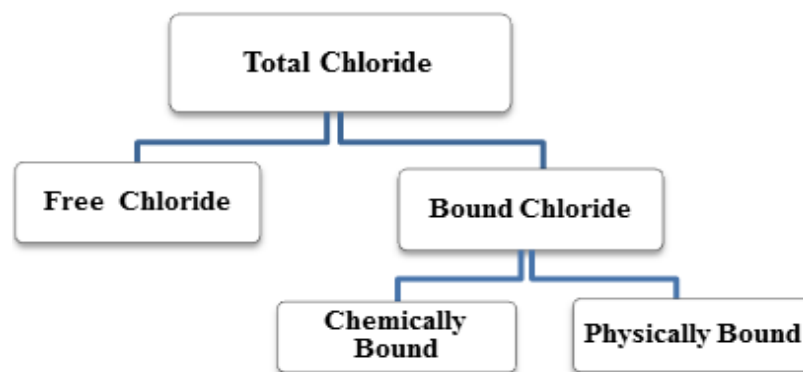


Figure 2.3 The presence of chloride in concrete

The free and bound chlorides normally exist together and maintain chemical equilibrium. The proportion of bound chloride present in the total chloride in conventional OPC concrete varies from 80% to 65% which means that the majority of total chloride is chemically bound to the hydration products or physically attached to the surface of C-S-H gel rather than dissolved in the pore solution [31].

The chemically bound chloride (acid-soluble) is a result of the reaction between the chloride ions with un-hydrated  $C_3A$  and  $C_4AF$  to form Friedel's salt ( $Ca_6Al_2O_6.CaCl_2.10H_2O$ ) and calcium chloroferrite ( $Ca_6Fe_2O_6.CaCl_2.10H_2O$ ). The physically bound chloride (water-soluble) occurs due to the adsorption of chloride on the surface of C-S-H gel. Therefore, the chemical binding of chloride in cementitious systems is dominated by the content of  $C_3A$  and  $C_4AF$  while the physical chloride binding is controlled by the amount of C-S-H gel [77, 78]. Chemically bound chloride (acid-soluble) represents most of the chloride in conventional OPC concrete and in current practice, the acid-soluble chloride values are used in the long-term prediction models for chloride ingress in concrete [79–82].

Bound chloride reduces the quantity of free chloride in the pore solution and, therefore, reduces the risk of reinforcement corrosion [83]. Free chloride can be a major durability problem only when its concentration exceeds a critical limit (known as a threshold) at the surface of the embedded steel. The limits of threshold, usually expressed as the percentage of chloride by mass of the binder, vary for different types of concrete. For example, the maximum corrosion threshold chloride concentration is 0.4% by mass of cement for reinforced concrete and 1% for non-reinforced concrete as given in the standard BS EN 206 [84]. Although the free chloride is considered to be responsible for initiating corrosion, determining its value by pore solution extraction under pressure is more difficult than conducting the total chloride content analyses by the acid-soluble method [85]. In practice, extraction of pore fluid requires special equipment and it is often not possible to obtain sufficient pore solution from concrete especially from cores obtained from concrete structures in the field which have inadequate moisture to release the pore fluid under pressure. In addition, this method is unsuitable for actual structures due to the practical difficulties of obtaining concrete cores for pore fluid extraction. It has been noted

that the use of this method is inaccurate and may overestimate the free chloride [86]. The state of moisture (degree of saturation of pores) in the concrete affects the value of free chloride concentration. Glass and Buenfeld [87] have provided evidence of the errors associated with the use of pore fluid extraction method. Therefore, in practical situations, a relationship between free and chemically bound (acid-soluble) chlorides is required since acid-soluble chloride is specified in standard BS EN 14629 [79] for the design of concrete structures against reinforcement corrosion. Some researchers have used the water-soluble chloride determined by dissolving the concrete powder in water (tests for physically bound chloride) as a measure of free chloride concentration [88–91].

Incorporation of supplementary cementitious materials (SCMs), such as fly ash, slag, silica fume has a significant impact on the resistance of concrete to chloride diffusion. Their effect on chloride binding is varied due to the differences in their chemical composition and physical properties which they impart to concrete. For instance, fly ash and ground granulated blast furnace slag (GGBS) generally show increased chloride binding capacity due to their relatively high reactive  $\text{Al}_2\text{O}_3$  contents while a lower chloride binding capacity is observed when silica fume is used due to its low  $\text{Al}_2\text{O}_3$  content [78, 92]. Coal fly ash reduces the free chloride ingress as chlorides chemically bind to the fly ash hydrates due to its high alumina content. The increase of cement replacement with fly ash in concrete reduces the rate of chloride ion penetration and provides greater protection to steel corrosion in concrete [83, 93, 94].

Existing literature lacks comprehensive data on the impact of biomass fly ash on chloride ingress in concrete; only limited data are available based on rapid chloride permeability (RCPT) test which showed lower chloride permeability than control OPC concrete [5, 11, 95]. However, the rapid chloride permeability test does not provide direct information on the chloride diffusion parameters of concrete which are required for the design and maintenance of concrete structure against reinforcement corrosion. In addition, rapid chloride permeability test is not recommended to evaluate chloride permeability of concrete incorporating supplementary cementing materials (SCMs). This is because it is a measurement of

the electrical conductivity of concrete, which depends on both pore structure and composition of the pore solution which can change due to the addition of SCMs. Analyses based on published results have indicated that the replacement of Portland cement with SCMs can reduce the electrical conductivity of concrete more than 90% due to the change in pore solution composition in the concrete [96]. Therefore, the bulk chloride diffusion test method for directly determining the basic parameters of the diffusion process was used in this research project, which involved the long-term exposure of test specimens in a chloride solution.

- **Chloride Ingress and Transport Mechanism**

Chloride penetrates into the concrete matrix by a combination of mechanisms such as absorption by capillary suction, permeation due to hydrostatic pressure and diffusion caused by the differences in chloride concentration within the concrete parts [97, 98]. The predominant mechanism is controlled by the environment to which the concrete is exposed as shown in Table 2.4. Among these three mechanisms, only diffusion can bring chloride ions up to the level of steel bars in the concrete as the effect of absorption is usually limited to a shallow region and permeation occurs rarely [97, 99]. Also in submerged areas where permeation occurs, the availability of oxygen to fuel the corrosion reaction may be reduced due to lower oxygen diffusion rates in submerged structures.

The rate of ingress of chlorides into concrete is mainly dependent on the pore structure of concrete which is in turn controlled by other factors such as water to binder ratio, the binder content, the inclusion of supplementary cementitious materials and the degree of hydration. However, other external factors such as curing condition, duration of exposure, temperature and the degree of saturation also control the transport of chloride ions [97, 99]. When the concrete is fully saturated (the case of the current study), the chloride moves from the high concentration medium (chloride solution) towards the lower concentration medium (concrete) to reach equilibrium, representing the predominant diffusion mechanism [98, 99].

**Table 2.4 Chloride transport mechanisms for various marine exposure conditions**[100]

<b>Exposure condition</b>	<b>Example of structure</b>	<b>Primary(predominant) transport mechanism</b>
Submerged	Substructures below low tide	Diffusion
	Basement exterior walls or transport tunnel liners below tide.	Permeation, diffusion and Wick's action
Tidal	Superstructures in tidal zone	Capillary absorption and diffusion
Splash & spray	Superstructures above high tide in the open sea	Capillary absorption and diffusion (also carbonation)
Coastal	land-based structures in coastal area or superstructures above high tide in river estuary	Capillary absorption (also carbonation)

- **Chloride Diffusion**

The response of concrete to chloride exposure is described by its chloride diffusion profiles. The chloride diffusion coefficient,  $D_c$ , and surface chloride concentration,  $C_0$ , are the main parameters used to assess the resistance of concrete to long term chloride ingress.

Fick's second law of diffusion, represented by equations 2.13 and 2.14, has been proposed by Collepardi et al. [101] as a suitable model for chloride diffusion in concrete:

$$\frac{\partial C}{\partial t} = D_c \frac{\partial^2 C}{\partial x^2} \quad 2.13$$

$$C_{(x,t)} = C_0 \left[ 1 - \operatorname{erf} \left( \frac{x}{2\sqrt{D_c t}} \right) \right] \quad 2.14$$

Where:  $C(x,t)$  is the chloride concentration (% by weight of binder) at distance  $x$  and exposure time  $t$ ;  $x$  is the distance from the concrete surface (m);  $t$  is the time (seconds);  $D_c$  is the diffusion coefficient ( $m^2/s$ );  $C_0$  is the chloride concentration (% by weight of binder) on the concrete surface and  $erf$  is the error function.

The equation 2.14 assumes that the values of  $D_c$  and  $C_0$  are constant during the chloride exposure period, however, other studies have proven that these values vary with time [82, 102, 103].

Mangat et al. [102] have proposed the following power function:

$$D_c = D_i \cdot t^{-m} \quad 2.15$$

Where:  $D_c$  is the diffusion coefficient at time  $t$ ;  $D_i$  is the diffusion coefficient at a reference time  $t_i$  and  $m$  is the age factor.

By introducing the time dependency of the diffusion coefficient  $D_c$  (equation 2.15) into Fick's second law (equation 2.14), the following equation is obtained[102]:

$$C_{(x,t)} = C_0 \left[ 1 - erf \left( \frac{x}{2 \frac{\sqrt{D_i \cdot t^{(1-m)}}}{\sqrt{(1-m)}}} \right) \right] \quad 2.16$$

Equation 2.15 can be used to predict long-term chloride diffusion coefficient while equation 2.16 predicts the chloride concentration profiles in concrete by knowing the values of  $m$ ,  $C_0$  and  $D_i$ .

Similarly, the time-dependent  $C_0$  has been shown to be proportional to the square root of chloride exposure period [104, 105] as given in the following equation:

$$C_0 = C_i + k\sqrt{t - t_i} \quad 2.17$$

Where:  $C_i$  and  $t_i$  are reference surface chloride concentration and reference time respectively;  $k$  is the age factor influencing the long-term surface chloride concentrations and  $C_0$  is the chloride concentration on the concrete surface at time  $t$ .

Many studies have been conducted on chloride ingress in cement-based materials under different marine exposure conditions to determine their chloride diffusion coefficients  $D_c$  at different periods of exposure in order to quantify the chloride ingress rate in concrete [99, 102, 106, 107]. Table 2.5 shows a wide range of  $D_c$  values determined by various methods for several concrete mixes. These values range between  $1 \times 10^{-12}$  to  $52.3 \times 10^{-12} \text{ m}^2/\text{s}$ . The table covers a wide range of mixes with w/c ratios varying from 0.4 to 0.65 and different concentrations of salt solution exposures. These values indicate that the  $D_c$  depends on several factors such as the type of binder, W/B ratio, the exposure condition and the test method.

For example, Polder [106] determined the  $D_c$  values of different fly ash concrete mixes from experimental results up to 14 weeks, then he applied an empirical model to predict  $D_c$  value at 1.5 years. A higher chloride diffusion coefficient of  $52.3 \times 10^{-12} \text{ m}^2/\text{s}$  is determined in fibre reinforced concrete after 28 days of exposure to wet/dry cycles in the laboratory with high salt concentration. The higher  $D_c$  value is due to the high w/c ratio of 0.58 which makes the concrete more permeable. However, the diffusion coefficient decreased to  $10 \times 10^{-12} \text{ m}^2/\text{s}$  after 270 days exposure period whereas the surface chloride concentration increased from 0.32% to 0.85% by weight of the binder between 28 and 270 days of exposure period [102]. A higher binder content and longer duration of exposure reduced the chloride diffusion coefficient to  $6.13 \times 10^{-12} \text{ m}^2/\text{s}$  at 154 days exposure and to  $2.81 \times 10^{-12} \text{ m}^2/\text{s}$  at 1250 days [107]. Chalee et.al [108] reported lower chloride diffusion coefficient,  $D_c$ , and surface chloride concentration,  $C_0$ , in reinforced fly ash concrete compared to control OPC concrete after 7 years exposure to hot and high-humidity climate marine conditions as shown in Figure 2.4.

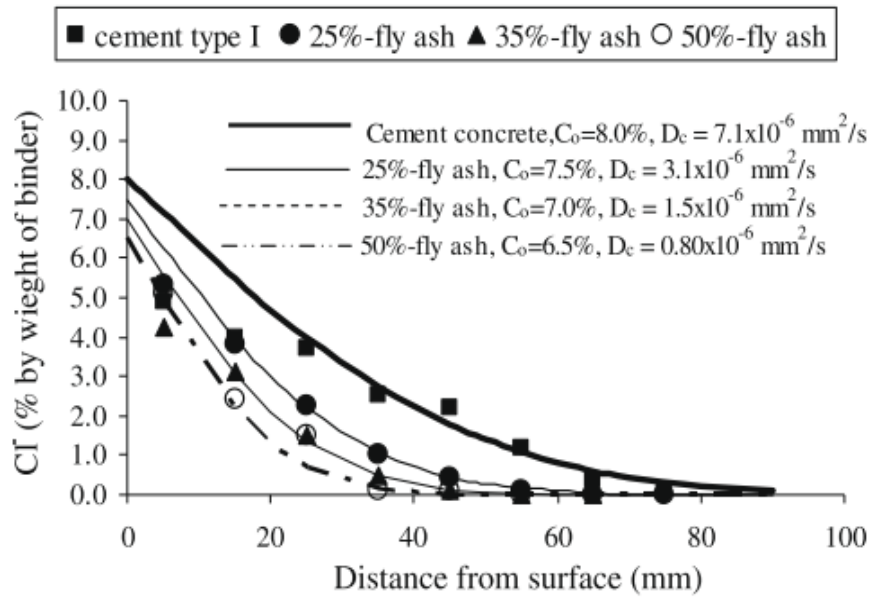


**Figure 2.4** The fitting curve of the solution of Fick's second law on chloride penetration profile in concrete with a W/B ratio of 0.65 at 7-year exposure[108]

Table 2.5 Chloride diffusion coefficient Dc values as Published in literature

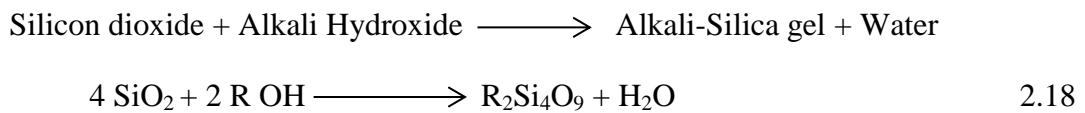
<b>Dc x10<sup>-12</sup> (m<sup>2</sup>/s)</b>	<b>W/C ratio</b>	<b>Curing age</b>	<b>Author</b>	<b>Concrete type &amp; Environment</b>
1.1 -4 2.5	0.4 - 0.54 0.43	1-14 weeks 1.5 year	R.B.Polder [106]	Fly ash concrete exposed to salt/dry cycle
15.3-0.42	0.44-0.68	2-10 years	Thomas &Matthews [109]	Fly ash concrete exposed to tidal zone of BRE marine site
3.65-1.19	0.5	2 Months	Zhang &Gjorv [110]	Theoretical analysis of concrete under RCPT test
52.3-10	0.58	28-270 days	Mangat& Molloy [102]	Steel fibre reinforced concrete exposed to wet/dry cycle
2.27-0.36	-	28-180 days	Mangat & Limbachiya [111]	Concrete repair materials immersed in 175g of NaCl per 1L of water solution in laboratory
6.13-2.81	0.4	154-1250 days	Mangat& Gurusamy [107]	Steel fibre reinforced concrete under marine exposure
7.1-0.8	0.45-0.65	7 years	W.Chalee et.al [108]	Reinforced fly ash concrete exposed to hot and high humidity climate in marine condition
7.3-2.5	0.486	55-270 days	Mangat &Ojedokun [81]	Concrete under bulk diffusion test immersed in 5% NaCl solution in laboratory

#### 2.5.2.3.4. Alkali silica reaction (ASR)

The alkalis present in concrete pore solution, which is dominated by Na, K, and OH (with minor amounts of Ca), reacts with the silica present in aggregates causing expansive reactions in the presence of sufficient moisture. The product of the reaction is an alkali-silica gel composed of Na, K, Ca, and Si. The gel imbibes water from the surrounding cement paste, expands and eventually the swelling pressures may exceed the tensile strength of the surrounding paste and cause cracking of the concrete which can in turn cause failure [112–114]. ASR affects many structures worldwide, including major dams and bridges.

ASR was first identified by Stanton in the early 1940s in California (USA) when he noticed that the concrete pavement and bridges in the Salinas Valley were failing due to cracking caused by expansive expansion. He recognized for the first time that alkalis, Na and K, in the paste combined with silica in the aggregate in a deleterious reaction which caused cracking [115].

The following is the simplest equation which can represent the ASR:



**Where:** R is sodium, Na, or potassium, K.

Alkali oxides such as  $\text{K}_2\text{O}$  and  $\text{Na}_2\text{O}$  are identified as the most significant contributors to ASR expansion. Cement is the major source of alkali in concrete; however, other concrete ingredients such as aggregates, water and SSMs may contain a certain amount of alkali and can contribute significantly to ASR damage.

Alkali released from cement is described as the total mass of “equivalent sodium oxide”,  $(\text{Na}_2\text{O})_{\text{eq}}$ , which is determined from the following Equation [116, 117]:

$$(\text{Na}_2\text{O})_{\text{eq}} (\%) = \text{Na}_2\text{O} (\%) + 0.658 \text{K}_2\text{O} (\%) \quad 2.19$$

Where: the constant 0.658 represents the atomic mass ratio of  $\text{Na}_2\text{O}$  (62.0 g/mol) over  $\text{K}_2\text{O}$  (94.2 g/mol).

Alkali has the ability to react with both crystalline and amorphous silica to form alkali silicate gel. With crystalline silica, the produced gel occupies greater volume than the volume of the reactants (swelling gel) whereas amorphous silica reacts more readily with alkali with little or no net expansion (non-swelling gel). The expansion of concrete depends on the type of reaction products, i.e. swelling alkali-silica gel or non-swelling lime-alkali-silica gel. The expansion will occur only when the swelling alkali-silica gel is formed. The calcium, Ca, ion concentration in concrete controls the formation of the type of reaction products because it reacts with both amorphous and crystalline silica. The calcium reactions with amorphous silica decrease the reaction rates of amorphous silica with the alkali, therefore, ASR reactions tend to increase with increasing calcium content. However, the ASR reaction with crystalline silica is slow, which is the reason that ASR damage commonly requires 20 or more years to become evident [3].

The reactivity of silica depends on the crystal structure rather than its chemical composition. For instance, both quartz and opal are silica minerals that have similar chemical composition, however, opal has a denser structure of silica spheres and is highly reactive whereas quartz has a well-ordered crystal structure of silica and is very stable (less reactive) in concrete at normal temperature [118].

The silica is not directly attacked by the alkali metal Na and K, the first stage of the alkali-silica reaction is the reaction between the hydroxyl ions ( $\text{OH}^-$ ) in the pore solution and reactive silica in the aggregate. The alkalis contribute initially to the high concentration of hydroxyl ions in solution and later to the formation of an expansive alkali-silica gel [112, 119].

Two main tests are used to screen aggregates for potential alkali-silica reactivity, ASTM C 1260 [120] and ASTM C 1293 [121]. Both are accelerated tests that put the material in aggressive conditions to increase the rate of reaction compared to the rate that would occur in the field. In ASTM C 1260, the reaction is accelerated by exposing the mortar sample to high temperature ( $80^\circ\text{C}$ ) and high concentration of hydroxide (1N NaOH) for 14 days. The length difference of the specimens between 1 day and 14 days indicates the expansion percentage of the specimens, where expansion of less than 0.1% is innocuous; 0.1- 0.2% represents potentially deleterious ASR; more

than 0.2% represents deleterious ASR attack. In contrast, ASTM C 1290 uses high alkali cement (total alkali content 1.25%) or alternatively alkalinity is increased by adding sodium hydroxide, NaOH, to the mixing water of concrete to obtain the alkali content required by this test. The concrete test samples are stored in an airtight container at 38 °C and 95% RH. The aggregate is considered potentially reactive if the expansion percentage of the concrete specimens at an age of one year exceeds 0.04%. Although ASTM C 1290 test has less aggressive conditions (lower concentration of hydroxide and lower temperature) than ASTM C 1260, it requires a year to complete. Thus, Accelerated mortar bar test ASTM C 1260 is preferred due to its time effectiveness [122].

- **The effect of fly ash on ASR**

The use of SCMs such as fly ash, slags and silica fumes has been shown to suppress the expansion due to ASR in accelerated laboratory tests such as ASTM C1260/1567 and ASTM C1293 and even in field exposure tests [123, 124]. Different mechanisms have been proposed for mitigation of ASR by fly ash such as reduction in pore solution alkalinity, reduction in the availability of calcium and refinement of the pore structure, thus reducing permeability and retarding ions transfer of concrete [125–128]. However, the primary role of fly ash in minimizing the deleterious expansion due to ASR is mainly attributed to the reduction in pore solution alkalinity by alkali dilution and binding of the alkalis in the hydration products [126]. The effect of fly ash on the alkalis available in solution depends on the composition of the ash, level of replacement and alkali content of the cement [129]. A fly ash is ineffective in depressing ASR expansion if its buffering effect cannot reduce the alkali content below the limits at which certain reactive aggregates undergo significant ASR [123].

During cement hydration, a certain amount of alkali ions can be released into the pore solution. When fly ash is used as a replacement of cement, the total alkalis in the mix reduces (dilution effect) thereby mitigates ASR. The silica present in the fly ash reacts with the alkalis present in cement to form a non-expansive calcium-alkali-silica gel, thus, reducing the free alkalis available to react with the aggregates. Binding the alkalis in the hydration products of the cement-fly ash system is controlled by CaO content of the fly ash. The binding increases as the calcium

content decrease. Low-calcium fly ashes are more effective at increasing the alkali binding capacity of C-S-H than high calcium fly ashes, therefore, the availability of alkalis for ASR increases when high calcium fly ashes are used [119, 130]. The inferior performance of high calcium fly ashes is largely due to differences in the pore solution chemistry of concretes with low or high calcium fly ash [130]. C-S-H hydrate with a low Ca/Si ratio are able to retain more alkalis (Na+K) compared to hydrates of higher lime to silica Ca/Si ratios. Glasser et al. [118, 131] explained the differences in alkali absorption of C-S-H which is dependent on the Ca/Si ratio. At high ratios, the charge is positive and the C-S-H tends to repel cations. As the Ca/Si ratio decreases the positive charge reduces becoming negative at low Ca/Si ratios.

Both pozzolanic reaction and alkali-silica reaction can simultaneously take place in the presence of fly ash under strong alkali condition. The overall effect is to reduce the possibility of reaction between alkali and aggregate. The pozzolanic reaction products (secondary C-S-H gel) can incorporate alkali metal ions into their structure and reduce the alkalinity of the pore solution. In addition, they fill the pores and reduce the permeability of concrete, consequently, reducing the free movement of alkali ions. The second effect (reduction of the permeability) is more important when there is a continuous supply of alkali from an outside source (groundwater, de-icing salts and the case of accelerated mortar bar test) because it slows down the supply of alkalis to concrete [114, 123].

Accelerated mortar bar test (AMBT) ASTM C 1567 [132] is widely used to assess the potential reactivity of the combination of SCMs and aggregates. The alkali in the pore solution of mortar bars is mainly a function of the availability of alkalis in the cementitious system and the quantity of alkalis that penetrate from the external solution of NaOH at 80°C. Thus the accelerated mortar bar test is actually testing the ability of the fly ash to lower the alkalinity of the pore solution (by binding alkalis in the hydrates) and to reduce the diffusivity of the mortar bar making it less accessible to the external alkali medium. As such it is a good simulation of practical conditions under which ASR occurs where both internal and external alkalis are available.

While Class F fly ashes are commonly used to mitigate aggregate reactivity, the influence of biomass and co-combustion fly ashes for mitigation of alkali-silica

reaction expansion requires more research to enable their application. According to Wang and Baxter [133], biomass fly ash from combined sawdust and switch grass has much better performance than class C fly ash in mitigating ASR expansion, despite its much higher alkali content. This could be due to lower capacity of binding the alkalis in the hydration products of the cement-fly ash system as it is controlled by the CaO content of the fly ash. Therefore, the availability of alkalis for ASR increases in the case of class C fly ash because it has higher amount of CaO than sawdust and switch grass biomass ashes. Similar behaviour was reported for wood bottom ash produced from a biomass power plant in Portugal by using it as 10 % cement replacement in mortar. It reduced the expansion caused by ASR compared with the control mortar [134]. In contrast, Shearer [5] observed no significant differences between expansion rates of mixes incorporating 25% co-combustion sawdust biomass fly ashes compared to their companion Class F coal fly ash sample mixes. Both ashes mitigated ASR expansion, whereas pure wood waste biomass ash at the same level of replacement was ineffective in controlling expansion.

In another study carried out by Esteves et al. [135], expansion results for mortar mixes containing reactive aggregate and 20 and 30% waste wood biomass fly ash showed a small improvement in resisting ASR compared to control OPC. But the incorporation of biomass fly ash in the blend along with metakaolin, 20% BFA + 10% MK, showed significant improvement in the expansion results, indicating the effective use of biomass fly ash along with metakaolin in mitigating ASR.

These mixed results encourage further research on the topic, especially given the differences in chemical compositions and the high alkali contents of the biomass ashes investigated in this study which may contribute significantly to ASR damage.

## 2.6. References

1. ASTM (2015) Standard Specification for Coal Fly Ash and Raw or Calcined Natural Pozzolan for Use C618:2015. 1–5 . doi: 10.1520/C0618-15.2
2. Rajamma R (2011) Biomass fly ash incorporation in cement based materials, PhD Thesis. Department of Ceramics and Glass Engineering, University of Aveiro
3. Wang S (2007) Biomass and Coal Fly Ash in Concrete : Strength , Durability , Microstructure , Quantitative Kinetics of Pozzolanic Reaction and Alkali Silica Reaction Investigations . PhD Thesis, Department of Chemical Engineering, Brigham Young University
4. Zulu SNF (2017) Optimizing the usage of fly ash in concrete mixes. Department of Civil Engineering and Surveying, Durban University of Technology
5. Shearer CR (2014) The Productive Reuse of Coal , Biomass and Co-Fired Fly Ash. PhD Thesis, School of Civil & Environmental Engineering, Georgia Institute of Technology
6. Steven H. Kostmatka, Beatrix Kerkhoff WCP (2002) Design and Control of Concrete Mixtures, EB001, 14th ed, Portland Cement Association
7. Vassilev S V., Vassileva CG (2007) A new approach for the classification of coal fly ashes based on their origin, composition, properties, and behaviour. Fuel 86:1490–1512 . doi: 10.1016/j.fuel.2006.11.020
8. Vassilev S V, Baxter D, Andersen LK, Vassileva CG (2010) An overview of the chemical composition of biomass. Fuel 89:913–933. doi:10.1016 /j.fuel. 2009.10.022
9. Tumuluru JS, Sokhansanj S, Wright CT, Boardman RD, Yancey NA (2011) A review on biomass classification and composition, co-firing issues and pretreatment methods. Am Soc Agric Biol Eng Annu Int Meet 2011, ASABE 2011 3:2053–2083
10. Kalemekiewicz J, Chmielarz U (2012) Ashes from co-combustion of coal and

- biomass : New industrial wastes. "Resources, Conserv Recycl 69:109–121 . doi: 10.1016/j.resconrec.2012.09.010
11. Cheah Chee Ban MRS (2011) The incorporation of wood waste ash as a partial cement replacement material for making structural grade concrete: An overview. Resour Conserv Recycl 55:669–685 . doi: 10.1016/j.asej.2014.11.005
  12. Vassilev S V., Baxter D, Andersen LK, Vassileva CG (2013) An overview of the composition and application of biomass ash. Part 1. Phase-mineral and chemical composition and classification. Fuel 105:40–76 . doi: 10.1016/j.fuel.2012.09.041
  13. Saraber A (2017) Fly ash from coal and biomass for use in concrete Origin, properties and performance. Master of Science in Environmental Science and Protection. TU Delft University
  14. Mourant D, Wang Z, He M, Wang XS, Garcia-Perez M, Ling K, Li CZ (2011) Mallee wood fast pyrolysis: Effects of alkali and alkaline earth metallic species on the yield and composition of bio-oil. Fuel 90:2915–2922 . doi: 10.1016/j.fuel.2011.04.033
  15. Bridgwater A V. (2012) Review of fast pyrolysis of biomass and product upgrading. Biomass and Bioenergy 38:68–94 .doi: 10.1016/j.biombioe.2011.01.048
  16. Sklivaniti V, Tsakiridis PE, Katsiotis NS, Velissariou D, Pistofidis N, Papageorgiou D, Beazi M (2017) Valorisation of woody biomass bottom ash in Portland cement: A characterization and hydration study. J Environ Chem Eng 5:205–213 . doi: 10.1016/j.jece.2016.11.042
  17. Siddique R (2012) Utilization of wood ash in concrete manufacturing. Resour Conserv Recycl 67:27–33 . doi: 10.1016/j.resconrec.2012.07.004
  18. Koppejan J (2012) The Handbook of Biomass Combustion and Co-firing. Handb Biomass Combust Co-firing. doi: 10.4324/9781849773041
  19. BS EN 450 (2012) Fly ash for concrete Part 1 : Definition , specifications and conformity criteria. BS EN Stand

20. Wang S, Baxter L (2007) Comprehensive study of biomass fly ash in concrete: Strength, microscopy, kinetics and durability. *Fuel Process Technol* 88:1165–1170 . doi: 10.1016/j.fuproc.2007.06.016
21. Lothenbach B, Scrivener K, Hooton RD (2011) Supplementary cementitious materials. *Cem Concr Res* 41:1244–1256. doi: 10.1016/j.cemconres.2010.12.001
22. Ataie FF (2013) Enhancement of Agricultural Residue Ash Reactivity in Concrete. PhD Thesis, Department of Civil Engineering, Kansas State University
23. Y CDA (2005) Strength properties of high-volume fly ash roller compacted and workable concrete, and influence of curing condition. *Cem Concr Res* 35:1112–1121 . doi: 10.1016/j.cemconres.2004.07.037
24. Burden D (2006) The durability of concrete containing high levels of fly ash. University of New Brunswick. Portland Cement Association (PCA) R&D Serial No. 2989 . <http://dspace.hil.unb.ca:8080/xmlui/handle/1882/43629>
25. Donatello S, Tyrer M, Cheeseman CR (2010) Comparison of test methods to assess pozzolanic activity. *Cem Concr Compos* 32:121–127 . doi: 10.1016/j.cemconcomp.2009.10.008
26. Berra M, Mangialardi T, Paolini AE (2015) Reuse of woody biomass fly ash in cement-based materials. *Constr Build Mater* 76:286–296 . doi: 10.1016/j.conbuildmat.2014.11.052
27. Felix F. Udoeyo; Hilary Inyang; David T. Young; and Edmund E. Oparadu (2006) Potential of Wood Waste Ash as an Additive in Concrete. *J Mater Civ Eng*. doi: [https://doi.org/10.1061/\(ASCE\)0899-1561\(2006\)18:4\(605\)](https://doi.org/10.1061/(ASCE)0899-1561(2006)18:4(605))
28. Wang S, Baxter L, Fonseca F (2008) Biomass fly ash in concrete: SEM, EDX and ESEM analysis. *Fuel* 87:372–379 . doi: 10.1016/j.fuel.2007.05.024
29. Elinwa AU, Mahmood YA (2002) Ash from timber waste as cement replacement material. *Cem Concr Compos* 24:219–222 . doi: 10.1016/S0958-

30. Elinwa AU, Ejeh SP, Mamuda AM (2008) Assessing of the fresh concrete properties of self-compacting concrete containing sawdust ash. *Constr Build Mater* 22:1178–1182 . doi: 10.1016/j.conbuildmat.2007.02.004
31. Neville A. (1995) *Properties of Concrete*, Forth Edit. Longman Group Limited
32. Rajamma R, Senff L, Ribeiro MJ, Labrincha JA, Ball RJ, Allen GC, Ferreira VM (2015) Biomass fly ash effect on fresh and hardened state properties of cement based materials. *Compos Part B* 77:1–9 . doi: 10.1016/j.compositesb.2015.03.019
33. Targan S, Olugun A, Erdogan Y, Sevinc V (2008) Effects of supplementary cementing materials on the setting time and early strength of concrete. *Cem Concr Res* 7:1551–1558
34. Rajamma R, Ball RJ, Tarelho LAC, Allen GC, Labrincha JA, Ferreira VM (2009) Characterisation and use of biomass fly ash in cement-based materials. *J Hazard Mater* 172:1049–1060 . doi: 10.1016/j.jhazmat.2009.07.109
35. Bullard JW, Jennings HM, Livingston RA, Nonat A, Scherer GW, Schweitzer JS, Scrivener KL, Thomas JJ (2011) Mechanisms of cement hydration. *Cem Concr Res* 41:1208–1223 . doi: 10.1016/j.cemconres.2010.09.011
36. Scrivener KL, Nonat A (2011) Hydration of cementitious materials, present and future. *Cem Concr Res* 41:651–665 . doi: 10.1016/j.cemconres.2011.03.026
37. Kosbab BD, Kurtis KE (2010) Effect of calcium chloride and initial curing temperature on expansion caused by sulfate exposure. *ACI Mater J* 107:632–639
38. Ballim Y, Graham PC (2009) The effects of supplementary cementing materials in modifying the heat of hydration of concrete. *Mater Struct Constr* 42:803–811 . doi: 10.1617/s11527-008-9425-3
39. Thongsanitgarn P, Wongkeo W, Chaipanich A, Poon CS (2014) Heat of hydration of Portland high-calcium fly ash cement incorporating limestone powder: Effect of limestone particle size. *Constr Build Mater* 66:410–417 .

doi: 10.1016/j.conbuildmat.2014.05.060

40. Schöler A, Lothenbach B, Winnefeld F, Ben M, Zajac M, Ludwig H (2017) Cement and Concrete Research Early hydration of SCM-blended Portland cements : A pore solution and isothermal calorimetry study. *Cem Concr Res* 93:71–82 . doi: 10.1016/j.cemconres.2016.11.013
41. Tkaczewska E, Małolepszy J (2009) Hydration of coal – biomass fly ash cement. *Constr Build Mater* 23:2694–2700 . doi: 10.1016/j.conbuildmat.2008.12.018
42. Tkaczewska E, Mróz R, Łój G (2012) Coal-biomass Fly Ashes for Cement Production of CEM II / A-V 42 . 5R. 28:633–639 . doi: 10.1016/j.conbuildmat.2011.10.022
43. Kearsley P.J WE. (2001) The effect of high fly ash content on the compressive strength of foamed concrete. *Cem Concr Res* 31:105–112
44. Poon CS, Lam L, Wong YL (2000) Study on high strength concrete prepared with large volumes of low calcium fly ash. *Cem Concr Res* 30:447–455 . doi: 10.1016/S0008-8846(99)00271-9
45. Abdullahi M (2006) Characteristics of Wood ASH / OPC Concrete. *Leonardo Electron J Pract Technol* 9–16
46. Johnson A, Catalan LJJ, Kinrade SD (2010) Characterization and evaluation of fly-ash from co-combustion of lignite and wood pellets for use as cement admixture. *Fuel* 89:3042–3050 . doi: 10.1016/j.fuel.2010.05.027
47. Yu Z, Ye G (2012) The pore structure and water permeability of cement paste blended with fly ash over a long period up to one year. *Concr Repair, Rehabil Retrofit III - Proc 3rd Int Conf Concr Repair, Rehabil Retrofit ICCRRR 2012* 296–301
48. Yu Z, Ma J, Ye G, van Breugel K, Shen X (2017) Effect of fly ash on the pore structure of cement paste under a curing period of 3 years. *Constr Build Mater* 144:493–501 . doi: 10.1016/j.conbuildmat.2017.03.182
49. Yu Z, Ye G (2013) The pore structure of cement paste blended with fly ash. *Constr Build Mater* 45:30–35 . doi: 10.1016/j.conbuildmat.2013.04.012

50. Chindaprasirt P, Rukzon S (2009) Pore Structure Changes of Blended Cement Pastes Containing Fly Ash , Rice Husk Ash , and Palm Oil Fuel Ash. *J Mater Civ Eng* 21:666–671 . doi: 10.1061/(ASCE)0899-1561-(2009)21:11(666)
51. Zeng Q, Li K, Fen-chong T, Dangla P (2012) Pore structure characterization of cement pastes blended with high-volume fly-ash. *Cem Concr Res* 42:194–204 . doi: 10.1016/j.cemconres.2011.09.012
52. Chindaprasirt P, Jaturapitakkul C, Sinsiri T (2005) Effect of fly ash fineness on compressive strength and pore size of blended cement paste. *Cem Concr Compos* 27:425–428 . doi: 10.1016/j.cemconcomp.2004.07.003
53. Li X, Dong Y, Yang H (2012) Hydration performance and pore structure of fly ash-cement pastes. 3867–3871. doi:10.4028/www.scientific.net/AMM.204-208.3867
54. Wang A, Zhang C, Sun W (2004) Fly ash effects: III. The microaggregate effect of fly ash. *Cem Concr Res* 34:2061–2066 . doi: 10.1016/j.cemconres.2003.03.002
55. John L.Provis VDJ (2015) Alkali Activated Materials State - of- the- Art Report,RILEM TC224-AAM
56. Hussain S, Bhunia D, Singh SB (2017) Comparative study of accelerated carbonation of plain cement and fly-ash concrete. *J Build Eng* 10:26–31 . doi: 10.1016/j.jobbe.2017.02.001
57. Rao NV, Meena T (2017) A review on carbonation study in concrete. *IOP Conf Ser Mater Sci Eng* 263: . doi: 10.1088/1757-899X/263/3/032011
58. Visser J (2012) Accelerated carbonation testing of mortar with supplementary cementing materials - Limitation of the acceleration due to drying. *Heron* 57:231–247
59. Ashraf W (2016) Carbonation of cement-based materials: Challenges and opportunities. *Constr Build Mater* 120:558–570 . doi: 10.1016/j.conbuildmat.2016.05.080
60. Lye, Chao-qun, Ravindra K. Dhir GSG (2015) Carbonation resistance of fly ash concrete. *Mag. Concr. Res.* 67:1150–1178

61. Papadakis VG (2000) Effect of supplementary cementing materials on concrete resistance against carbonation and chloride ingress. *Cem Concr Res* 30:291–299 . doi: 10.1016/S0008-8846(99)00249-5
62. Ye H, Radlińska A, Neves J (2017) Drying and carbonation shrinkage of cement paste containing alkalis. *Mater Struct Constr* 50: . doi: 10.1617/s11527-017-1006-x
63. Chen JJ, Thomas JJ, Jennings HM (2006) Decalcification shrinkage of cement paste. *Cem Concr Res* 36:801–809 . doi: 10.1016/j.cemconres.2005.11.003
64. Sisomphon K, Franke L (2007) Carbonation rates of concretes containing high volume of pozzolanic materials. *Cem Concr Res* 37:1647–1653 . doi: 10.1016/j.cemconres.2007.08.014
65. Cengiz Duran A (2003) Accelerated carbonation and testing of concrete made with fly ash. *Constr Build Mater* 17:147–152 . doi: 10.1016/S0950-0618(02)00116-2
66. Ramos T, Matos AM, Sousa-Coutinho J (2013) Mortar with wood waste ash: Mechanical strength carbonation resistance and ASR expansion. *Constr Build Mater* 49:343–351 . doi: 10.1016/j.conbuildmat.2013.08.026
67. Cheah CB, Ramli M (2012) Mechanical strength, durability and drying shrinkage of structural mortar containing HCWA as partial replacement of cement. *Constr Build Mater* 30:320–329 . doi: 10.1016/j.conbuildmat.2011.12.009
68. Sudheen Anantharaman (2008) Sulfate And Alkali Silica Resistance Of Class C & F Fly Ash Replaced Blended Cements. Master of Science, Arizona State University
69. Persson B (2003) Sulphate resistance of self-compacting concrete. *Cem Concr Res* 33:1933–1938 . doi: 10.1016/S0008-8846(03)00184-4
70. P. K. Mehta (1986) Effect of Fly Ash Composition on Sulfate Resistance of Cement. *ACI J* 83:994–1000
71. El-Khatib JM (1991) Durability related properties of PFA, slag and silica fume concrete. PhD Thesis, University of Aberdeen ,Department of

## Engineering

72. Dimic,D and Droljc S (1986) The influence of a lite content on the sulphate resistance of portland cement. In: 8th Int.Conf.on the Chemistry of cement. pp 195–199
73. Park YS, Suh JK, Lee JH, Shin YS (1999) Strength deterioration of high strength concrete in sulfate environment. *Cem Concr Res* 29:1397–1402 . doi: 10.1016/S0008-8846(99)00106-4
74. Tikalsky PJ, Carrasquillo RL (1989) The Effect Of Fly ASH On The Sulfate Resisance Of Cncrete.Research Study 3-5/9-87-481,Center for Transportation Research The University of Texas at Austin
75. Wedding P, Dunstan E (1980) A Possible Method for Identifying Fly Ashes That Will Improve the Sulfate Resistance of Concretes. *Cem Concr Aggregates* 2:20–30 . doi: 10.1520/cca10175j
76. E Tkaczewska JM (2009) The sulphate resistance of mortars made with fly ashes from co-burning bituminous coal and biomass. *Silic Ind* 47:163–170
77. Justnes H (1996) A Review of Chloride Binding in Cementitious Systems, Cement and concrete. *Nord Concr Res* 21:1–6
78. Yuan Q, Shi C, De Schutter G, Audenaert K, Deng D (2009) Chloride binding of cement-based materials subjected to external chloride environment - A review. *Constr Build Mater* 23:1–13 . doi: 10.1016/j.conbuildmat.2008.02.004
79. BS EN 14629 (2007) Products and systems for the protection and repair of concrete structures - Test methods - Determination of chloride content in hardened concrete. Br Stand
80. Drilled T, Statements B (2006) Standard Test Method for Acid-Soluble Chloride in Mortar and Concrete 1 ASTM. 15:5–8 . doi: 10.1520/C1152
81. Mangat PS, Ojedokun OO (2019) Bound chloride ingress in alkali activated concrete. *Constr Build Mater* 212:375–387 . doi: 10.1016/j.conbuildmat.2019.03.302
82. Chalee W, Jaturapitakkul C (2009) Effects of W/B ratios and fly ash

- finenesses on chloride diffusion coefficient of concrete in marine environment. *Mater Struct Constr* 42:505–514 . doi: 10.1617/s11527-008-9398-2
83. Cheewaket T, Jaturapitakkul C, Chalee W (2010) Long term performance of chloride binding capacity in fly ash concrete in a marine environment. *Constr Build Mater* 24:1352–1357 . doi: 10.1016/j.conbuildmat.2009.12.039
  84. BS EN 206 (2013) Concrete — Specification , performance , production and conformity. Br Stand
  85. C.Shi, F.He, C.Chen XA (2015) Relationship between water-soluble and free chloride concentrations in cement-based materials. *Mater Res Innov* 19:348–353 . doi: 10.1179/1432891715Z.0000000001700
  86. Haque MN, Kayyali OA (1995) Free and water soluble chloride in concrete. *Cem Concr Res* 25:531–542 . doi: 10.1016/0008-8846(95)00042-B
  87. Glass GK, Buenfeld NR (1995) The Determination of Chloride Binding Relationship. *RILEM Int Work Chloride Penetration into Concr* 3:3–9
  88. Simčič T, Pejovnik S, De Schutter G, Bosiljkov VB (2015) Chloride ion penetration into fly ash modified concrete during wetting-drying cycles. *Constr Build Mater* 93:1216–1223 . doi: 10.1016/j.conbuildmat.2015.04.033
  89. Byung Hwan SJ (2005) Experimental Investigation on the Threshold Chloride Concentration for Corrosion Initiation in Reinforced Concrete Structures. In: 18th International Conference on Structural Mechanics in Reactor Technology (SMiRT 18) Beijing, China, August 7-12, 2005. pp 2389–2396
  90. Arya C, Buenfeld NR, Newman JB (1987) Assessment of Simple Methods of Determining the Free Chloride. *Cem Concr Res* 17:907–918
  91. Pavlík V (2000) Water extraction of chloride, hydroxide and other ions from hardened cement pastes. *Cem Concr Res* 30:895–906 . doi: 10.1016/S0008-8846(00)00261-1
  92. Thomas MDA, Hooton RD, Scott A, Zibara H (2012) The effect of supplementary cementitious materials on chloride binding in hardened cement paste. *Cem Concr Res* 42:1–7 . doi: 10.1016/j.cemconres.2011.01.001

93. Sengul O, Tasdemir C, Tasdemir MA (2005) Mechanical properties and rapid chloride permeability of concretes with ground fly ash. *ACI Mater J* 102:414–421
94. Sujjavanich S, Sida V, Suwanvitaya P (2005) Chloride permeability and corrosion risk of high-volume fly ash concrete with mid-range water reducer. *ACI Mater J* 102:177–182
95. Wang S, Llamazos E, Baxter L, Fonseca F (2008) Durability of biomass fly ash concrete: Freezing and thawing and rapid chloride permeability tests. *Fuel* 87:359–364 . doi: 10.1016/j.fuel.2007.05.027
96. Caijun Shi, Julia A. Stegemann and RJC (1998) Effect of Supplementary Cementing Materials on the Specific Conductivity of Pore Solution and Its Implications on the Rapid Chloride Permeability Test (AASHTO T277 and ASTM C1202) Results. *ACI Mater J* 95:389–394
97. Joshi P and Chan C (2002) Rapid Chloride Permeability Testing. *Concr Constr*.doi: [https://s3.amazonaws.com/academia.edu.documents/34937844/Rapid\\_Chloride\\_Permeability\\_Testing\\_.pdf](https://s3.amazonaws.com/academia.edu.documents/34937844/Rapid_Chloride_Permeability_Testing_.pdf)
98. Poulsen.E (1993) Chloride Profiles — Analysis and Interpretation of Observations. AEC Consult Eng Ltd, Vedbaek Denmark
99. Stanish KD, Hooton RD, Thomas MDA (1997) Testing the Chloride Penetration Resistance of Concrete: A Literature Review. FHWA Contract DTFH61-97-R-00022 31 . doi: <https://rosap.ntl.bts.gov/view/dot/35971>
100. Cement Concrete & Aggregates Australia (2009) Chloride Resistance of Concrete.doi:<https://www.concrete.org/publications/internationalconcreteabstractsportal/m/details/id/51682546>
101. Collepari M, Marcialis A TR (1970) The kinetics of Chloride ions Penetration in Concrete. *II Cem* 67:157–164
102. Mangat PS& M (1994) Prediction of long term chloride concentration in concrete. *Mater Struct* 27:338–346
103. Costa A, Appleton J (1999) Chloride penetration into concrete in marine environment—Part I: Main parameters affecting chloride penetration. *Mater*

Struct 32:252–259 . doi: 10.1007/bf02479594

104. Luping T, Gulikers J (2007) On the mathematics of time-dependent apparent chloride diffusion coefficient in concrete. *Cem Concr Res* 37:589–595 . doi: 10.1016/j.cemconres.2007.01.006
105. Petcherdchoo A (2013) Time dependent models of apparent diffusion coefficient and surface chloride for chloride transport in fly ash concrete. *Constr Build Mater* 38:497–507 . doi: 10.1016/j.conbuildmat.2012.08.041
106. Polder R.P (1997) Chloride diffusion and resistivity testing of five concrete mixes for marine environment. *RILEM Int Work Chloride Penetration into Concr* 225–233
107. Mangat PS, Gurusamy K (1987) Chloride Diffusion in Steel Fiber Reinforced Concrete Containig PFA. *Cem Concr Res* 1987:1–49
108. Chalee W, Ausapanit P, Jaturapitakkul C (2010) Utilization of fly ash concrete in marine environment for long term design life analysis. *Mater Des* 31:1242–1249 . doi: 10.1016/j.matdes.2009.09.024
109. Thomas MDA, Matthews JD (2004) Performance of pfa concrete in a marine environment - 10-year results. *Cem Concr Compos* 26:5–20 . doi: 10.1016/S0958-9465(02)00117-8
110. Zang T, Gjørsv O (1994) An electrochemical method for accelerated testing of chloride diffusivity in concrete. *Cem Concr Res* 24:1534–1548
111. Mangat PS, Limbachiya MC (1999) Effect of initial curing on chloride diffusion in concrete repair materials. *Cem Concr Res* 29:1475–1485 . doi: 10.1016/S0008-8846(99)00130-1
112. Rajabipour F, Giannini E, Dunant C, Ideker JH, Thomas MDA (2015) Alkali-silica reaction: Current understanding of the reaction mechanisms and the knowledge gaps. *Cem Concr Res* 76:130–146 . doi: 10.1016/j.cemconres.2015.05.024
113. Lindgård J, Andiç-çak Ö, Fernandes I, Rønning TF, Thomas MDA (2012) Alkali – silica reactions ( ASR ): Literature review on parameters influencing laboratory performance testing. *Cem Concr Res* 42:223–243 . doi:

10.1016/j.cemconres.2011.10.004

114. Xu GJZ, Watt DF, Hudec PP (1995) Effectiveness of mineral admixtures in reducing ASR expansion. *Cem Concr Res* 25:1225–1236 . doi: 10.1016/0008-8846(95)00115-S
115. Stanton TE (1940) Influence of Cement and Aggregate on Concrete Expansion. *Eng News-Record* 124:171–173
116. Fernandes I, Broekmans MATM (2013) Alkali-Silica Reactions: An Overview. Part I. *Metallogr Microstruct Anal* 2:257–267 . doi: 10.1007/s13632-013-0085-5
117. Leemann A, Lothenbach B (2008) The influence of potassium-sodium ratio in cement on concrete expansion due to alkali-aggregate reaction. *Cem Concr Res* 38:1162–1168 . doi: 10.1016/j.cemconres.2008.05.004
118. Glasser FP (1992) “Chemistry of the alkali-aggregate reaction” in: Swamy R.N. (Ed.), *The Alkali-Silica Reaction in Concrete*. Blackie, London, p 96–121.
119. Shehata MH, Thomas MDA (2006) Alkali release characteristics of blended cements. *Cem Concr Res* 36:1166–1175 . doi: 10.1016/j.cemconres.2006.02.015
120. ASTM Committee (2014) ASTM C1260-14 Standard Test Method for Potential Alkali Reactivity of Aggregates ( Mortar-Bar Method). *Annu B ASTM Stand Vol 0402* 1–5 . doi: 10.1520/C1260-14.2
121. ASTM Committee (2015) ASTM C 1290-15 Standard Test Method for Determination of Length Change of Concrete Due to Alkali-Silica Reaction. *ASTM Stand* 1–7 . doi: 10.1520/C1293-08BR15.2
122. Thomas M.D.A, Innis FA (1999) Use of the accelerated mortar bar test for evaluating the efficacy of mineral admixtures for controlling expansion due to alkali-silica reaction. *Cem Concr Aggregates* 21:157–164 . doi: 10.1520/cca10429j
123. Thomas M.D.A (1996) Review of the effect of fly ash and slag on alkali - aggregate reaction in concrete. *Building Research Establishment Report*, 61

BR314, Construction Research Communication, Watford, UK

124. Thomas M.D.A (1996) Field studies of fly ash concrete structures contain ing reactive aggregates. *Mag Concr Res* 48:265–279
125. Thomas M.D.A (2011) The effect of supplementary cementing materials on alkali-silica reaction: A review. *Cem Concr Res* 41:1224–1231 . doi: 10.1016/j.cemconres.2010.11.003
126. Shayan A, Diggins R, Ivanusec I (1996) Effectiveness of fly ash in preventing deleterious expansion due to alkali-aggregate reaction in normal and steam-cured concrete. *Cem Concr Res* 26:153–164 . doi: 10.1016/0008-8846(95)00191-3
127. Shafaatian SMH, Akhavan A, Maraghechi H, Rajabipour F (2013) How does fly ash mitigate alkali – silica reaction ( ASR ) in accelerated mortar bar test. *Cem Concr Compos* 37:143–153 . doi: 10.1016/j.cemconcomp.2012.11.004
128. Duchesne J, Bérubé MA (1994) The effectiveness of supplementary cementing materials in suppressing expansion due to ASR: Another look at the reaction mechanisms part 2: Pore solution chemistry. *Cem Concr Res* 24:221–230 . doi: 10.1016/0008-8846(94)90047-7
129. Bleszynski RF, Thomas MDA, Ash F (1998) Microstructural Studies of Alkali-Silica Reaction in Fly Ash Concrete Immersed in Alkaline Solutions. *Adv Cem Based Mater* 7:66–78
130. Shehata MH, Thomas MDA (2000) Effect of fly ash composition on the expansion of concrete due to alkali-silica reaction. *Cem Concr Res* 30:1063–1072 . doi: 10.1016/S0008-8846(00)00283-0
131. Glasser F.P. MJ (1985) The alkali binding potential of OPC and blended cements. *Cemento* 82:85–94
132. ASTM Committee (2017) ASTM C1567-13 Standard Test Method for Determining the Potential Alkali-Silica Reactivity of Combinations of Cementitious Materials and Aggregate ( Accelerated Mortar-Bar Method ) 1. 1–6 . doi: 10.1520/C1567-13.2
133. Wang S, Baxter L (2007) Comprehensive study of biomass fly ash in

concrete : Strength , microscopy , kinetics and durability. *Fuel Process Technol* 88:1165–1170 . doi: 10.1016/j.fuproc.2007.06.016

134. Matos AM, Sousa-Coutinho J (2016) ASR and sulphate performance of mortar containing industrial waste. *Struct Concr* 17:84–95 . doi: 10.1002/suco.201400095
135. Esteves TC, Rajamma R, Soares D, Silva AS, Ferreira VM, Labrincha JA (2011) Use of biomass fly ash for mitigation of alkali-silica reaction of cement mortars. *Constr Build Mater* 1–7 . doi: 10.1016/j.conbuildmat.2011.06.075

# **CHAPTER 3 CHARACTERIZATION OF BIOMASS FLY ASHES**

## **3.1. Introduction**

Proper characterization of each fly ash before employing it to partially replace cement in concrete is necessary to assess its suitability as a supplementary cementitious material (SSMs). Each fly ash used in this study was characterized in terms of chemical, mineralogical and physical properties by using different testing techniques. Three types of fly ash, depending on the combustion technology used in the power plants, were used in this investigation. An enhanced pozzolanic biomass ash identified as (EBA) generated in Drax power station, Yorkshire, by burning 30 tonnes of wood pellets with 5 tonnes of coal fly ash by proportion. Coal fly ash was added to the wood before combustion to prevent the reaction of potassium with chloride and sulphur to form several potassium compounds. Potassium has the ability of binding with alumina and silicate phases of coal fly ash and becomes part of the glass phase. Combustion of wood pellets usually produces low ash content of around 1-2%. Thus, 30 tonnes of wood pellets produce 0.6 tonnes of biomass fly ash which combines with 5 tonnes of coal fly ash used in the combustion process. The second type of fly ash used in this project was wood biomass ash identified as (WBA) generated in Lynemouth power station by burning only pure virgin wood pellets. The third material was standard class F coal fly ash identified as (CFA) conforming to EN450, which is commonly used in concrete production. All materials were supplied in 25 Kg drums, the EBA and CFA were supplied by Power Minerals Ltd while WBA was supplied directly from Lynemouth power station.

## **3.2. Experimental Techniques**

### **3.2.1. Chemical Characterization**

X-ray Fluorescence (XRF) technique was used to determine the chemical composition of the three types of fly ash by using Philips PW2400 XRF

spectrometer. The sample was irradiated by an X- ray beam and the elements present were identified by the energies of the emitted X- rays. Then, the intensity of X- rays was used to determine the concentration of each element. The loss of ignition (LOI), which is a measure of the amount of unburnt carbon in fly ash, was also determined by heating the samples up to 950°C during the analysis process. The weight loss of the sample after heating is considered as loss of ignition, which is expressed as a percentage of the original sample weight before heating.

### **3.2.2. Mineralogical Characterization**

The mineralogical composition of the fly ash samples was determined by X-ray Diffraction (XRD) analysis. A Philips X- Pert diffractometer with a Cu K $\alpha$  radiation source (40 KV, 40 mA and wavelength  $\lambda=0.1540$  nm) was used. Each sample was loaded into a separate XRD flat plate sample holder for a 30 minutes scan between (10°C - 80°C) and the data were collected over an angle  $2\theta$  . An internal standard method based on the addition of a known amount of standard silicon (10%) was employed to quantify the amorphous content of the sample [1].

### **3.2.3. Physical Characterization**

#### **3.2.3.1. Particle Size Distribution**

The ash particle size distribution (PSD) was measured using the laser diffraction technique. The Malvern Mastersizer 3000 analyser shown Figure 3.1 was used with dry dispersion laser diffraction. The detecting diffraction of the device covers a size range from 40 nm to 2000  $\mu\text{m}$ . The measurement uses a laser beam passing through the dispersed particulate sample and the angular variation in the intensity of the scattered light is measured. The basic principle of this method is that the large particles scatter light at small angles while small particles scatter light at large angles. The angular scattering intensity data is then analysed by applying Mie theory to calculate the size of the particles.



**Figure 3.1 Malvern Mastersizer 3000 analyser**

### **3.2.3.2. Specific Surface Area**

The specific surface area of both ashes was measured based on BET (Stephen Brunauer, P.H. Emmett and Edward Teller) method [2]. A probing gas that does not chemically react with the material, such as Nitrogen, is used in this method to determine the surface area based on the amount of gas adsorbed by the sample at a known pressure. The software is programmed to measure the specific surface area based on the pressure differences. BET theory relies on some assumptions such as the gas molecules behave ideally and the surface is homogeneous as well as all its sites are equal. Figure 3.2 shows the Micromeritics ASAP 2020 M volumetric adsorption analyser which was used in this study.

### **3.2.3.3. Morphology**

Gold-sputtered ash samples were prepared and examined in a Nova- Nano 200 SEM (Scanning Electron Microscope) at varying magnifications under accelerating voltage of 5 kV. The sample was first attached to aluminium stubs and a layer of gold was applied for 90 seconds. The sample was then transferred to the SEM device and exposed to an electron beam inside. The electrons generate signals which reveal

information about the sample's morphology. Figure 3.3 shows Nova- Nano 200 SEM which was used in this study.



**Figure 3.2 Micromeritics ASAP 2020 volumetric adsorption BET analyser.**



**Figure 3.3 Nova- Nano 200 SEM analyser**

#### 3.2.3.4. Pozzolanic Activity Index (PAI)

Various test methods have been reported in the literature to assess the pozzolanic activity of fly ash in mortar and concrete. Direct methods measure the amount of  $\text{Ca}(\text{OH})_2$  by using X-ray diffraction (XRD) and thermo-gravimetric analyses (TGA) while indirect methods measure the influence of the pozzolanic behaviour on some physical properties such as compressive strength and electrical conductivity [3]. In this study, pozzolanic behaviour was tested by measuring the pozzolanic activity index (PAI) in accordance with BS EN 450-1 [4]. PAI is a physical method used to measure the reactivity of pozzolanic materials, which involves measuring the 28, 90 days compressive strength of fly ash cement mortar relative to control 100% OPC mortar. The control OPC mortar was prepared by mixing 1350 g sand, 450 g Portland cement and 225 g water. The blended fly ash mortars were prepared in the same manner except that 25% by weight of the Portland cement was replaced with fly ash and the quantity of water was altered to give the same workability (flow) value as the control mortar ( $\pm 10\text{mm}$ ).

Cement and fly ash binders were mixed by hand until homogeneity was achieved. The binder was then placed into the bowl of a Hobart mixer and water was added carefully within 10 seconds. Immediately the mixing was started at low speed for 30 seconds. Then, the sand was added gradually during the following 30 seconds while mixing continued. The mixer was switched to high speed for an additional 60 seconds. After about 2 minutes, the mixing was stopped and the mix was briefly mixed by hand to remove accumulated materials from the paddle and the base of the bowl. This was followed by mixing at high speed for 60 seconds. The flow tests were conducted according to EN 1015-3 standard [5]. A detailed procedure of the flow test is given in chapter 4 (section 4.3.1.2).

The mortar samples were then cast in 40 x 40 x 160 mm prism moulds in the laboratory environment (20°C, 60% RH), demoulded after 24 h and cured in water at 20°C until the age of testing. The prisms were first tested under three-point bending, then each part was tested under compression (equivalent cube) according to BS EN 196-1 standard [6] as shown in Figure 3.4. Three samples were tested at each age

and their average was determined. The pozzolanic activity index (PAI) was calculated as follows:

$$PAI = \left(\frac{A}{B}\right) * 100 \quad \% \quad 3.1$$

Where: A is the average compressive strength of blended fly ash-cement mortar (MPa) and B is the average strength of the control OPC mortar (MPa) at the same age.

According to the standard, the tested material is considered as pozzolanic (reactive) if the activity index is higher than 75 % at 28 days and 85 % at 90 days.

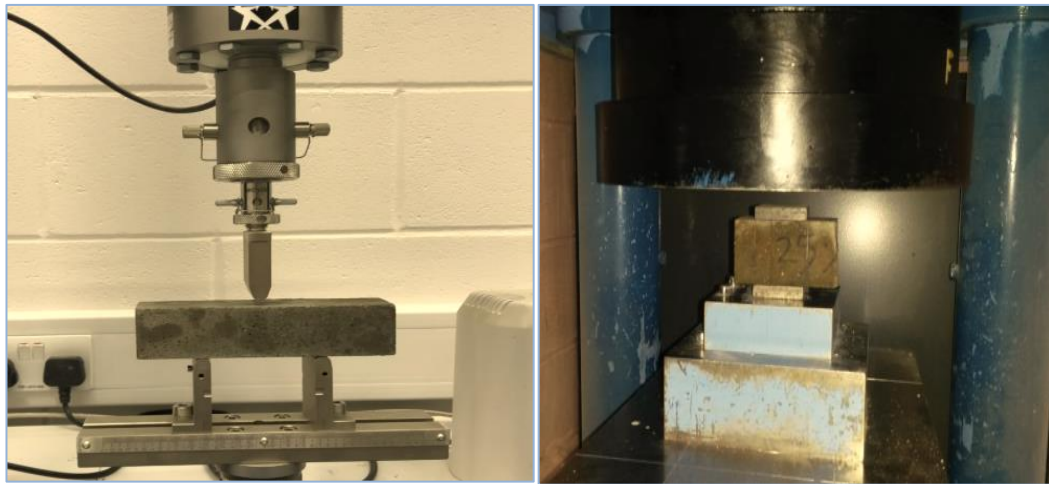


**Figure 3.4 Three-point bending and equivalent cube compressive strength tests**

### **3.3. Results and Discussion**

#### **3.3.1. Chemical Characterization**

The major chemical elements of the ashes obtained by XRF analysis are presented in Table 3.1. Considering that no specific standard covers biomass fly ash, its properties were compared with the requirements for coal fly ash as specified in BS EN 450-1 [4] and ASTM C618-12 [7]. Table 3.1 shows that both EBA and CFA comprise of silica ( $\text{SiO}_2$ ) and alumina ( $\text{Al}_2\text{O}_3$ ) which are the important components in the cementitious and pozzolanic reactions. The CFA contains higher amounts of silicon dioxide ( $\text{SiO}_2$ ), aluminium oxide ( $\text{Al}_2\text{O}_3$ ) and iron oxide ( $\text{Fe}_2\text{O}_3$ ) compared to

EBA which might result in better pozzolanic and mechanical properties of CFA whereas EBA is much richer in calcium oxide (CaO), alkali sodium and potassium oxides (Na<sub>2</sub>O, K<sub>2</sub>O). Both ashes have a total content of main oxides (SiO<sub>2</sub> + Al<sub>2</sub>O<sub>3</sub> + Fe<sub>2</sub>O<sub>3</sub>) greater than 70% and total calcium content, represented by calcium oxide (CaO), lower than 10%. Thus, both ashes meet the requirement of main oxides with 73.04% and 81.35% for EBA and CFA respectively and the total calcium content requirement with 8.10% and 3.10% for EBA and CFA respectively. Therefore, both would be classified as Class F according to ASTM C618-12 based on their chemical compositions.

Calcium oxide (CaO) is the main component in WBA (Table 3.1), which accounts for 25.4% of the ash mass whereas the main oxides SiO<sub>2</sub>, Al<sub>2</sub>O<sub>3</sub> and Fe<sub>2</sub>O<sub>3</sub> are present in lower quantities than EBA and CFA. The total content of the main oxides (SiO<sub>2</sub>=12.5%), aluminium oxide (Al<sub>2</sub>O<sub>3</sub>= 2.55%) and iron oxide (Fe<sub>2</sub>O<sub>3</sub> = 1.71%) is 16.76%. This is less than the minimum limits of 50% and 70% prescribed for pozzolanic ashes by ASTM C618-12 and BS EN450 -1 respectively. In addition, the chemical composition of WBA indicates very high LOI (42.48%) which is more than the limit of 6% required for ASTM C618-12 and 9% required for BS EN 450 -1. LOI is a very important factor for determining the quality of fly ash for use in concrete as it represents residual carbon material that may have negative impact on air-entrained concrete and loss of strength due to higher water demand [8].

The alkali content (expressed as total alkali equivalent = Na<sub>2</sub>O + 0.66 K<sub>2</sub>O), is below the acceptable limit of BS EN 450-1 (≤ 5% by mass) with 4.23% and 2.24% for EBA and CFA respectively while it is above the limit in WBA with 6.49%. The high alkali content of both biomass ashes (EBA and WBA) increases their risk of alkali-silica reaction. The other chemical components of all ashes met the BS EN 450-1 requirements of SO<sub>3</sub> < 3%, MgO < 4%, P<sub>2</sub>O<sub>5</sub> < 5%. Generally, the silica and alumina content of wood biomass fly ashes is lower than coal fly ash whereas they contain abundant potassium as the most volatile element in raw biomass [9–12].

**Table 3.1 The chemical analyses of CFA, EBA and WBA fly ashes**

Element	EBA(wt. %)	WBA (wt. %)	CFA (wt. %)
SiO <sub>2</sub>	41.46	12.5	47.64
Al <sub>2</sub> O <sub>3</sub>	23.49	2.55	25.32
Fe <sub>2</sub> O <sub>3</sub>	8.10	1.71	8.39
MgO	2.27	2.66	2.11
SO <sub>3</sub>	0.17	0.12	-
TiO <sub>2</sub>	1.48	-	0.57
C <sub>a</sub> O	8.10	25.4	3.10
K <sub>2</sub> O	5.57	8.81	3.16
P <sub>2</sub> O <sub>5</sub>	0.75	1.52	0.22
Na <sub>2</sub> O	0.56	0.68	0.16
MnO	0.46	1.25	-
ZnO	0.12	0.098	-
SrO	0.25	0.067	0.11
BaO	0.21	-	0.36
LOI	8.91	42.48	7.0

A wide variation in the chemical composition of biomass fly ashes has been reported in the literature which makes their categorization very difficult. Therefore, it is very important to know the source and the burning conditions of biomass fly ash in order to characterize these parameters and identify their category.

### 3.3.2. Mineralogical Characterization

The importance of XRD patterns is to give an indication of the reactivity of fly ash by determining its amorphous content. The initial XRD patterns on all samples had relatively weak peaks and high backgrounds; this suggests a high amorphous (non-crystalline) component in the samples. Therefore, the samples were put back on the X'Pert XRD machine overnight and the test was rerun with 10% standard silicon added to do longer scans. It was possible to determine the percentage of amorphous content in these samples by including a known amount of standard silicon (Standard Addition technique to determine the amorphous content) [1]. XRD results indicate that the mineralogical structure of all ashes is mainly amorphous with the presence

of some crystalline phases. The amorphous content is 88 %, 84 % and 80 % for CFA, EBA and WBA respectively. Qualitative XRD analyses determined the main crystalline phases for all ashes. The XRD patterns of EBA ash given in Figure 3.5 show the presence of quartz ( $\text{SiO}_2$ ), lime ( $\text{CaO}$ ) and hematite ( $\text{Fe}_2\text{O}_3$ ) as the major crystalline mineral components. The main phases identified for CFA, were quartz ( $\text{SiO}_2$ ) and mullite ( $\text{Al}_2\text{O}_3\cdot\text{SiO}_2$ ) as shown in Figure 3.6. These minerals are usually present in class F fly ashes as reported in the literature [9, 10, 13]. The result of the mineralogical analyses of WBA is presented in Figure 3.7. Quartz ( $\text{SiO}_2$ ), Arcanite ( $\text{K}_2\text{SO}_4$ ) and dicalcium silicate ( $\text{Ca}_2\text{SiO}_4$ ) are the main crystalline phases. In addition, small peaks of calcite ( $\text{CaCO}_3$ ) were also detected.

The reactive component of fly ash is related to the non-crystalline (amorphous) phase. Therefore, all fly ashes, EBA, WBA and CFA can be considered reactive as they consisted of 84 %, 80 % and 88% amorphous phases respectively.

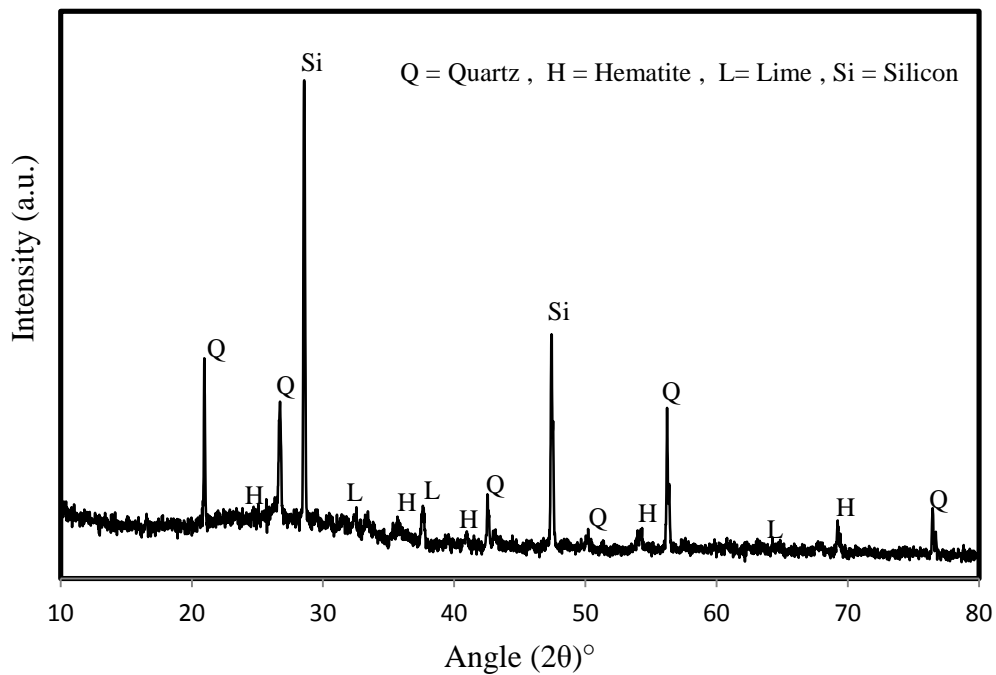


**Figure 3.5 XRD patterns of EBA**

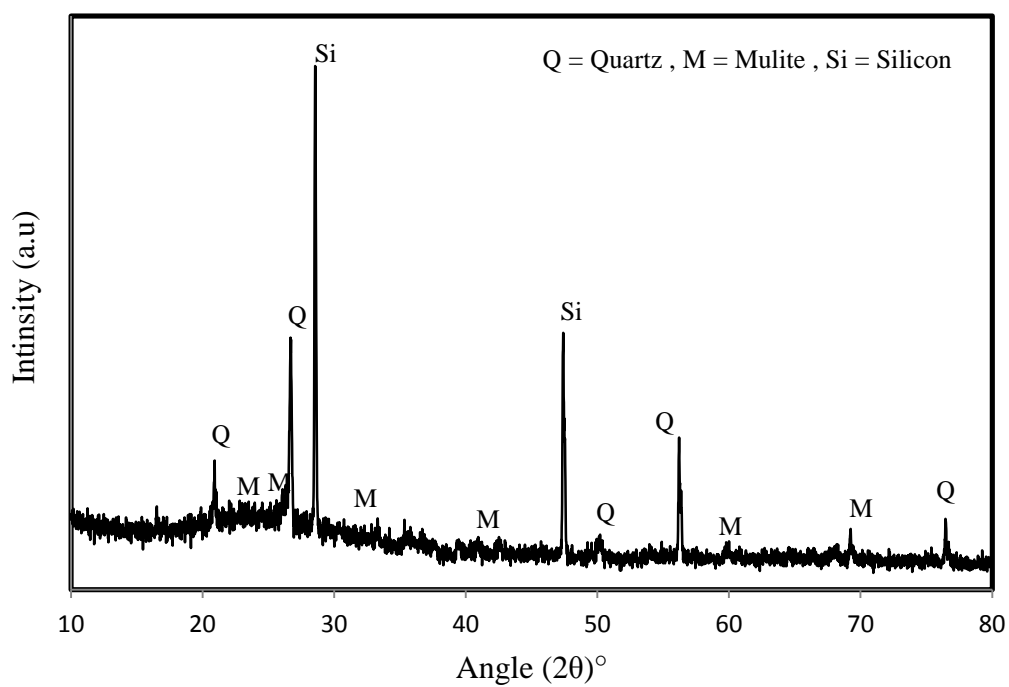


Figure 3.6 XRD patterns of CFA

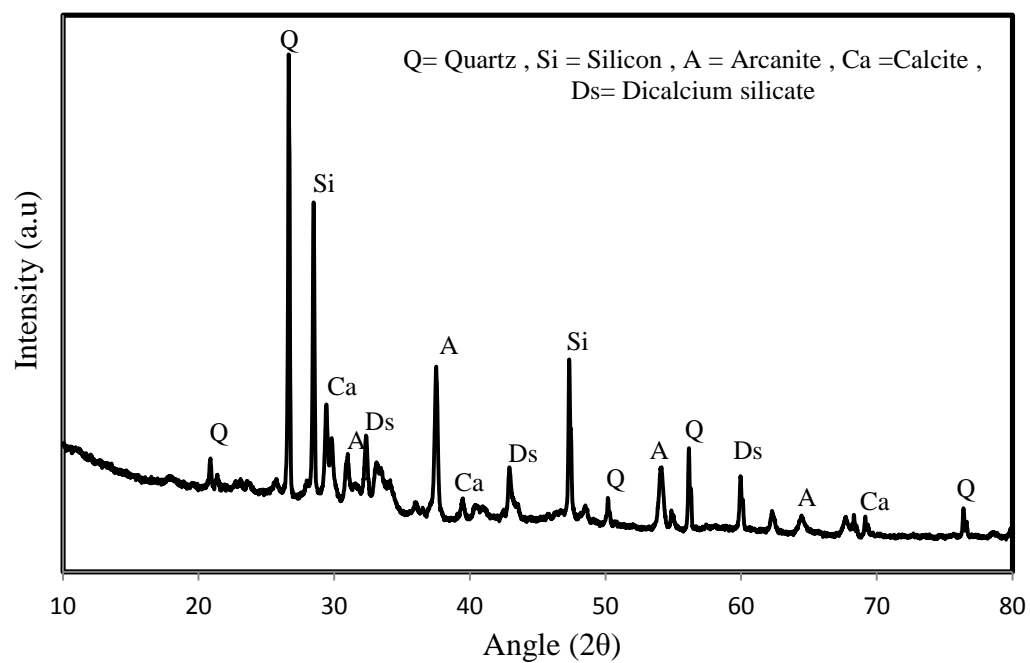


Figure 3.7 XRD patterns of WBA

### 3.3.3. Physical Characterization

#### 3.3.3.1. Particle Size Distribution

The particle size distribution (PSD) of all ashes as determined by laser diffraction is shown in Figure 3.8. The cumulative size distribution calculated at 10% ( $d_{10}$ ), 90% ( $d_{90}$ ) and the median size of the curve 50 % ( $d_{50}$ ) are summarized in Table 3.2.

**Table 3.2 Particle size distribution by laser diffraction**

Sample	Particle Size Distribution		
	Median ( $d_{50}$ ) $\mu\text{m}$	( $d_{10}$ ) $\mu\text{m}$	( $d_{90}$ ) $\mu\text{m}$
CFA	17.3	2.46	148
EBA	49.7	6.43	246
WBA (Sieved by 500 $\mu\text{m}$ sieve)	68.9	6.25	308
WBA (Un-Sieved)	86.4	8.6	516

About 90% of EBA exhibits a grain size smaller than 246  $\mu\text{m}$  whereas 90% of WBA particles are less than 516  $\mu\text{m}$  before sieving and 308  $\mu\text{m}$  after sieving.

The analyses revealed that both biomass ash particles are coarser than coal fly ash particles. The median diameter ( $d_{50}$ ) is 17.3  $\mu\text{m}$ , 49.7  $\mu\text{m}$  and 86.4  $\mu\text{m}$  for CFA, EBA and Un-Sieved WBA respectively. The maximum particle size is around 760  $\mu\text{m}$  for EBA ash and about 350  $\mu\text{m}$  for CFA while it exceeds 1 mm (1000  $\mu\text{m}$ ) in un-sieved WBA. The particle size distribution of both biomass ashes EBA and WBA is unimodal and the most numerous ranges are around 100  $\mu\text{m}$  whereas CFA distribution is triple modal. The biggest first mode is located at 5  $\mu\text{m}$ , whereas the second and third modes are at 28 and 140  $\mu\text{m}$  respectively.

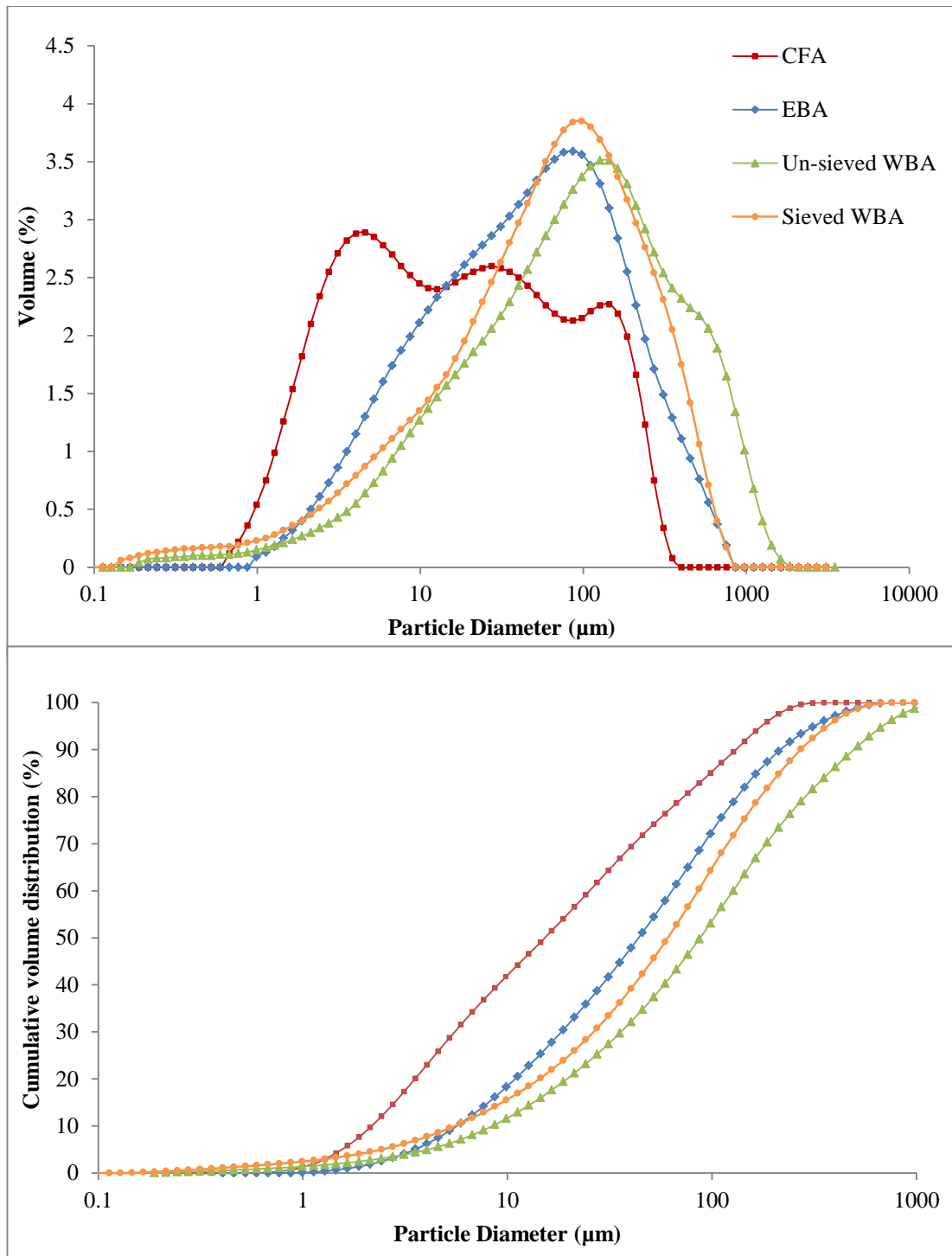


**Figure 3.8 Particle size distribution (PSD) of EBA, CFA and WBA**

Based on physical observation and as shown in Figure 3.9, large particles of size exceeding 1mm unburned wood were observed in WBA which might not be detected by laser diffraction as the detecting diffraction of the device only covers a size range

from 40 nm to 2000  $\mu\text{m}$ . Therefore, the particle size distribution of WBA was also determined by manual sieving and is presented in Figure 3.10.



**Figure 3.9 Manual sieve analyses of WBA**

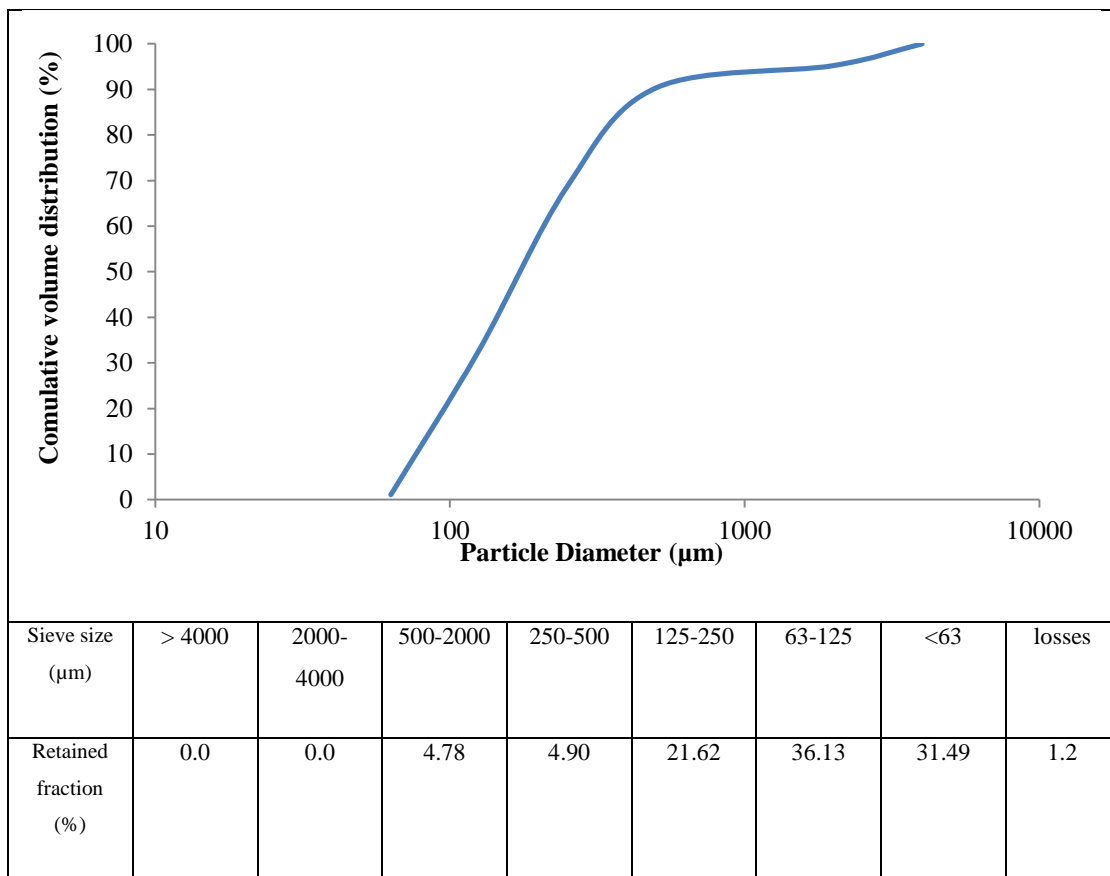


**Figure 3.10 Particle size distribution of WBA by manual sieving**

After sieving, the material retained on 500 $\mu\text{m}$  sieve was rejected and the particle size distribution for the finer WBA which passed through 500  $\mu\text{m}$  sieve was determined by laser diffraction. Table 3.2 and Figure 3.8 show the differences between un-sieved and sieved samples. The median diameter ( $d_{50}$ ) reduced from 516  $\mu\text{m}$  to 308  $\mu\text{m}$  after sieving. However, WBA particles are still the coarser between all ashes (CFA and EBA).

### 3.3.3.2. Specific Surface Area (SSA)

Table 3.3 shows the specific surface areas of all ashes as determined by nitrogen adsorption using BET method. The WBA has higher surface area than both EBA and CFA. This can be due to the irregular and porous nature of the biomass fly ash particles which contribute to the overall higher specific surface area [14, 15] especially when the quantity of unburnt material is relatively high as in the case of WBA. The fineness of the ash particles and their irregular shapes play a significant role in the surface area.

**Table 3.3 Specific surface area of fly ashes**

Sample	Specific surface area ( $\text{m}^2/\text{g}$ )
CFA	$3.06 \pm 0.02$
EBA	$6.38 \pm 0.05$
WBA (Sieved)	$61.7 \pm 0.04$
WBA (Un-sieved)	$77.9 \pm 0.07$

### 3.3.3.3. Morphology

Figure 3.11 shows that the colour of both biomass ashes is significantly different from coal fly ash. WBA is black and EBA is dark grey while CFA ash is medium grey. It has been reported that the fly ash colour depends on the content of unburnt carbon and some chemical elements such as lime and iron [15]. However, the difference in colour of the investigated biomass and coal fly ashes can alternatively

be attributed to the content of unburnt carbon as the burning technology and temperature used for the three ashes are different. The lime (CaO) content which provides a lighter colour is much greater in the biomass ashes but their colour is dominated by the unburnt carbon content as the LOI in both biomass ashes is higher than CFA especially in WBA (LOI = 42.48 %).



**Figure 3.11 The appearance of EBA, WBA and CFA**

Figures 3.12 to 3.14 show SEM images at different magnifications for CFA, EBA and WBA respectively. Figures 3.12 and 3.13 reveal that the particles of both CFA and EBA are mainly spherical which is the typical morphology of coal fly ash. However, a small portion of unburnt or partially burnt wood was observed in EBA sample. Long, fibrous, irregular in shape and size and agglomerated fused woody particles were observed in WBA (Figure 3.14). This indicates that the raw biomass used to produce WBA was not fully combusted. These agglomerates are the result of the ash-forming process in the boiler due to the presence of potassium.

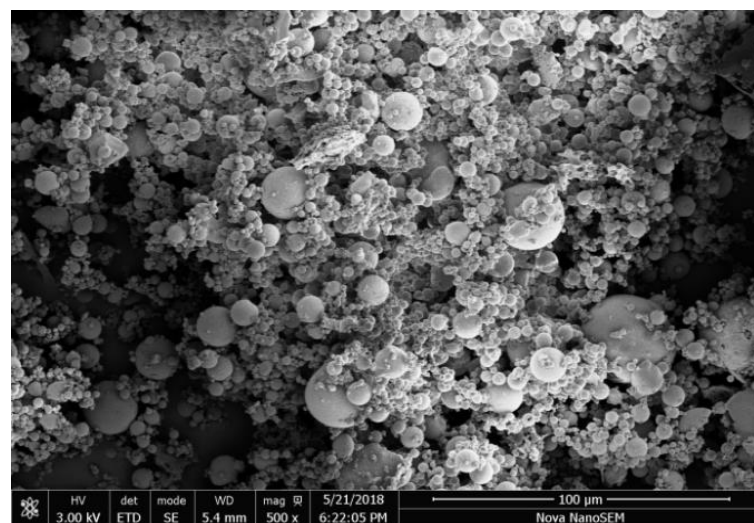
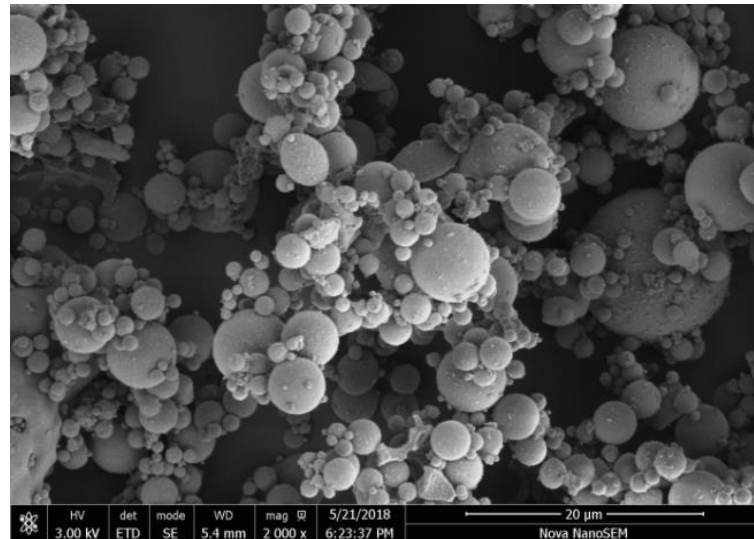


**Figure 3.12 SEM images of CFA**

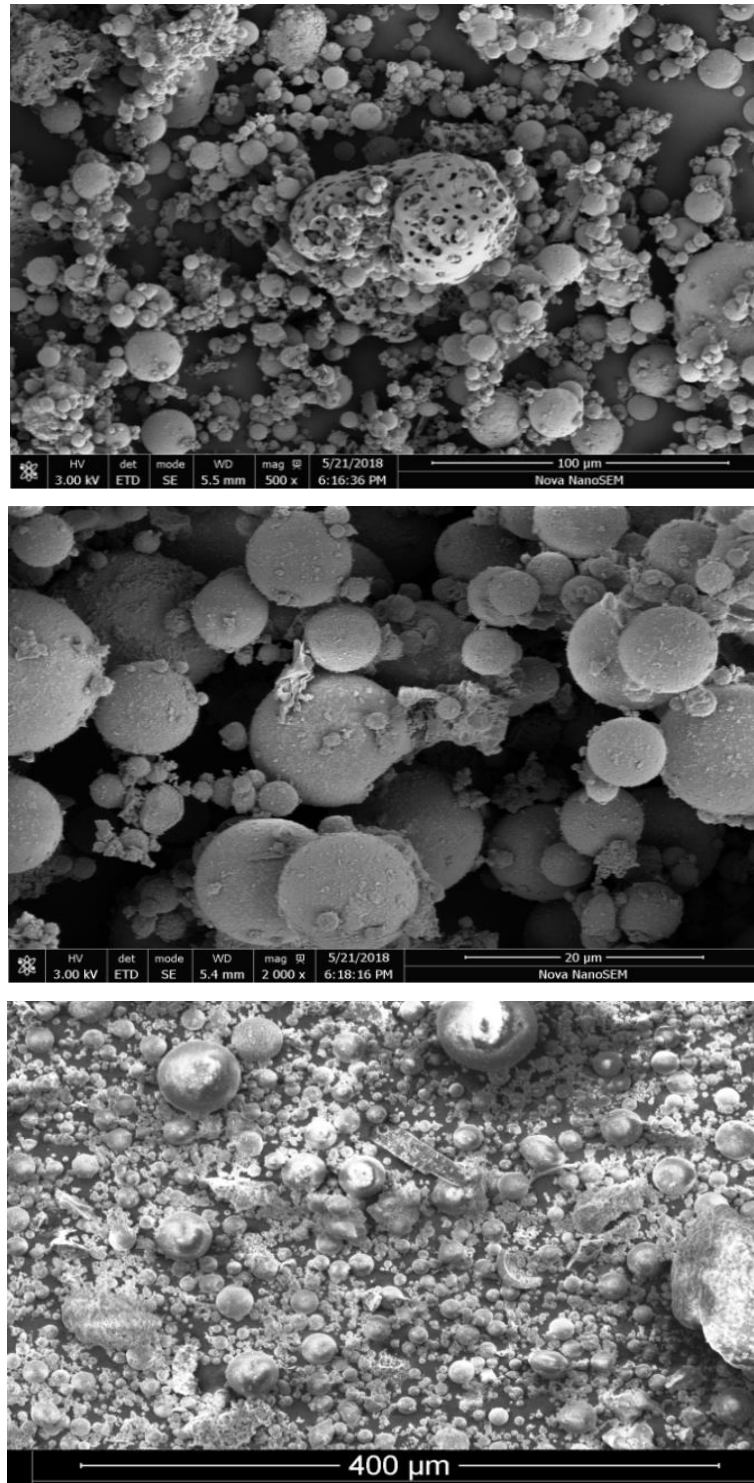
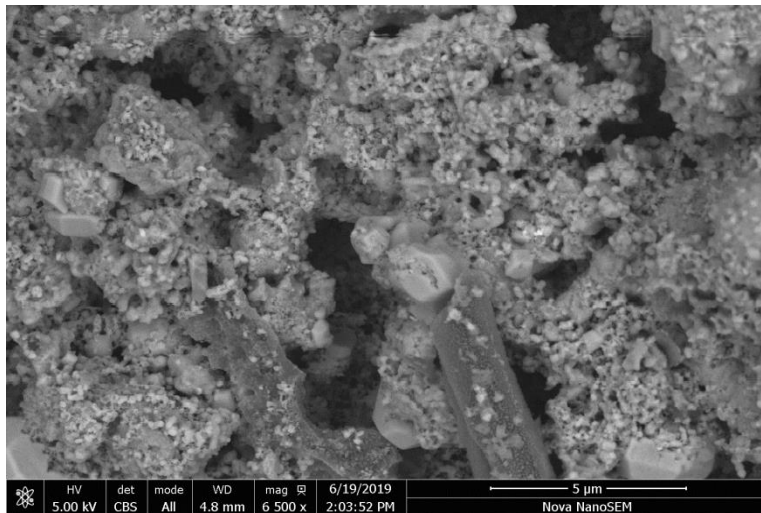
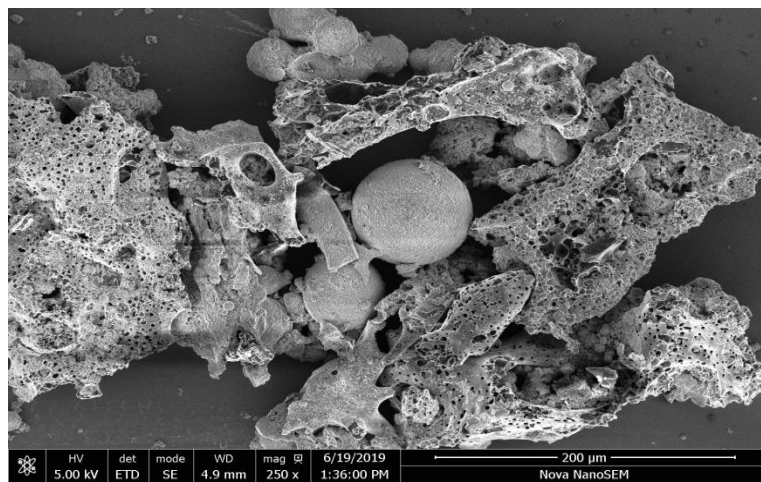
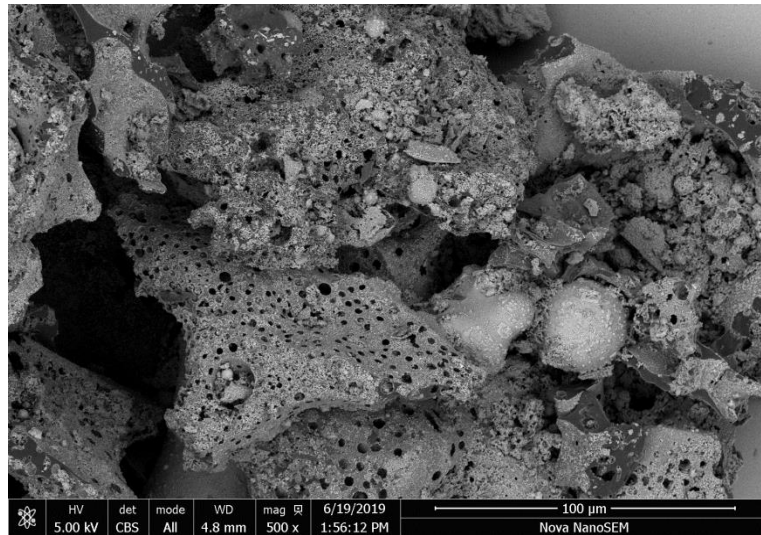


Figure 3.13 SEM images of EBA



**Figure 3.14 SEM images of WBA**

### 3.3.3.4. Pozzolanic Activity Index

The compressive strength and pozzolanic activity index (PAI) of all blended ash cement mortars are presented in Table 3.4. CFA shows considerably higher PAI than EBA and WBA. At 28 days, the PAI for CFA, EBA and WBA is 99%, 85% and 67% of the control OPC mortar respectively whereas it is 109%, 95.3% and 76.7% at 90 days.

The superior strength of CFA compared to EBA and WBA could be attributed to the combined effect of its finer particle size, higher amorphous content and higher content of silica and alumina which are the important components in the cementitious and pozzolanic reactions. Analyses of literature data indicate that the pozzolanic activity of fly ash is influenced by factors such as chemical, mineralogical compositions, particle size distribution and specific surface area, however, the strength development is strongly affected by the fineness of fly ash [16, 17]. Tkaczewska [18] investigated the effect of fly ash fineness on the hydration and properties of cement. The results confirmed that finer fly ash fractions have higher pozzolanic activity.

**Table 3.4 Compressive strength and pozzolanic activity index**

Sample	28-days compressive strength (MPa)	Activity Index at 28-days %	90-days compressive strength (MPa)	Activity Index at 90-days %
OPC	37.18	100%	40.64	100 %
25% EBA	31.67	85%	38.75	95.3 %
20% WBA	24.83	67%	31.2	76.7%
25% CFA	36.9	99%	44.7	109 %

According to BS EN 450-1 standard, both CFA and EBA satisfied the strength activity requirements since their activity index at 28 and 90 days is greater than 75% and 85% respectively while WBA failed to meet the required limit. Therefore, EBA can be suitable as supplementary cementitious material as its activity index is within

the required limits whereas WBA might be used either at lower level of cement replacement or in applications where high strength is not required. However, research on the durability properties of EBA and WBA based concrete is needed to determine their suitability for use in concrete.

### **3.4. Conclusions**

The chemical and mineralogical characteristics of both biomass fly ashes (EBA and WBA) were investigated. The physical properties of particle size distribution, specific surface area, morphology and strength activity index were also investigated relative to coal fly ash (CFA). The analyses and experimental results give the following conclusions:

1. The enhanced biomass ash (EBA) has a composition more similar to coal fly ash (CFA) than wood biomass ash (WBA). Both EBA and CFA are mainly composed of  $\text{SiO}_2$  and  $\text{Al}_2\text{O}_3$  and the content of the total oxide of ( $\text{SiO}_2 + \text{Al}_2\text{O}_3 + \text{Fe}_2\text{O}_3$ ) is more than 70%. This value is suitable for pozzolanic materials which are used in cement production. In contrast, the chemical composition of WBA indicates very high LOI, high alkali content and low  $\text{SiO}_2$  and  $\text{Al}_2\text{O}_3$  content resulting in oxide content of 16.76% which is below the acceptable limits for pozzolanic ash.
2. Both EBA and CFA are a low calcium fly ashes class F according to ASTM C618-12. In addition, both ashes satisfy the BS EN 450-1 requirements for the main oxides and other chemical components of  $\text{SO}_3 < 3\%$ ,  $\text{MgO} < 4\%$  and  $\text{P}_2\text{O}_5 < 5\%$ .
3. The virgin wood biomass ash (WBA) has high alkali content, LOI and low calcium and alumina content, thus it does not satisfy the ASTM C618-12 and BS EN 450-1 requirements.
4. The mineralogical structure of the three ashes is mainly amorphous with the presence of quartz, calcite and hematite as crystalline phases in EBA. The main crystalline phases in CFA are quartz and mullite whereas they are Quartz, Arcanite and di-calcium silicate in WBA.

5. CFA has finer particles with a median diameter of 17.3  $\mu\text{m}$  compared to 49.7  $\mu\text{m}$  and 86.4  $\mu\text{m}$  in EBA and WBA respectively.
6. WBA has a higher surface area than both EBA and CFA. This is correlated to higher carbon contents due to the high internal porosity of unburned carbon.
7. Both CFA and EBA particles are mainly spherical which is the typical morphology of coal fly ash whereas the morphology of WBA particles is different as evidenced by the presence of Long, fibrous irregular in shape and size which indicates that the raw wood biomass was not fully combusted.
8. Both EBA and CFA ashes satisfy the strength activity requirements of ASTM C618-12 and BS EN 450-1 since their pozzolanic activity index (PAI) at 28 and 90 days is greater than 75 % and 85 % respectively whereas WBA failed to meet the requirements of these standards.

### 3.5. References

1. Snellings R, Machiels L, Mertens G, Elsen J (2010) Rietveld refinement strategy for quantitative phase analysis of partially amorphous zeolitized tuffaceous rocks. *Geol Belgica* 13:183–196
2. Brame J, Griggs C (2016) Surface Area Analysis Using the Brunauer-Emmett-Teller (BET) Method. *Scient. Eng Res Dev Cent* 23 . <https://doi.org/39180-6199>
3. Donatello S, Tyrer M, Cheeseman CR (2010) Comparison of test methods to assess pozzolanic activity. *Cem Concr Compos* 32:121–127 . <https://doi.org/10.1016/j.cemconcomp.2009.10.008>
4. BS EN 450 (2012) Fly ash for concrete Part 1 : Definition , specifications and conformity criteria. BS EN Stand
5. BS EN 1015-3 (2006) Methods of test for mortar for masonry — Part 3: Determination of consistence of fresh mortar (by flow table). Br Stand
6. BS EN 196-3 (2016) Methods of testing cement -- Part 3: determination of setting times and soundness. Br Stand 1–18 . <https://doi.org/10.1111/j.1748-720X.1990.tb01123.x>
7. ASTM C618 (2010) Standard Specification for Coal Fly Ash and Raw or Calcined Natural Pozzolan for Use. *Annu B ASTM Stand* 3–6 . <https://doi.org/10.1520/C0618>
8. Zulu SNF (2017) Optimizing the usage of fly ash in concrete mixes. Department of Civil Engineering and Surveying, Durban University of Technology
9. Vassilev S V., Baxter D, Andersen LK, Vassileva CG (2013) An overview of the composition and application of biomass ash. Part 1. Phase-mineral and chemical composition and classification. *Fuel* 105:40–76 . <https://doi.org/10.1016/j.fuel.2012.09.041>
10. Shearer CR (2014) The Productive Reuse of Coal , Biomass and Co-Fired Fly Ash. PhD Thesis, School of Civil & Environmental Engineering, Georgia

Institute of Technology

11. Wang S, Baxter L (2007) Comprehensive study of biomass fly ash in concrete: Strength, microscopy, kinetics and durability. *Fuel Process Technol* 88:1165–1170 . <https://doi.org/10.1016/j.fuproc.2007.06.016>
12. Rajamma R, Ball RJ, Tarelho LAC, Allen GC, Labrincha JA, Ferreira VM (2009) Characterisation and use of biomass fly ash in cement-based materials. *J Hazard Mater* 172:1049–1060 . <https://doi.org/10.1016/j.jhazmat.2009.07.109>
13. Vassilev S V., Vassileva CG (2007) A new approach for the classification of coal fly ashes based on their origin, composition, properties, and behaviour. *Fuel* 86:1490–1512 . <https://doi.org/10.1016/j.fuel.2006.11.020>
14. Cheah CB, Ramli M (2012) Mechanical strength, durability and drying shrinkage of structural mortar containing HCWA as partial replacement of cement. *Constr Build Mater* 30:320–329 . <https://doi.org/10.1016/j.conbuildmat.2011.12.009>
15. Rajamma R (2011) Biomass fly ash incorporation in cement based materials, PhD Thesis. Department of Ceramics and Glass Engineering, University of Aveiro
16. Tkaczewska E, Małolepszy J (2009) Hydration of coal – biomass fly ash cement. *Constr Build Mater* 23:2694–2700 . <https://doi.org/10.1016/j.conbuildmat.2008.12.018>
17. Tkaczewska E, Mróz R, Łój G (2012) Coal-biomass Fly Ashes for Cement Production of CEM II / A-V 42 . 5R. 28:633–639 . <https://doi.org/10.1016/j.conbuildmat.2011.10.022>
18. Tkaczewska E MJ (2007) Effect of fly ash fineness on the fly ash cement hydration and properties. *Cem wapno Bet* 12:279–302

# CHAPTER 4 PROPERTIES OF BIOMASS FLY ASH PASTES AND MORTARS

## 4.1. Introduction

This chapter evaluates the properties of the biomass fly ashes as supplementary cementitious materials (SCMs) in cement pastes and mortars. The effect of partial substitution of Portland cement with enhanced biomass (EBA), wood biomass (WBA) and coal (CFA) fly ash was investigated and compared for their impact on the fresh and hardened properties. The ashes were used at replacement level of 10, 20 and 30% by weight of the total binder except for the WBA which was used as 10% and 20% replacement only due to the difficulty of producing a workable mix at 30% replacement with WBA. The properties of fresh material investigated include workability (flow), consistency, initial and final setting time and heat of hydration. The compressive and flexural strength of the hardened material was determined. In addition, the microstructure and hydrated phase development of blended fly ash mixes were studied using Mercury porosimetry (MIP) and Quantitative x- ray diffraction (QXRD).

## 4.2. Test Programme

The overall investigated properties along with the test methods used to assess each property are summarised in Table 4.1.

**Table 4.1 Test programme**

Test	Property	Test method	Standard
Fresh properties	Setting time	Vicat needle	BS EN 196-3
	Consistency	Mortar flow	EN 1015-3
	Heat of hydration	Isothermal calorimetry	ASTM C1702
Mechanical properties	Compressive & flexural strength	Mortar strength	BS EN 196-1
Microstructure	Porosity & pore size distribution	Mercury intrusion porosimetry	na
Phase analysis	Hydrated phases	X- ray diffraction	na

## 4.2.1. Materials

### 4.2.1.1. Cement

Ordinary Portland cement (CEM I: 52.5 N) conforming to EN 197-1 supplied by Rugby cement was used in this investigation. The chemical composition of the cement was determined by XRF analysis. It is shown in Table 4.2.

**Table 4.2** Chemical composition of CEM I 52.5 N

Element	SiO <sub>2</sub>	Al <sub>2</sub> O <sub>3</sub>	Fe <sub>2</sub> O <sub>3</sub>	CaO	MgO	SO <sub>3</sub>	K <sub>2</sub> O	P <sub>2</sub> O <sub>5</sub>
Content (%)	15.9	4.73	2.73	69.8	0.57	3.54	1.45	0.78

### 4.2.1.2. Fly Ash

Enhanced biomass fly ash (EBA) generated in Drax power station, virgin wood biomass ash (WBA) produced in Lynemouth power station and commercial coal fly ash (CFA) were used as supplementary cementitious materials to prepare pastes and mortars. CFA and EBA were supplied by Power Minerals Ltd. WBA was sieved through 500µm sieve, the retained material was rejected and the finer WBA was used. The chemical composition of all ashes, determined by XRF analysis, is shown in Table 4.3. Further information on the chemical and physical properties of the materials is given in chapter 3.

### 4.2.1.3. Aggregates

The fine aggregate used for making mortars is a local sharp medium grade siliceous sand supplied by Frank Key Ltd. The sand was sieved through a 2 mm sieve before using in the mixtures to be within the same range of standard sand grading [1]. The grading of the sand particles was determined by manual sieving. It is shown in Figure 4.1. The coarse aggregate used for making concrete is 10 mm un-crushed gravel. It was supplied by Frank Key Ltd, Sheffield and its grading curve is shown in Figure 4.2.

**Table 4.3 The chemical analyses of fly ashes**

Element	EBA (wt. %)	WBA (wt. %)	CFA (wt. %)
SiO <sub>2</sub>	41.46	12.5	47.64
Al <sub>2</sub> O <sub>3</sub>	23.49	2.55	25.32
Fe <sub>2</sub> O <sub>3</sub>	8.10	1.71	8.39
MgO	2.27	2.66	2.11
SO <sub>3</sub>	0.17	0.12	-
TiO <sub>2</sub>	1.48	-	0.57
CaO	8.10	25.4	3.10
K <sub>2</sub> O	5.57	8.81	3.16
P <sub>2</sub> O <sub>5</sub>	0.75	1.52	0.22
Na <sub>2</sub> O	0.56	0.68	0.16
MnO	0.46	1.25	-
ZnO	0.12	0.098	-
SrO	0.25	0.067	0.11
BaO	0.21	-	0.36
LOI	8.91	42.48	7.0

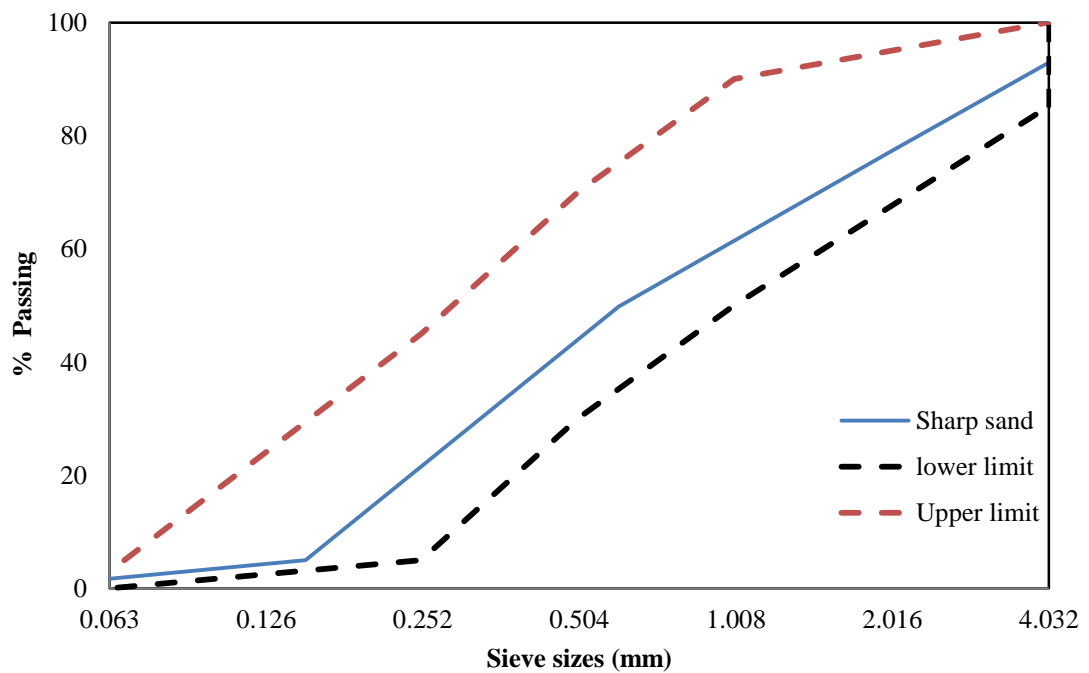


**Figure 4.1 Grading curve of sand by manual sieving**

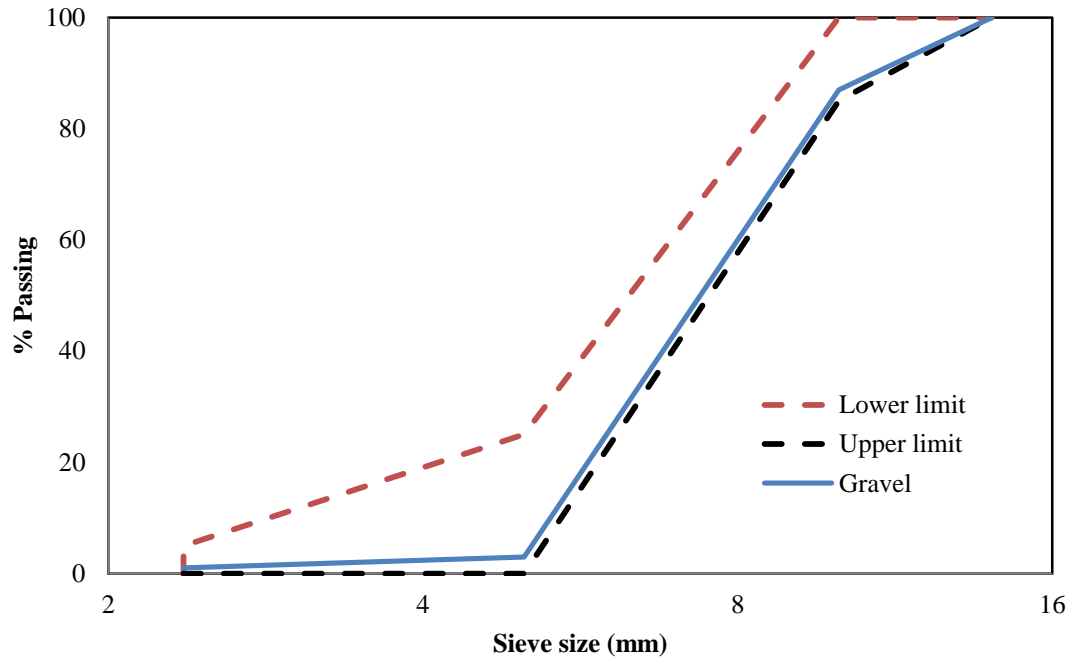


Figure 4.2 Grading curve for 10 mm gravel

#### 4.2.1.4. Superplasticizer

Oscreed superplasticizer was used in the paste and mortar formulations. It is manufactured by OSCERET UK Ltd and conforms to the requirements of BS EN 934-2. It is a multifunctional high molecular weight polymer-based admixture which can reduce the water by up to 25% without affecting the mix integrity. It was only used with wood biomass ash (WBA) mixes to provide workability due to their high water demand.

#### 4.2.1.5. Water

Tap water was used in mortar and concrete mixtures while distilled (ionized) water was used for paste mixtures, preparation of  $\text{NaSO}_4$  and  $\text{NaOH}$  solutions (chapter 6),  $\text{NaCl}$  solution and dissolving the concrete powder into a solution for chloride analysis (chapter 7).

### 4.2.2. Mix Proportion

Cement pastes and mortars were prepared by replacing ordinary Portland cement with different amounts of biomass and coal fly ashes at 10, 20 and 30% in a dry condition. These percentages were chosen based on previous research which

suggested that the optimum limit to monitor the behaviour of blended cementitious material is up to 30% [2].

Table 4.4 shows the mix proportions of the pastes and mortars. Mix 1 represents the reference mix of 100% cement and mixes 2 to 9 contain different blends of cement and fly ash. The mix ID (column 2) of mixes 2 to 9 represents the replacement percentage of each fly ash. For example, 10EBA contains 10% enhanced biomass ash and 90% cement by weight of the binder. Mortar mixes corresponding to the paste mixes 1 to 9 were also prepared using the same proportion given in Table 4.4. The cement to aggregate to water ratio was 1:3:0.5 for all mortar mixes whereas the cementitious pastes were prepared with a w/c of 0.4.

**Table 4.4 Details of paste and mortar mixes**

<b>Mix no</b>	<b>Mix ID</b>	<b>Cement (% weight of binder)</b>	<b>Fly ash (% weight of binder)</b>
1	OPC	100	0
2	10EBA	90	10
3	20EBA	80	20
4	30EBA	70	30
5	10WBA	90	10
6	20WBA	80	20
7	10CFA	90	10
8	20CFA	80	20
9	30CFA	70	30

### **4.3. Experimental Methods**

#### **4.3.1. Fresh Properties**

##### **4.3.1.1. Water Demand and Setting Times**

Vicat apparatus was used to measure the initial and final setting time of control cement and blended fly ash pastes of standard consistency according to BS EN 196-3 [3]. The water required to obtain a paste with an appropriate consistency was determined first by trial penetrations of pastes with different water contents until one

was found suitable for the plunger to penetrate to the depth of  $(5\pm 1)$  mm from the base of the mould. Once the water required for standard consistency was determined, the initial and final setting time was measured following the procedure provided in BS EN 196-3. The initial setting time is the elapsed time (in minutes) from zero time (start of mixing) until the moment when the penetration depth of the needle is  $5\pm 1$  mm from the mould base. The final setting time was determined from zero time until the Vicat needle penetrates only 0.5 mm. The initial setting time refers to the beginning of hardening while the final setting time refers to the sufficient hardening of the mixture. Figure 4.3 shows the initial and final setting time measurement stages.

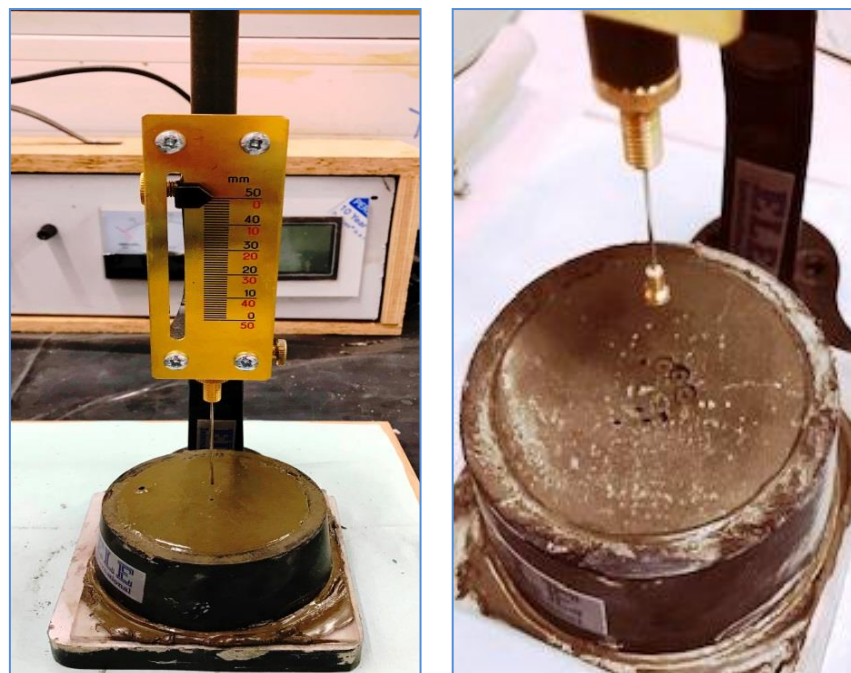


**Figure 4.3 Initial and final setting time measurements**

#### **4.3.1.2. Consistency (flow /workability) of Cement Mortars**

Consistency is defined as a measure of the fluidity of fresh mortar or measurement of its deformability when subjected to a certain type of stress. The flow tests were conducted on mortars of control cement and blended fly ash mortars according to EN 1015-3 standard [4]. Material proportions given in BS EN 450-1 [5] were used; one part of cement to 3 parts of fine aggregate and 0.5 water to binder ratio (w/b). Control mortar was prepared by mixing 1350 g sand, 450 g Portland cement CEM I

and 225 g water. Other mortars were prepared in the same manner except that the Portland cement was replaced with 10%, 20% and 30% of fly ash. Superplasticizer was only used with wood biomass ash (WBA) mixes to control the water requirement and keep constant w/b ratio for all mixes. However, it was not possible to produce a workable mix at 30% replacement by WBA even by using the maximum dosage limit of the superplasticizer (1.5% by weight of binder). Thus, only 10 and 20% replacement of WBA was used. The mixing was conducted as described in chapter 3 (section 3.1.3.4). After mixing, the fresh mortar was placed in two layers on a flow table disc; each layer was compacted by 10 short strokes of a tamper. The excess mortar was skimmed off by a palette knife and the free area around the disk was wiped to remove any water. Then, the mould was slowly raised vertically and the mortar was spread out by 15 jolts of the flow table (approximately one jolt per second). The diameter of the mortar was measured at a right angle in four directions and the mean value was taken as the flow in mm. The mixing and flow measurements are shown in Figure 4.4.

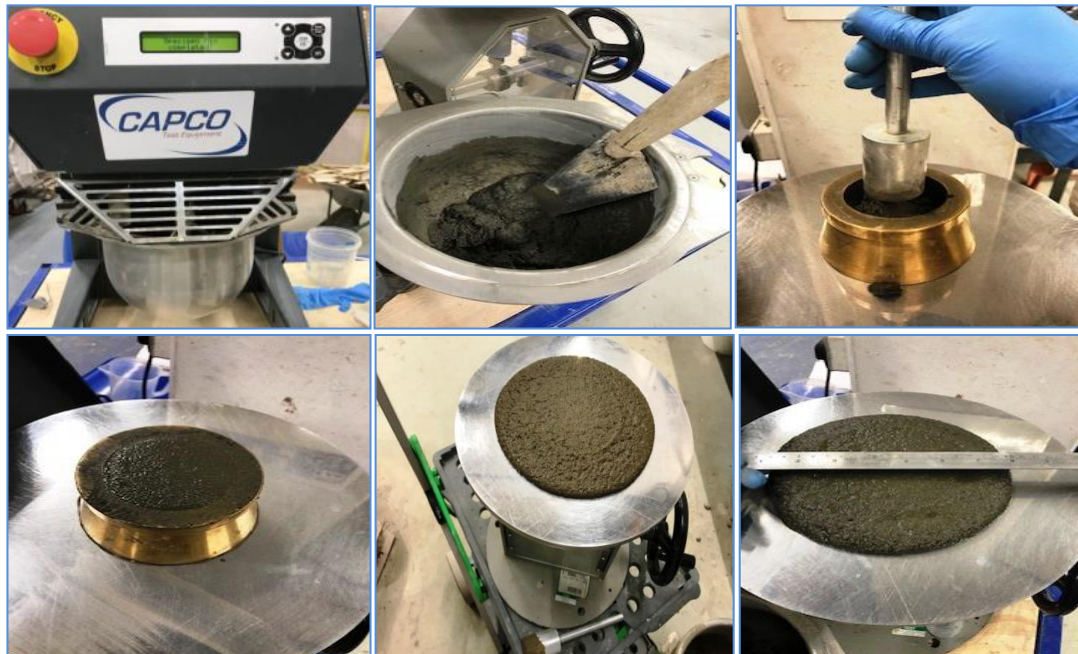


**Figure 4.4** Mixing and flow measurements

### 4.3.1.3. Heat of Hydration

The heat of hydration of plain cement and fly ash blended cement pastes at 10%, 20% and 30% of cement replacement was measured by isothermal calorimetry according to ASTM C1702 [6] using TAM air calorimeter set at 25°C. The water to the binder ratio (w/b) was 0.4 for all mixes. The dry components (cement + fly ash) were combined before adding the deionized water, and the paste was mixed by hand for 2 minutes to ensure homogeneity. Then, about 20 g of the paste was inserted into the small HDPE bottle, capped and placed into the calorimeter channels and the heat flow was recorded for 72 hours. Figure 4.5 shows the TAM AIR calorimeter measurements.

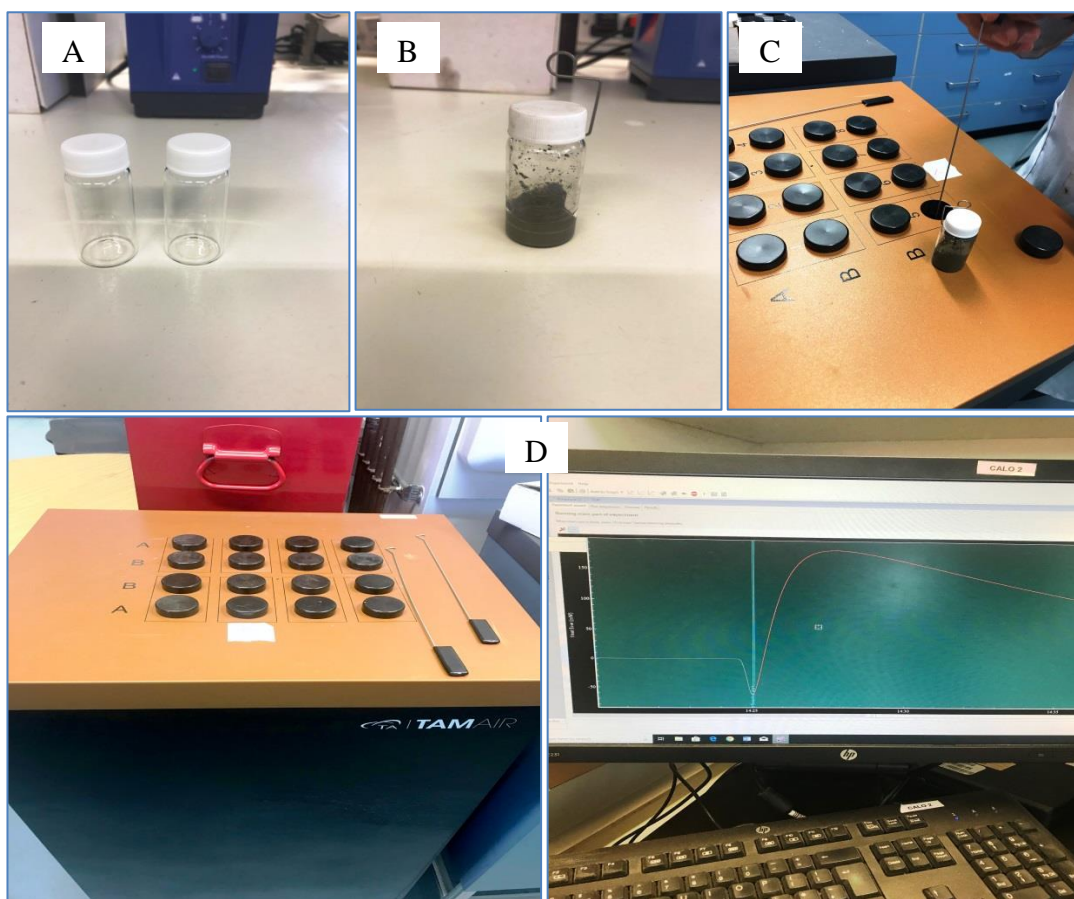


**Figure 4.5 Heat of hydration measurements**

A. HDPE bottle, B. 20 g of the paste was inserted into the bottle, C. The bottle placed inside the calorimeter channel and D. TAM air calorimeter connected to computer for data collection.

### 4.3.2. Hardened Properties

Mortars of plain cement and blended with fly ash were used to assess mortar flexure and compressive strength development using the same mixes that were used for the mortar flow tests (Table 4.4) in section 4.3.1.2. After conducting the flow test, the mortar was placed into prism steel moulds of dimensions 40 x 40 x 160 mm in two layers; each layer was compacted on a vibrating table for 5 seconds. The moulds were lubricated with mould oil prior to casting. All moulds were then placed in a mist curing room for 24 hours. All samples were then removed from their moulds and cured in water at 20°C until the age of testing. The prisms were first tested in three-point bending mode to measure flexural strength then each part was tested under compression (equivalent cube test) according to BS EN 196.1 standard. Three samples were tested for each age and the average was determined. The strength was recorded at 7, 28, 90 and 180 days for all mixes.

The flexural strength was calculated by using equation 4.1 as follows

$$F_s = 1.5 \frac{fl}{bh^2} \quad 4.1$$

Where:  $F_s$  is the flexural strength in (MPa);  $f$  is the fracture load in (N);  $l$  is the length between the supports of the mortar sample in (mm);  $b$  is the width of the sample in (mm) and  $h$  is the height of sample in (mm).

The compressive strength was calculated by equation 4.2 as follows

$$C_s = \frac{F_c}{A} \quad 4.2$$

Where:  $C_s$  is the compressive strength in (MPa);  $F_c$  is the maximum load at fracture in (N) and  $A$  is the area of the cross-section in (mm<sup>2</sup>).

### 4.3.3. Microstructure Analyses

Mercury intrusion porosimetry (MIP) technique was used to measure the porosity and pore size distribution of plain cement and blended fly ash pastes. PASCAL 140/240 Porosimeter shown in Figure 4.6 was used in this study. The control cement and fly ash blended cement pastes were prepared with (w/b) = 0.4 at 10%, 20% and 30% percentage of cement replacement. The paste mixes were prepared by placing

the binder in the mixer bowl which was then placed into the Hobart mixer and mixed until homogeneity was achieved. The water was added carefully within 10 seconds while mixing continued at low speed for about 3 minutes. The paste was placed in two layers in cubic steel moulds of size 50 mm on a vibrating table. The moulds were lubricated with mould oil prior to casting. The fresh samples were covered with a plastic sheet to prevent evaporation and stored in a mist curing room. After 24 hours, all samples were removed from their moulds and cured in water at 20°C until the age of testing.

At the desired test age, the cubes were crushed in the compression machine and samples weighing between 1 and 2 g were taken from the middle of the crushed cube. The samples were dried in an oven at 70°C for about 48 hours to remove moisture. Then, they were placed in an airtight bottle and stored in a desiccator containing silica gel to prevent moisture migration from the air. The samples were kept in the desiccator until MIP analyses were conducted.



**Figure 4.6 Pascal 140/240 mercury intrusion porosimetry device used for analyses**

MIP testing was performed using a Pascal 140/240 Porosimeter which measures the pore sizes within the range of 0.007–100  $\mu\text{m}$ . It was connected to an external computer for data analysis. The apparatus is in two parts, Pascal 140 and Pascal 240

both of which apply pressure to a sample confined in mercury. The mercury under pressure intrudes into the pores of the sample. Pascal 140 applies pressure of up to 100 MPa which allow mercury to intrude into the large pore of the paste matrix. Pascal 240 applies pressure of up to 200 MPa to aid intrusion of mercury through the pore size down to 0.0073  $\mu\text{m}$ . The device records the intrusion pressure and the amount of mercury intruded into the sample. The computer microprocessor then translates the collected data on applied pressures to pore radius based on Washburn equation as given below:

$$r = \frac{-4\delta \cos \theta}{P} \quad 4.3$$

Where: P is the applied pressure (Pa); r is the radius of pores ( $\mu\text{m}$ );  $\delta$  is the surface tension of mercury (0.48 N/m) and  $\theta$  is the contact angle between mercury and cement paste (assumed as  $140^\circ$ ).

The total porosity and the graph of pore size distribution were obtained at the end of MIP analysis.

#### **4.3.4. Phase Analyses**

The influence of biomass ashes on the phase formation of blended fly ash cement pastes was investigated. X- ray diffraction (XRD) technique was used to identify the crystalline phases in blended fly ash cement pastes. The pastes were prepared by replacing ordinary Portland cement with biomass and coal fly ashes at the rate of 10, 20 and 30 % by weight. The samples used for XRD analyses were taken from the middle of the same cubes which were crushed and dried for MIP testing. The dried samples were ground to a powder before placing in airtight bags as shown in Figure 4.7 until testing. XRD analyses followed by quantitative X- ray diffraction using Rietveld method were conducted on the samples. Standard silicon was introduced in each test sample to enable the measurement of amorphous content.



Figure 4.7 XRD samples stored in self-sealing bags

## 4.4. Results and Discussion

### 4.4.1. Fresh Properties

#### 4.4.1.1. Water Demand and Setting Time

The water required for the consistency of the fly ash cement pastes, expressed as a percentage of total binder weight, is shown in Figure 4.8. The figure shows that the water demand for both CFA and EBA blended cement pastes is lower than that of the control OPC paste. Increasing the content of fly ash leads to a decrease in water demand in both cases. This can be attributed to the spherical glass structure of fly ash which has low water absorption [7, 8]. The decrease in water demand in comparison to control OPC paste for 10%, 20% and 30% CFA is 5.8%, 11.7% and 14.7% respectively. The corresponding values for 10%, 20% and 30% EBA is 2.9%, 5.8% and 8.8% respectively.

In the case of WBA, the water demand is higher than OPC mix. The increase in water demand compared to OPC mix is 2.9 % for 10% WBA and 11.76% for 20% WBA. These results on virgin wood biomass ash are in agreement with the findings of some researchers who used sawdust and waste (recycled) wood ashes [2, 9].

It was observed that the WBA requires more water compared to CFA and EBA. The fineness and the higher surface area, which were reported in chapter 3, of WBA are

the most likely factors responsible for its higher water demand compared to CFA and EBA. WBA has the highest surface area ( $61.7\text{m}^2/\text{g}$ ) compared to  $6.38\text{ m}^2/\text{g}$  and  $3.06\text{ m}^2/\text{g}$  for EBA and CFA respectively. It has been reported that the physical properties of fly ash such as fineness and surface area have the main influence on the consistency [8, 10].

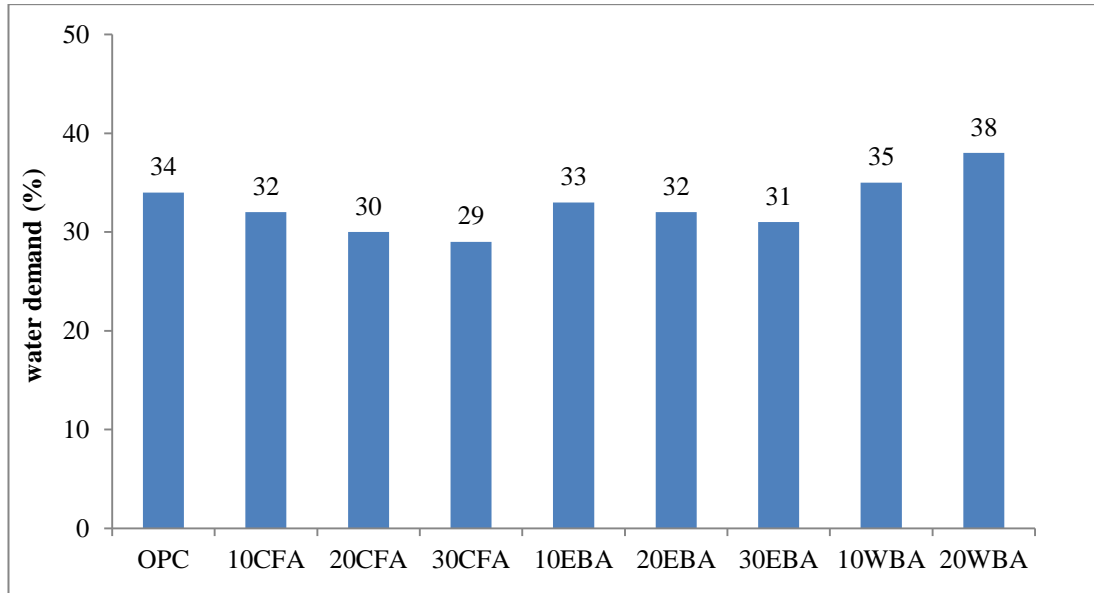


**Figure 4.8 water demand for normal consistency for OPC, CFA, EBA and WBA pastes**

Vicat apparatus was also used to determine the effect of fly ash on initial and final setting times and the results are presented in Figure 4.9. A delay in setting time was observed for both CFA and EBA blended mixes. The addition of CFA and EBA fly ashes causes an increase of setting time due to the dilution effect of fly ash on the initial hydration reaction. CFA mixes delayed the initial setting by 4-25 minutes and final setting by 5-41 minutes. On the other hand, EBA delayed the initial setting by 6-22 minutes and final setting by 15-24 minutes compared to the plain cement paste. The delay in setting time increases with increasing the content of both EBA and CFA fly ashes, however, the setting time was not significantly affected by 10 % substitution.

The behaviour of WBA is different from both EBA and CFA, the setting time being accelerated by the inclusion of WBA. The high surface area of WBA and high alkalinity contributed to accelerated initial setting time. The chemical composition of

WBA reveals that it is less reactive than OPC and the setting should be delayed because of reduced initial hydration. However, the accelerated setting times obtained for 10 and 20% WBA mortars are due to the drying of the mortar caused by the water adsorption of the wood biomass fly ash and its high carbon content, expressed as LOI, which absorbs the mixing water leading to fast drying. The setting time of WBA, therefore, is more a reflection of its stiffening caused by drying rather than chemical reaction as will be shown in section 4.4.1.3.

The results show that the minimum initial setting time obtained for all mixes was greater than 30 minutes and the maximum final setting time was less than 600 minutes which are within the specified limits set by BS EN 196-3 standard [3].

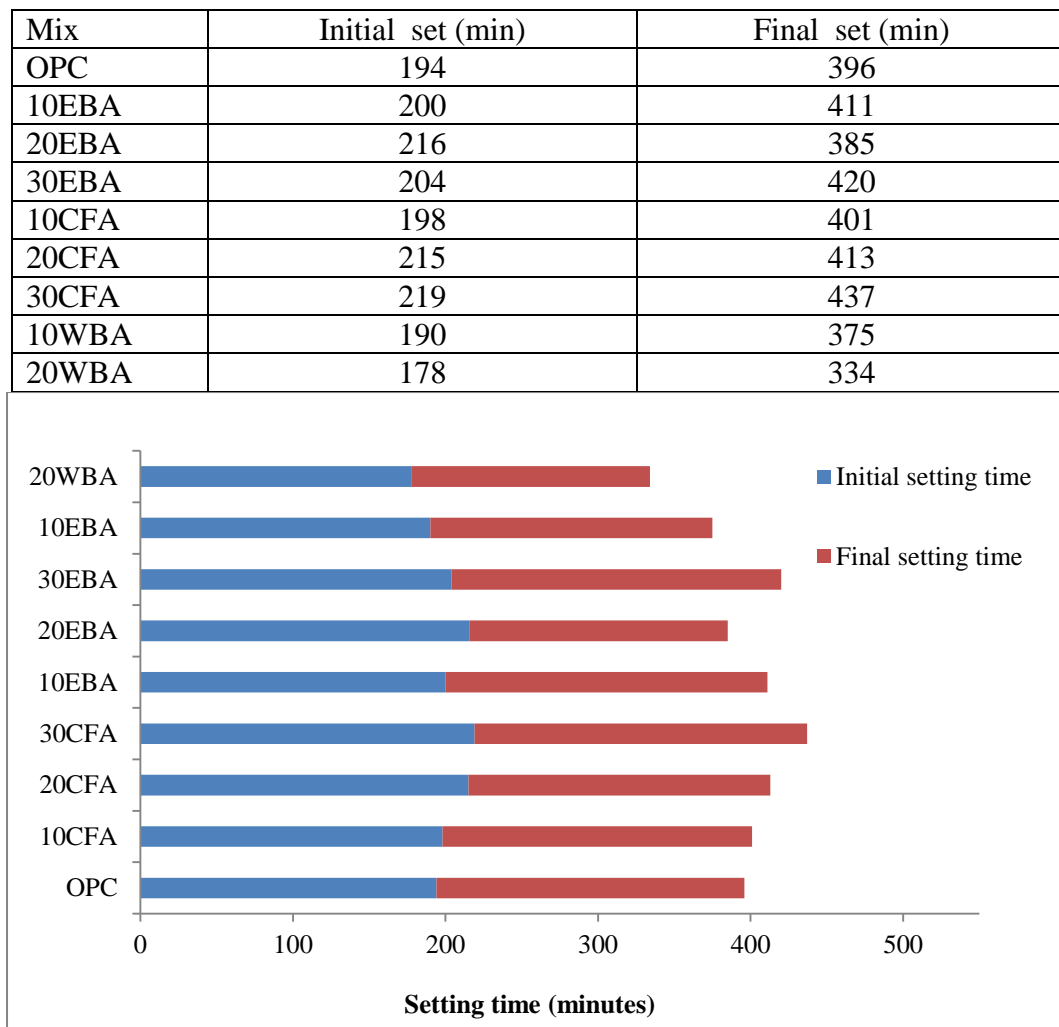


**Figure 4.9 Initial and final setting times for EBA, CFA, WBA and OPC pastes**

#### 4.4.1.2. Consistency (flow) of Cement Mortars

Mortar flow results of OPC and blended fly ash mortars at different levels of replacement are shown in Figure 4.10. It shows that both CFA and EBA increase the workability of mortar whereas the addition of WBA reduces the workability. CFA mixes improved the workability by up to 13.8% with 20% replacement, however, when the replacement was 30%, the increase in workability reduced to 10%. Similar trend was observed with EBA mixes but to a lesser extent, the increase in workability was only up to 5.5% at 20% replacement. On the other hand, the workability was reduced by 17% at 20% replacement by WBA.

It is generally accepted that the rheological behaviour (workability) in blended fly ash cement mixtures is highly influenced by the physical properties of fly ash such as the particle size distribution, morphology (shape and texture of fly ash particles) and LOI. The fine and spherical particles of CFA increased the workability of the mortar whereas the high LOI, irregularly shaped, coarse and porous particles of WBA tend to absorb more water, reducing its availability in the mix and decrease the workability of the mortar [11]. Biomass ashes produced from waste (recycled) wood biomass sources and sawdust ashes also reduce the workability of mortar compared to OPC control mortar [2, 12].

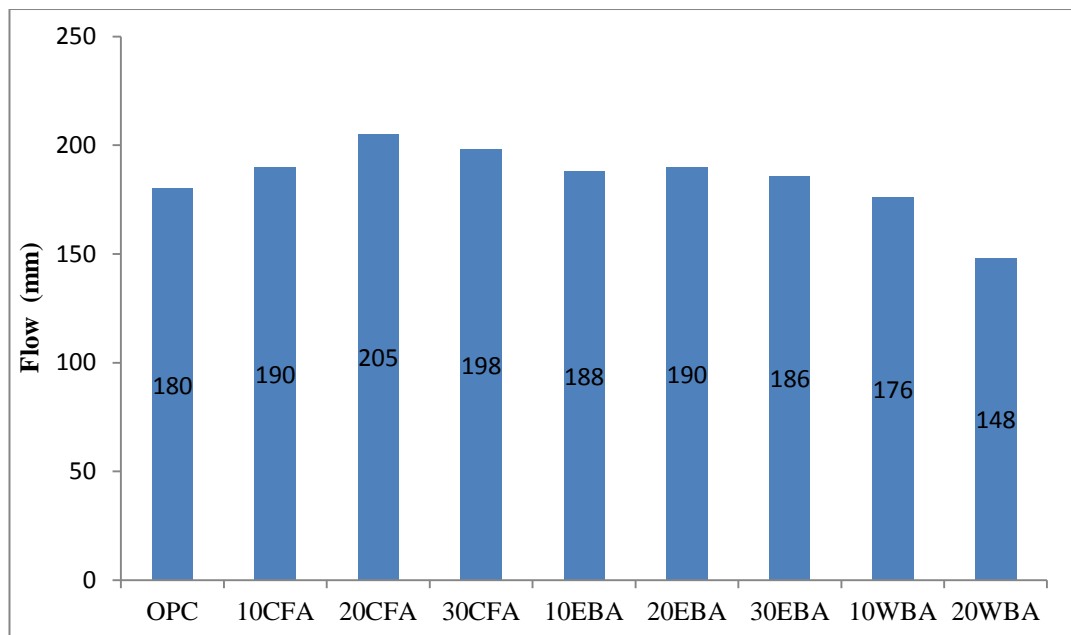


Figure 4.10 Mortar flow for EBA, CFA, WBA and OPC mixes

The mortar flow increases with increasing fly ash content as evidenced by the subsequent decrease in water demand of EBA and CFA mixes whereas the opposite is true in the case of WBA.

#### 4.4.1.3. Heat of Hydration

Calorimetric curves of control OPC and fly ash blended mixtures measured at 25°C for 72 h are presented in Figure 4.11. The graphs show the rate of heat evolution (Figure 4.11-A) and the total (cumulative) heat evolved (Figure 4.11-B) for all mixes. The cumulative heat flow was obtained by integration of heat flow versus time data over the time interval of the test ( $t_0$  to  $t_e$ , in units of seconds) as shown in Eq 4.4 [6].

$$Q_t = \int_{t_0}^{t_e} P \cdot dt \quad 4.4$$

Where:  $t_0$  is the time the cement and water are mixed, taken as zero, and  $t_e$  is the end of the test.

All values are normalized per gram of the total binder (i.e., the mass of cement + fly ash). Overall, the measured values of heat released show that all blended fly ash cement pastes generated less heat flow than OPC control at different percentage of cement replacement. All samples reached a steady-state heat flow after two days.

Generally, two peaks appear in all heat evolution curves, the first peak is related to  $C_3S$  hydration, which appears right after the addition of water, and the second is related to the hydration of  $C_3A$  [8]. The highest heat flow is observed in OPC cement paste after a period of approximately 9 hrs. The peak heat decreases as the content of fly ash increases indicating a reduction in the hydrating phases of the fly ash cement pastes. The slope of the acceleration period curve in all blended fly ashes pastes is reduced due to less  $C_3S$  being hydrated.

The early age hydration behaviour of EBA is quite similar to CFA. This is particularly clear in Figure 4.11-B where the curves of both ashes almost coincide at 10% and 20% replacement. It is noticeable that the heat released by CFA and EBA mixes was considerably higher than the virgin wood biomass mixes (WBA) indicating a higher rate of hydration of CFA and EBA compared to WBA. According

to Shearer [8, 13], the height of the peak correlates to particle size, the smallest median particle size exhibiting the highest peak. This observation is in agreement with the results in Figure 4.11-A, as the median particle size of CFA and EBA is smaller than WBA (chapter 3, section 3.3.3.1).

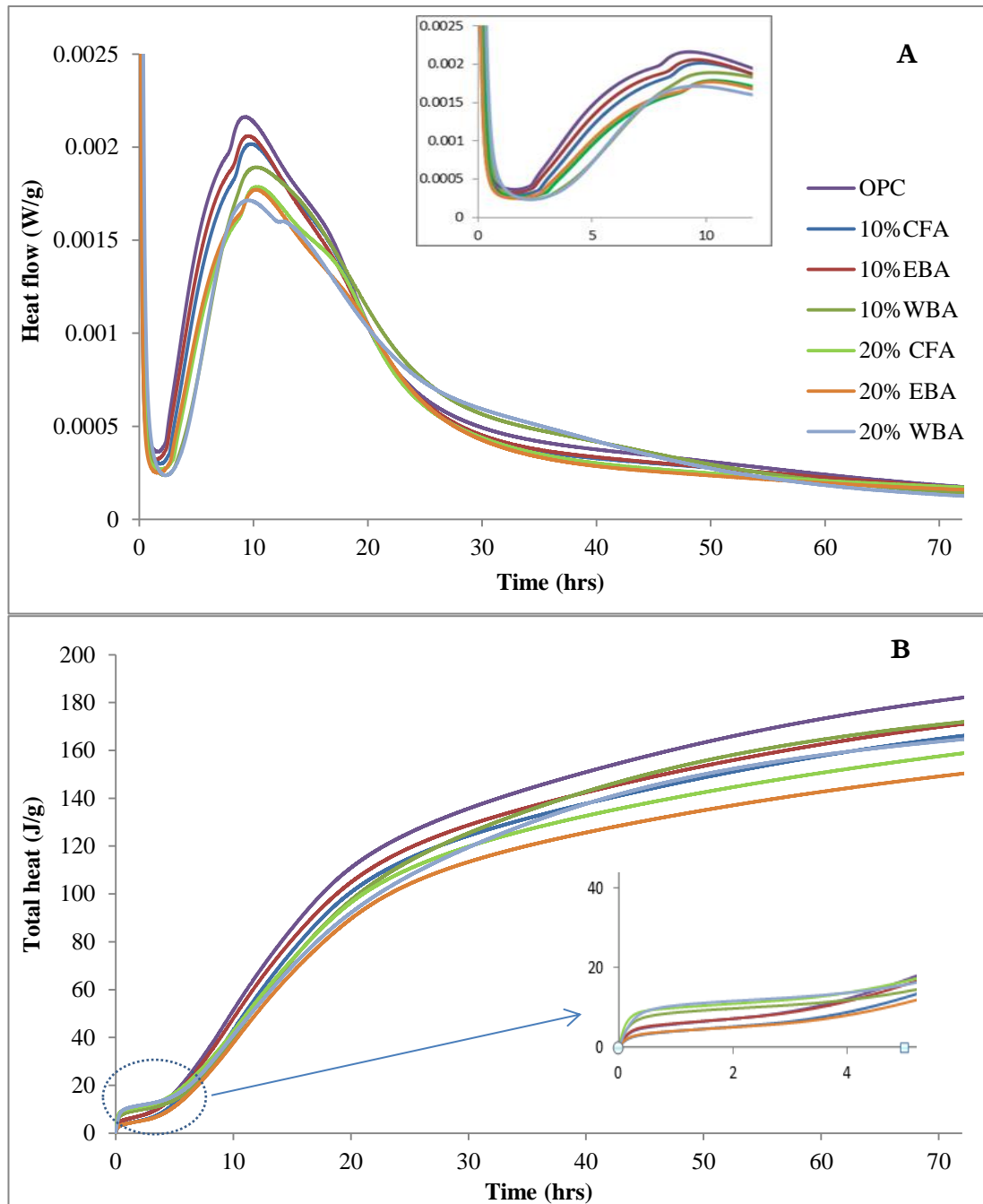


Figure 4.11 Calorimetric curves of OPC and fly ash mixtures measured at 25°C

The WBA pastes show a quite different trend compared to CFA and EBA. With the addition of WBA, the hydration peak is accelerated compared to CFA and EBA pastes as shown by slight shift to the left of 20% WBA paste in Figure 4.11-A. The cumulative heat released after 72 hrs by this mix is the highest (164.3 J/g) compared to 20% EBA (158.4 J/g) and 20% CFA (149.9 J/g) mixes. However, it is less than the total heat produced by the control OPC past (181.7 J/g). The shift in hydration peak could be influenced by the high amount of alkalis present in WBA [2].

Interestingly, both 10% and 20% WBA mixes produced higher cumulative (total) heat than OPC during the first 5 hrs as shown in Figure 4.11-B. The high surface area along with the high water demand due to absorption of WBA are the main reasons for the acceleration of the early-age heat flow as they reduce the effective w/b ratio available for hydration and produce more heat. It has been reported that high calcium fly ash do not always reduce the heat evolution because of its cementitious property [14].

The values of heat evolved after 24 and 72 hours of hydration are given in Table 4.5. The heat evolved decreases with the addition of fly ashes. The reduction of hydration heat is due to the dilution effect (less cement available compared to the control OPC mix) [10, 15].

**Table 4.5 Total heat evolved during hydration of OPC and fly ash mixtures**

Sample	Total (cumulative) heat (J/g)	
	24h	72h
OPC	153	181.7
10% EBA	116.8	170.4
20% EBA	105.5	150
10% CFA	114.1	165.8
20% CFA	109.5	158.4
10% WBA	118	171.6
20% WBA	107.7	164.3

## 4.4.2. Mechanical Properties

### 4.4.2.1. Compressive Strength

The results of equivalent cube tests at different periods of water curing are shown in Figure 4.12. The compressive strength at all ages decreases gradually as the percentage of fly ash in the mix increases. At early age, the pozzolanic reaction of fly ash is slower than the cement hydration. Therefore, all blended fly ash mixes have less strength compared to control OPC. However, the reduction in early strength is often compensated by an increase in long term strength and as the curing age increases the differences in strength get smaller. The 7- day strengths for 10, 20 and 30% replacement by coal fly ash are about 87, 71 and 58% of the control mix respectively while they are 98, 89 and 74% compared to control OPC at 28 days. The high strength gain at 28 days can be mainly attributed to continuous cement hydration and additionally to the pozzolanic reaction. However, from 28 days onwards, the relative compressive strength increased due to the acceleration of pozzolanic reaction, which consumes the  $\text{Ca(OH)}_2$  produced by cement hydration to form additional cementitious C-S-H gels. Thus, the long term strength increases due to the higher pozzolanic reaction. The rate of strength gain depends on the level of cement replacement.

At 90 days age, the compressive strength of mortar with 10% and 20% CFA exceeded the compressive strength of OPC mortar. The 30% CFA mortars maintained a marginal difference in compressive strength relative to the OPC mortar. This can be due to insufficient amount of  $\text{Ca(OH)}_2$  present in the system to activate the high level of fly ash.

Similar trends of strength gain are observed for EBA mixes but at a lower rate as shown in Figure 4.12. At 90 days age, the compressive strength of mortar with 10% EBA exceeded the compressive strength of control mortar by 11.4% while at 20% and 30% replacement EBA mortars maintained a marginal difference in compressive strength relative to the OPC mortar.

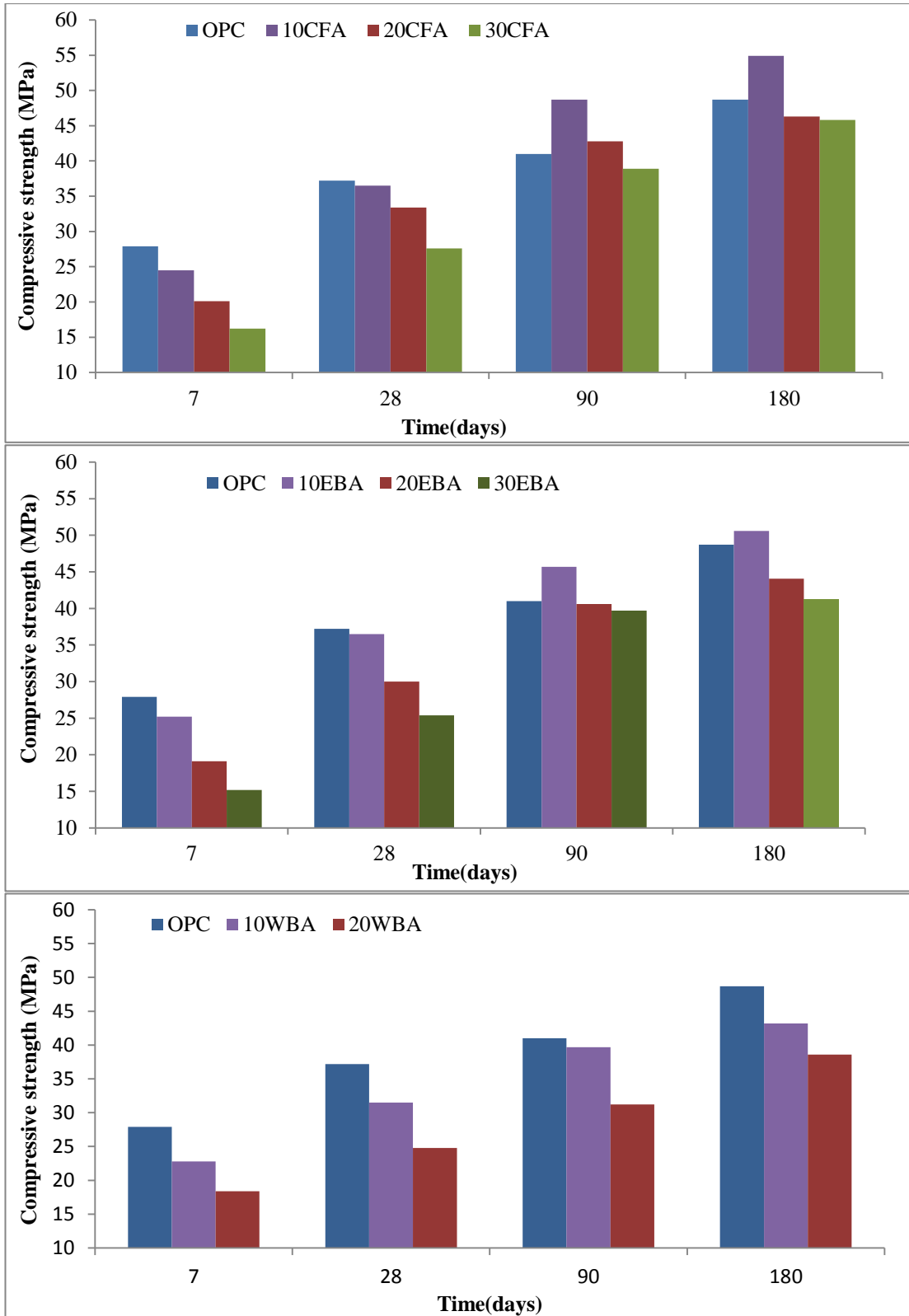


Figure 4.12 Compressive strength development in OPC, EBA and WBA blended mortars

In the case of virgin wood biomass ash, the strength of OPC mortar was higher than 10% WBA and 20% WBA mixes at all ages. The compressive strength of CFA mixes is higher than EBA mixes while WBA strength was the lowest at all ages. The superior strength of CFA mortars compared to EBA and WBA can be attributed to its higher fineness, higher silica and alumina content and a relatively higher amount of amorphous content. The results reported in chapter 3 revealed that the median diameter ( $d_{50}$ ) was 17.3  $\mu\text{m}$ , 49.7  $\mu\text{m}$  and 86.4  $\mu\text{m}$  for CFA, EBA and WBA respectively while the amorphous content was 88%, 84% and 80% respectively. In addition, QXRD results of all blended fly ash mortars, which are presented in section 4.3.5 (Table 4.8), show that 10% and 20% WBA mixes had a lower amorphous content compared to all other mixes indicating less hydration products formation, including C-S-H formation which is responsible for strength gain.

Results reported in literature reveal that the use of waste wood (recycled) ash as a partial replacement of cement ranging between 5-30% reduces the compressive strength compared to control OPC concrete [9, 12, 16, 17]. Table 4.6 shows a comparison between the strength of both EBA and WBA fly ashes and the results reported by Rajamma [10, 16] on two types of waste wood ash FA1 and FA2 from two distinct wood biomass power plants and at the same levels of cement replacement used in this investigation.

**Table 4.6 Comparison of compressive strength at various curing ages**

Age days	Rajamma's results [10, 16]					Current results				
	OPC	WA	10 %	20 %	30 %	OPC	WA	10 %	20 %	30 %
7	28.3	FA1	31.1	27.2	21.3	27.8	EBA	25.2	19.1	15.2
		FA2	30.8	25	22.1		WBA	22.8	18.4	-
28	41.4	FA1	41.3	32.5	22.5	37.2	EBA	36.5	30	25.4
		FA2	35.7	30.1	26.7		WBA	31.5	24.8	-
90	49.4	FA1	43.7	41.2	37.3	41	EBA	45.7	40.6	39.7
		FA2	38.6	34.5	34.1		WBA	39.7	31.2	-
180	55	FA1	51.7	44.4	42.6	48.7	EBA	50.6	44.1	41.2
		FA2	50.2	42.1	43.8		WBA	-	-	-

The strength decreased by the increase in wood ash content and only 10% replacement level gave similar strength to control OPC after 28 days age. The OPC used in Rajamma's mixes was CEM I- 42.5 R which is different from the OPC used in this investigation so the differences are due to both the OPC and fly ash differences (chemical and physical).

#### **4.4.2.2. Flexural Strength**

The results of three-point bending tests for flexural strength of mortars with various levels of cement replacement by all ashes are presented in Figure 4.13.

Generally, the effect of fly ash incorporation on flexural strength is similar to its effect on compressive strength, with increasing cement replacement reducing the flexural strength. At 7 day age, the flexural strength of control OPC mortar was the highest compared to all blended fly ash mixes. From 28 days onwards, both CFA and EBA mortars exhibited higher flexural strength than the control OPC. For example, the control OPC mortar achieved a strength of 6.3 MPA at 7 days and 8 MPA at 90 days whereas the flexural strength of EBA mixes varied between 4.5 to 5.8 MPA at 7 days and between 9 to 9.6 MPA at 90 days. The highest flexural strength of CFA mortars is greater than EBA mortars while WBA mortars had the lowest strength at all ages. Results reported in literature reveal that the use of waste wood (recycled) ash as a partial replacement of cement reduces the flexural strength compared to control OPC concrete [2, 17]. Udoeyo et al. [17] studied the flexural strength behaviour of waste wood biomass ash concrete as a partial cement replacement at 5 to 30 % compared to control OPC concrete. They found that the strength decreased by the inclusion of waste wood ash at all replacement levels. For example, at 28 days, the flexural strength for OPC concrete is 5.57 MPa compared to 5.20 and 3.74 MPa for 5 % and 30 % wood waste ash respectively.

The flexural strength development is also attributed to the hydration process of cement matrix and the pozzolanic reactivity of fly ashes as discussed in section 4.3.3.1.

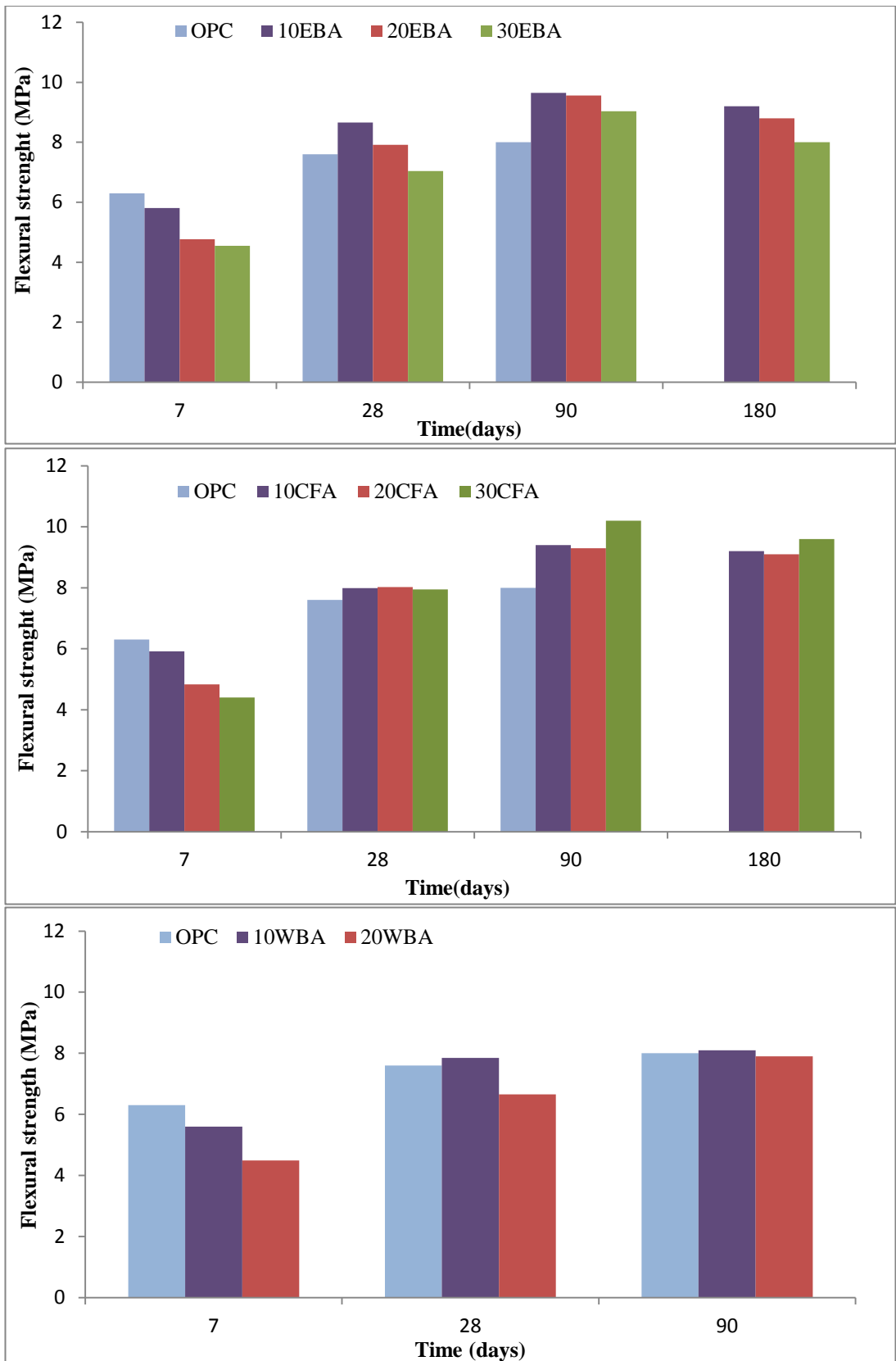


Figure 4.13 Flexural strength development in OPC, EBA and WBA blended mortars

Figure 4.14 shows the relationship between the flexural strength and compressive strength for OPC and all blended fly ashes mortars at 7, 28 and 90 days. A nonlinear relationship is evident with a correlation factor of 0.8827. At 28 days, the flexural strength is 20% of the compressive strength for OPC mortar compared to 23.7%, 24% and 21.8% for 10EBA, 10WBA and 10CFA respectively. The flexural/compressive ratio increases as the replacement level (fly ash content) increases.

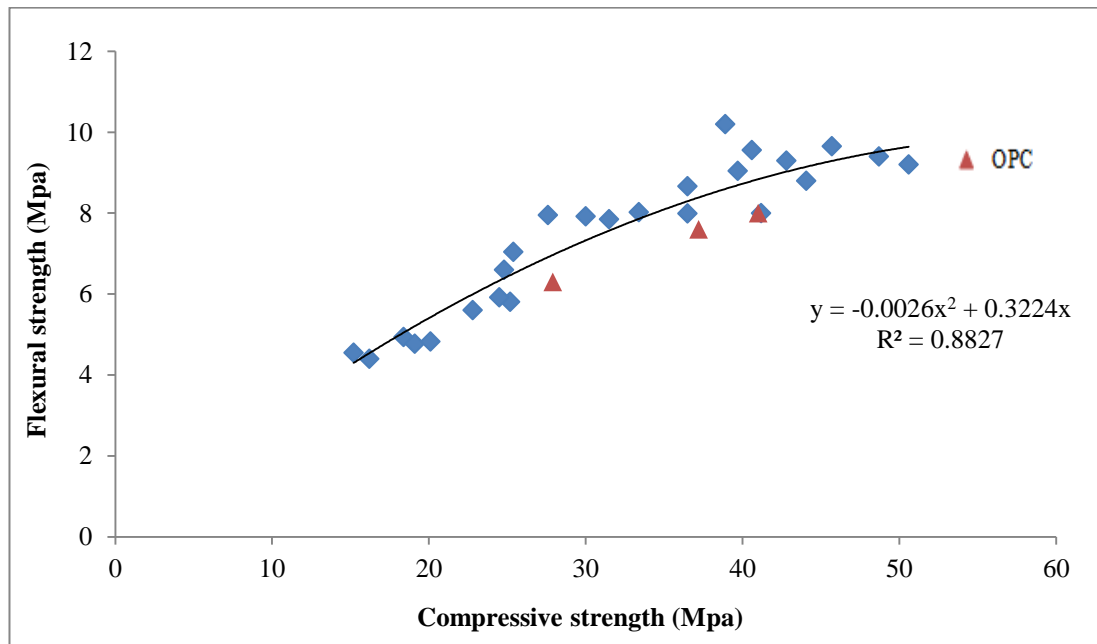


Figure 4.14 Flexural-compressive strength relationship for OPC, EBA, WBA and CFA mortars

#### 4.4.3. Microstructure development

Mercury intrusion porosimetry (MIP) technique was used to investigate the effect of biomass fly ash on the microstructure of blended cement pastes. The results are compared with pastes containing coal fly ash at the same percentage of replacement and control OPC paste. The porosity, pore size distribution and critical pore diameter are the main parameters characterizing the pore structure of hydrated cement paste. The porosity is obtained from the cumulative particle size distribution (PSD) curve whereas the development of pore structure (pore type and size) is identified from the logarithmic differential pore volume curve.

#### 4.4.3.1. Total intruded porosity

The total intruded porosity of control OPC cement paste and blended fly ash pastes at 28 and 90 days of curing was determined and is plotted in Figure 4.15. The effect of curing age and fly ash content on the total porosity is discussed.

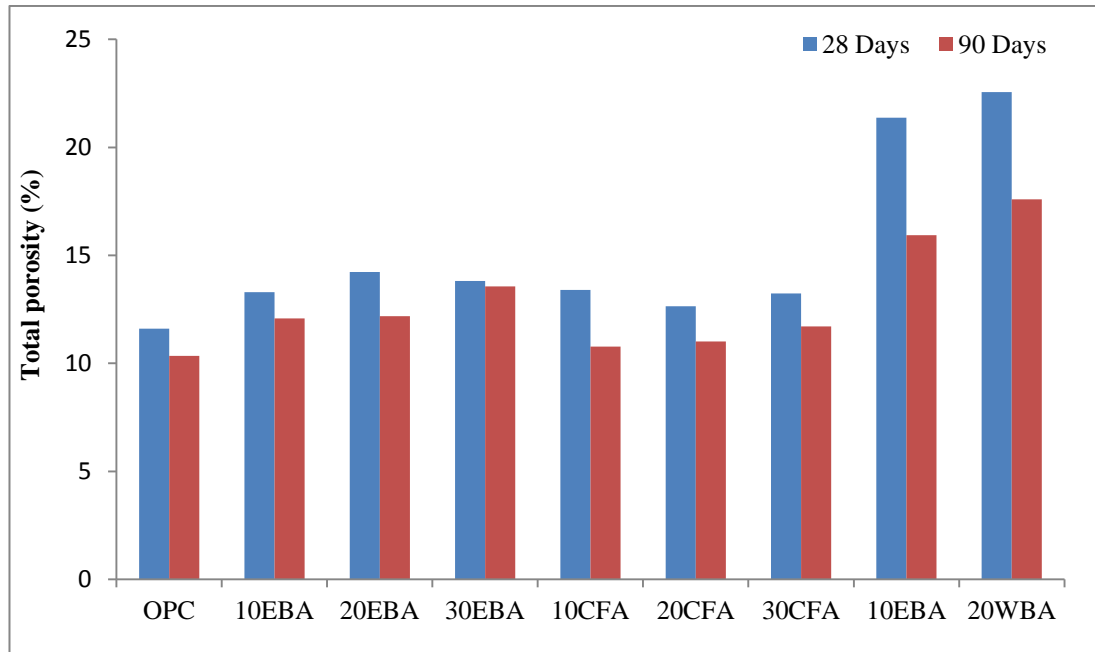


Figure 4.15 The total porosity of control OPC paste and blended fly ash pastes at 28 and 90 days age

##### 4.4.3.1.1. Effect of curing age

Figure 4.15 shows the effect of curing age on total porosity of all mixes. The general trend is of total porosity decreasing with increasing curing age. As the hydration proceeds, solid hydration products (i.e. C-S-H gel) are produced which result in lower porosity and denser microstructure. The total porosity of OPC paste decreased with time from 11.61% to 10.34% between 28 and 90 days. Similar trend was observed in all blended pastes as seen in Figure 4.15. When fly ash is blended into cement and with the progress of cement hydration, additional C-S-H and C-A-H hydration products will be formed due to the pozzolanic reaction. The hydration products fill the open capillary pores which inevitably results in improved pore structure and lower total porosity.

#### 4.4.3.1.2. Effect of fly ash content

Figure 4.15 shows that the reference OPC sample has the lowest total porosity at both ages and the incorporation of fly ash increases the total porosity. This is consistent with other studies which indicated that the incorporation of pozzolanic materials such as fly ash in blended cement paste results in higher total porosity [18, 19]. Fly ash generates less hydration products in blended cement pastes especially at early age when the degree of pozzolanic reaction is much less than in the cement paste. High dosage of fly ash leads to higher total porosity. For instance, after 90 days of curing the total porosity for 30% EBA is 13.56% while at 10% EBA it is 12.08%. The corresponding values for 30% CFA and 10% CFA are 11.71% and 10.78 % respectively.

The total porosity of all CFA pastes was less than EBA and WBA pastes suggesting that the degree of pozzolanic reaction of both biomass ashes is less than coal fly ash. However, it is still greater than the PC paste at all replacements levels and both ages. This is due to the greater fineness of CFA ( $D_{50} = 17.3 \mu\text{m}$ ) than EBA and WBA ( $D_{50} = 49.7 \mu\text{m}$ ,  $68.9 \mu\text{m}$ ) respectively which is reported in chapter 3 (section 3.3.3.1). Similar result was reported by Chindaprasirt et al. [20] who investigated the effect of fly ash fineness on compressive strength, porosity, and pore size distribution of cement pastes. They used Class F fly ash with two fineness ( $D_{50} = 19.1$  and  $6.4 \mu\text{m}$ ) at 20%, and 40% replacement level by weight and 0.35 w/b ratio. They found that the total porosity of the blended cement paste containing finer fly ash was significantly lower than that with coarser fly ash.

Rajamma [2] investigated the impact of two types of waste wood biomass ashes from different sources (BFA1 and BFA2) on the total porosity. The ash replaced 10%, 20 and 30 % of the cement by weight to prepare blended fly ash cement pastes. He found that the porosity of 10% and 20% BFA1 is 15.10% and 16.69% respectively whereas it is 16.77% and 18.71% for BFA2 compared to 15.66% for OPC. He concluded that the addition of both biomass fly ashes increases the total porosity and the variation in the porosity between both ashes is due to the differences in their pozzolanic reactivity.

#### **4.4.3.2. Pore Structure of Fly Ash Blended Cement Paste**

The differential and cumulative pore volume curves of reference OPC and blended fly ash cement pastes at 28 and 90 days of curing are shown in Figures 4.16 to 4.21. The pore size distribution of the control OPC and all blended fly ash pastes show a similar single range (unimodal) of pore volume with most of the pores within the range of 0.01-0.1  $\mu\text{m}$  pore diameter. Similar values are reported in the literature for OPC pastes [21, 22].

Generally, pores in cement-based materials are classified into capillary pores which have diameter  $> 0.01 \mu\text{m}$  (10 nm) while the pores that lie below 0.01  $\mu\text{m}$  are defined as gel pores. Another classification divides the pores into ranges of large pores ( $> 0.1 \mu\text{m}$ ) and small pores ( $< 0.1 \mu\text{m}$ ) [23]. However, the most common classification is by dividing the pores into ranges that affect specific properties such as strength and permeability. Mehta [24] reported that strength and permeability characteristics are more affected by larger pore sizes  $> 50 \text{ nm}$ , which refer to as capillary pores, due to the difficulty of water movement across small pores  $< 50 \text{ nm}$ . It was found that when the pores exceed a diameter of 0.1  $\mu\text{m}$ , the permeability is highly affected [25].

In order to determine the influence of biomass fly ash on the pore structure of cement paste, the pores are divided into small pores  $< 0.1 \mu\text{m}$  and large pores  $> 0.1 \mu\text{m}$ .

##### **4.4.3.2.1. Volume of small pores $< 0.1\mu\text{m}$**

The volume of small pores is determined and presented in Table 4.7. It is noticeable that the mixtures with fly ash have higher volume of small pores than control OPC cement paste at 28 and 90 days. As the content of fly ash increases, the volume of small pores increases. Between 28 and 90 days, the volume of small pores decreased for the control cement paste and all fly ash blended pastes. Zhuiqin Yu et al. [25] investigated the influence of low calcium coal fly ash on pore structure in blended cement paste at long-term curing age up to 2 years. He reported that the volume of small pores in cement and fly ash blended cement pastes increases sharply during early age up to 28 days and then decrease from 28 days to 3years. However, the EBA and WBA are different from the coal fly ash used by Zhuiqin Yu et al. [25, 26].

#### 4.4.3.2.2. Volume of large pores > 0.1 $\mu\text{m}$

Table 4.7 shows the volume of large pores of control OPC and fly ash blended cement pastes. A reduction in the proportion of large pore accompanied by an increase of the small pores is expected as a result of the progress of cement hydration and pozzolanic reaction. At 28 days, the pastes blended with 10% and 20% EBA and CFA have less pores larger than the diameter of 0.1  $\mu\text{m}$  compared to OPC paste. In contrast, the pore structure at 30% replacement by both ashes was coarser than the reference OPC mix. This indicates that replacing cement with both ashes improves the pore structure by reducing the volume of pores lying above 0.1 $\mu\text{m}$ . However, when the replacement level exceeds 30%, the pore structure is affected in a negative way. At 90 days, coal fly ash was more effective in refining the pore structure whereas only 20% replacement of EBA mix has less proportion of large pores compared to OPC mortar.

The behaviour of WBA is different from both EBA and CFA. Its porosity and volume of large pores were the highest between all mixes. This can be attributed to its coarse particles and lower pozzolanic activity. The influence of pore structure on the durability properties will be discussed in later chapters.

**Table 4.7 The influence of CFA, EBA and WBA fly ashes on the pore structure of blended cement pastes.**

Mix ID	28- days of curing			90-days of curing		
	Total porosity (%)	Small pores < 0.1 $\mu\text{m}$	Large pores > 0.1 $\mu\text{m}$	Total porosity (%)	Small pores < 0.1 $\mu\text{m}$	Large pores > 0.1 $\mu\text{m}$
OPC	11.61	10.42	1.19	10.34	8.78	1.56
10EBA	13.3	12.19	1.11	12.08	9.61	2.47
20EBA	14.23	13.50	0.73	12.18	10.7	1.48
30EBA	13.81	11.99	1.82	13.56	11.64	1.92
10CFA	13.4	12.67	0.73	10.78	10.26	0.52
20CFA	12.65	11.43	1.22	11.02	10.37	0.65
30CFA	13.23	11.50	1.73	11.71	11.21	0.5
10WBA	21.37	12.83	8.54	15.94	13.54	2.4
20WBA	22.55	16	6.55	17.60	15.32	2.28

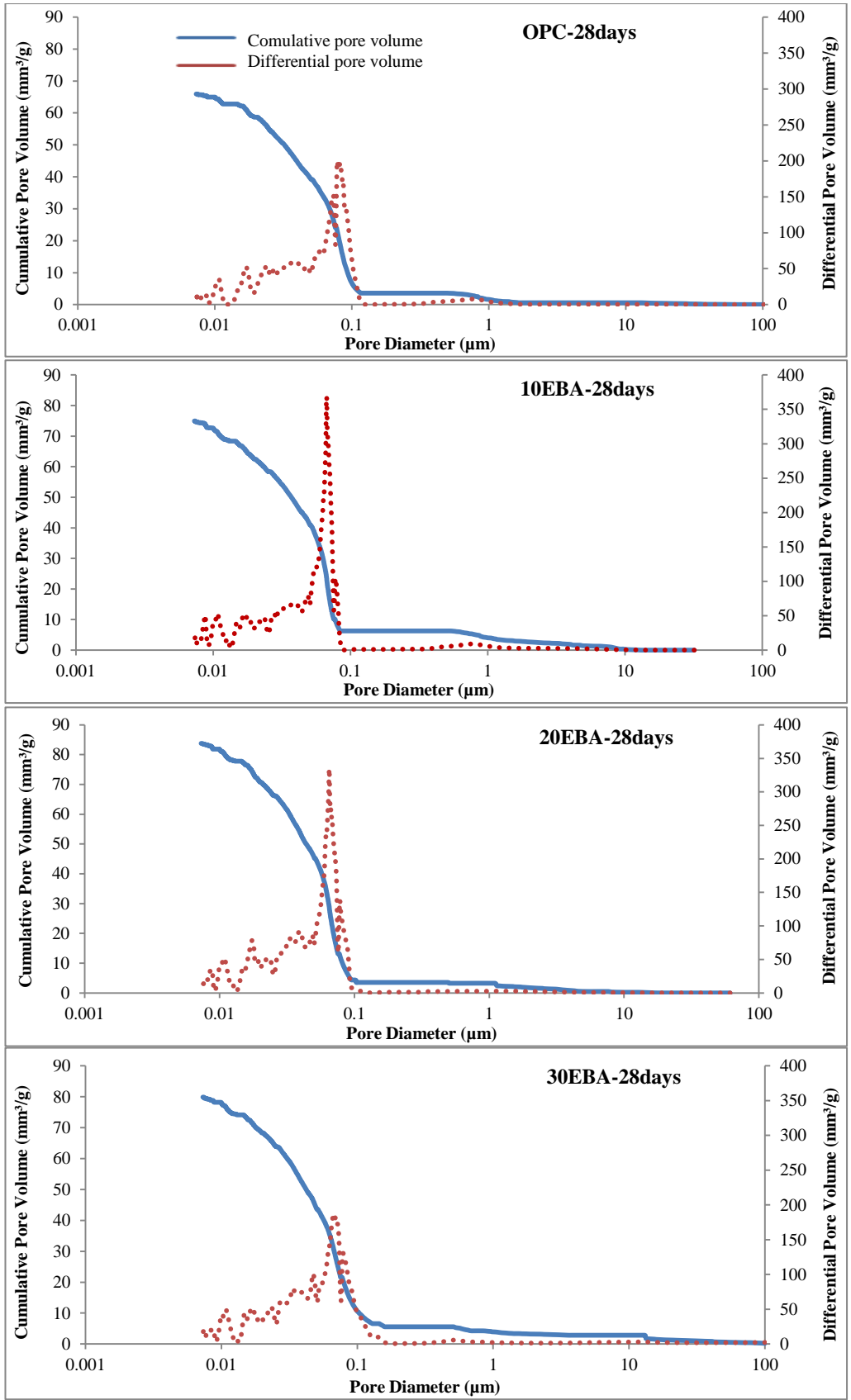
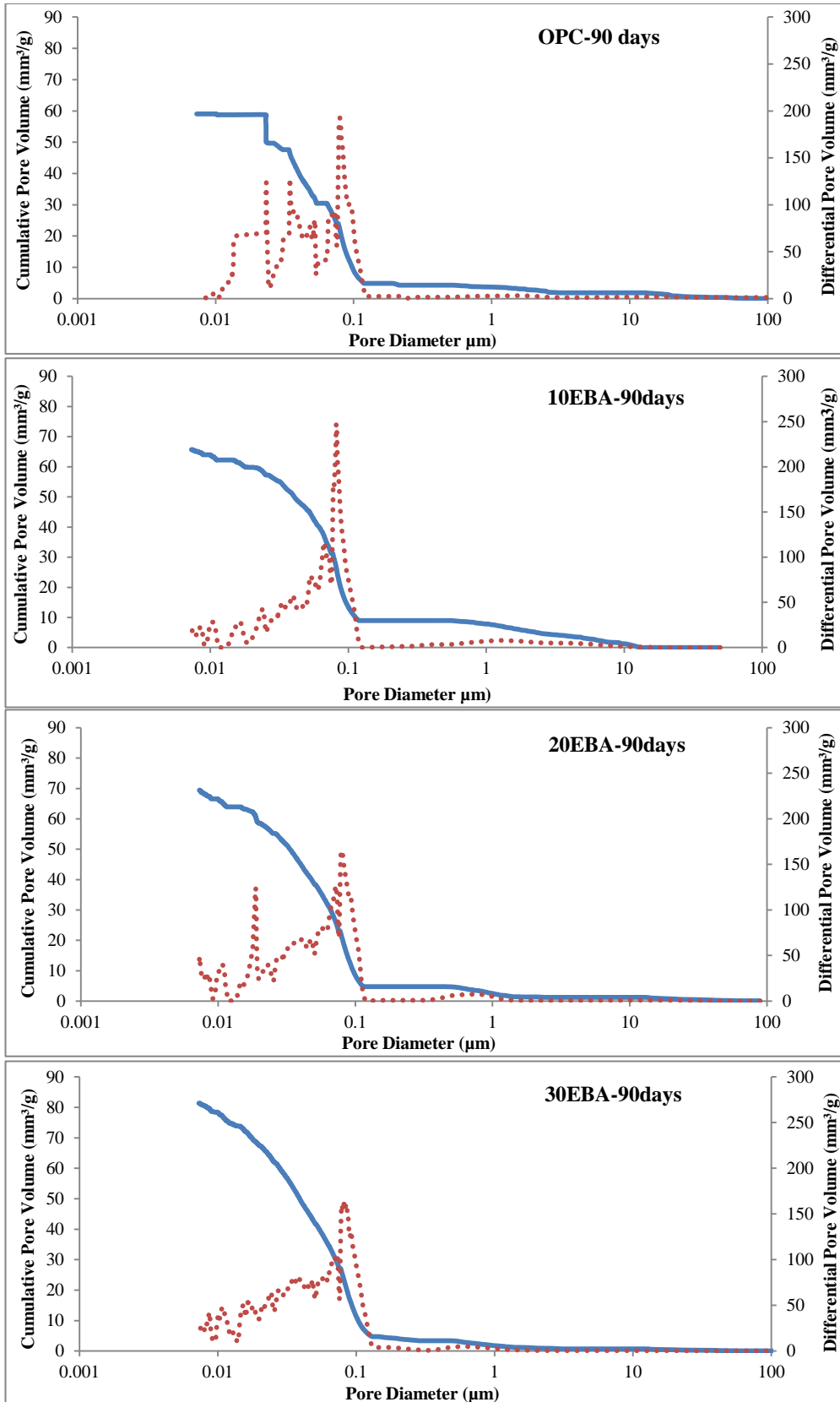


Figure 4.16 The differential and cumulative pore volume curves of OPC and EBA cement pastes at 28 days of curing



**Figure 4.17** The differential and cumulative pore volume curves of OPC and EBA cement pastes at 90 days of curing

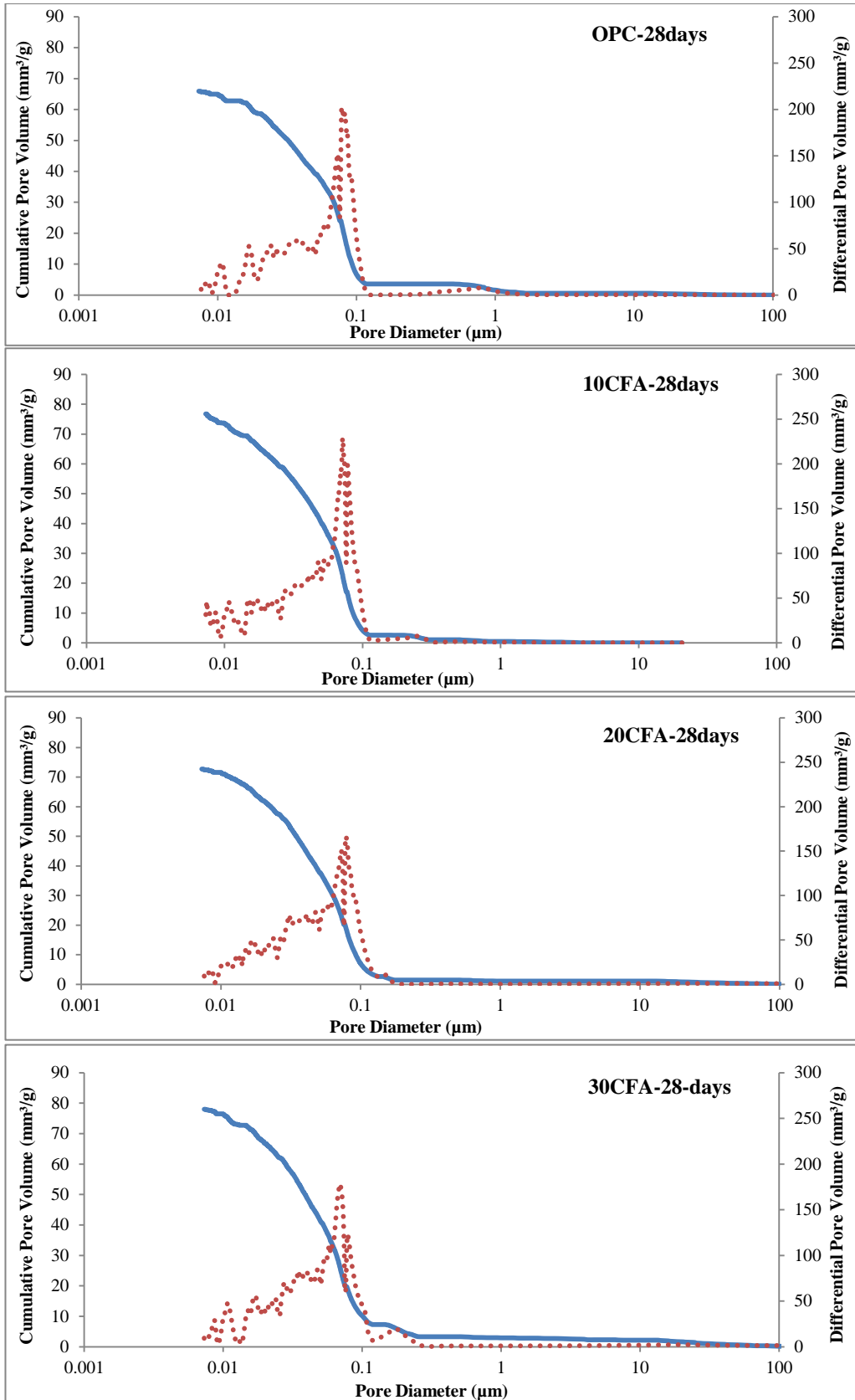


Figure 4.18 The differential and cumulative pore volume curves of OPC and CFA cement pastes at 28 days of curing

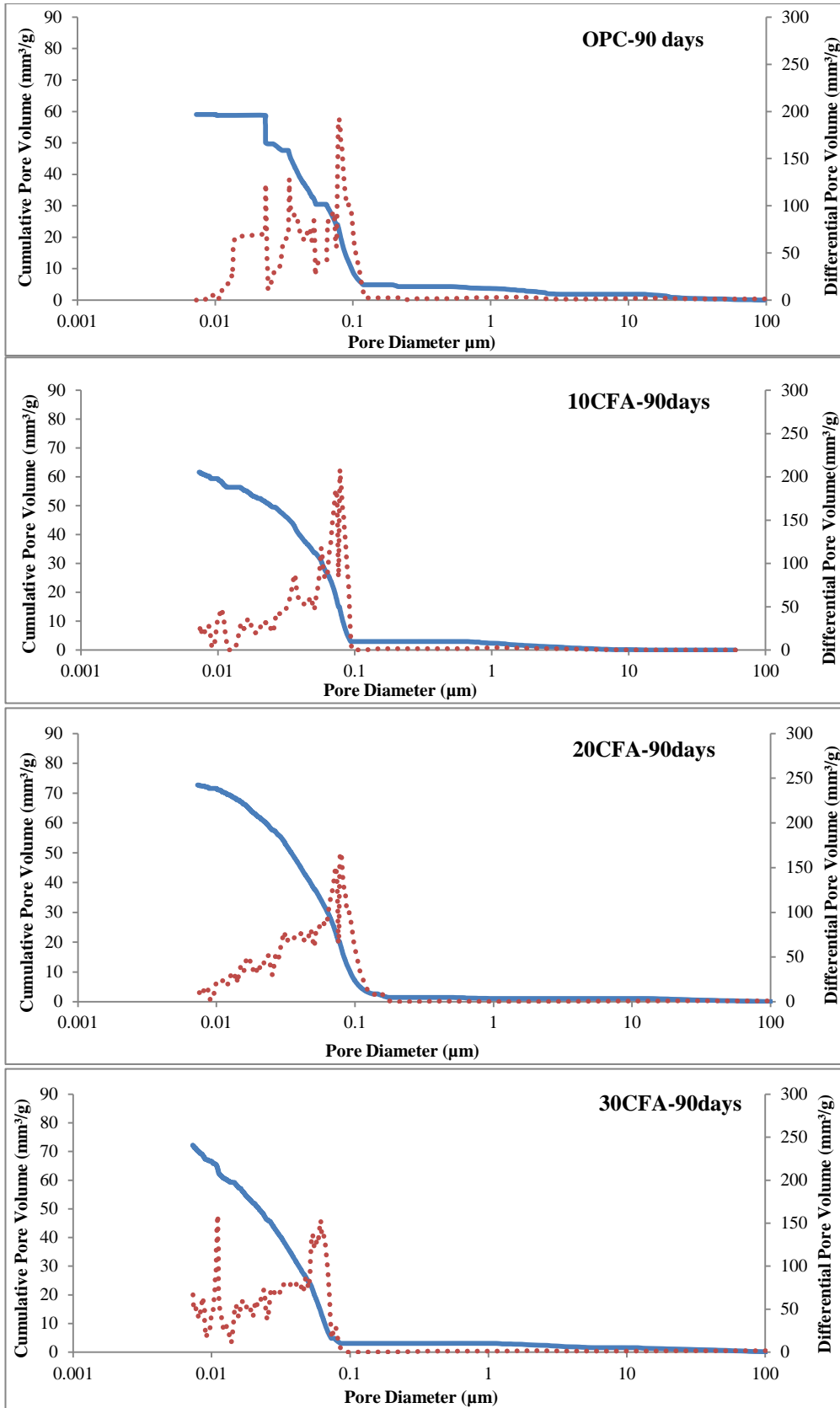
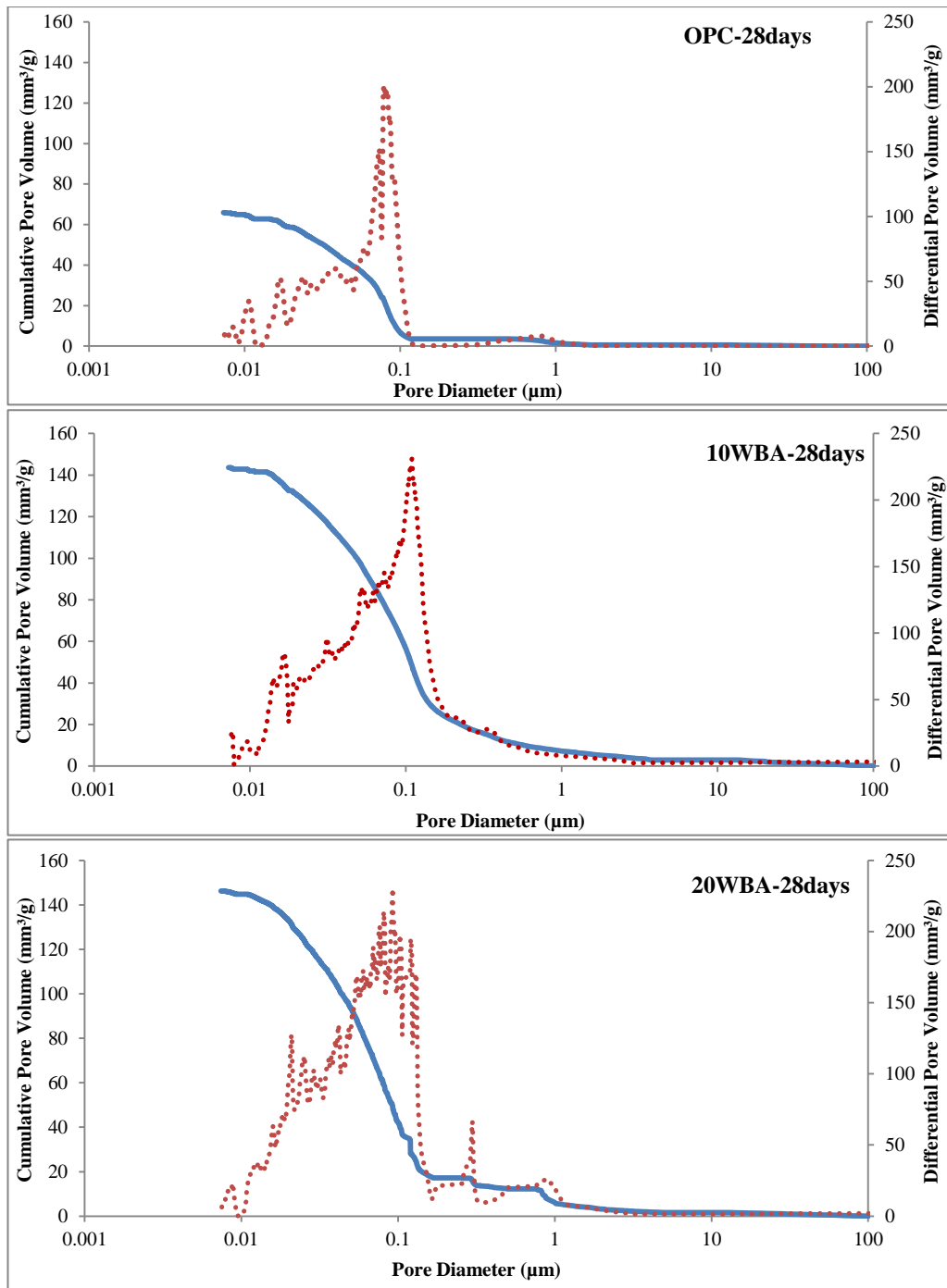
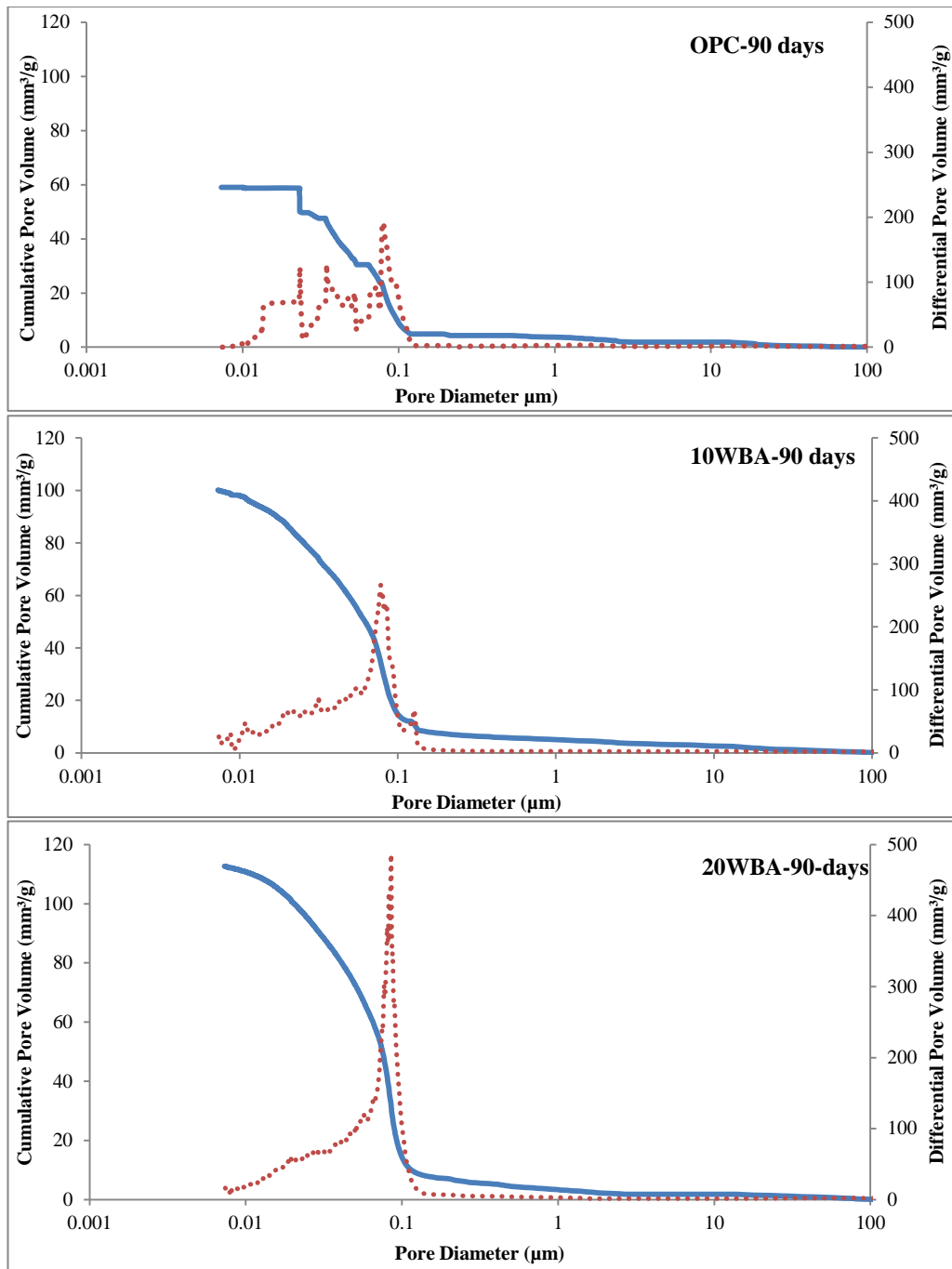


Figure 4.19 The differential and cumulative pore volume curves of OPC and CFA cement pastes at 90 days of curing



**Figure 4.20** The differential and cumulative pore volume curves of OPC and WBA cement pastes at 28 days of curing



**Figure 4.21** The differential and cumulative pore volume curves of OPC and WBA cement pastes at 90days of curing

It is clear that the shape of the differential pore volume curve for OPC paste at 90 days looks a bit odd at the end which suggests that an experimental error with the test in the high- pressure stage (Pascal 240). The curve flattened in the region of 0.01 µm where it is expected to have a shape similar to the 28 days sample.

#### 4.4.4. Hydrated Phases

The mineralogical composition of control OPC and blended fly ash cement pastes at 28 and 90 days of curing was analysed by means of X- ray Diffraction (XRD) analysis followed by quantitative X- ray diffraction (QXRD) using Rietveld method. The XRD patterns on all samples had relatively weak peaks and high backgrounds; this suggests a high "amorphous" (non- crystalline) component in the samples. This is confirmed by the quantitative phase analyses using the Rietveld method to determine the percentage of amorphous contents in these samples. The amorphous contents of all samples at 90 days are presented in Table 4.8. It shows that the control OPC paste has the highest amorphous content with 91.3% while the 20% WBA substitution has the lowest content at 79.72%.

**Table 4.8 The amorphous and CH contents of all paste samples at 90 days**

Mix ID	Amorphous content (%)	Ca(OH) <sub>2</sub> (%)
OPC	91.3	19.76
10BFA	85.28	16.87
20BFA	86.28	14.60
30BFA	82.16	15.85
10CFA	87.4	15.72
20CFA	87.52	13.58
30CFA	85.48	12.85
10WBA	82.31	19.6
20WBA	79.72	18.2

Diffraction patterns of all blended fly ash pastes show the presence of the same phases that are found in control OPC paste. Table 4.9 shows the main crystalline phases of the pastes, the prominent peaks are quartz, portlandite, and calcite. Peaks from Gypsum, Haturite were also found.

Generally, CH or calcium hydroxide  $\text{Ca(OH)}_2$  is the main hydration product formed during the hydration reaction. Therefore, the amount and intensity of  $\text{Ca(OH)}_2$  give an indication of the degree of hydration. The pozzolanic reaction of fly ash can be monitored by the decrease of the amount of  $\text{Ca(OH)}_2$  in the mix. Table 4.8 shows the decrease in the quantity of  $\text{Ca(OH)}_2$  in all blended fly ash mixes compared to control OPC. The percentage of portlandite decreased with increasing content of fly ash. It is clear that the pozzolanic reactivity of WBA is the lowest compared to EBA and CFA as the quantity of  $\text{Ca(OH)}_2$  is higher indicating less pozzolanic reaction.

The intensity peaks of  $\text{Ca(OH)}_2$  appeared at  $18.1^\circ$ ,  $28.8^\circ$ ,  $34.14^\circ$ ,  $47.8^\circ$  and  $50.9^\circ$  of  $2\theta$  in the XRD patterns of control OPC and all blended fly ash cement pastes as can be seen in Figures 4.22 to 4.25.

**Table 4.9 Main crystalline phases of the pastes**

Crystalline phase	Chemical formula
Quartz(Q)	$\text{SiO}_2$
Portlandite(CH)	$\text{Ca(OH)}_2$
Calcite	$\text{CaCO}_3$
Haturite(CS)	$\text{Ca}_3\text{SiO}_5$
Gypsum	$\text{CaSO}_4 \cdot 2\text{H}_2\text{O}$

Figure 4.22 shows the XRD patterns of control OPC paste at 28 and 90 days. It shows an increase in the peak intensities of  $\text{Ca(OH)}_2$  with curing time due to the continuous hydration of  $\text{C}_2\text{S}$  and  $\text{C}_3\text{S}$  [27]. At 28 days, the  $\text{Ca(OH)}_2$  intensity peaks of all blended fly ash pastes were almost similar to that of OPC and are not significantly affected by the incorporation of fly ash. This is because the hydration reaction was dominant at early age while the pozzolanic reaction was minimal [28]. At 90 days, the intensity peaks of  $\text{Ca(OH)}_2$  decreased by the inclusion of fly ash compared to control OPC peaks as shown in Figures 4.23 to 4.25. As the content of fly ash increases, the  $\text{Ca(OH)}_2$  content decreases gradually. This is due to the decrease in OPC which is the main source of  $\text{Ca(OH)}_2$  and the enhanced rate of pozzolanic reaction with increasing age of hydration [27, 28]. In addition, the results

indicate that CFA was more effective in reducing the intensity peaks of  $\text{Ca}(\text{OH})_2$  due to greater consumption of  $\text{Ca}(\text{OH})_2$  caused by higher pozzolanic reactivity of the fly ash with greatest fineness. This can explain why CFA, which had a smaller particle size and higher amorphous content, was more reactive than EBA and WBA. Studies on the effect of coal fly ash fineness on microstructure of hardened blended cement pastes have also shown that high fineness accelerates the pozzolanic reaction leading to high  $\text{Ca}(\text{OH})_2$  consumption [28].

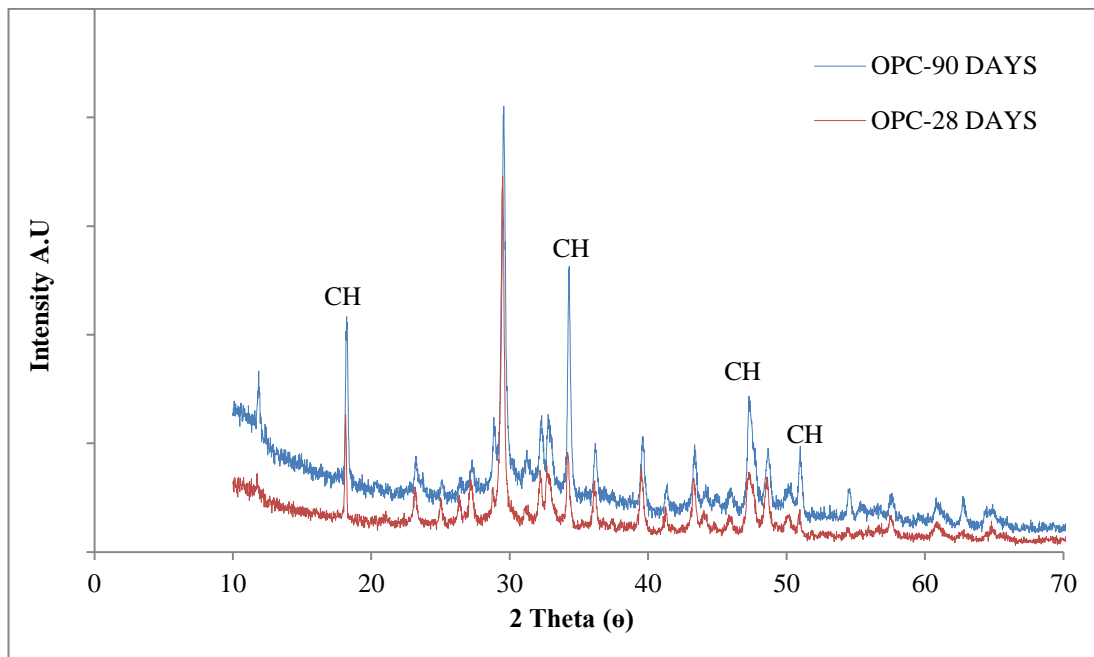


Figure 4.22 XRD of OPC paste at 28, 90 days of curing

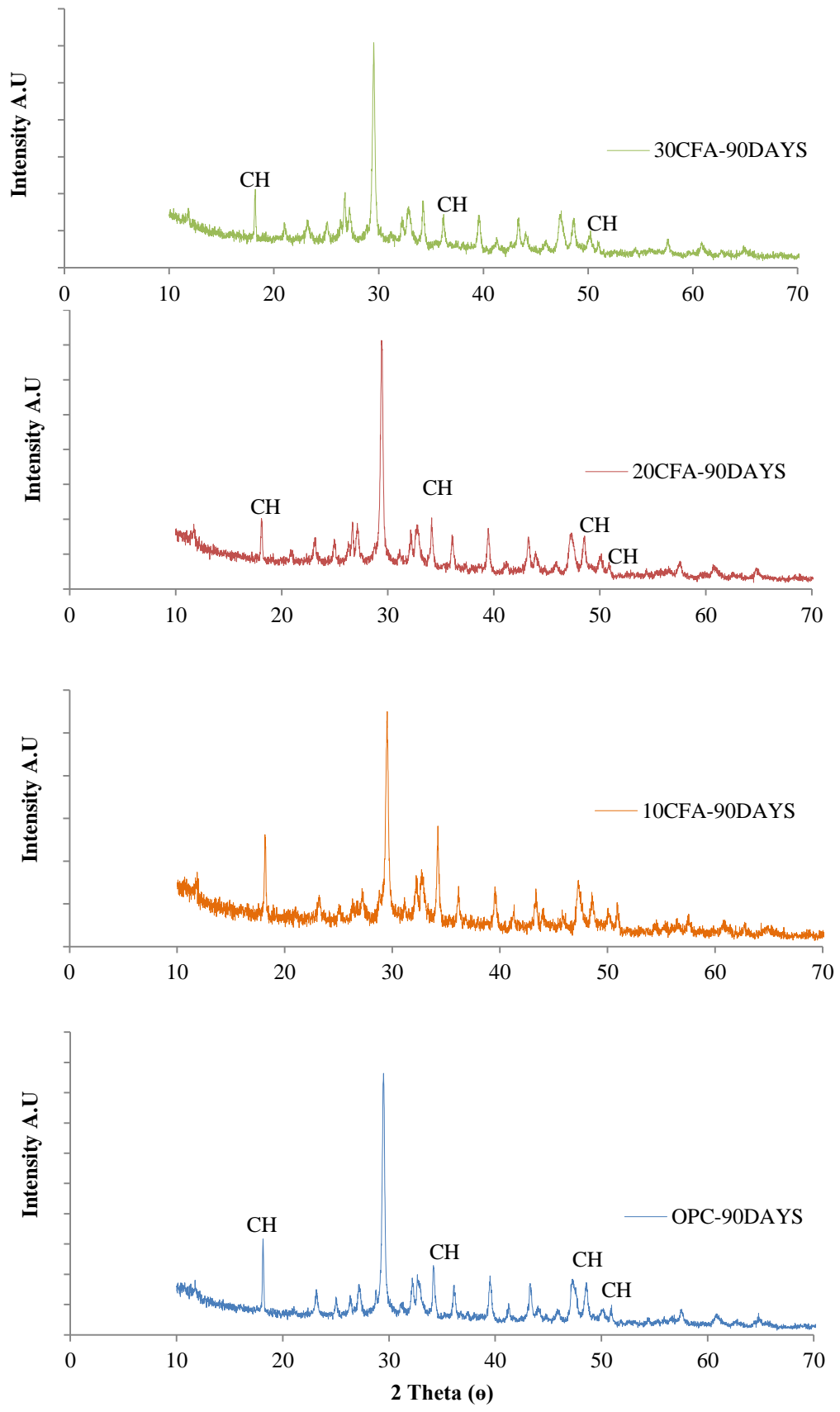


Figure 4.23 XRD of OPC, 10, 20, 30 CFA at 90 days of curing

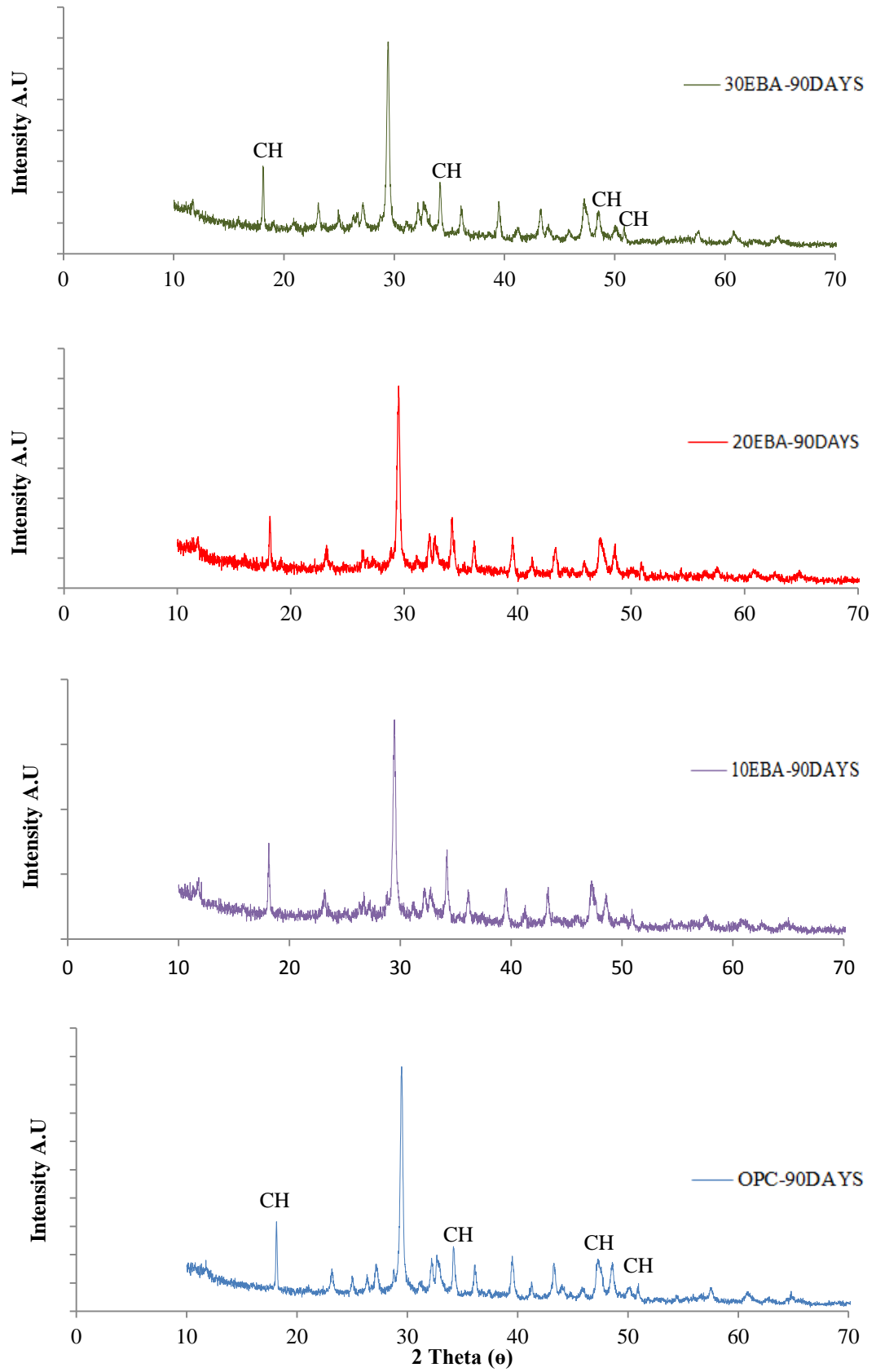


Figure 4.24 XRD of OPC, 10, 20, 30 EBA at 90 days of curing

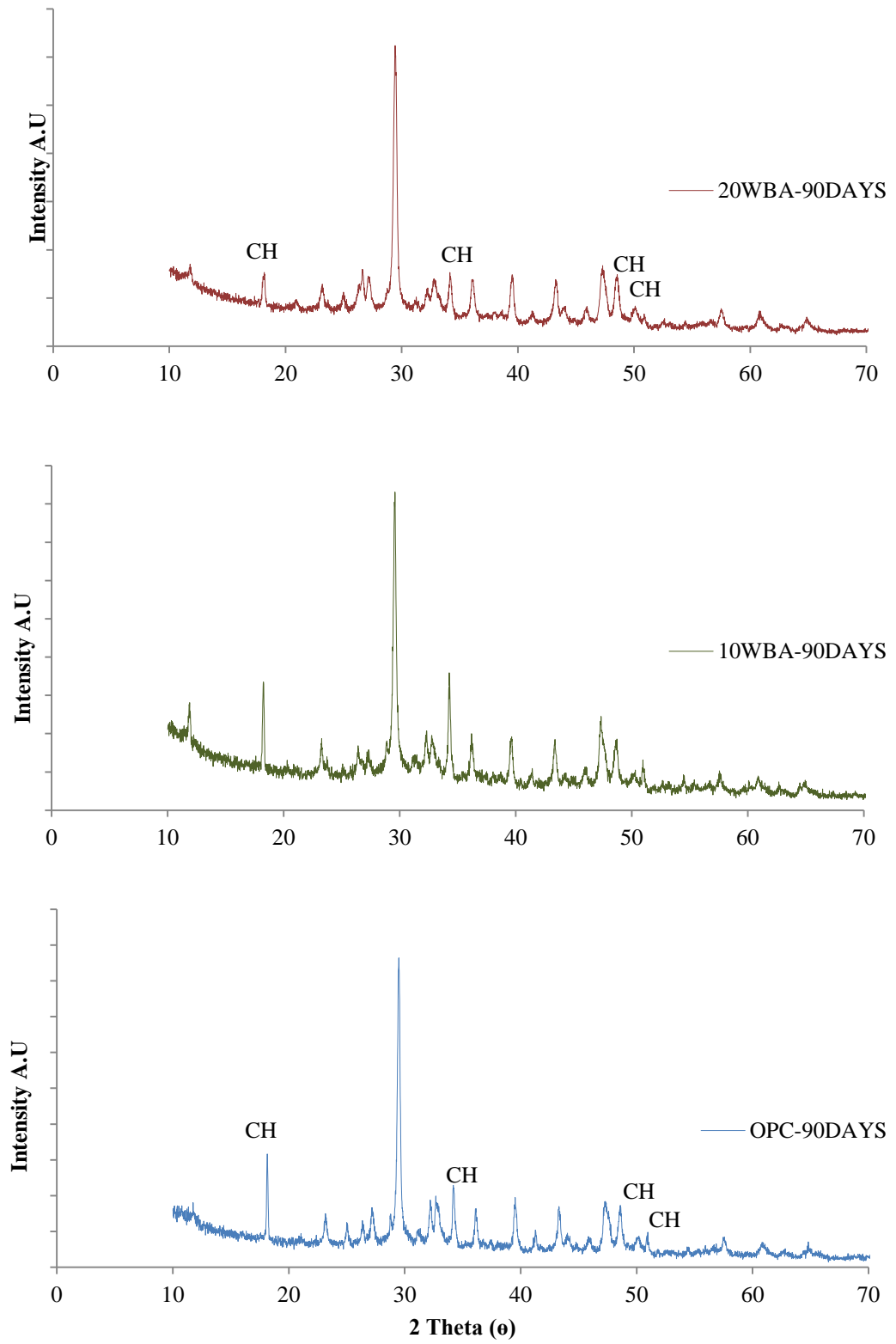


Figure 4.25 XRD of OPC, 10, 20 WBA at 90 days of curing

## 4.5. Conclusions

The partial replacement of Portland cement by enhanced biomass (EBA), wood biomass (WBA) and coal (CFA) fly ash was investigated and compared in terms of their impact on the fresh and hardened properties. The main conclusions derived from the results can be summarized as follows:

- **Water demand, setting time and flow(workability)**

1. The water demand decreases with increasing content of EBA and CFA in the mix while the initial and final setting time increases.
2. The coarse and high surface area of WBA particles contribute to its higher water requirement and accelerate the initial and final setting time.
3. The mortar workability (flow) increases with increasing fly ash content due to decrease in water demand of EBA and CFA mixes. This can be attributed to the spherical glass structure of both ashes.
4. High LOI, high water demand and non - spherical morphology of WBA reduces the workability.

- **Heat of hydration**

1. The early age hydration behaviour of EBA is quite similar to CFA. Both delay cement hydration and generate less heat than OPC.
2. The peak heat decreases as the content of fly ash increases indicating a reduction in the hydrating phases of the fly ash cement pastes.
3. The CFA and EBA mixes release considerably higher heat than WBA mixes over the first 72h indicating a higher rate of hydration of CFA and EBA compared to WBA.
4. 10% and 20% WBA mixes produce higher cumulative (total) heat than OPC during the first 5hrs due to the high water demand along with the high surface area.

- **Strength development**

1. The compressive and flexural strength decreases gradually as the percentage of fly ash in the mix increases.

2. The long term strength increases due to the acceleration of pozzolanic reaction; the rate of strength gain depends on the level of cement replacement.
3. The compressive strength of CFA mixes is higher than EBA mixes while WBA mixes give the lowest strength.
4. The superior strength of CFA mortars compared to EBA and WBA can be attributed to its higher fineness and a relatively higher amorphous content.

- **Microstructure development**

1. The incorporation of CFA, EBA and WBA increase the total porosity of cement pastes. The total porosity of OPC paste is the lowest of all blended fly ash pastes.
2. The porosity of CFA pastes is less than EBA and WBA pastes due to the higher degree of pozzolanic reaction of CFA compared to both biomass ashes (EBA and WBA).
3. The additional (C-S-H) hydrations products, resulting from the pozzolanic reaction of fly ashes, fill the open capillary pores and improve the pore structure. CFA is more effective than both EBA and WBA in refining the pore structure.

- **Hydrated phases**

1. Diffraction patterns of all blended fly ash pastes show the presence of the same phases that are found in control OPC paste. The main crystalline phases of all pastes are quartz, portlandite,  $\text{Ca(OH)}_2$ , and calcite.
2. The intensities of  $\text{Ca(OH)}_2$  peaks decrease with the partial substitution of OPC by EBA, CFA and WBA due to the decrease of OPC content which is the main source of  $\text{Ca(OH)}_2$ .
3. CFA is more effective in reducing the intensity peaks of  $\text{Ca(OH)}_2$  due to greater consumption of  $\text{Ca(OH)}_2$  caused by higher pozzolanic reactivity of the fly ash.

4. The pozzolanic reaction of fly ashes is indicated by the decrease of  $\text{Ca(OH)}_2$  in the mix. The pozzolanic reactivity of WBA is the lowest compared to EBA and CFA as the quantity of  $\text{Ca(OH)}_2$  is higher.

#### 4.6. References

1. BS EN 196-1 (2016) Methods of Testing Cement Part 1: Determination of Strength. Br Stand. doi: 10.1590/S1413-294X2011000200001
2. Rajamma R (2011) Biomass fly ash incorporation in cement based materials, PhD Thesis. Department of Ceramics and Glass Engineering, University of Aveiro
3. BS EN 196-3 (2016) Methods of testing cement — Part 3: determination of setting times and soundness. Br Stand 1–18 . doi: 10.1111/j.1748-720X.1990.tb01123.x
4. BS EN 1015-3 (2006) Methods of test for mortar for masonry — Part 3: Determination of consistence of fresh mortar (by flow table). Br Stand
5. BS EN 450 (2012) Fly ash for concrete Part 1 : Definition , specifications and conformity criteria. BS EN Stand
6. ASTM (2017) C1702-17: Standard test method for measurement of heat of hydration of hydraulic cementitious materials using isothermal conduction calorimetry. 1–9 . doi: 10.1520/C1702-17.2
7. Wang S (2007) Biomass and Coal Fly Ash in Concrete : Strength , Durability , Microstructure , Quantitative Kinetics of Pozzolanic Reaction and Alkali Silica Reaction Investigations . PhD Thesis, Department of Chemical Engineering, Brigham Young University
8. Shearer CR (2014) The Productive Reuse of Coal , Biomass and Co-Fired Fly Ash. PhD Thesis, School of Civil & Environmental Engineering, Georgia Institute of Technology
9. Elinwa AU, Mahmood YA (2002) Ash from timber waste as cement replacement material. Cem Concr Compos 24:219–222 . doi: 10.1016/S0958-9465(01)00039-7
10. Rajamma R, Ball RJ, Tarelho LAC, Allen GC, Labrincha JA, Ferreira VM (2009) Characterisation and use of biomass fly ash in cement-based materials. J Hazard Mater 172:1049–1060 . doi: 10.1016/j.jhazmat.2009.07.109

11. Hamood A, Khatib JM, Williams C (2017) The effectiveness of using Raw Sewage Sludge (RSS) as a water replacement in cement mortar mixes containing Unprocessed Fly Ash (u-FA). *Constr Build Mater* 147:27–34 . doi: 10.1016/j.conbuildmat.2017.04.159
12. Elinwa AU, Ejeh SP, Mamuda AM (2008) Assessing of the fresh concrete properties of self-compacting concrete containing sawdust ash. *Constr Build Mater* 22:1178–1182 . doi: 10.1016/j.conbuildmat.2007.02.004
13. Shearer CR, Yeboah N, Kurtis KE, Burns SE (2011) The Early Age Behavior of Biomass Fired and Co-fired Fly Ash in Concrete. *World Coal Ash*
14. R C Joshi RPL (1997) Fly Ash in Concrete-Production, Properties and Uses. Gordon and Breach Science Publishers
15. Shearer CR, Kurtis KE (2015) Use of Biomass and Co-Fired Fly Ash in Concrete. *ACI Mater Journal*, V 112 209–218 . doi: 10.14359/51686827
16. Rajamma R, Senff L, Ribeiro MJ, Labrincha JA, Ball RJ, Allen GC, Ferreira VM (2015) Biomass fly ash effect on fresh and hardened state properties of cement based materials. *Compos Part B* 77:1–9 . doi: 10.1016/j.compositesb.2015.03.019
17. Felix F. Udoeyo; Hilary Inyang; David T. Young; and Edmund E. Oparadu (2006) Potential of Wood Waste Ash as an Additive in Concrete. *J Mater Civ Eng*. doi: [https://doi.org/10.1061/\(ASCE\)0899-1561\(2006\)18:4\(605\)](https://doi.org/10.1061/(ASCE)0899-1561(2006)18:4(605))
18. Yu Z, Ma J, Ye G, van Breugel K, Shen X (2017) Effect of fly ash on the pore structure of cement paste under a curing period of 3 years. *Constr Build Mater* 144:493–501 . doi: 10.1016/j.conbuildmat.2017.03.182
19. Chindapasirt P, Rukzon S (2009) Pore Structure Changes of Blended Cement Pastes Containing Fly Ash , Rice Husk Ash , and Palm Oil Fuel Ash. *J Mater Civ Eng* 21:666–671 . doi: 10.1061/(ASCE)0899-1561-(2009)21:11(666)
20. Chindapasirt P, Jaturapitakkul C, Sinsiri T (2005) Effect of fly ash fineness on compressive strength and pore size of blended cement paste. *Cem Concr Compos* 27:425–428 . doi: 10.1016/j.cemconcomp.2004.07.003
21. Mangat P, Lambert P (2016) 18 – Sustainability of alkali-activated

cementitious materials and geopolymers, Second Edi. Elsevier Ltd.

22. Mangat PS, Ojedokun OO (2018) Influence of curing on pore properties and strength of alkali activated mortars. *Constr Build Mater* 188:337–348 . doi: 10.1016/j.conbuildmat.2018.07.180
23. Kalliopi k, Aligizaki (2006) Pore structure of cement based materials. Taylor & Francis
24. Mehta PK, Monteiro PJM (2003) *Concrete , Microstructure, Properties, and Materials*. McGraw-Hill Publishing
25. Yu Z, Ye G (2013) The pore structure of cement paste blended with fly ash. *Constr Build Mater* 45:30–35 . doi: 10.1016/j.conbuildmat.2013.04.012
26. Khatib JM, Wright L, Mangat P (2016) Effect of desulphurised waste on long-term porosity and pore structure of blended cement pastes. *Sustain Environ Res* 26:230–234 . doi: 10.1016/j.serj.2016.02.002
27. Abo-El-Enein SA, El-kady G, El-Sokkary TM, Ghariieb M (2015) Physico-mechanical properties of composite cement pastes containing silica fume and fly ash. *HBRC J* 11:7–15 . doi: 10.1016/j.hbrcj.2014.02.003
28. Chindaprasirt P, Jaturapitakkul C, Sinsiri T (2007) Effect of fly ash fineness on microstructure of blended cement paste. *21:1534–1541* . doi: 10.1016/j.conbuildmat.2005.12.024

# CHAPTER 5 CARBONATION OF ENHANCED BIOMASS FLY ASH CONCRETE

## 5.1. Introduction

Carbonation has been recognized as one of the main causes of concrete deterioration and reinforcement corrosion. Generally, all cement-based materials undergo a certain level of carbonation during the in-service life which affects the durability of the concrete structure. Carbonation takes place in the surface layers of concrete and proceeds inwards at a slow rate due to the diffusion of atmospheric carbon dioxide,  $\text{CO}_2$ , into concrete and its reaction with the main hydration products of cement paste,  $\text{Ca}(\text{OH})_2$  and C-S-H, to form insoluble calcium carbonate,  $\text{CaCO}_3$ . This reaction results in induced stresses in cement paste and a reduction in the pH (alkalinity) of concrete which is essential to protect the steel reinforcement from corrosion [1, 2]. The steel reinforcement will be prone to corrosion when the carbonation front progresses up to it and lowers the pH [1, 3]. In addition, the induced stresses in cement paste can cause shrinkage and cracking of the cementitious matrix, however, the magnitude of carbonation shrinkage in concrete is small compared to its long-term drying shrinkage.

Carbonation has a positive impact on some of the engineering properties of concrete. It reduces the total porosity as the volume of calcium carbonate (carbonation reaction product) is greater than the original hydration product (calcium hydroxide). In addition,  $\text{CO}_2$  accelerates the hydration reaction of  $\text{C}_3\text{S}$  and  $\text{C}_2\text{S}$  which results in rapid strength gain, therefore, carbonation curing of OPC concrete is sometimes used to improve some properties such rapid strength gain [3, 4]. The concrete density, quality, age and the surrounding environmental conditions (temperature and humidity) have the main influence on the rate of carbonation [5, 6]. The rate of carbonation is very slow since the  $\text{CO}_2$  concentration in the atmosphere is very low (approximately 0.04 %). Therefore, an accelerated carbonation test is used to simulate the carbonation in service life, then, the actual rate of carbonation can be calculated by knowing the ratio between the accelerated  $\text{CO}_2$  concentration and the atmospheric  $\text{CO}_2$  concentration (0.04 %) [7].

This chapter aims to investigate the influence of enhanced biomass ash (EBA) on the resistance of concrete to carbonation. A parallel investigation on control samples of commercial coal fly ash (CFA) and normal OPC concrete designed for similar strength was also conducted for comparison.

## **5.2. Experimental Programme**

The aim of the experimental programme is to investigate the effect of enhanced biomass fly ash (EBA) on the carbonation resistance of concrete in terms of carbonation depth and carbonation shrinkage. An accelerated carbonation process of the samples is used since, in practice, the process is too slow under ambient conditions due to the low CO<sub>2</sub> concentration in the atmosphere (approximately 0.04 %). The samples were exposed to 3- 4% CO<sub>2</sub> in a carbonation chamber, the temperature and relative humidity in the chamber were controlled at 20 ± 2 °C and 50-70%, respectively. The 4 % CO<sub>2</sub> concentration is 100 times higher than the atmospheric concentration of 0.04 %. BS 1881-210 [8] test procedures were used in this investigation. The depth of carbonation was determined at regular intervals of exposure by using 0.1% alcoholic solution of phenolphthalein indicator as a standard method used to locate the carbonation front. The standard method for measuring drying shrinkage BS ISO 1920-8 [9] of concrete was used to measure carbonation shrinkage since there is no specific method to measure the carbonation shrinkage of concrete.

### **5.2.1. Materials**

Ordinary Portland cement (CEM I: 52.5 N) conforming to EN 197-1, supplied by Rugby cement, was used as the main binder. Enhanced biomass fly ash (EBA) generated from Drax power station which is one of the UK's largest energy producers and commercial coal fly ash (CFA) supplied by Power Minerals Ltd were used as supplementary cementitious materials. Locally supplied sharp medium grade siliceous sand and 10 mm nominal size gravel aggregate supplied by Frank Key were used as fine and coarse aggregates. Further information on the materials is given in chapters 3 and 4.

### 5.2.2. Mix Design and Proportions

The DOE (Department of Environment) [10] method for concrete mix design was used to design a grade 40 MPa mix of normal OPC concrete and fly ash concrete with 20 % cement replacement. This method gives mix design procedures for normal concrete and modification for mixes with fly ash. A part of cement was replaced by fly ash along with an adjustment in the amount of fine aggregate and water. Therefore, the fly ash concrete mix had a total binder weight (cement + fly ash) higher than the weight of cement in the control OPC mix to overcome the reduction in early age strength [11, 12]. Trial mixes were performed to achieve practical workability with the required strength prior to selection of the mix proportions used for the experimental investigation. The mix proportions used in one cubic meter of the control OPC and fly ash concrete are presented in Table 5.1.

**Table 5.1 Mix proportions**

MIX	Cement (kg/m <sup>3</sup> )	Fly ash (kg/m <sup>3</sup> )	Fine aggregate (kg/m <sup>3</sup> )	Coarse aggregate (kg/m <sup>3</sup> )	Water (kg/m <sup>3</sup> )	Effective water to binder ratio W/(C+kF)*
OPC	368	0	732	1100	180	0.49
20EBA	323	81	680	1136	170	0.49
20FCA	323	81	680	1136	170	0.49

\* The k value is given in the design guide for adjusting the amount of fly ash (K= 0.3).

### 5.2.3. Mixing

All aggregates were in a saturated surface dry state before mixing. Half of the aggregate content was first poured inside cretangle concrete mixer of 150 Kg capacity followed by the binder composition. The binder (fly ash + cement) were first mixed together by hand until homogeneity was achieved. The remaining half of the aggregate content was then added to cover the binder before the start of mixing for one minute. The water was added carefully while mixing continued for an extra two minutes. To ensure homogeneity, the mix was briefly mixed by hand to remove

accumulated materials sticking around the edge and corner of the mixer. The mixture was then mixed for a further two minutes before casting.

#### **5.2.4. Sample Preparation**

Nine concrete prismatic specimens of size 75 x 75 x 300 mm were cast for each mix. Three samples were for carbonation depth measurements, three for carbonation shrinkage measurements and the last three for drying shrinkage measurements. Prior to casting, all moulds were slightly lubricated with mould oil. The mix was placed in two layers; each layer was compacted using a vibrating table for 5 seconds. Then, all specimens were covered with a plastic sheet to prevent drying and stored in the laboratory environment at  $20 \pm 2^\circ\text{C}$  and 65 % RH. All samples were demoulded after 24h and cured in water at  $20^\circ\text{C}$ . After 7 days of water curing, the specimens were put into two groups. The first group of six specimens were removed from water and allowed to dry in the laboratory air for carbonation and drying shrinkage measurements. The second group of three specimens was cured in water for 28 days, then removed and allowed to cure for 14 days in the laboratory air ( $20 \pm 2^\circ\text{C}$  and 65% RH) for carbonation depth measurements.

##### **5.2.4.1. Carbonation Depth Specimens**

After removing and drying the prism samples (group 2), the top and bottom longitudinal faces and the two end faces of the samples were sealed with two coats of bitumen paint. The remaining two side faces were left uncoated as shown in Figure 5.1 to be exposed to  $\text{CO}_2$ . The samples were left in the laboratory to dry the bitumen coating for two days followed by 14 days air curing as suggested in the standard BS 1881-210 [8] before the exposure to accelerated carbonation inside a carbonation chamber (Figure 5.2) for one year. The accelerated carbonation tests were started at 45 days age of the specimens. The concentration of  $\text{CO}_2$  in the chamber was maintained at 3- 4%, the temperature and humidity were kept at  $20 \pm 2^\circ\text{C}$  and 50 – 70% respectively. The carbonation depth was determined by using phenolphthalein indicator method at 90, 180, 240, 300 and 360 days of accelerated carbonation exposure.



**Figure 5.1** Four faces coated with bitumen paint and the remaining two side longitudinal faces left uncoated.



**Figure 5.2** The samples exposed to 3- 4 % CO<sub>2</sub> inside the carbonation chamber

#### **5.2.4.2. Carbonation and Drying Shrinkage Specimens**

After 7 days of water curing, the samples were removed from water and dried. Mechanical stainless steel studs (demec points) were attached along the two parallel longitudinal (300 x 75mm) faces of each prism specimen at a gauge length of 200mm as shown in Figure 5.3. No bitumen paint was applied to the faces of samples. The carbonation shrinkage samples were left in the laboratory air at  $20 \pm 2^\circ\text{C}$  and 65 % RH to stabilize the moisture condition within the concrete matrix before exposing to CO<sub>2</sub>. Then, they were put inside the carbonation chamber at 45 days age together with carbonation test samples described in section 5.2.4.1. The readings of carbonation shrinkage were taken at regular intervals up to 300 days with

a demec extensometer. The test procedure for carbonation shrinkage is detailed in section 5.2.5.2.

The drying shrinkage samples were cured in the laboratory air at  $20 \pm 2^\circ\text{C}$  and 65% RH after the initial 7 days of water curing. The initial (datum) reading was recorded on day 7 after removing the samples from water and then, the readings of drying shrinkage were taken at regular intervals up to 200 days.

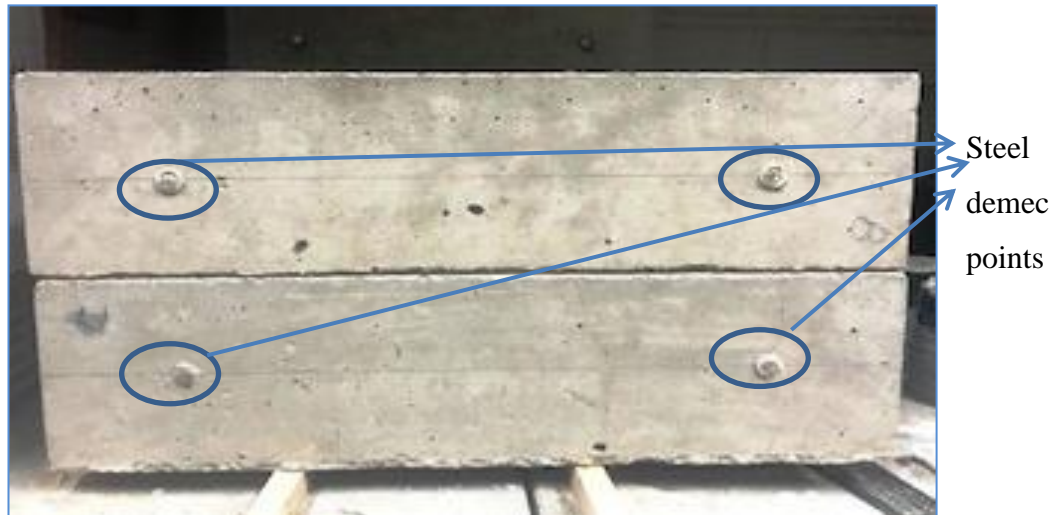


**Figure 5.3 Steel demec points attached along the two parallel longitudinal faces**

## **5.2.5. Experimental Procedures**

### **5.2.5.1. Carbonation Depth Measurement**

The carbonation depth was determined by the phenolphthalein indicator method at 90, 180, 240, 300 and 360 days of accelerated carbonation curing. After the process of accelerated carbonation, a 50 mm thick slice from one end of the prism length (300 mm) was split by applying a tensile split compression load across the cross-section of the prism. The split slice had a cross-section of 75 x 75 mm of the split face and length of 50 mm. A solution of 1g phenolphthalein indicator dissolved in 70ml ethyl alcohol and diluted with distilled water to 100 ml was sprayed on the freshly broken surfaces as shown in Figure 5.4. The phenolphthalein solution is colourless and used as an acid-base indicator. The colour of the solution changes into purple when the pH is higher than 9. Therefore, when the solution is sprayed on a broken concrete surface, the non-carbonated area turns purple whereas the

carbonated area does not change colour (Figure 5.4). The carbonation depth from the split faces was measured at different locations (eight points each side) after about 75 minutes of spraying the solution as shown in Figure 5.5. The average depth was calculated by taking the mean depth of carbonation for each face. Subsequently, the remaining whole prism (minus the split slice) was transferred back to the carbonation chamber for future carbonation measurements after resealing the split surface with bitumen paint as shown in Figure 5.6.

#### **5.2.5.2. Carbonation Shrinkage Measurement**

The existing method for drying shrinkage measurement was used for measuring the carbonation shrinkage since there is no standard method to measure the carbonation shrinkage of concrete. After 7 days of water curing followed by 38 days of laboratory air curing, the datum reading was taken before exposing the specimens to CO<sub>2</sub> in the accelerated carbonation chamber. Measurements were recorded at regular intervals using a demec extensometer. The carbonation shrinkage strain was determined by taking the difference between the datum reading and the periodical readings using the following equation:

$$\varepsilon = (X_0 - X_i) * G * 10^6 \quad 5.1$$

Where:  $\varepsilon$  is the shrinkage strain in microstrain;  $X_0$  is the initial (datum) gauge reading;  $X_i$  is the gauge reading at time  $t$  and  $G$  is the gauge factor of the extensometer.

The mean value of measurements taken on two opposite faces of three specimens is considered as carbonation shrinkage.

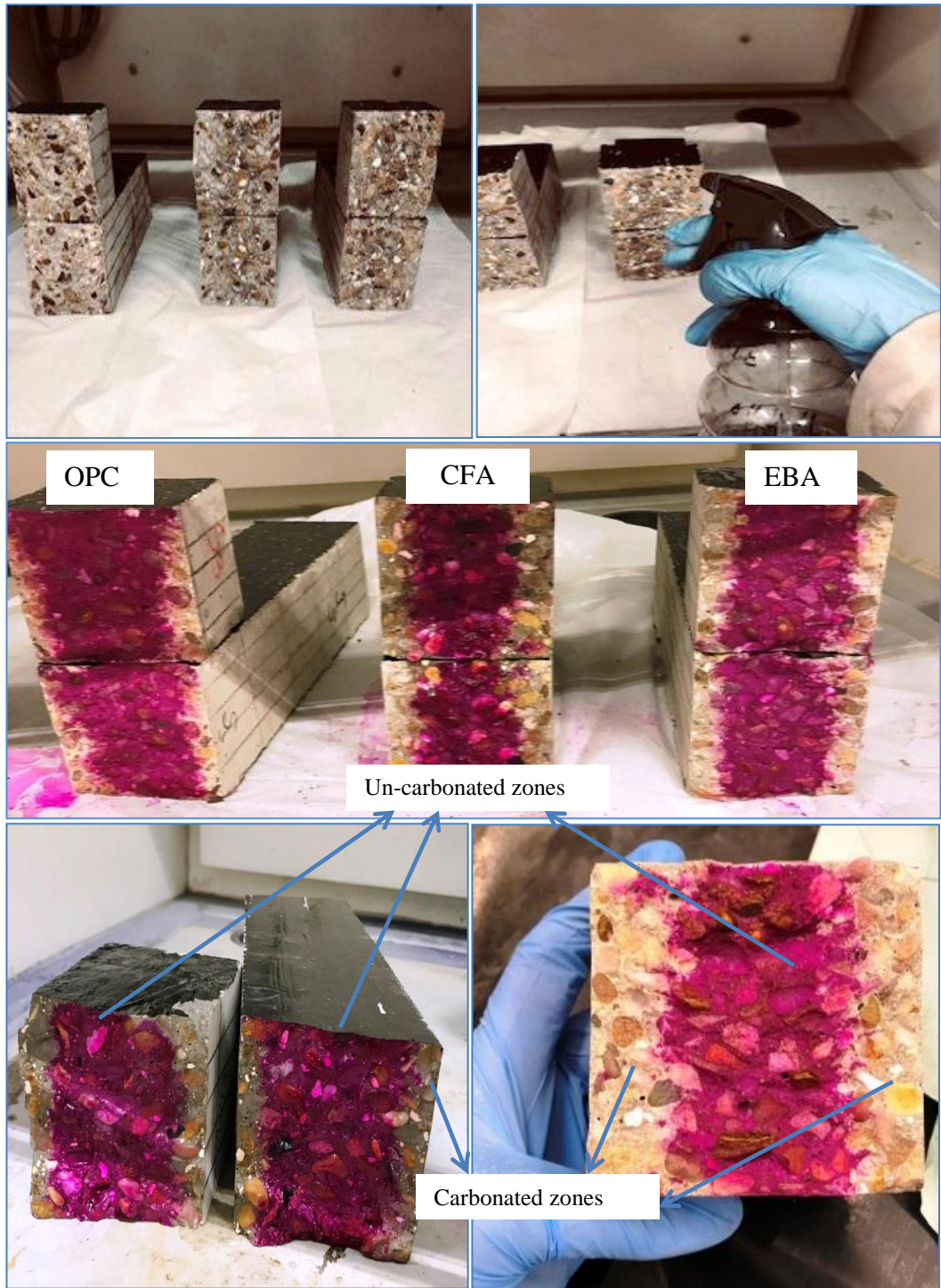


**Figure 5.4 Phenolphthalein indicator applied to the freshly cut faces**



**Figure 5.5 Carbonation depth measurements at different locations**



**Figure 5.6 The split surface of the samples resealed with bitumen paint**

### **5.3. Results and Discussion**

#### **5.3.1. Carbonation Depth**

The depth of carbonation for EBA, CFA and OPC mixes at different times of 4% CO<sub>2</sub> exposure is presented in Figure 5.7. The presented values are the average of 16 depths of carbonation readings from two cut faces of the specimen. Generally, the depth of carbonation for all mixes has increased with the duration of carbonation. A lower depth of carbonation was observed in OPC concrete mix compared to EBA

and CFA concrete mixes, which is consistent with the trend observed in concrete for various pozzolanic materials due to the reduction of  $\text{Ca(OH)}_2$  and PH [3]. After 90 days of  $\text{CO}_2$  exposure, the depth of carbonation is 4 mm for OPC concrete while it is 7.2 mm and 9.6 mm for EBA and CFA respectively. The corresponding values of the carbonation depth after one-year exposure are 11.8 mm, 15.2 mm and 19.75 mm respectively. The increase in carbonation depth in both EBA and CFA is due to a decrease in  $\text{Ca(OH)}_2$  caused by the pozzolanic reaction [1, 13, 14]. This dissipation of  $\text{Ca(OH)}_2$  decreases the alkalinity of concrete, thus resulting in higher carbonation [1]. The reaction in blended binders between the amorphous minerals (silica and alumina) present in both fly ashes and  $\text{Ca(OH)}_2$  produced from the hydration of cement, forms calcium-silicate-hydrate (C-S-H) gel, thereby leaving less free lime  $\text{Ca(OH)}_2$ . As a result, less  $\text{CO}_2$  is required to react with the remaining  $\text{Ca(OH)}_2$  to form calcium carbonate ( $\text{CaCO}_3$ ) [1, 15, 16]. Thus, the carbonation depth in both EBA and CFA is higher than OPC concrete. The increase in carbonation rate when replacing the cement with fly ash is not only because the calcium hydroxide is carbonated, but also the calcium silicate hydrate (C-S-H), which is the main product of the pozzolanic reaction, is also carbonated [3, 4, 17]. In addition, fly ash delays the hydration and increases the porosity of concrete which allows faster diffusion for  $\text{CO}_2$  in the pore system. Therefore, the higher porosity of fly ash concretes (EBA and CFA) as determined by MIP test and reported in chapter 4 also contributed to the increase in the depth of carbonation zone compared to OPC concrete.

Figure 5.7 shows that the highest average carbonation depth at all ages is exhibited by the CFA mix. The consumption of free lime  $\text{Ca(OH)}_2$  is highly influenced by the pozzolanic activity of the fly ash. The XRF results, given in chapter 3 (section 3.3.1), show that EBA has a lower silica content of 41.46% than 47.64% of CFA. In addition, the amorphous content of mineral, as determined by the Rietveld refinement method and presented in chapter 3 (section 3.3.2), is lower in EBA (84%) than in CFA (88%). Therefore, the lower carbonation depth of the EBA concrete compared to CFA concrete is because of the combined effect of its relatively lower pozzolanic activity due to its low silica content and lower chemical reaction caused by lower amorphous content. The carbonation depth is greater when the amount of  $\text{Ca(OH)}_2$  present in the mix is lower [16]. Although the porosity of EBA (12.18%) is

higher than CFA (11.02%), it shows better resistance against carbonation. This could be because the effect of  $\text{Ca}(\text{OH})_2$  is more dominant which indicates that the chemical processes mainly control carbonation resistance rather than physical processes.

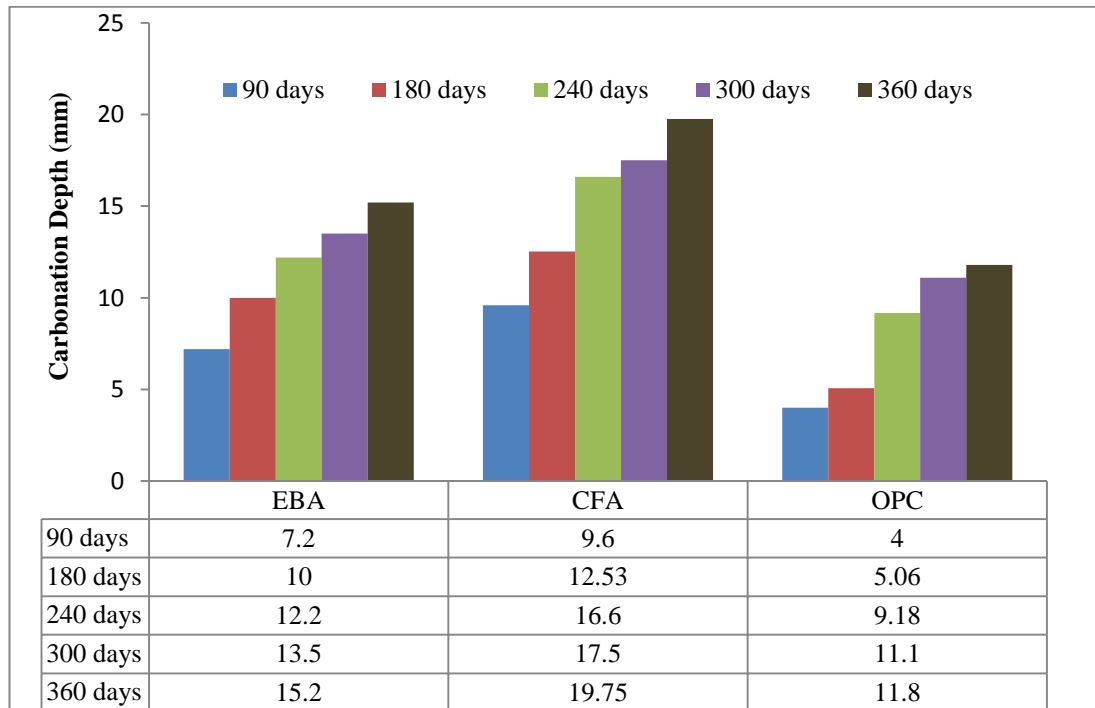


**Figure 5.7 Carbonation depth of control OPC, CFA and EBA**

### 5.3.2. Rate of Carbonation

It is generally established that the carbonation depth increases with the duration of exposure to  $\text{CO}_2$ , however, the rate of carbonation decreases with time. According to Fick's law and assuming steady-state diffusion of  $\text{CO}_2$ , the carbonation depth is considered proportional to the square root of time as shown in equation 5.2.

This formula has been adopted by many researchers and generally used to compare the carbonation resistance of concrete and also to predict the rate of carbonation [13, 15, 18].

$$d = k \sqrt{t} \quad 5.2$$

Where:  $d$  is the depth of carbonation in (mm);  $t$  is the period of exposure in (years) and  $k$  represents the coefficient of carbonation in ( $\text{mm}/\text{year}^{0.5}$ ).

The measured carbonation depth for EBA, CFA and OPC mixes is plotted against  $\sqrt{t}$  (years) in Figure 5.8. A linear relationship with a strong correlation factor ranging from 0.94 to 0.99 is evident. The carbonation coefficient  $k$  ( $\text{mm}/\text{year}^{0.5}$ ) is determined by regression analyses.

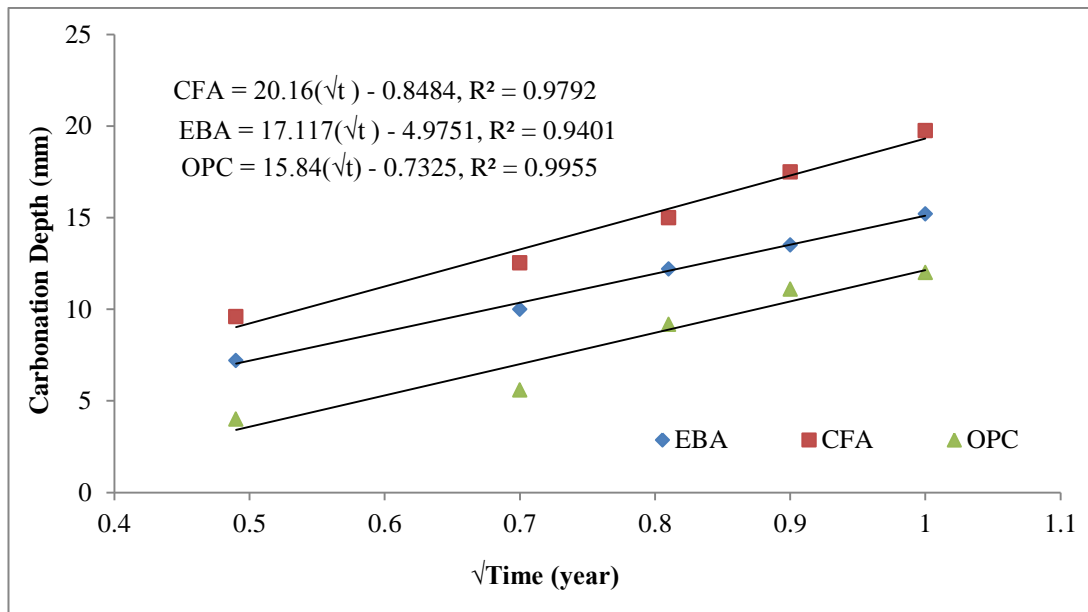


**Figure 5.8 Rate of carbonation for EBA, CFA and OPC concrete**

Figure 5.9 shows the carbonation coefficient  $k$  for CFA and EBA compared to OPC concrete. The high value of carbonation coefficient  $k$  indicates a higher rate of carbonation. The OPC concrete has the lowest carbonation coefficient of  $15.84 \text{ mm}/\text{year}^{0.5}$  followed by EBA concrete by  $17.11 \text{ mm}/\text{year}^{0.5}$  whereas the coefficient of CFA is the highest at  $20.16 \text{ mm}/\text{year}^{0.5}$ .

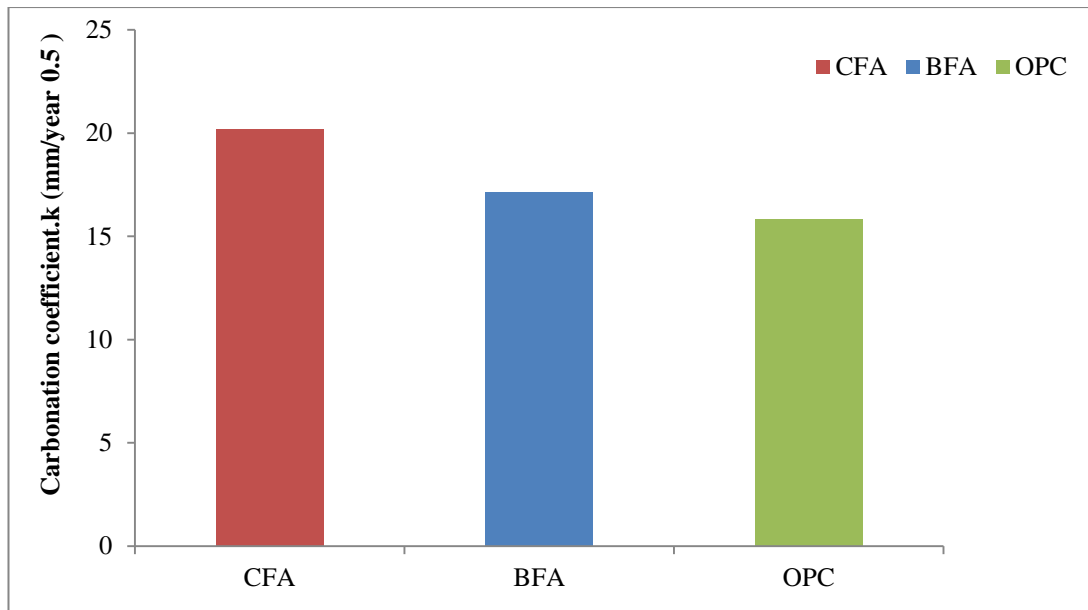


Figure 5.9 The coefficient of carbonation for CFA, EBA and OPC concrete

### 5.3.3. Shrinkage of EBA, CFA and OPC Concrete

#### 5.3.3.1. Carbonation Shrinkage

The carbonation shrinkage of EBA, CFA and OPC concrete cured in accelerated carbonation chamber for 300 days was calculated and plotted in Figure 5.10. At age of 45 days, the samples were exposed to 3-4 % CO<sub>2</sub> in a carbonation chamber, the temperature and relative humidity were controlled at 20 ± 2°C and 50-70% respectively. During the first two months, the carbonation shrinkage of all samples was almost similar and seems to be not highly affected by both ashes. Afterward, low carbonation shrinkage is observed in CFA compared to EBA and OPC concretes. After 300 days of exposure(345 days age), the carbonation shrinkage of CFA was the lowest at 312 microstrains compared to 329.8 and 337.7 microstrains for EBA and OPC respectively. OPC mix has lower porosity but higher volume of large pores than CFA and EBA concrete as reported in chapter 4 (section 4.3.4.2.2). The high volume of large pores facilitates the diffusion of moisture from the mix. Therefore, the shrinkage in OPC concrete is higher. In addition, the carbonated zone in hardened cement paste is becoming denser due to the precipitation of a large amount of CaCO<sub>3</sub> which fills the large pores and reducing the induced stresses

during carbonation [19]. Therefore, the shrinkage in CFA concrete is lower than OPC and EBA as its carbonated zone is wider.

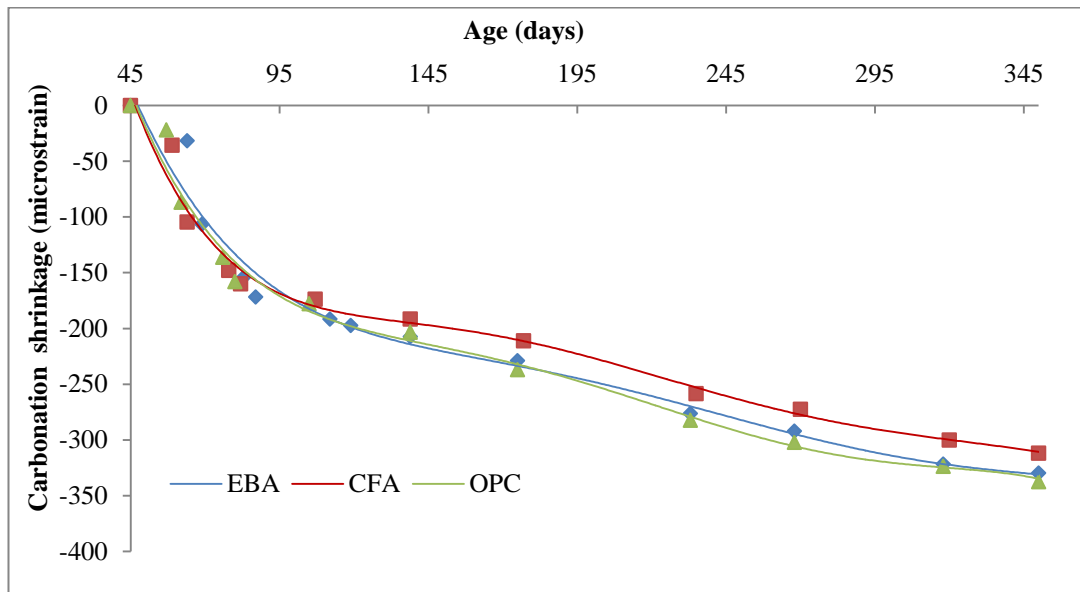


Figure 5.10 Carbonation shrinkage of CFA, EBA and OPC concrete

### 5.3.3.2. Drying Shrinkage

The drying shrinkage of both EBA and CFA compared to OPC concrete is shown in Figure 5.11. All samples were cured in the laboratory environment at  $20 \pm 2^\circ\text{C}$  and 65% RH for 200 days subsequent to 7 days of water curing. Generally, shrinkage of all samples (EBA, CFA and OPC) was observed to occur at a higher rate during the first two months, through which no significant impact of the inclusion of both ashes on drying shrinkage was noted. After that and up to 90 days, the samples undergo further shrinkage but at a lower rate as can be clearly seen from the figure. Afterward, the change in drying shrinkage for all mixes was similar, all of which continue to exhibit a very low rate of shrinkage up to 207 days. At 207 days age, the reference OPC mix exhibited 9% higher shrinkage than EBA and 13% higher than CFA. The inclusion of both EBA and CFA ashes as a partial replacement of cement resulted in a reduction of drying shrinkage. Drying shrinkage occurs due to the removal of inter-crystalline water from C-S-H gel [20]. Thus, a decrease in the formed C-S-H gel as a consequence of the retardation effect of fly ash will reduce the drying shrinkage. In addition, the reduction of the rate and degree of hydration reaction due to the presence of fly ash decreases the adsorbed water on the surface of

C-S-H gel particles. As a result, fly ash concrete exhibits lower drying shrinkage compared to OPC concrete [21–23]. The high shrinkage strain for OPC concrete is attributed to the high volume of large pores compared to CFA and EBA. Moreover, the shrinkage restraining effect of coarse aggregate [20] could be another reason for higher shrinkage as the aggregate content in OPC concrete,  $1100 \text{ kg/m}^3$ , is lower than the  $1136 \text{ kg/m}^3$  in CFA and EBA concrete.

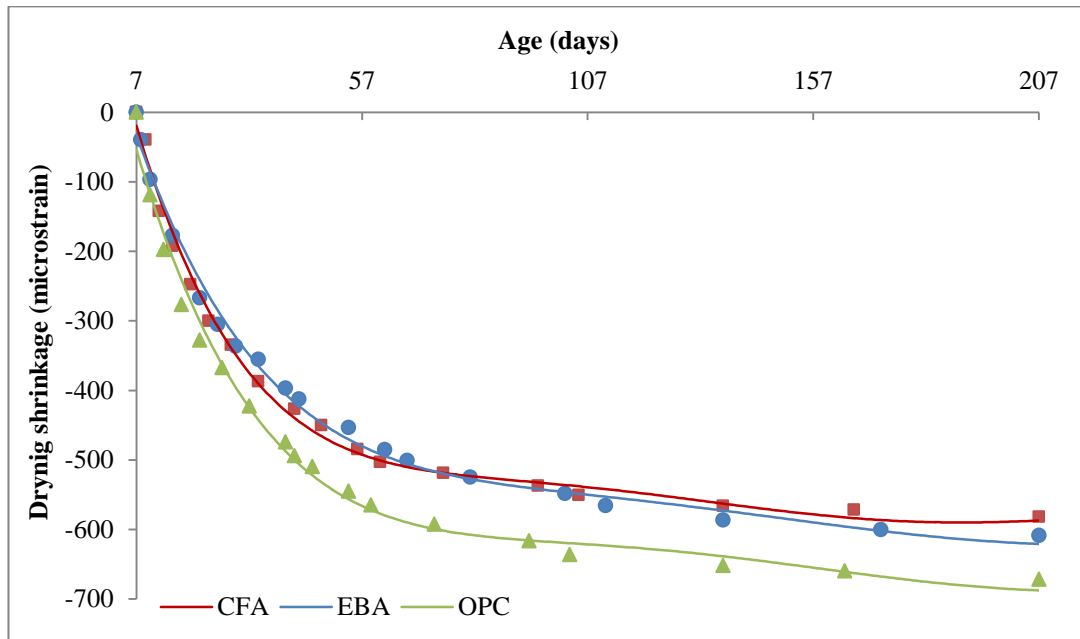


Figure 5.11 Drying shrinkage of EBA, CFA and OPC concrete

Drying shrinkage reduction of fly ash concrete has been reported in the literature [24, 25]. Naik et.al [24] investigated the drying shrinkage of wood waste ash as a partial cement replacement at 5, 8 and 12% up to 232 days. They found that drying shrinkage of control OPC concrete at 232 days is 520 microstrains whereas the shrinkage values of concrete with 5%, 8% and 12% wood ash are 270, 130 and 440 microstrains respectively. Similar trend was observed by using class F fly ash, the shrinkage at 180 days reduced from 435 microstrains (OPC concrete) to 362 microstrains for concrete with 40% cement replacement by fly ash [25].

Figure 5.11 also shows that CFA is more effective in reducing long-term shrinkage compared to EBA due to its lower porosity and lower volume of the large pores.

### 5.3.3.3. Carbonation and Drying Shrinkage

The carbonation and drying shrinkage graphs for EBA, CFA and OPC concretes from 45 up to 140 days are illustrated in Figure 5.12. The two graphs are identical from 7 to 45 days as all samples were in the same conditions (drying only) and the carbonations process was started on day 45. The solid lines represent the best fit lines of the combination of carbonation and drying shrinkage values whereas the dashed lines represent the best fit lines of drying shrinkage values alone. Therefore, the carbonation shrinkage is considered as the difference between both as shown in the figure.

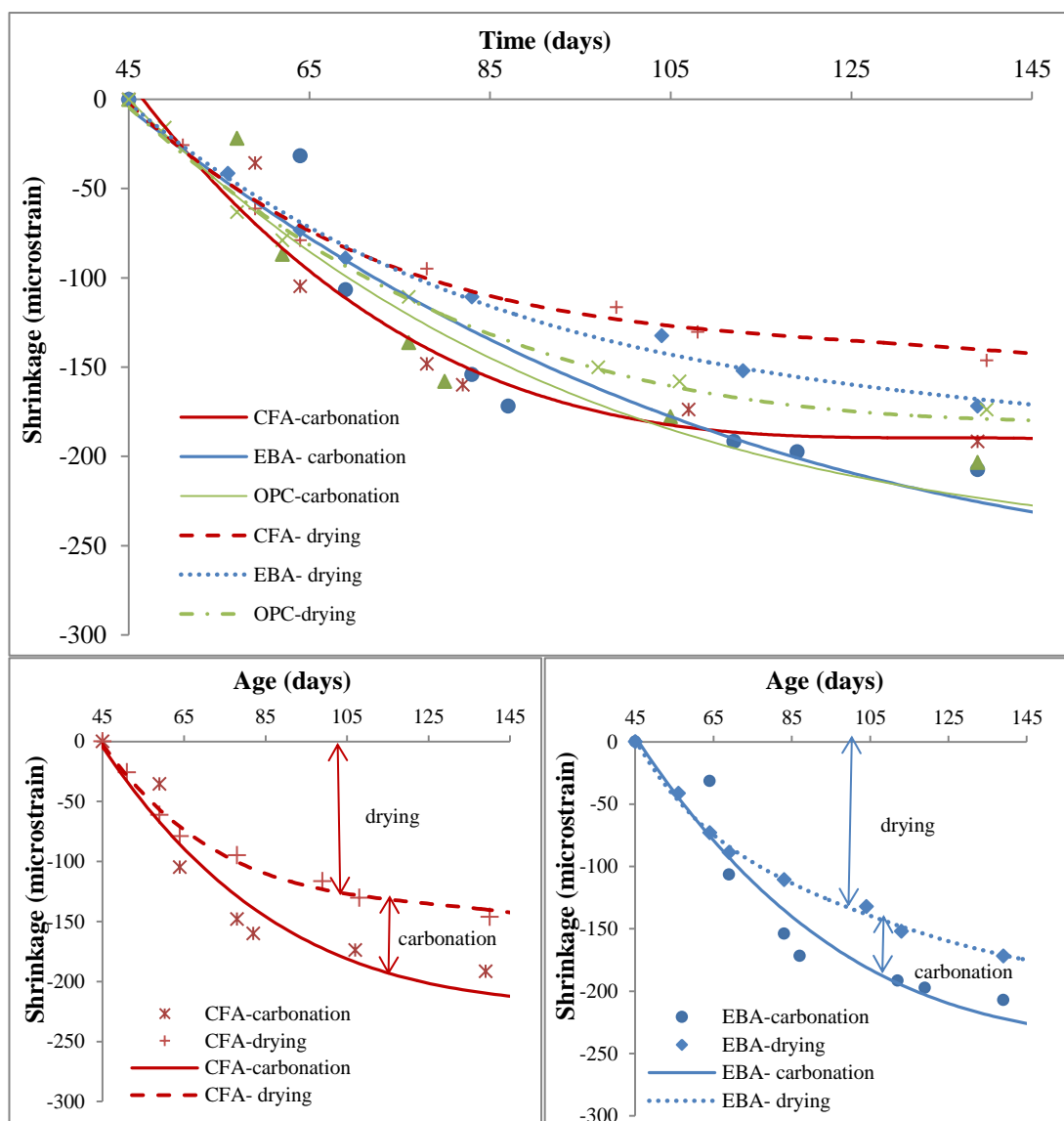


Figure 5.12 Carbonation and drying shrinkage of CFA, EBA and OPC concrete

It is clearly seen that the magnitude of drying shrinkage is greater than the carbonation shrinkage. The higher drying shrinkage can be attributed to the higher water loss compared to carbonation shrinkage as the curing conditions are different. The drying shrinkage samples were cured in the laboratory environment at  $20 \pm 2^\circ\text{C}$  and 65% R.H whereas the carbonation shrinkage samples were cured in a chamber where 4%  $\text{CO}_2$  were continuously introduced. The carbonation process releases water in addition to calcium carbonate which fills the pores and eliminates the induced stresses in cement paste by water loss during shrinkage whereas the pore spaces in drying conditions are usually filled with air.

#### **5.4. Conclusions**

The influence of enhanced biomass ash (EBA) on carbonation resistance of concrete was investigated and compared with coal fly ash (CFA) and normal OPC concretes. The samples were exposed to 3- 4%  $\text{CO}_2$  in a carbonation chamber, the temperature and relative humidity in the chamber were controlled at  $20 \pm 2^\circ\text{C}$  and 50-70%, respectively. The depth of carbonation and carbonation shrinkage were determined at different times of exposure. The following conclusions can be drawn based on the reported results.

1. A higher carbonation depth was observed in both EBA and CFA concretes compared to control OPC concrete. For instance, at 360 days, the carbonation depth is 15.2 mm for EBA and 19.75 mm for CFA. The corresponding depth for OPC is 11.8 mm. This is due to a decrease in  $\text{Ca}(\text{OH})_2$  caused by the pozzolanic reaction which makes the concrete sensitive to  $\text{CO}_2$  and reduces its resistance against the carbonation.
2. EBA is more effective than CFA in resisting the carbonation because of its lower pozzolanic reactivity due to its lower silica and amorphous content compared to CFA.
3. The rate of carbonation is higher in fly ash concrete than OPC concrete. It is  $17.11 \text{ mm/year}^{0.5}$  and  $20.16 \text{ mm/year}^{0.5}$  in EBA and CFA concretes respectively whereas it is  $15.84 \text{ mm/year}^{0.5}$  for OPC concrete.

4. The carbonation shrinkage is lower in both fly ashes (CFA and EBA) compared to OPC concrete. For example, after 300 days of exposure, the carbonation shrinkage is 312 microstrain for CFA, 329.8 for EBA compared to 337.7 microstrain for OPC concrete.
5. The drying shrinkage of both ashes (CFA and EBA) concrete is lower than OPC concrete due to the high volume of large pores in OPC concrete, which controls the diffusion of moisture from the mix.
6. Drying shrinkage values are greater than carbonation shrinkage for both fly ash and OPC concretes as shown in figure 5.12. This is because the drying process causes high water loss while in the carbonation process, the precipitation of  $\text{CaCO}_3$  fills the pores and restricts further shrinkage.

## 5.5. References

1. Rao NV, Meena T (2017) A review on carbonation study in concrete. IOP Conf Ser Mater Sci Eng 263: . doi: 10.1088/1757-899X/263/3/032011
2. Lye, Chao-qun, Ravindra K. Dhir GSG (2015) Carbonation resistance of fly ash concrete. Mag. Concr. Res. 67:1150–1178
3. Ashraf W (2016) Carbonation of cement-based materials: Challenges and opportunities. Constr Build Mater 120:558–570 . doi: 10.1016/j.conbuildmat.2016.05.080
4. Šavija B, Luković M (2016) Carbonation of cement paste: Understanding, challenges, and opportunities. Constr Build Mater 117:285–301 . doi: 10.1016/j.conbuildmat.2016.04.138
5. Shebani Y (2016) Durability of Incinerator Fly Ash Concrete Durability of Incinerator Fly Ash Concrete. Dr Theses, Covntry Univ
6. John L.Provis VDJ (2015) Alkali Activated Materials State - of- the- Art Report,RILEM TC224-AAM
7. Visser J (2012) Accelerated carbonation testing of mortar with supplementary cementing materials - Limitation of the acceleration due to drying. Heron 57:231–247
8. British Standard Institution (2013) BS 1881-210:2013 Testing hardened concrete - Part 210: Determination of the potential carbonation resistance of method
9. British Standard Institution (2009) Testing of concrete Part 8: Determination of drying shrinkage of concrete for samples prepared in the field or in the laboratory. Br Stand BS ISO 1920-82009. doi: 10.1016/0041-624X(66)90307-6
10. British Standard Institution (1988) DOE METHOD OF CONCRETE MIX DESIGN
11. R.Kosalram,G.S.Vijayabhaskara MBA (2015) Mix Design of Fly Ash based concrete using DOE Method. Int J Eng Technol 10:7–12

12. Sankaralingam T, Roy C, Pandey SN (2013) Resource For High Strength and Durability of Structures at Lower Cost. NTPC Limited,A-11, NFL Premises Sector-24, Noida-201301
13. Hussain S, Bhunia D, Singh SB (2017) Comparative study of accelerated carbonation of plain cement and fly-ash concrete. *J Build Eng* 10:26–31 . doi: 10.1016/j.jobbe.2017.02.001
14. Morandea A, Thiéry M, Dangla P (2015) Impact of accelerated carbonation on OPC cement paste blended with fly ash. *Cem Concr Res* 67:226–236 . doi: 10.1016/j.cemconres.2014.10.003
15. Khunthongkeaw J, Tangtermsirikul S, Leelawat T (2006) A study on carbonation depth prediction for fly ash concrete. *Constr Build Mater* 20:744–753 . doi: 10.1016/j.conbuildmat.2005.01.052
16. Cheah CB, Ramli M (2012) Mechanical strength, durability and drying shrinkage of structural mortar containing HCWA as partial replacement of cement. *Constr Build Mater* 30:320–329 . doi: 10.1016/j.conbuildmat.2011.12.009
17. Papadakis VG (2000) Effect of supplementary cementing materials on concrete resistance against carbonation and chloride ingress. *Cem Concr Res* 30:291–299 . doi: 10.1016/S0008-8846(99)00249-5
18. Sulapha P, Wong S. F, Wee T. H, and Swaddiwudhipong S (2003) Carbonation of Concrete Containing Mineral Admixtures. *Mater Civel Eng* 15: . doi: [https://doi.org/10.1061/\(ASCE\)0899-1561\(2003\)15:2\(134\)](https://doi.org/10.1061/(ASCE)0899-1561(2003)15:2(134))
19. Puertas F, Palacios M, Vázquez T (2006) Carbonation process of alkali-activated slag mortars. *J Mater Sci* 41:3071–3082 . doi: 10.1007/s10853-005-1821-2
20. Neville A. (1995) *Properties of Concrete*, Forth Edit. Longman Group Limited
21. L.Wright (2003) *Properties of Concrete Containing Desulphurised Waste*. Dr Theses,sheff Hallam Univ
22. Saha AK (2018) Effect of class F fl y ash on the durability properties of concrete. *Sustain Environ Res* 28:25–31 . doi: 10.1016/j.serj.2017.09.001

23. Khatib JM, Mangat PS WL (2016) Mechanical and Physical Properties of Concrete Containing FGD Waste. *Mag Concr Res* 68:550–560 . doi: <https://doi.org/10.1680/macr.15.00092>
24. Naik BTR, Kraus RN (2002) Demonstration of manufacturing technology for concrete and CLSM utilizing wood ash from Wisconsin. Report No. CBU-2002-30, Report for Year 1 activities submitted to the Wisconsin Department of Natural Resources, Madison, WI, for Project # 01-06 UWM Center . 124
25. Nath P, Sarker P (2011) Effect of Fly Ash on the Durability Properties of High Strength Concrete. *Procedia Eng* 14:1149–1156 . doi: [10.1016/j.proeng.2011.07.144](https://doi.org/10.1016/j.proeng.2011.07.144)

## **CHAPTER 6 SULPHATE ATTACK AND ALKALI-SILICA REACTION OF BIOMASS FLY ASH MORTARS**

### **6.1. Sulphate Attack**

Concrete structures are subjected to deterioration caused by external factors which affect its service life. Sulphate attack is one of the most common deterioration processes which occur when concrete is exposed to sulphate rich environments such as soils, groundwater and seawater. Sulphate attack causes a chemical breakdown by sulphate ions attacking compounds of cement hydration products and causing excessive expansion, cracking and strength loss due to the formation of ettringite and gypsum [1, 2]. Generally, two main factors control the sulphate resistance of concrete, which are the chemistry of cement and concrete permeability. The content of  $C_3A$  in cement makes an important contribution to the sulphate reactions, therefore, the sulphate resistance improves by reducing its amount [3]. Lower water /cement ratio results in reducing permeability which in turn reduces sulphate attack by hindering the movement of sulphate ions throughout the concrete matrix. However, the rate of sulphate attack also depends upon the concentration and type of sulphate solution (i.e. sodium, magnesium) to which the concrete is exposed [4].

In this chapter, sulphate resistance of mortars containing cement and biomass fly ash with different levels of replacement is investigated. The aim of the experimental programme was to evaluate the influence of biomass fly ash on the sulphate resistance of cement mortars containing 10, 20 and 30% replacement of cement by enhanced biomass fly ash (EBA). In order to understand and evaluate the effect of biomass fly ash against sulphate attack, a parallel investigation was also conducted on coal fly ash (CFA) blended cement mortars by using the same cement replacement levels together with control specimens of mortar made with 100% OPC cement for comparison. A brief literature review on the important aspects of sulphate attack which are relevant to this study is given in chapter 2.

### **6.1.1. Experimental Programme**

Different test methods have been developed to study the sulphate resistance of cementitious materials, however, ASTM C 1012 [5] is considered the most common approach and much data are available in the literature based on this test method. The current investigation was conducted according to this test method.

#### **6.1.1.1. Materials**

Ordinary Portland cement (Cem I: 52.5 N) conforming to EN 197-1 supplied by Rugby cement, Enhanced biomass ash (EBA) and commercial coal fly ash (CFA) were used as cementitious materials to prepare the mortars. The enhanced biomass ash was generated from Drax power station which is one of the UK's largest energy producers. The class F commercial coal fly ash (CFA) conforming to EN450 was supplied by Power Minerals Ltd. Locally produced sharp medium grade sand supplied by Frank Key Sheffield was sieved through a 2 mm mesh before using it in the mortar mixes. Further information on the chemical and physical properties of the materials is given in chapter 3.

#### **6.1.1.2. Mix Proportions for Sulphate Attack Test**

Sulphate resistance tests were conducted on seven mortar mixes prepared according to ASTM C1012M standard procedures [5]. The proportions of binder to sand by mass were kept constant at 1: 2.75 for all mixes. One minor modification was performed when following the ASTM C1012M procedure to minimize the parameters. The water to binder ratio was kept constant at 0.485 for the control (OPC) mix with 100 % cement and all fly ash blended cement mixes, instead of adjusting the quantity of water for fly ash blended cement mixes to give a flow within  $\pm 10$ mm of the control mortar as specified in the standard. However, the flow of all blended fly ash mortars was almost within this limit. Table 6.1 shows the proportions of evaluated mixes.

Mix 1 represents a reference mix of 100% OPC cement and mixes 2 to 7 contain different blends of cement and fly ash. The mix ID (column 2) for mixes 2 to 7 represents the replacement percentage of cement by fly ash. For example, 10EBA contains 10% enhanced biomass fly ash and 90% cement by weight of the binder.

**Table 6.1 The proportion of evaluated mixes for sulphate attack test**

Mix no	Mix ID	Cement (g)	Fly ash(g)	Sand(g)	Water(g)	Flow(mm)
1	OPC	491	0	1350	238.1	195
2	10EBA	441.9	49.1	1350	238.1	187
3	20EBA	392.8	98.2	1350	238.1	185
4	30EBA	343.7	147.3	1350	238.1	183
5	10CFA	441.9	49.1	1350	238.1	188
6	20CFA	392.8	98.2	1350	238.1	193
7	30CFA	343.7	147.3	1350	238.1	197

### **6.1.1.3. Mixing**

The mixing procedure was as follows:

1. The binder (Cement and fly ash) were placed into the bowl and mixed by hand until homogeneity was achieved.
2. The bowl was placed into the Hobart mixer and water was added carefully within 10 seconds.
3. The mixing was started immediately at low speed for 30 seconds. Then, the sand was added steadily during the next 30 seconds while mixing continued.
4. The mixer was switched to high speed for an additional 60 seconds.
5. After about 2 minutes from the start, the mixing was stopped and the mix was briefly mixed by hand to remove accumulated materials from the paddle and the base of the bowl.
6. The mixture was then mixed at high speed for a further 60 seconds. The total period of mixing was about 5 minutes and the mortar was regularly mixed by hand during sample preparation to avoid bleeding.

### **6.1.1.4. Casting**

Three prisms of dimensions 40mm x 40mm x160mm were cast for each mix in steel moulds. The moulds were lubricated with mould oil prior to casting. Then, the fresh mortar was placed in the prism moulds in two layers; each layer was compacted on a vibrating table for five seconds.

#### 6.1.1.5. Curing

After casting, all the moulds were placed in a mist curing room at 20°C for 24 hours. Then, all samples were demoulded and cured in water at 20°C until 28 days to develop sufficient strength for the sulphate resistance test.

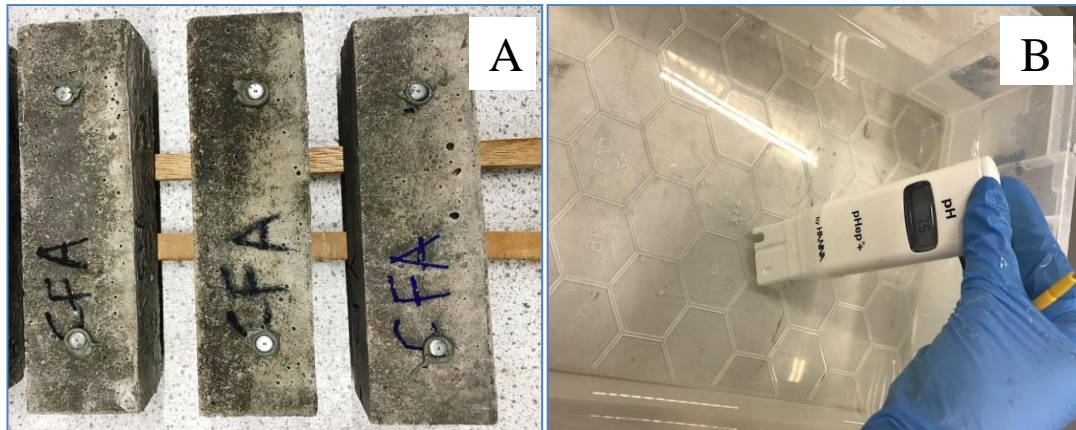
#### 6.1.1.6. Testing

The specimens were removed from the water after 28 days of water curing and dried. Stainless steel demec points were fixed along two parallel longitudinal faces of each specimen at a gauge length of 100 mm. An epoxy resin was used to glue the demec points on the specimens as shown in Figure 6.1.A. Extensometer measurements were taken for each sample across the demec points on the two faces. These initial readings provided the datum values for the test. The weight of each specimen was also recorded prior to placing the samples in a plastic tank containing 5% sodium sulphate solution. The solution was prepared a day before as specified by ASTM C1012M [5] by dissolving 50 g of sodium sulphate ( $\text{Na}_2 \text{SO}_4$ ) in 900 ml of water and further diluted with distilled water to obtain 1L of solution. The Solution pH was maintained in the range of 6 to 8 (Figure 6.1.B). The volume of the solution in the plastic container was  $4 \pm 0.5$  times the volume of mortar bars to ensure complete immersion of the samples (Figure 6.1.C). The plastic container was kept covered to prevent solution evaporation and it was stored in the laboratory at 20°C, 65% RH (Figure 6.1.D). The solution was replaced every 2 months during the whole immersion period to maintain the sulphate concentration as much as possible.

The expansion of the prisms was measured at regular intervals using demec extensometer (once a week in the first month, and then once a month up to 420 days). Expansion strain was determined by taking the mean value of measurements from the two opposite faces of three test specimens. The expansion strain at any age due to sulphate attack was calculated as follows:

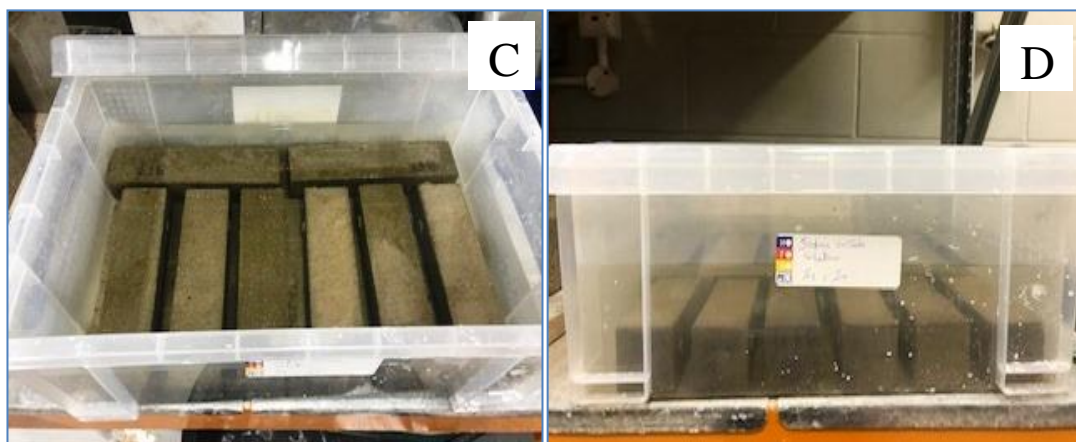
$$\varepsilon = (X_t - X_i) \times GF \times 10^6 \quad 6.1$$

Where:  $\varepsilon$  is the expansion in microstrain;  $X_t$  is the gauge reading at time  $t$ ;  $X_i$  is the initial (datum) gauge reading and  $GF$  is the gauge factor of the extensometer.



A. Samples with demec points.

B. Solution preparation in plastic tank and pH measurement.



C. Samples submerged in 5% Na<sub>2</sub>SO<sub>4</sub> solution.

D. Samples stored in the laboratory at 20°C, 65 % RH in a plastic tank with led.

**Figure 6.1 Samples preparation for sulphate resistance test**

All samples were examined visually after measuring the expansion to identify any visual changes such as discolouration, cracking and disintegration. At the end of the test, the average weight for all samples was recorded and expressed as a percentage of weight change with respect to the initial weight which was recorded after 28 days curing in water before immersion in the sulphate solution. The weight change was calculated as follows:

$$W(\%) = \frac{(W_f - W_0)}{W_0} \times 100 \quad 6.2$$

Where:  $W$  is the weight change in %;  $W_0$  is the initial weight after 28 days of water curing and  $W_f$  is the final weight after 420 days of immersion in Na<sub>2</sub>SO<sub>4</sub> solution.

Finally, the samples were crushed in the compression machine for strength measurements. Then, a few pieces of the fractured surface of some mortar samples were taken for SEM analyses in order to determine any variation in their morphology. The microstructures were investigated using SEM analyses equipped with EDX spectrums for element identification. The mortar sample was first attached to aluminium stubs and a layer of carbon was applied by sputtering using SPI coater equipment. The sample was then transferred to the QUANTA 650 SEM device and exposed to an electron beam inside. The electrons generate signals which reveal information about the morphology of the sample. Figure 6.2 shows QUANTA 650 SEM which was used in this study.

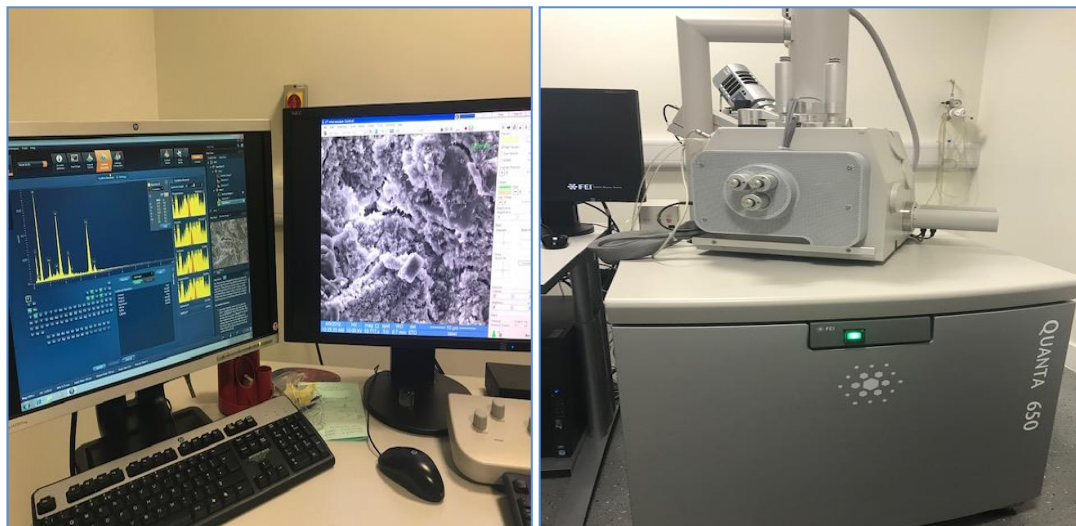


**Figure 6.2 QUANTA 650 SEM equipped with EDX spectrums**

### **6.1.2. Results**

The expansion rates of OPC and fly ash blended cement mortars stored in the 5% sodium sulphate,  $\text{Na}_2\text{SO}_4$ , solution have been monitored and illustrated in Figures 6.3 and 6.6. It is clearly seen that OPC control mortars showed the highest expansion between all mixes by the end of the testing period of 420 days. The replacement of cement with fly ash has a significant effect on the sulphate resistance. Incorporation of fly ash reduces the expansions, however, the reduction was dependant on the level of replacement and the type of fly ash. The effect of both ashes against the sulphate attack will be discussed in the following sections.

### 6.1.2.1. Effect of Coal Fly Ash (CFA)

The expansion of control OPC mortars and the samples containing 10, 20 and 30% coal fly ash by weight are presented in Figure 6.3. The samples expanded in the solution with the increase of immersion time and only control OPC samples showed significant expansion during 420 days of immersion in  $\text{Na}_2\text{SO}_4$  solution. During the first 120 days, all samples including the control OPC mortars showed a gradual increase in expansion but there was no visible destruction, scaling or spalling in all samples. However, white water-soluble substances were formed only on the surface of the reference OPC samples after about 90 days.

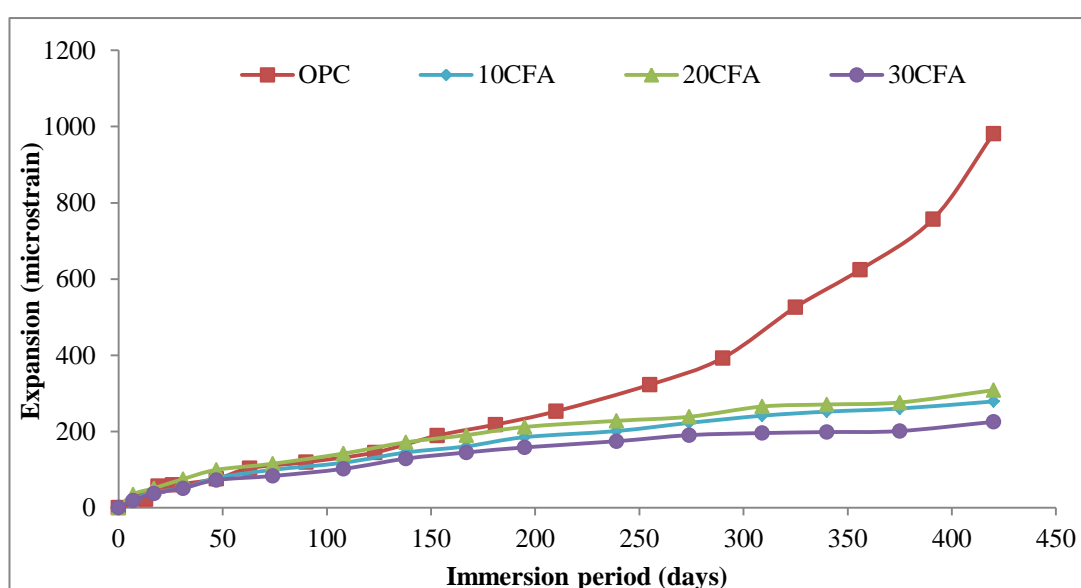
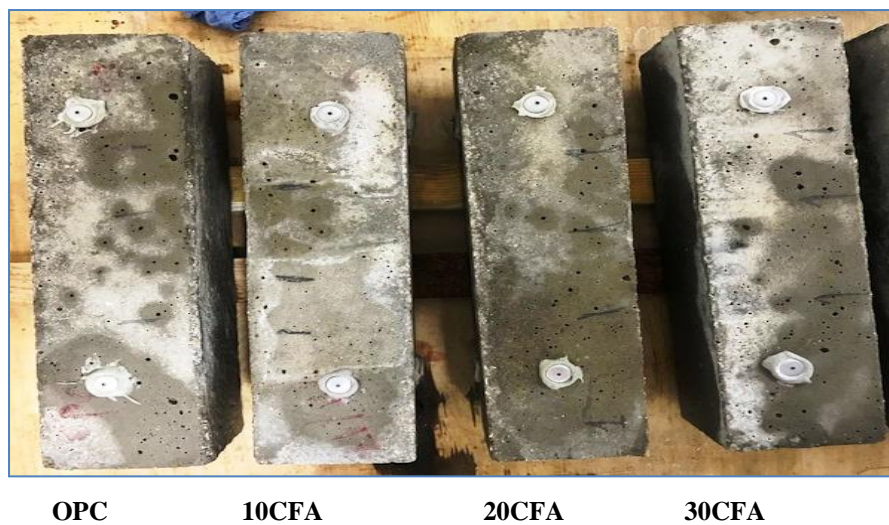


Figure 6.3 The effect of coal fly ash on sulphate resistance of mortars

An accelerating expansion rate of OPC mortars started to be obvious from 150 days onward whereas no obvious acceleration in expansion rate was observed in all blended coal fly ash mortars. After 150 days storage of OPC mortars in  $\text{Na}_2\text{SO}_4$  solution, slight cracking was observed which was more prominent around the edges and on the surface indicating significant sodium sulphate attack. Between 300 and 420 days, the expansion of OPC samples increased significantly, almost three times, exceeding 981 microstrains at the end of the test. This increase in the expansion was accompanied by increased cracking and loss of material. On the contrary, the blended coal fly ash mortars showed almost a linear pattern of expansion after about 150 days, however, 30% of cement replacement exhibited the lowest expansion

during the whole immersion period. It is clearly evident that the replacement of cement with coal fly ash at these levels (10, 20 and 30%) reduced the expansion which indicated improved resistance to sulphate attack. This improvement in sulphate resistance was also reflected in the physical deterioration.

Physical observation showed that the deterioration of OPC mortars was more obvious compared to coal fly ash blended samples which showed less deterioration (hair-line cracks) especially at 20% and 30% substitutions of fly ash. Figure 6.4 shows the appearance of OPC and blended coal fly ash mortars after 150 days of storage in 5%  $\text{Na}_2\text{SO}_4$  solution. No visible cracks appear on the top face of samples.



**Figure 6.4** The appearance of OPC and blended coal fly ash mortar samples after 150 days of immersion in 5%  $\text{Na}_2\text{SO}_4$  solution.

Figure 6.5 shows the appearance of OPC and blended coal fly ash mortars at the end of the test (after 420 days of storage in  $\text{Na}_2\text{SO}_4$  solution). It shows significant continuous, deep cracks and loss of material around the edges of OPC mortar samples while minimal cracking around the edges and corners appeared on coal fly ash samples especially at 20 and 30 % replacement of cement.

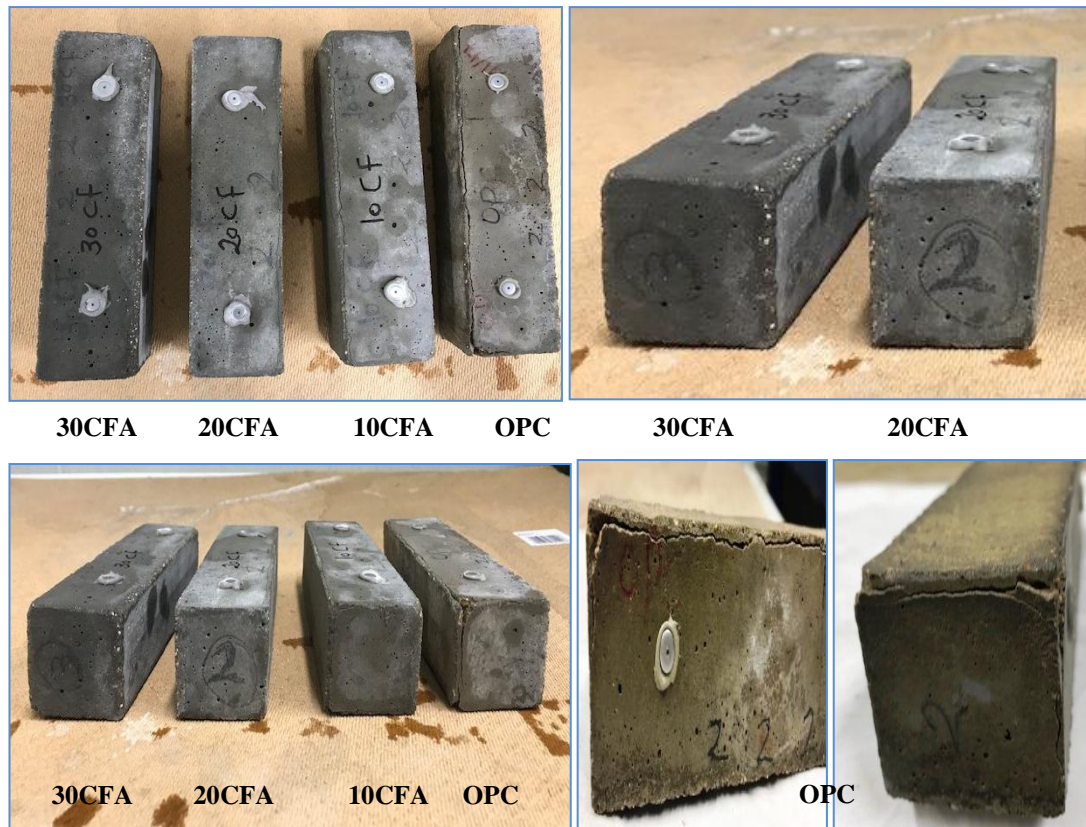


**Figure 6.5** The appearance of OPC and blended coal fly ash mortars after 420 days of immersion in 5 %  $\text{Na}_2\text{SO}_4$  solution.

#### **6.1.2.2. Effect of Enhanced Biomass Ash (EBA)**

Figure 6.6 shows the expansion rate of mortar samples containing 10, 20 and 30% EBA by weight immersed in 5%  $\text{Na}_2\text{SO}_4$  solution for 420 days. Generally, the samples expanded in the solution with time and only the control OPC mortars and the mix containing 10% EBA exhibited significant expansion after 420 days of immersion. During the first 150 days, all samples including the control OPC mortars showed a gradual increase in expansion but there is no visible destruction or cracks appearing on the surface. An accelerating expansion rate of OPC and 10 % EBA mortars started to be obvious from 150 days onward, however, the expansion rate was lower for 10% EBA mortars than OPC. At 420 days, the expansion of 10% EBA mortars was 775.86 microstrain compared to 981.3 microstrains for OPC mortars. The mortars with 20% and 30% EBA showed low expansion which indicated improvement in sulphate resistance. A few cracks appeared on the surface of the control OPC and 10% EBA samples after about 150 days of immersion. The visual

observations agreed with expansion results. Figure 6.7 shows that the OPC and 10% EBA mortars underwent significant deterioration and cracks around the ends and corners whereas 20% and 30% EBA show lower signs of deterioration.

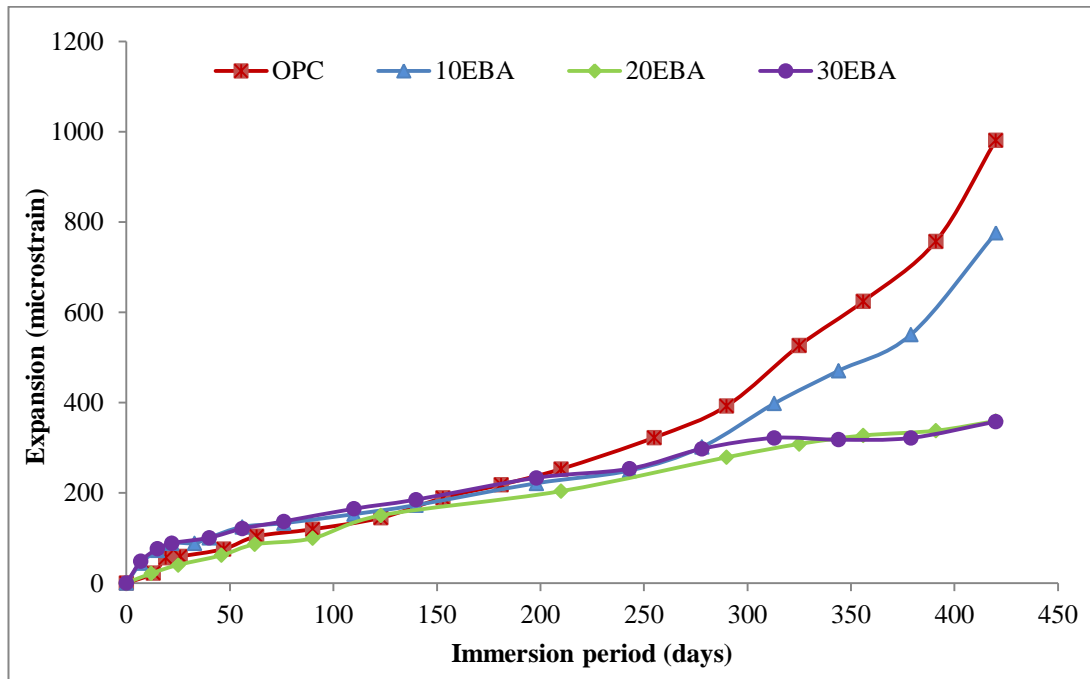


Figure 6.6 The effect of enhanced biomass ash on sulphate resistance of mortars

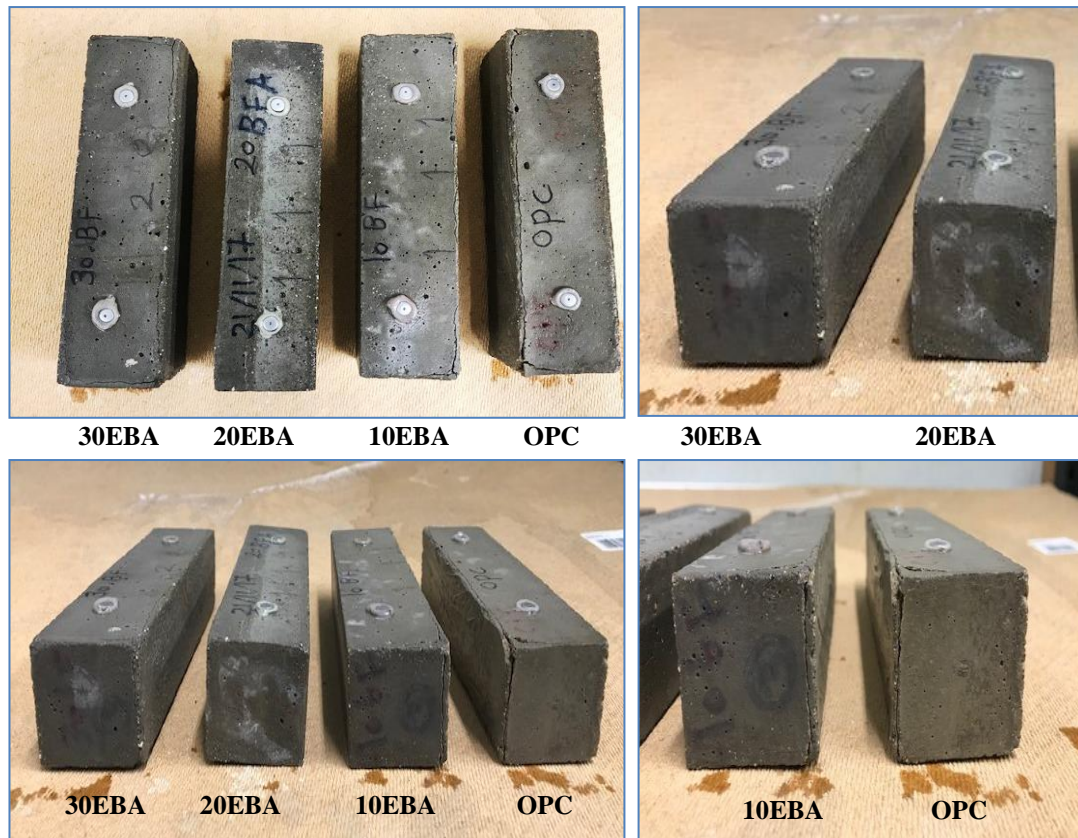
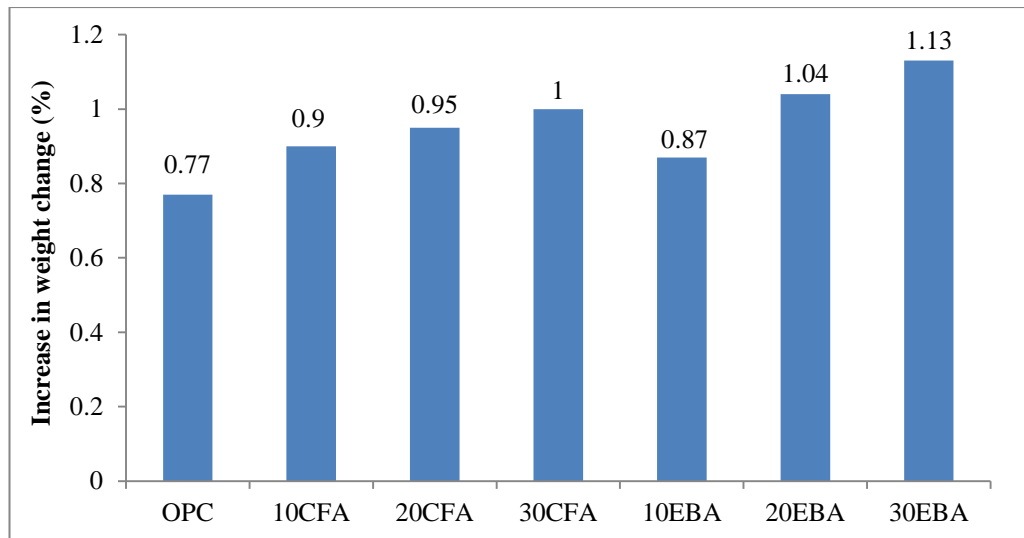


Figure 6.7 The appearance of OPC and enhanced biomass ash blended mortar samples after 420 days of immersion in 5 % Na<sub>2</sub>SO<sub>4</sub> solution.

### 6.1.2.3. Weight Change

The average weight of all samples was recorded at the end of the test and expressed as a percentage of weight change with respect to the initial weight which was recorded after 28 days curing in water and before the immersion in the sulphate solution. The average weight change of control OPC and blended fly ash mortar samples which were exposed to 5% Na<sub>2</sub>SO<sub>4</sub> solution up to 420 days is presented in figure 6.8. All samples showed a weight gain after 420 days immersion period. The weight changes of the samples were in the range of 0.77 - 1.13% at the end of the test. The least mass increase was found in control OPC mix followed by 10% EBA while the weight gain increased by increasing the replacement level of both ashes. These results are discussed in section 6.1.3.3.



**Figure 6.8** The weight change of the mortars after 420 days of immersion in 5%  $\text{Na}_2\text{SO}_4$  solution.

#### **6.1.2.4. SEM/EDX Examination**

Some mortar samples at a depth of about 2 mm from the surface were investigated by SEM/EDX analyses after immersion in 5% sodium sulphate solution for 420 days. SEM images and EDX spectra of control OPC, 10 % EBA and 30 % CFA specimens are presented in Figures 6.9, 6.10 and 6.11 respectively. Ettringite was very prominent as long needles in OPC and 10% EBA mortar samples. It was identified by EDX where the S, Al, Ca and O peaks are the characteristic of this mineral as shown in Figures 6.9 C and 6.10 C. In 30% CFA mortar sample, ettringite was also detected as short needles but in much less quantity than in OPC and 10% EBA mortar samples. As the content of fly ash increases, the quantity of ettringite decreases. Massive precipitation of gypsum crystals was easily observed in OPC and 10% EBA samples while no gypsum was detected in 30% CFA mortar sample.

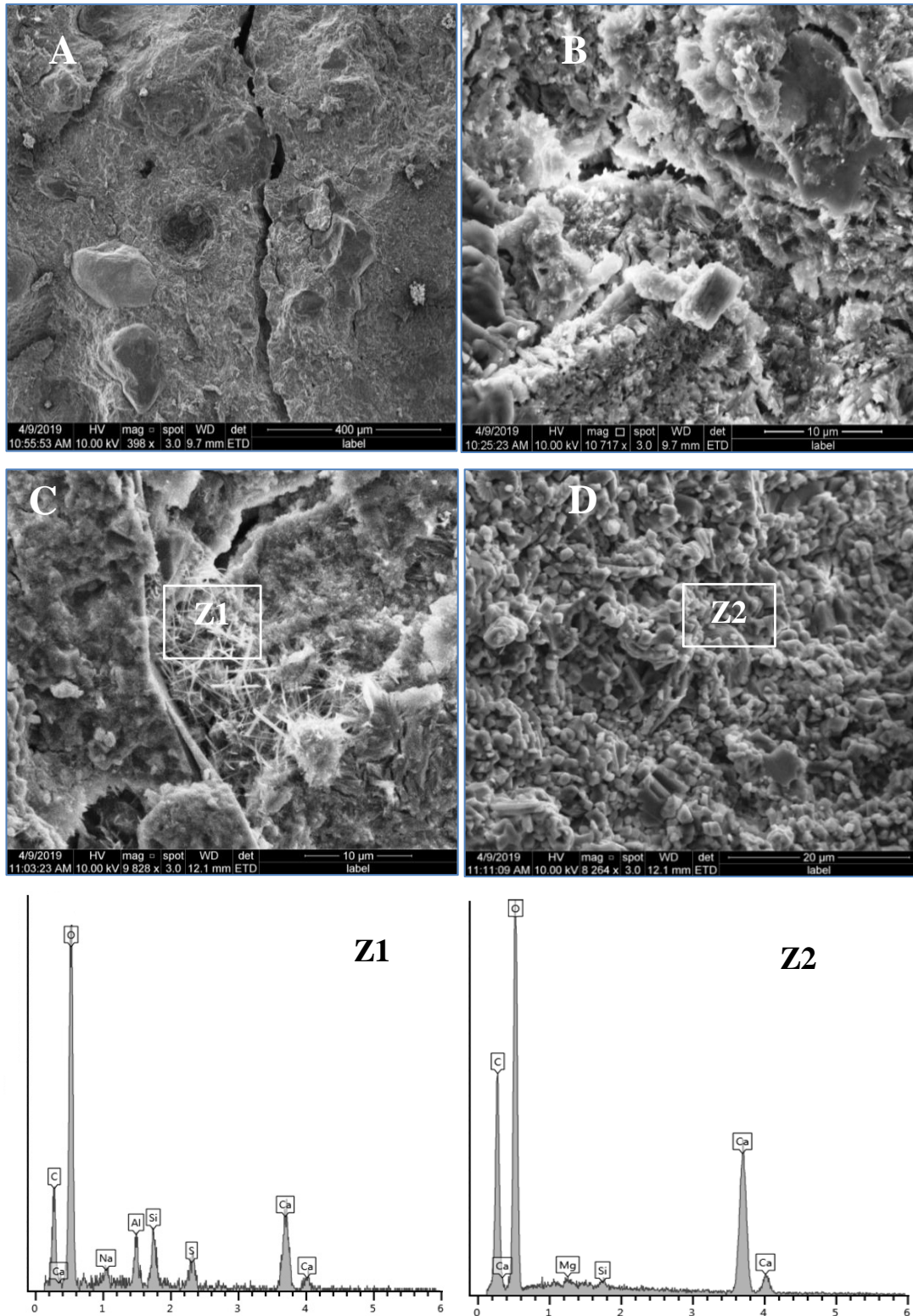


**Figure 6.9 SEM micrograph on OPC mortar after 420 days of immersion in  $\text{Na}_2\text{SO}_4$  solution.**

A. General view, B. The appearance of ettringite needles and gypsum crystals, C. Long ettringite needles & EDX spectrum of Z1 indicating mainly ettringite, D. Gypsum crystals & EDX spectrum of Z2 indicating mainly Gypsum.

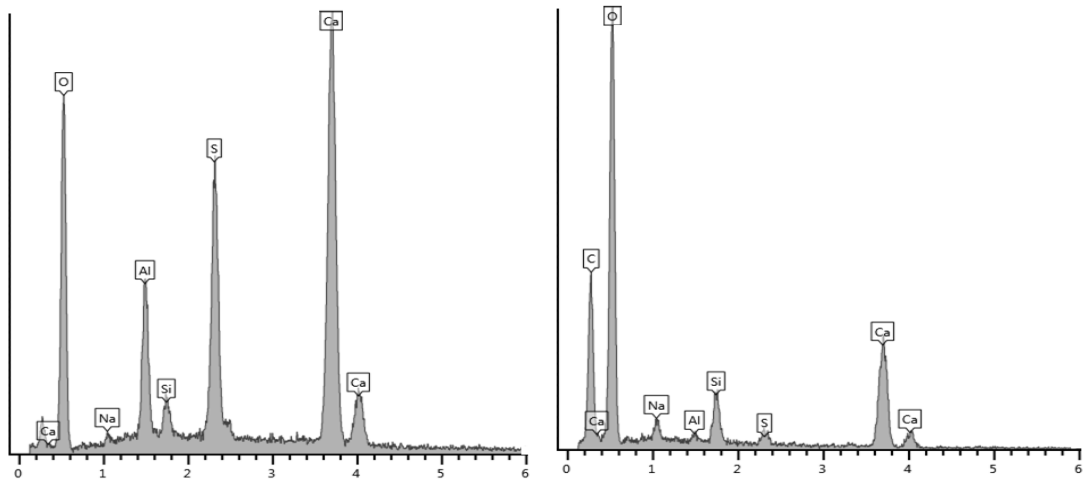
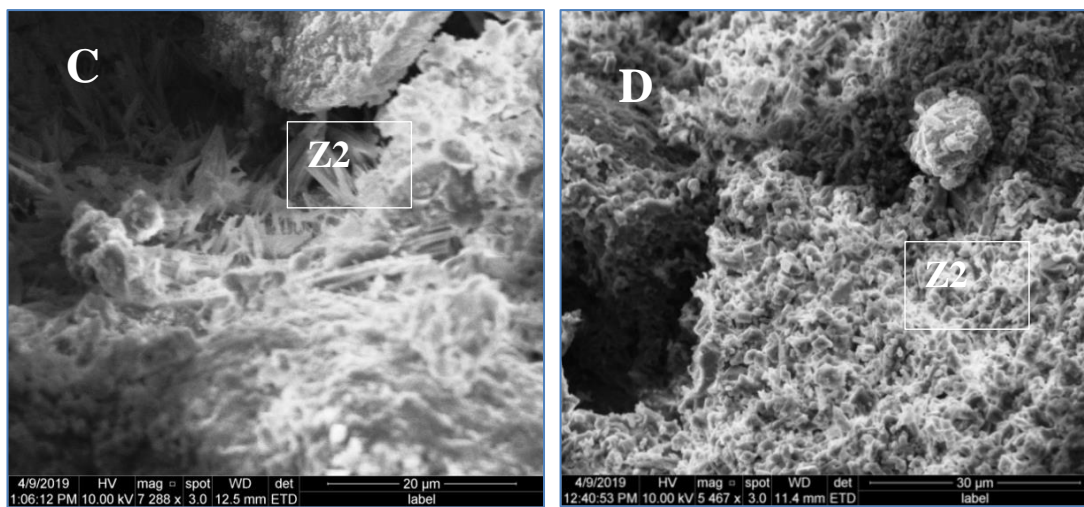
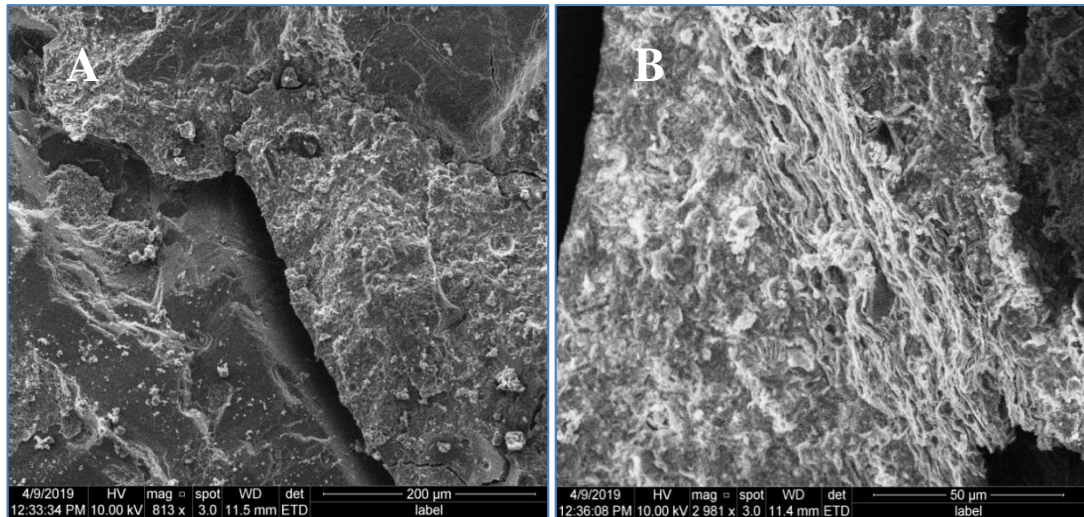


**Figure 6.10 SEM micrograph on 10% EBA mortar after 450 days of immersion in  $\text{Na}_2\text{SO}_4$  solution.**

A. General view, B. The appearance of ettringite needles and gypsum crystals, C. Long ettringite needles & EDX spectrum of Z1 indicating ettringite, D. Gypsum crystals & EDX spectrum of Z2 indicating mainly gypsum.

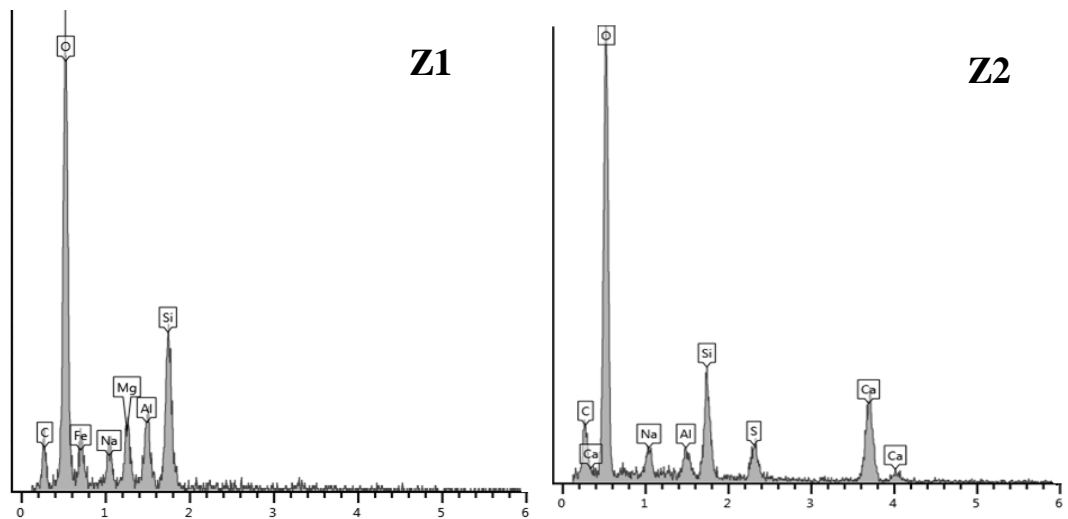
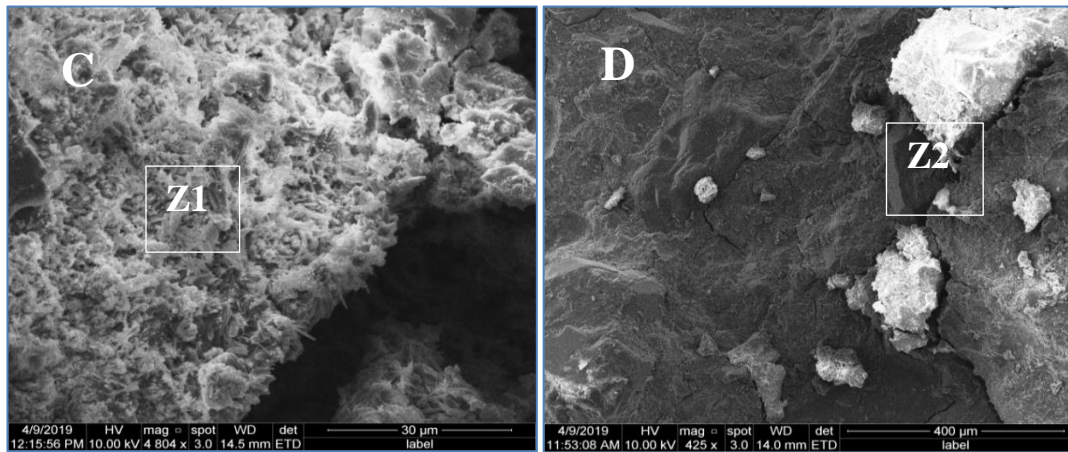
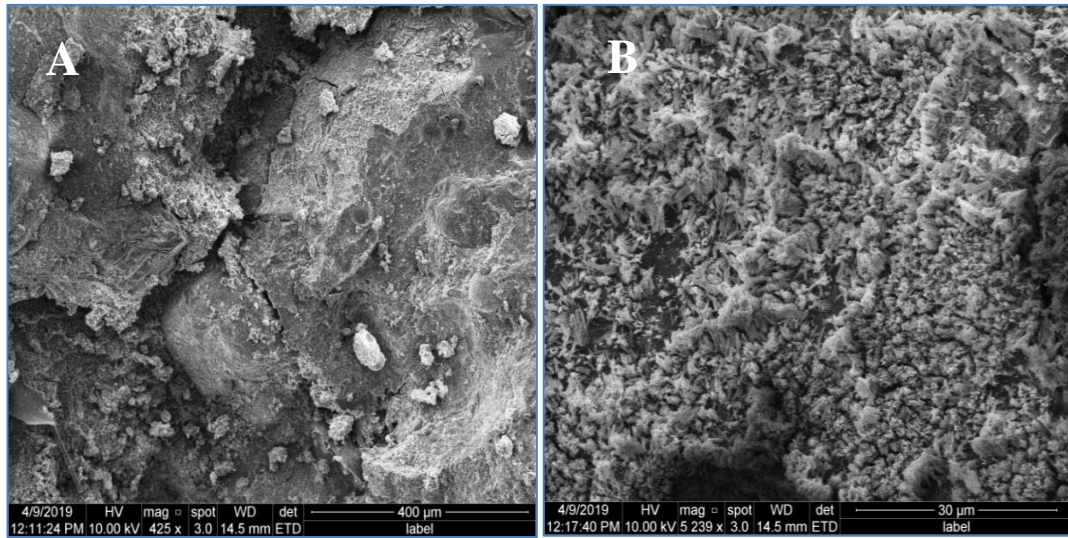


**Figure 6.11 SEM micrograph on 30% EBA mortar after 450 days of immersion in  $\text{Na}_2\text{SO}_4$  solution.**

A. General view, B& C. The appearance of short ettringite needles, D.EDX spectrum of Z1 & Z2 indicating just ettringite.

### 6.1.3. Discussion

In order to compare the effect of both ashes (EBA and CFA) on the sulphate resistance of mortars, the expansion results of all samples are plotted in Figure 6.12.

The results of the experimental programme show that the performance of the control OPC mortar samples is different from the blended fly ash mortar samples. The replacement of OPC cement with both EBA and CFA improved the sulphate resistance which is reflected by the reduction in expansion, cracks and disintegration. The control OPC mortar samples underwent an attack process when exposed to the sodium sulphate solution, which caused rapid expansion, cracks and spalling of material around the edges. The mortar samples containing EBA performed better than OPC mortar specimens. Rapid expansion and cracking were not observed, except in 10% EBA samples. The severity of attack decreased as the fly ash content increased.

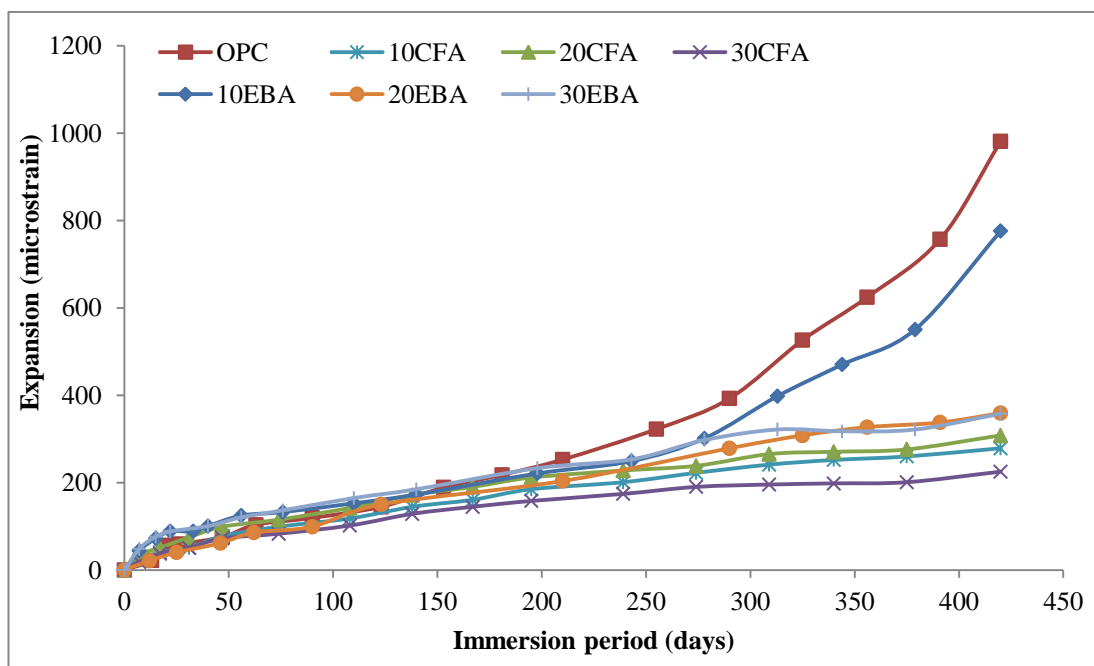


Figure 6.12 Comparison of sulphate resistance of OPC, CFA and EBA mortar samples

It is clearly seen that although both fly ashes decreased the expansion rate, mortars containing coal fly ash showed less expansion and, therefore, better sulphate resistance compared to enhanced biomass ash mortars. For example, at 420 days of immersion, the expansion of OPC mortars, 10%, 20% and 30% coal fly ash mortars

is 981.32, 278.72, 308.2 and 255.12 microstrains respectively. The corresponding values for mortars with 10%, 20% and 30% enhanced biomass fly ash are 775.8, 359.12 and 357.78 microstrains respectively. This indicates that the degree of sulphate resistance depended on the type of fly ash. Tkaczewska and Malolepszy [6] investigated the sulphate resistance of mixtures incorporating fly ash produced from the co-combustion of coal and wood biomass compared to mixtures incorporating coal fly ash alone. The wood biomass accounts 10% of the total mass of fuel. The ash replacement was 40% by mass of cement. They found that the mortars made with fly ash produced by the co-combustion of coal and biomass exhibited lower resistance to sulphate attack than the mortars made with coal fly ash only. The inferior resistance to sulphate attack of the mortar incorporating co-combustion of coal and biomass is attributed to its lower pozzolanic activity which also resulted in increased permeability and reduced volume stability of mortars. This co-combustion biomass ash is clearly different from the EBA investigated in this thesis since it uses coal as the combustion fuel instead of fly ash in the case of EBA.

The variation in sulphate resistance between the two ashes (EBA and CFA) could be attributed to several factors such as the variation in their chemical and mineralogical composition, porosity and pore structure as will be discussed in the following sections.

#### **6.1.3.1. Effect of Chemical and Mineralogical Compositions**

Coal fly ash has been known to be effective in improving sulphate resistance due to its chemical and mineralogical composition [7]. Table 6.2 shows the chemical composition of OPC cement and both ashes used in this investigation. The CFA contains higher amounts of silicon dioxide ( $\text{SiO}_2$ ), aluminium oxide ( $\text{Al}_2\text{O}_3$ ) and iron oxide ( $\text{Fe}_2\text{O}_3$ ) compared to EBA which result in better pozzolanic properties whereas EBA is much richer in calcium oxide CaO which does not contribute to the pozzolanic activity. The results reported in chapter 3 (section 3.3) on the chemical and physical properties of both ashes revealed that the pozzolanic activity and the amorphous silica and alumina content of EBA are less than CFA. Although EBA was less effective in resisting the sulphate attack than CFA, the principle behind their improvement in sulphate resistance relative to OPC mortar is similar. The

replacement of cement with fly ash reduces the content of C<sub>3</sub>A and CaO which contribute to sulphate reactions (dilution effect or less cement). In addition, the amorphous minerals (silica and alumina) present in fly ash undergo long-term pozzolanic reaction which consumes the calcium hydroxide that is released by the hydration process, leaving less portlandite Ca(OH)<sub>2</sub> available to react with sulphates. Consequently, the formulation of gypsum will be minimized [8]. The higher rate of expansion observed in EBA mixes is due to its lower pozzolanicity compared to CFA. Therefore, the quantity of free Ca(OH)<sub>2</sub> available to react with sulphate ions is higher in EBA blended mortar. Moreover, the higher content of CaO in EBA (8.10%) is another reason for its higher expansion rate as it is more than twice the CaO content in CFA (3.10%). These results agree with previous research on different types of coal fly ashes [9, 10] when compared with OPC which has CaO content of 69.8 % (Table 6.2).

**Table 6.2 The chemical composition of cement, CFA and EBA**

Material	SiO <sub>2</sub>	Al <sub>2</sub> O <sub>3</sub>	Fe <sub>2</sub> O <sub>3</sub>	CaO	MgO	SO <sub>3</sub>	K <sub>2</sub> O	P <sub>2</sub> O <sub>5</sub>
OPC	15.9	4.73	2.73	69.8	0.57	3.54	1.45	0.78
CFA	47.64	25.32	8.39	3.10	2.66	-	3.16	0.22
EBA	41.46	23.49	8.10	8.10	2.27	0.17	5.57	0.75

Dunstan [9] correlated the ability of fly ash to resist sulphate attack with its chemistry by introducing the simple factor 'R' in equation 6.3, which is mainly dependent on the content of calcium and iron oxides (CaO and Fe<sub>2</sub>O<sub>3</sub>) in the fly ash.

$$R = \frac{CaO-5}{Fe_2O_3} \quad 6.3$$

Based on this factor, decreasing the calcium oxide content and/or increasing iron oxide content would improve the sulphate resistance. Limits have been established for R values to increase sulphate resistance as shown in Table 6.3. According to these limits, the sulphate resistance increases if R values are less than 1.5 whereas, values greater than 3 reduce the sulphate resistance.

Dunstan's equation with the R factor was developed for 25% volumetric replacement of Type II cement with fly ash at a water to cement plus fly ash ratio, W/(C+P), of

0.45. He stated that the R factor may change for different replacements, other types of cement and probably the equation is not valid for  $W/(C+P)$  ratios exceeding 0.5. However, this expression has been extensively used to predict the sulphate attack of fly ash concrete despite that other studies have found that R factor is not sufficient to determine the resistance of the fly ash concrete [2, 11]. Khatib [11] found that 10% fly ash replacement performed worse than control OPC despite the R factor of the used fly ash being  $2.75 (< 3)$ , which according to Dunstan's equation would represent highly improved resistance to sulphate attack.

**Table 6.3 R-Factor limits as proposed by Dunstan [9]**

R	Sulphate resistance
< 0.75	Highly improved
0.75 to 1.5	Moderately improved
1.5 to 3	No significant effect
> 3	Reduced

In the current investigation, the R factor is - 0.22 and 0.38 for CFA and EBA respectively which correspond to the value of < 0.75 in Table 6.3 representing highly improved sulphate resistance of both ashes compared to control OPC mix. The lower value of - 0.22 for CFA than 0.38 for EBA explains the superior resistance of CFA compared to EBA (Figure 6.12). However, cement replacement with 10% EBA performed similarly to the control OPC despite the R factor of EBA being 0.38. This supports the claim that only the right proportion of fly ash, which generally lies between 20 - 30%, would improve the sulphate resistance and the R factor is only valid for these percentage (20 - 30%) [2].

An attempt is made to calculate the R factor for different types of fly ashes which have been investigated for their resistance to sulphate attack from selected papers including current results to compare their practical behaviour with the expected behaviour according to R-values. Table 6.4 shows this comparison. It is clear that not all results correlated well with the expected results based on R-value. For example, in Sudheen's investigation in the case of class F fly ash, the actual behaviour for all fly ash replacement levels (10 - 40%) was improvement in sulphate resistance. The expected behaviour according to R-value (0.23), is highly improved resistance

corresponding to the value of  $< 0.75$  (Table 6.3). The actual and expected behaviour is the same even when the fly ash is used as low as 10 % cement replacement. The trend is similar to the sulphate resistance of CFA used in this investigation (Figure 6.12) which is also a class F fly ash. In the case of class C fly ash and according to its R-value (1.68), the sulphate resistance should not be affected (remain similar to OPC) corresponding to the values of 1.5 to 3 (Table 6.3). In practice, the substitution of 20 to 40% fly ash results in improved sulphate resistance compared to OPC whereas 10% cement replacement reduced the sulphate resistance. This indicates that the R factor is not valid for class C fly ash as the actual and expected behaviour are opposite.

Another example of the variation between the actual and expected results is Rajamma's study. In the case of biomass B1, 10% cement replacement moderately improved the sulphate resistance compared to the OPC mix whereas 20 and 30% cement replacement reduced the sulphate resistance. The expected behaviour based on its R-value, 2.46, is no significant effect. The addition of biomass B2 at 10 and 20% cement replacement moderately improved the sulphate resistance compared to OPC mix whereas 30% cement replacement reduced the sulphate resistance. The expected behaviour based on its R-value of 9.27 is reducing the sulphate attack resistance. Again, the actual and expected behaviour are different. The author attributed the lower resistance of both biomass ashes to their higher porosity compared to OPC.

This variation reveals that relying on the R-value to predict the sulphate resistance produced by fly ash is not valid for all types and at all replacement levels and in some cases the physical properties (porosity and pore structure) become more dominant than the chemical composition of the fly ash.

**Table 6.4 Comparison between the practical and expected behaviour according to R values**

Author	Sulphate solution/duration	w/b ratio	CaO %	Fe <sub>2</sub> O <sub>3</sub> %	Type of ash	R	Porosity (%)	Replacement level (%)	Actual behaviour	Expected behaviour according to R
Sudheen [1]	5% Na <sub>2</sub> SO <sub>4</sub> for 6 months	0.4-0.6	16.44	6.78	Class C	1.68	-	10	Reduced the resistance	No significant effect
			6.17	5.03	Class F	0.23	-	20-40	Improved the resistance	
								10-40	Improved at all replacement	Highly improved
Kaiwei et al [12]	5% Na <sub>2</sub> SO <sub>4</sub> for 19 months	0.55	4.48	5.24	Class F	-0.01	10.84-10.78	20, 40	Improved	Highly improved
Sumer[13]	15% Mg SO <sub>4</sub> for 12 months	0.76 - 0.43	15.1	8.26	Class C	1.22	-	10,17	Improved	Moderately improved
			1.55	6.97	Class F	-0.49	-	10,17	Improved	Highly improved
Shearer [14]	Na <sub>2</sub> SO <sub>4</sub> for 18 months	0.5	1.26 - 2.85	7.98 - 14.01	Class F	-0.46 to -0.08	-	25	Improved	Highly improved
			2.53 -0.77	13.18 - 6.67	Co-combustion	-0.48 to -0.07	-	25	Improved	Highly improved
			24.5	0.6	Biomass	32.5	-	25	Reduced	reduced
Tkaczewska et al.[6]	Na <sub>2</sub> SO <sub>4</sub> for 13 months	0.5	3.7 - 3.3	7.1 - 6.8	Class F	-0.24 to -0.19	-	40	Improved	Highly improved
			10.3 - 9.4	9 - 8.5	Co-combustion biomass	0.49 to 0.62	-	40	Improved	Highly improved
Rajamma [15]	5% Na <sub>2</sub> SO <sub>4</sub> + 5% MgSO <sub>4</sub> for 12 months	0.55	11.4	2.6	Wood waste biomass B1	2.46	15.10	10	Moderately improved	No significant effect
			25.4	2.2	Wood waste biomass B2	9.27	16.69	20-30	Reduced the resistance	
							16.77	10-20	Moderately improved	Reduced
						18.71	30	Reduced the resistance		
Current study	5% Na <sub>2</sub> SO <sub>4</sub> for 15 months	0.485	3.10	8.39	CFA	-0.22	10.78-11.02	10-30	Highly improved	
			8.10	8.10	EBA	0.38	12.08	10	Similar to OPC	Highly improved
							12.18-13.56	20-30	highly improved	

### 6.1.3.2. Effect of Pore Structure

The replacement of cement with fly ash improves the sulphate resistance not only due to chemical factors but also physical properties. Fly ash improves the sulphate resistance by changing the microstructure and reducing the permeability by refining and blocking the pores [8]. The pozzolanic reaction product (calcium-silicate- hydrate gel) fills the capillary pores and makes the material denser. The sulphate ions, therefore, cannot easily penetrate the concrete and combine with the tri-calcium aluminate  $C_3A$  to form ettringite [8, 16]. Table 6.5 shows the total porosity and pore size distribution as determined by MIP measurements (chapter 4) conducted on pastes containing the same level of cement replacement by CFA and EBA as evaluated for the sulphate resistance investigation.

The percentage of small pores  $< 0.1 \mu\text{m}$  for the mixes containing both ashes is higher compared to control OPC and CFA was more effective in refining the pores. It also shows that the lowest percentage of small pores was found in OPC and 10% EBA mixes respectively which may explain why they exhibited more aggressive sulphate attack (higher rate of expansion and deterioration between all mixes).

**Table 6.5 Total porosity and pore size distribution of OPC and blended fly ash (CFA and EBA) samples**

<b>Mix ID</b>	<b>Total porosity (%)</b>	<b>Small pores &lt; 0.1 <math>\mu\text{m}</math> (%)</b>	<b>Large pores &gt; 0.1 <math>\mu\text{m}</math> (%)</b>
OPC	10.34	8.78	1.56
10EBA	12.08	9.61	2.47
20EBA	12.18	10.7	1.48
30EBA	13.56	11.64	1.92
10CFA	10.78	10.26	0.52
20CFA	11.02	10.37	0.65
30CFA	11.71	11.21	0.5

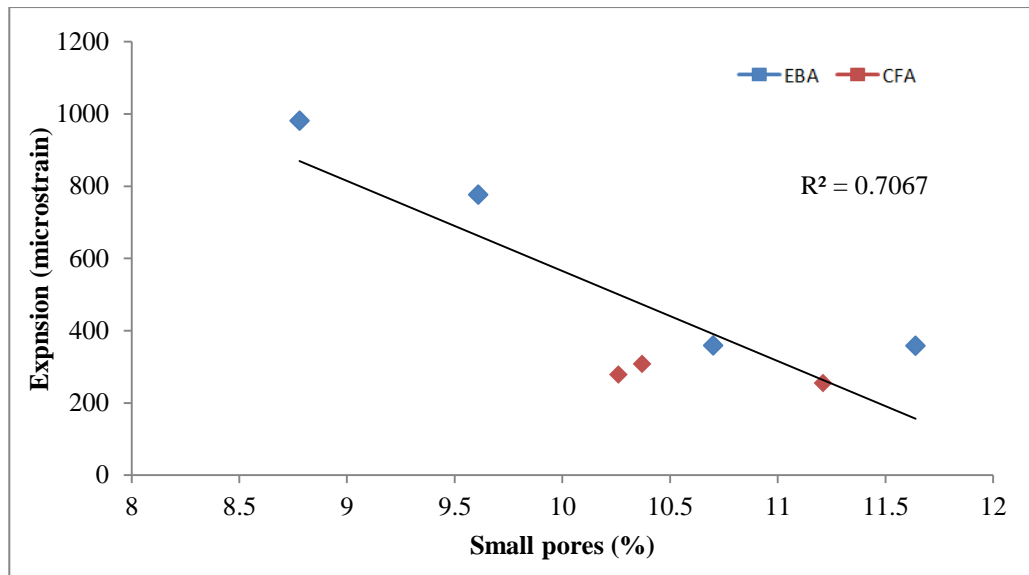


**Figure 6.13 Effect of small pores on the expansion caused by sulphate attack**

Figure 6.13 shows a linear relationship between the volume of small pores (%) and the expansion caused by sulphate attack, with a coefficient of correlation 0.706. A decrease in the expansion is observed at higher percentage of small pores. In addition, the effect of small pore volume is more significant in EBA than CFA which is more dominated with the effect of chemical composition on sulphate resistance.

### 6.1.3.3. Weight Change

All samples showed an increase in weight at the end of the test (Figure 6.8). The increase of weight was the result of continuous water absorption which indicates the formation of additional hydration products. Additionally, the mass increase is due to swelling caused by the formation of expansive reaction products (gypsum and/or ettringite ) and filling up of pores, thereby densifying the hardened concrete mixtures and increasing the weight [13, 17].

Specimens typically gained mass after being exposed to the sulphate solution until cracking occurred. The specimens generally began spalling after cracking, thereby resulting in mass loss [7]. The least mass increase was found in control OPC mortar followed by 10% EBA despite their expansion being the highest. The deterioration of OPC and 10% EBA mortars was defined by widening of cracks around the corners which cause a loss of material around the edges as

shown in Figure 6.7. This is the cause of a decrease in weight once the cracks were formed.

The weight gain increases with increasing replacement level of both ashes while the less expansion occurred in blended fly ash mixes compared to control OPC mix. These observations are different from the result reported by Sumer [13] who investigated the sulphate resistance of concrete containing Turkish class C and class F fly ashes exposed to 15% magnesium sulphate solution. He found that there was continuous mass increase throughout one year immersion period in all samples, however, the weight increase decreases by increasing the replacement level of both types of coal fly ash. The variation in the solution type and concentration could explain the contrary results since magnesium sulphate solution causes more aggressive sulphate attack by reacting with the calcium-silicate-hydrate products.

#### **6.1.3.4. Correlation between SEM, Expansion and Visual Observation Results**

The results of SEM analyses shown in Figures 6.9 to 6.11 correlate well with the expansion and visual observation results. The morphology of the examined samples suggests that there is a close link between ettringite formation and expansion. The high and accelerated expansion pattern of OPC and 10% EBA mortar samples is associated with the formation of ettringite while the low expansion rate of 30% CFA is due to the lack of ettringite. The high quantity of identified gypsum crystals in OPC and 10% EBA is the main cause of spalling destruction (loss of material). It has been reported in the literature that the cracks and expansion result from ettringite formation in hardened concrete while gypsum is the main cause of surface spalling[6, 8, 12]. The role of gypsum precipitation in cement exposed to a sulphate solution is to open up cracks which were already present [18].

## **6.2. Alkali-silica Reaction (ASR)**

One of the important aspects of concrete durability is its resistance to alkali-silica reaction (ASR) which is an expansive reaction between reactive mineral phases in aggregates and alkali hydroxide and/or calcium hydroxide in the pore solution of cement paste. The major source of alkali in concrete are sodium (Na) or potassium (K) ions from cement, however, alkalis can also penetrate concrete from external sources such as groundwater and de-icing salts [19–21]. The concentration of alkali metal hydroxides in solution depends on a number of factors such as the alkali content of the cement, the water/cement ratio (w/c) and the degree of hydration [22]. ASR reaction produces a hydrophilic alkali-silica gel which by itself is not expansive but it has a very high capacity to absorb water from the pore solution and expand causing cracking and failure of the concrete [20, 22, 23]. Thus, high alkali content in concrete, reactive aggregate and sufficient moisture are essential for ASR to occur.

The use of SCMs such as fly ash, slags and silica fume are known to control the expansion due to ASR mainly by their ability to reduce the alkalinity of the pore solution and binding the alkalis in the hydration products [20, 24–28]. The effect of fly ash on the alkalis available in solution depends on the composition of the ash, level of replacement and alkali content of the cement [29]. In this section, the efficiency of biomass fly ashes in mitigating ASR was investigated. The aim of the experimental programme was to evaluate the influence of biomass fly ash on the expansion due to ASR of blended cement mortars containing 20% replacement of cement by enhanced biomass fly ash (EBA) and wood biomass ash (EBA). A parallel investigation was also conducted on coal fly ash (CFA) blended cement mortar by using the same cement replacement level together with control specimens of mortar made with 100% OPC cement for comparison. A brief literature review on alkali-silica reaction in concrete which is relevant to this study is given in chapter 2.

### **6.2.1. Experimental Programme**

Accelerated mortar bar test (AMBT) is widely used to assess the potential risk of alkali-silica reaction (ASR) in concrete due to its simplicity and time

effectiveness. ASR investigation was carried out in accordance with the accelerated mortar bar tests ASTM C 1260/1567 standards [30, 31]. ASTM C 1567 is a modified version of ASTM C 1260, used to assess the potential reactivity of the combination of SCMs and aggregates. This test method can be used to evaluate the effectiveness of supplementary cementitious materials (SCMs) in reducing the expansion due to ASR. High temperature of 80°C and high concentration of hydroxide (1 N NaOH) is used in this method to accelerate the reaction.

#### **6.2.1.1. Materials**

Ordinary Portland cement (CEM I: 52.5 N) conforming to EN 197-1 supplied by Rugby was used in this investigation. Enhanced biomass fly ash (EBA) generated in Drax power station, virgin wood biomass ash (WBA) produced in Lynemouth power station and commercial coal fly ash (CFA) were used as supplementary cementitious materials to prepare mortars. The fine aggregate used for making mortars is standard CEN sand given in BS EN 196-1 standard [32], this sand was found to be potentially reactive.

#### **6.2.1.2. Mix proportions For ASR Test**

ASR tests were conducted on four mortar mixes prepared according to ASTM C 1567 standard. The proportions of binder to sand to water by mass were kept constant at 1: 2.25: 0.47 for all mixes (OPC mix with 100% cement and all fly ash blended cement mixes). The control OPC mortar was prepared by mixing 1125 g sand, 500 g Portland cement and 235 g water. The blended fly ash mortars were prepared in the same manner except that 20% by weight of the Portland cement was replaced with fly ash. Table 6.6 shows the proportions of evaluated mixes.

One minor modification was performed when following the procedure in ASTM C 1567. Instead of using the specific particle size distribution of the (reactive) aggregate (sand) given in the ASTM C 1567 standard, the particle size distribution used was the one for standard CEN sand given in BS EN 196-1

standard [32]. Table 6.7 gives the grading of the tow sands, which are quite similar.

**Table 6.6 The proportion of evaluated mixes for ASR test**

Mix no	Mix ID	Cement (g)	Fly ash(g)	Sand(g)	Water(g)
1	OPC	500	0	1125	235
2	20 EBA	400	100	1125	235
3	20 WBA	400	100	1125	235
4	20 CFA	400	100	1125	235

**Table 6.7 Grading requirements in ASTM C 1567 and grading for CEN sand**

ASTM C 1567 grading requirements		CEN sand grading	
Retained on sieve size (mm)	Mass (%)	Retained on sieve size (mm)	Mass (%)
2.36	10	2.0	0
1.18	25	1.60	7
0.60	25	1.00	26
0.30	25	0.50	34
0.15	15	0.16	20

### 6.2.1.3. Sample Preparation and Testing

Cement and fly ash binders were mixed by hand until homogeneity was achieved. The binder was then placed into the bowl of a Hobart mixer and water was added carefully within 10 seconds. The mixing was started immediately at low speed for 30 seconds. Then, the sand was added gradually during the following 30 seconds while mixing continued. The mixer was switched to high speed for an additional 60 seconds. After about 2 minutes, the mixing was stopped and the mix was briefly mixed by hand to remove accumulated materials from the paddle and the base of the bowl. This was followed by mixing at high speed for 60 seconds. Three specimens for each mortar mix were cast in 25 x 25 x 250 mm prism moulds (Figure 6.14.A) with embedded gauge

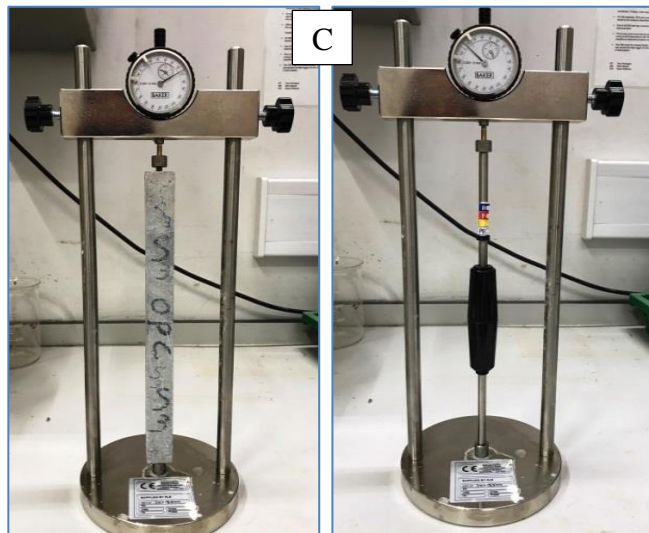
studs at the end to facilitate length measurements. Immediately after casting, the moulds were covered by a plastic sheet, stored in the laboratory environment (20°C, 60% RH) and demoulded after 24h (Figure 6.14.B). Then they were preconditioned for a further 24 h in water maintained at 80 °C inside an oven. The lengths of these mortar bars, after 24 h immersion in hot water, were measured using the length comparator as shown in Figure 6.14.C. This measurement provided the initial reading ( $L_0$ ). The mortar bars were subsequently transferred to a plastic container filled with 4 % sodium hydroxide solution (NaOH), covered with a lid to prevent evaporation of the solution and maintained at 80 °C inside the oven (Figure 6.14.D). The plastic container could withstand the high temperature of 80°C and was resistant to the sodium hydroxide solution. The solution was prepared a day before by dissolving 40 g of sodium hydroxide (NaOH ) in 900ml of water and further diluted with distilled water to obtain 1L of solution. The volume of the soak solution in the plastic container was  $4 \pm 0.5$  times the volume of mortar bars to ensure complete immersion of the samples. The length of mortar bars was periodically measured over 28 days of exposure. The expansion was determined by taking the mean value of measurements from three test specimens.

The expansion of each specimen at day x was calculated as follows:

$$E = \frac{(L_x - L_0)}{250} \times 100 \% \quad 6.4$$

Where: E is the expansion in %;  $L_x$  is the gauge comparator reading of specimen at day x;  $L_0$  is the initial (datum) gauge comparator reading of specimen and 250 is the gauge length.

According to ASTM C 1567, any expansion value less than 0.1% at 14 days indicates a low risk of deleterious expansion and will qualify the combination of materials for use in concrete. Any value greater than 0.2% at 14 days indicates a high risk of deleterious expansion and will not qualify the combination of materials for use in concrete. Any value between 0.1- 0.2% indicates potentially deleterious expansion and should be subjected to further testing.



A. Casting

B. Demoulding

C. Length measurements



D. Samples exposed to NaOH solution maintained at 80°C inside the oven

E. The specimens at the end of ASR test

**Figure 6.14 ASR test procedures**

### 6.2.2. Results and Discussion

The AMBT expansion results of control OPC, CFA, EBA and WBA are shown in Figure 6.15. The standard 14- day AMBT period is indicated by the vertical dotted line and the ASTM C1260/1576 limits of the expansion at the age of 14 days are shown as horizontal dotted lines. These results provide a comparison of the effect of biomass fly ashes in resisting ASR compared to OPC and CFA. The figure clearly shows that all fly ash blended mixes showed less expansion than control OPC mix throughout the exposure time. OPC mortar has the highest expansion whereas CFA mortar has the lowest expansion and EBA and WBA have expansion between both. However, EBA shows a much better resistance to ASR than WBA. After two weeks exposure time, both OPC and WBA specimens showed greater expansions than the specified ASTM C 1260/1576 limit of 0.1% for 14days exposure time. The expansion of EBA and CFA are 0.095% and 0.054% respectively which are lower than the limit of 0.1%. The corresponding expansions values after 4 weeks exposure time for OPC and WBA were also higher than limit of 0.2 specified by ASTM C1576. Both EBA and CFA reduced the expansion to the level of low deleterious risk according to ASTM C1260/1576. Although WBA reduced the expansion compared to control OPC, the reduction was not sufficient to reduce the expansion from the level of potentially deleterious to low risk deleterious.

The results clearly indicate that high calcium and alkali content in the fly ash provides the least mitigation of ASR expansion. This agrees with the existing literature [21, 22, 29, 33, 34] on mitigation of ASR by fly ash. The chemical composition of the fly ashes (based on calcium, silica and alkali content) in addition to their physical properties such as the fineness can be used to explain their performance in the AMBT test.

The most important chemical elements leading to ASR expansion are calcium, Ca, and leachable sodium and potassium (Na, K). The advantages of coal fly ash in mitigating ASR correlated to the amount of alkali (Na, K), CaO, SiO<sub>2</sub> and the ratio of CaO/ SiO<sub>2</sub> [25, 35, 36]. The mechanisms of mitigating the ASR by the

biomass fly ashes are likely to be similar to coal fly ash and depend on the same factors.

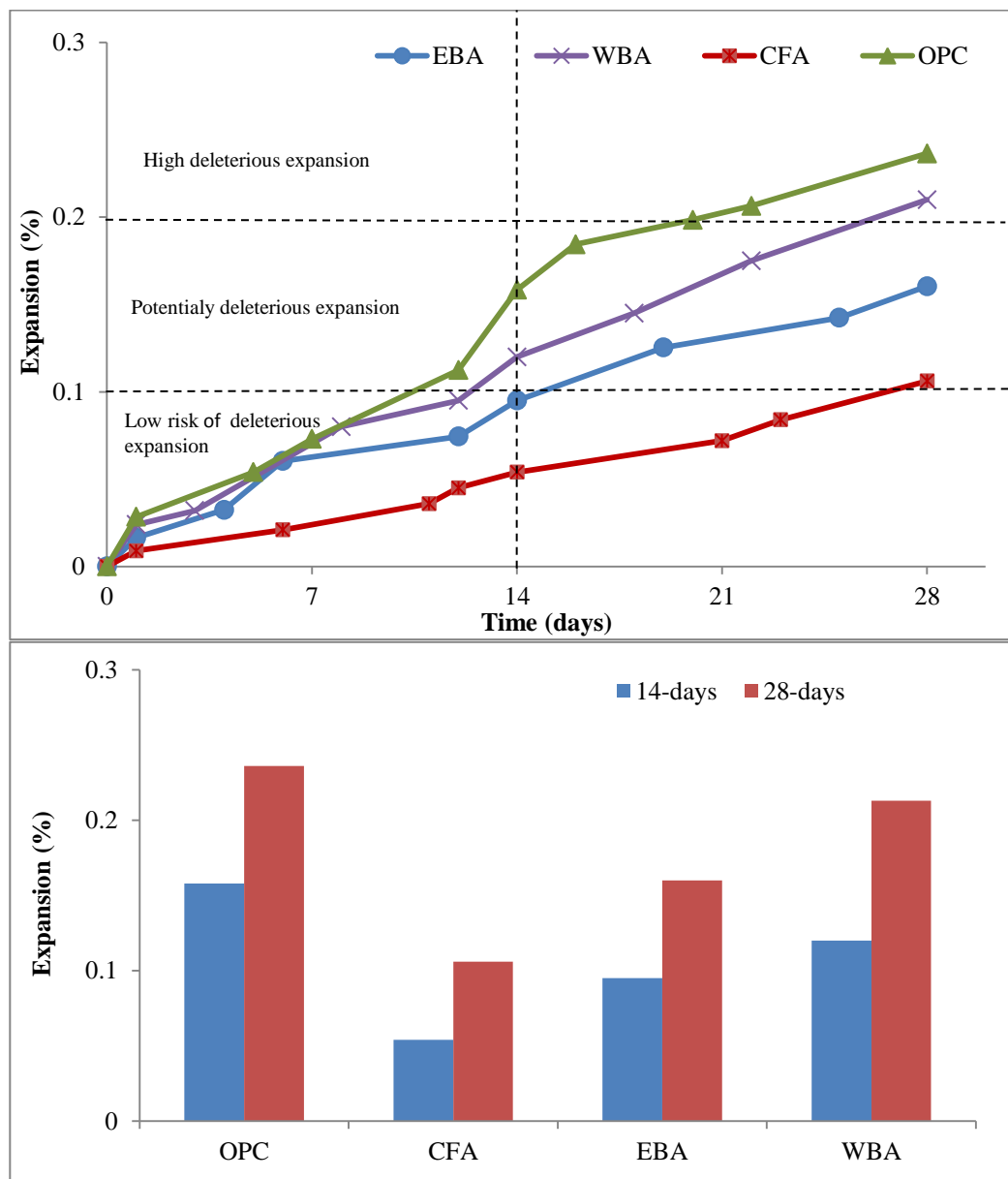


**Figure 6.15** The expansion of OPC, CFA, EBA and WBA due to ASR

Fly ashes with higher alkali or calcium contents are less effective in controlling expansion due to ASR and have to be used at higher levels of cement replacement to prevent damaging expansion [14, 25, 33]. Lower CaO/ SiO<sub>2</sub> ratios are less susceptible to deterioration than higher CaO/SiO<sub>2</sub> ratios and higher silica content binders increase the resistance to ASR deterioration [1].

The reduction of pH of the pore solution is attributed to the incorporation of alkalis by low CaO/ SiO<sub>2</sub> in the presence of fly ash [20].

With respect to the role of alkali in the fly ashes on ASR, WBA has the highest equivalent alkali content followed by EBA while CFA has the lowest content (Table 6.8), therefore, the expansion is higher in WBA compared to EBA and CFA. It has been reported that fly ashes that do not reduce pore solution alkalinity are less effective in controlling ASR expansion [25].

**Table 6.8 The important chemical elements leading to ASR expansion**

Element (%)	CFA	EBA	WBA
CaO	3.10	8.10	25.4
SiO <sub>2</sub>	47.64	41.46	12.5
CaO/ SiO <sub>2</sub>	0.065	0.19	2.03
Na <sub>2</sub> O (equivalent) = (Na <sub>2</sub> O + 0.658K <sub>2</sub> O)	2.24	4.23	6.49

Figure 6.16 shows linear relationship between the equivalent alkali content of the fly ashes and the expansion of the mortars. It shows that as the alkali content of the fly ash increases the expansion also increases.

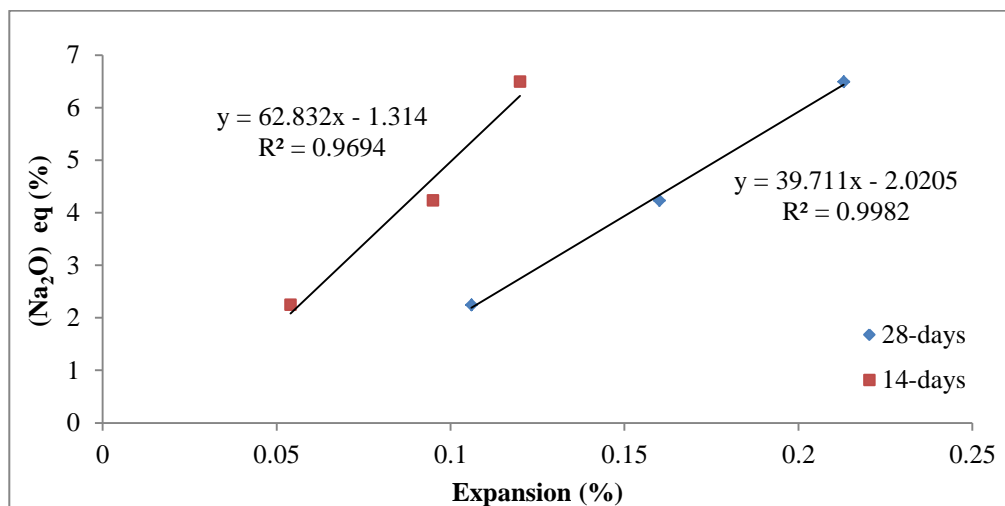


**Figure 6.16 The effect of alkali (equivalent) content of fly ash on the expansion of mortar bars.**

The expansion is also higher in the fly ashes with higher calcium content. It is generally agreed that high calcium fly ash (Class C) is not very effective in reducing ASR expansion. Although EBA is classified as Class F and has almost the same amount of silica as CFA, it exhibited higher expansion than CFA due to its higher calcium and alkali contents.

On the basis of the amount of CaO, SiO<sub>2</sub> and the ratio of CaO/ SiO<sub>2</sub>, the ashes fall into three groups. CFA with a low ratio of CaO/ SiO<sub>2</sub> (0.065) and the least amount of CaO (3.10 %), EBA with a medium ratio of CaO/ SiO<sub>2</sub> (0.19) and CaO content (8.10 %) and WBA with the highest ratio of CaO/ SiO<sub>2</sub> (2.03) and CaO content (25.4 %). Therefore, CFA is the most efficient in depressing ASR expansion, EBA is the second and WBA is the least.

In addition, the greater pozzolanic reactivity of the finer particle size of CFA ( $d_{50} = 17.3\mu\text{m}$ ), compared to EBA ( $d_{50} = 49.7\mu\text{m}$ ) and WBA ( $d_{50} = 68.9\mu\text{m}$ ), could have contributed to the reduction of expansion by the consumption of portlandite, Ca(OH)<sub>2</sub>, during the pozzolanic reaction and limiting transport of ions especially in the presence of external source of alkali such as NaOH in the case of AMBT.

As the pozzolanic reaction of the fly ash is very slow at early age, the influence of pore refinement of fly ash mortar and permeability (limiting ions transport) on the mortar expansion for these mixes is unclear and may not be captured by the use of the AMBT due to the short curing time in this test. However, curing the mortars in water at 80°C for 24h and the alkalinity of the system promote the pozzolanic reaction at early age leading to lower ion transport which is one of the mechanisms by which fly ash suppresses ASR [21].

It is difficult to conclusively determine from the AMBT test which ash characteristic (i.e., particle size, alkali or calcium contents) has the greater influence on ASR expansion. Further experimentation using the concrete prism test for long term ASR assessment according to ASTM C 1293 standard and pore solution study may clarify these issues and provide a better understanding of the effect of these ashes on mitigation ASR expansion.

## **6.3. Conclusions**

The influence of biomass fly ash on the sulphate resistance of cement mortars containing 10, 20 and 30% replacement of cement by enhanced biomass fly ash (EBA) was investigated. The degree of sulphate attack was evaluated by measuring the expansion of the mortars, the final weight change, visual observation and the morphology. The influence of biomass fly ash on the expansion due to ASR of blended cement mortars containing 20 % replacement of cement by enhanced biomass fly ash (EBA) and wood biomass ash (EBA) was also studied. A parallel investigation on coal fly ash (CFA) blended cement mortar by using the same cement replacement levels together with control specimens of mortar made with 100% OPC cement was conducted for comparison.

The following conclusions can be drawn based on the results presented above:

### **6.3.1. Sulphate Attack**

1. The expansion of the control OPC mortars caused by sulphate attack is much higher than those made with coal and enhanced biomass ashes. The control OPC mortar samples underwent an attack process which caused rapid expansion, cracks and spalling of material around the edges.
2. The incorporation of both ashes improves the sulphate resistance which reflects in a reduction in expansion and physical deterioration. This improvement is dependent on the level of replacement and the type of fly ash. Higher fly ash contents provide higher sulphate resistance. For example, Between 300 and 420 days, the expansion of OPC samples increased significantly, almost three times, exceeding 981 microstrains at the end of the test. On the contrary, the blended coal fly ash mortars showed little expansion after about 150 days.
3. At the same level of replacement, CFA is more effective than EBA in resisting sulphate attack. For example, at 420 days of immersion, the expansion of 10%, 20% and 30% CFA is 278.72, 308.2 and 255.12 microstrain respectively. The corresponding values for mortars with 10%,

20% and 30% EBA are 775.8, 359.12 and 357.78 microstrain respectively.

4. The lower resistance of EBA to sulphate attack compared to CFA is due to its lower pozzolanic activity and higher content of CaO. The content of CaO in EBA is 8.10%, which accounts more than twice the CaO content in CFA (3.10%)
5. The rate of weight gain under sulphate exposure increases by increasing the replacement level of both ashes (CFA and EBA). For example, the increase in weight change is 0.87% in 10% EBA whereas it is 1.13% in 30% EBA.
6. The SEM micrographs show the massive morphology of ettringite needles and gypsum crystals formed in control OPC mortar compared to 10% EBA and 30% CFA mortars. Gypsum is also formed in fly ash blended cement prisms but in much smaller quantities.
7. R-value alone is not an indication of the resistance of fly ash to sulphate attack and cannot be used to distinguish between different types of fly ashes. The physical properties (porosity and pore structure) become more dominant than the chemical composition of the fly ash as they have direct influence on the permeability.

### **6.3.2. Alkali-silica Reaction**

1. Replacing cement with 20% fly ashes reduces the ASR expansion, however, CFA is more effective in limiting the expansion than both biomass ashes (EBA and WBA). The expansion of 20% EBA and 20% CFA at 14 days of exposure are 0.095 % and 0.054% respectively compared to 0.15% of OPC.

2. The effectiveness of CFA is due to smaller particle size, higher pozzolanic reactivity and chemical compositions (less alkali and calcium contents).
3. WBA is less effective than EBA and CFA in controlling expansion caused by ASR due to its higher alkali and calcium contents.
4. The study shows linear relationship between the equivalent alkali content of the fly ashes and the expansion of the mortars. The expansion increases as the alkali content of the fly ash increases.
5. The influence of pore refinement of fly ashes and permeability (limiting ions transport) may play a role in mitigating ASR.

#### 6.4. References

1. Sudheen Anantharaman (2008) Sulfate And Alkali Silica Resistance Of Class C & F Fly Ash Replaced Blended Cements. Master of Science, Arizona State University
2. Mehta P. K. (1986) Effect of Fly Ash Composition on Sulfate Resistance of Cement. *ACI J* 83:994–1000
3. Dimic,D and Droljc S (1986) The influence of a lite content on the sulphate resistance of portland cement. In: 8th Int.Conf.on the Chemistry of cement. pp 195–199
4. Park YS, Suh JK, Lee JH, Shin YS (1999) Strength deterioration of high strength concrete in sulfate environment. *Cem Concr Res* 29:1397–1402 . doi: 10.1016/S0008-8846(99)00106-4
5. ASTM C1012/C1012M-15 (2015) Standard Test Method for Length Change of Hydraulic-Cement Mortars Exposed to a. 1–8 . doi: 10.1520/C1012
6. E Tkaczewska JM (2009) The sulphate resistance of mortars made with fly ashes from co-burning bituminous coal and biomass. *Silic Ind* 47:163–170
7. Tikalsky PJ, Carrasquillo RL (1989) The Effect Of Fly ASH On The Sulfate Resisance Of Cncrete.Research Study 3-5/9-87-481,Center for Transportation Research The University of Texas at Austin
8. Whittaker M, Black L (2015) Current knowledge of external sulfate attack. *Adv Cem Res* 27:532–545 . doi: 10.1680/adcr.14.00089
9. Wedding P, Dunstan E (1980) A Possible Method for Identifying Fly Ashes That Will Improve the Sulfate Resistance of Concretes. *Cem Concr Aggregates* 2:20–30 . doi: 10.1520/cca10175j
10. Archuleta Jr, Tikalsky PJ, Carrasquillo RL (1986) Production of Concrete Containing Fly Ash for structural applications.Research Report 364-1,Center for Transportation Research,The University of Texas at Austin

11. El-Khatib JM (1991) Durability related properties of PFA, slag and silica fume concrete. PhD Thesis, University of Aberdeen ,Department of Engineering
12. Liu KW, Deng M, Mo LW (2013) Effect of Fly Ash on Resistance to Sulfate Attack of Cement-Based Materials. *Key Eng Mater* 539:124–129 . doi: 10.4028/www.scientific.net/kem.539.124
13. Sumer M (2012) Compressive strength and sulfate resistance properties of concretes containing Class F and Class C fly ashes. *Constr Build Mater* 34:531–536 . doi: 10.1016/j.conbuildmat.2012.02.023
14. Shearer CR (2014) The Productive Reuse of Coal , Biomass and Co-Fired Fly Ash. PhD Thesis, School of Civil & Environmental Engineering, Georgia Institute of Technology
15. Rajamma R (2011) Biomass fly ash incorporation in cement based materials, PhD Thesis. Department of Ceramics and Glass Engineering, University of Aveiro
16. Matos AM, Sousa-Coutinho J (2016) ASR and sulphate performance of mortar containing industrial waste. *Struct Concr* 17:84–95 . doi: 10.1002/suco.201400095
17. Rozière E, Loukili A, El Hachem R, Grondin F (2009) Durability of concrete exposed to leaching and external sulphate attacks. *Cem Concr Res* 39:1188–1198 . doi: 10.1016/j.cemconres.2009.07.021
18. Schmidt T, Lothenbach B, Romer M, Neuenschwander J, Scrivener K (2009) Physical and microstructural aspects of sulfate attack on ordinary and limestone blended Portland cements. *Cem Concr Res* 39:1111–1121 . doi: 10.1016/j.cemconres.2009.08.005
19. Rajabipour F, Giannini E, Dunant C, Ideker JH, Thomas MDA (2015) Alkali- silica reaction : Current understanding of the reaction mechanisms and the knowledge gaps. *Cem Concr Res* 76:130–146 . doi: 10.1016/j.cemconres.2015.05.024
20. Lindgård J, Andiç-çak Ö, Fernandes I, Rønning TF, Thomas MDA

- (2012) Alkali – silica reactions ( ASR ): Literature review on parameters in influencing laboratory performance testing. *Cem Concr Res* 42:223–243 . doi: 10.1016/j.cemconres.2011.10.004
21. Shafaatian SMH, Akhavan A, Maraghechi H, Rajabipour F (2013) How does fly ash mitigate alkali – silica reaction ( ASR ) in accelerated mortar bar test. *Cem Concr Compos* 37:143–153 . doi: 10.1016/j.cemconcomp.2012.11.004
  22. Thomas M.D.A (2011) The effect of supplementary cementing materials on alkali-silica reaction : A review. *Cem Concr Res* 41:1224–1231 . doi: 10.1016/j.cemconres.2010.11.003
  23. Thomas M.D.A, Innis FA (1999) Use of the accelerated mortar bar test for evaluating the efficacy of mineral admixtures for controlling expansion due to alkali-silica reaction. *Cem Concr Aggregates* 21:157–164 . doi: 10.1520/cca10429j
  24. Moser RD, Jayapalan AR, Garas VY, Kurtis KE (2010) Assessment of binary and ternary blends of metakaolin and Class C fly ash for alkali-silica reaction mitigation in concrete. *Cem Concr Res* 40:1664–1672 . doi: 10.1016/j.cemconres.2010.08.006
  25. Shehata MH, Thomas MDA (2000) Effect of fly ash composition on the expansion of concrete due to alkali-silica reaction. *Cem Concr Res* 30:1063–1072 . doi: 10.1016/S0008-8846(00)00283-0
  26. Duchesne J, Bérubé MA (1994) The effectiveness of supplementary cementing materials in suppressing expansion due to ASR: Another look at the reaction mechanisms part 2: Pore solution chemistry. *Cem Concr Res* 24:221–230 . doi: 10.1016/0008-8846(94)90047-7
  27. Joshi P and Chan C (2002) Rapid Chloride Permeability Testing. *Concr Constr*.doi:[https://s3.amazonaws.com/academia.edu.documents/34937844/Rapid\\_Chloride\\_Permeability\\_Testing\\_.pdf](https://s3.amazonaws.com/academia.edu.documents/34937844/Rapid_Chloride_Permeability_Testing_.pdf)
  28. Shayan A, Diggins R, Ivanusec I (1996) Effectiveness of fly ash in preventing deleterious expansion due to alkali-aggregate reaction in normal and steam-cured concrete. *Cem Concr Res* 26:153–164 . doi:

10.1016/0008-8846(95)00191-3

29. Bleszynski RF, Thomas MDA, Ash F (1998) Microstructural Studies of Alkali-Silica Reaction in Fly Ash Concrete Immersed in Alkaline Solutions. *Adv Cem Based Mater* 7:66–78
30. ASTM Committee (2017) ASTM C1567-13 Standard Test Method for Determining the Potential Alkali-Silica Reactivity of Combinations of Cementitious Materials and Aggregate ( Accelerated Mortar-Bar Method ) 1. 1–6 . doi: 10.1520/C1567-13.2
31. ASTM Committee (2014) ASTM C1260-14 Standard Test Method for Potential Alkali Reactivity of Aggregates ( Mortar-Bar Method). *Annu B ASTM Stand Vol 0402* 1–5 . doi: 10.1520/C1260-14.2
32. BS EN 196-1 (2016) Methods of Testing Cement Part 1: Determination of Strength. *Br Stand*. doi: 10.1590/S1413-294X2011000200001
33. Wang S, Baxter L (2007) Comprehensive study of biomass fly ash in concrete : Strength , microscopy , kinetics and durability *Comprehensive study of biomass fly ash in concrete : Strength , microscopy , kinetics and durability*. *Fuel Process Technol* 88:1165–1170 . doi: 10.1016/j.fuproc.2007.06.016
34. Shearer CR, Kurtis KE (2015) Use of Biomass and Co-Fired Fly Ash in Concrete. *ACI Mater Journal*, V 112 209–218 . doi: 10.14359/51686827
35. Wang S, Miller A, Llamazos E, Fonseca F, Baxter L (2008) Biomass fly ash in concrete : Mixture proportioning and mechanical properties. *Fuel* 87:365–371 . doi: 10.1016/j.fuel.2007.05.026
36. Xu GJZ, Watt DF, Hudec PP (1995) Effectiveness of mineral admixtures in reducing ASR expansion. *Cem Concr Res* 25:1225–1236 . doi: 10.1016/0008-8846(95)00115-S

# **CHAPTER 7 CHLORIDE DIFFUSION IN ENHANCED BIOMASS FLY ASH CONCRETE**

## **7.1. Introduction**

Chloride attack is the main cause of deterioration in reinforced concrete structures exposed to marine environment or de-icing salts. The ingress of chloride in concrete is a major durability problem when its concentration exceeds threshold limits at the surface of the embedded steel. This problem has received great attention because of its frequent occurrence and the associated high cost of repairs. Therefore, the ability of concrete to resist the penetration of chloride ions is a critical parameter in determining the service life of reinforced concrete structures.

Chloride ions in concrete can exist either in the pore solution as free chloride, physically attached to the surface of C-S-H gel or chemically bound to the hydration products [1–3]. Among these chloride forms, free chloride is generally considered to be responsible for reinforcement corrosion. Chloride binding plays an important role in the service life of concrete structures as it reduces the free chloride concentration, thus, lowering the chance of reinforcement corrosion. The ingress of chloride in concrete is a complex interaction of both physical and chemical processes which are predominantly affected by the physical and chemical composition of the cement gel structure and the environment to which the concrete is exposed [4].

Replacement of cement by supplementary cementitious materials (SCMs) such as fly ash and ground granulated blast furnace slag increases the chloride binding due to the formation of additional calcium silicate hydrates (C-S-H) by their pozzolanic reaction [3, 5]. Numerous data are available in the literature on the effect of individual pozzolanic materials such as coal fly ash on chloride diffusion, however, very limited data are available on the influence of biomass fly ash on chloride ingress.

In this chapter, the effect of replacing cement with enhanced biomass ash (EBA) on chloride diffusion has been investigated. A parallel investigation on two control

samples, one replaced with class F coal fly ash (CFA) and the other without any cement replacement (100 % OPC concrete) have been conducted for comparison. A direct bulk diffusion test under exposure to 4% sodium chloride solution was conducted to obtain long term data in accordance with the Nord Test 443 [6] and CEN/TS 12390-11 [7] standards test methods for accelerated chloride diffusion. A higher chloride concentration of 4% was used for the solution of exposure than the chloride concentration under normal marine exposure (for example, seawater has a chloride concentration of 1.9%) in order to accelerate chloride diffusion since the penetration of chloride ions into the concrete is a slow process. Chapter 2 gives a brief literature review on the important aspects which are relevant to this subject.

## **7.2. Experimental Programme**

The experimental programme was conducted in order to study the chloride diffusion parameters for three concrete mixtures (20% EBA, 20% CFA and OPC) during long term periods of exposure to a chloride solution (up to 400 days). Accelerated diffusion (bulk diffusion) tests according to Nord Test 443 [6] and CEN/TS 12390-11 [7] procedures were used in this investigation which represents higher chloride concentrations than the chloride concentration under normal marine exposure in order to accelerate the chloride ingress. Both tests are similar in their procedures but the chloride concentration is different, Nord Test 443 specifies exposure to 165 g NaCl per  $\text{dm}^3$  whereas CEN/TS 12390-11 specifies 3% chloride solution by weight. In the current investigation, the samples were exposed to 4% sodium chloride solution and stored in the laboratory at  $20 \pm 2^\circ \text{C}$  after 28 days of water curing at  $20^\circ \text{C}$  to attain full saturation of concrete pores, therefore, the chloride ion transport is by diffusion only.

### **7.2.1. Materials**

Ordinary Portland cement (CEM I: 52.5 N) conforming to EN 197-1, Enhanced biomass ash (EBA) and commercial coal fly ash (CFA) were used as cementitious materials. Sharp, medium grade siliceous sand and gravel coarse aggregate of 10 mm nominal size were used as fine and coarse aggregates in all mixes. All the aggregates were in a saturated surface dry condition. Further details of the materials are given in

chapter 3 (section 3.3) and chapter 4 (section 4.2.1). No superplasticizer or air-entraining agent was used.

### 7.2.2. Mix Proportions

DOE (Department of Environment) method [8] for concrete mix design was used to design a grade 40 MPa mix of normal OPC concrete and fly ash concrete with 20% cement replacement. Trial mixes were performed to achieve practicable workability with high strength prior to selection of the mix proportions. The same mix proportions used for the carbonation investigation in chapter 5 were used in the chloride ingress study. A Compressive strength of more than 52 MPa was achieved at the age of 28 days of water curing; the slump was between 60 - 100 mm. The quantities in one cubic metre of the control OPC and fly ash concrete are presented in Table 7.1.

**Table 7.1 Mix proportions**

MIX	Cement (kg/m <sup>3</sup> )	Fly ash (kg/m <sup>3</sup> )	Fine aggregate (kg/m <sup>3</sup> )	Coarse aggregate (kg/m <sup>3</sup> )	Water (kg/m <sup>3</sup> )	Effective water/ binder W/(C+kF)*	28 days strength (MPa)
OPC	368	0	732	1100	180	0.49	60.5
20EBA	323	81	680	1136	170	0.49	53.3
20FCA	323	81	680	1136	170	0.49	58.1

\* The k value is given in the design guide for adjusting the amount of fly ash (K=0.3).

### 7.2.3. Mixing, Casting and Curing

The binder (fly ash + cement) were blended thoroughly. Half of the coarse and fine aggregate was placed first inside the cretangle concrete mixer of 150 Kg capacity followed by the binder composition. Then, the remaining half of the aggregate was added to cover the binder and mixed for one minute. The water was added slowly and mixing continued until the consistency of the mix was achieved. After about 2 minutes, mixing was stopped and the mix was briefly mixed by hand to remove accumulated materials from the paddle and the base of the mixer. The material was then mixed for a further two minutes before casting.

All moulds were slightly oiled prior to casting, to prevent the hardened concrete from sticking to the surface. A total of 10 slabs for each mix were cast in 250 x 250 x 75 mm dimension polystyrene moulds for the chloride diffusion test (Figure 7.1) and 75 x 75 x 75 mm dimension steel moulds were used for casting 9 cube specimens for compressive strength tests. The moulds were filled in three layers, each of which was compacted on a vibrating table to minimize the presence of voids. After the concrete surface was finished, all samples were covered with polythene sheets and stored in the laboratory air at  $20 \pm 2^{\circ}\text{C}$  and 60% RH. The samples were demoulded after 24 hours and cured in water at  $20^{\circ}\text{C}$ . The cubes were stored in water until the age of testing (3, 7, 28 days) while the slabs were cured in water for 28 days at  $20^{\circ}\text{C}$  to attain full saturation of the pores thus ensuring that the chloride ion transport occurred by diffusion only.

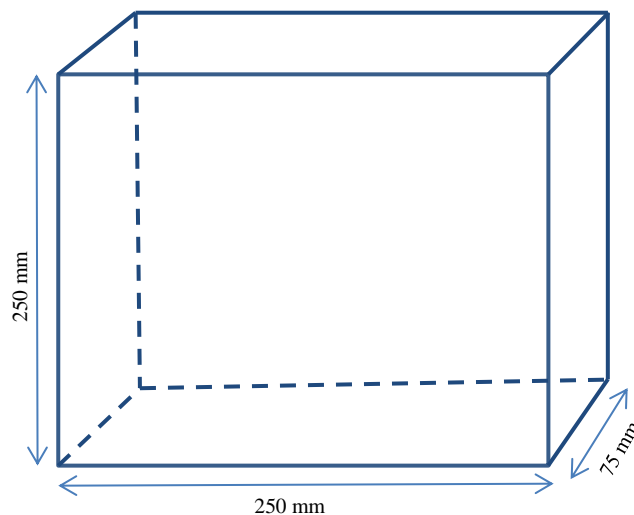
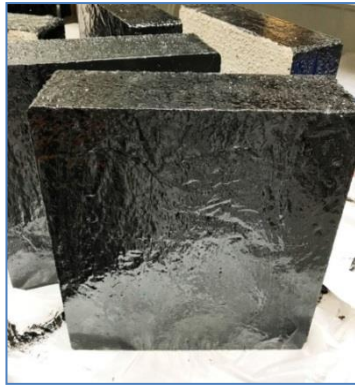


**Figure 7.1 Sample dimensions**

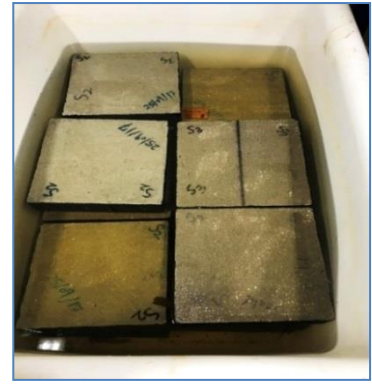
#### **7.2.4. Sample Preparation and Powder Collection**

After 28 days of water curing, all slab samples were removed from water and left for 3 hours in the laboratory air to dry. Then, two layers of bituminous paint were applied to all samples on five faces except the 250 mm x 250 mm bottom face (in the mould) to ensure that chlorides penetrated only from this face as shown in Figure 7.2a. The coated specimens were left in the laboratory air for 24 hours to allow the

bituminous paint to dry before they were fully immersed in 4% by weight sodium chloride solution as shown in Figure 7.2b. The higher limit of 3-5% (4% in this study) chloride concentration specified by the Nord Test 443 [6] and CEN/TS 12390-11[7] was used to accelerate the chloride ingress through the uncoated face. The solution was replaced every three months to maintain the chloride concentration. After the period of 90, 210, 300 and 400 days of immersion in the chloride solution, two slab specimens for each mix were taken out of the solution. Each slab was wet-cut into two equal halves by a masonry saw as shown in Figures 7.2c,d. Each uncoated cut face was drilled at six locations at 8, 5, 25, 35, 50 and 65 mm depth from the uncoated surface by means of a hammer drill using 4mm diameter SDS drill bits. A minimum of six holes were drilled per depth at about 20 mm distance from the corners to avoid any edge errors in chloride concentration, as shown in Figure 7.2e. The first 5 mm depth of powder drilled from each hole was discarded to minimize the effect of wet cutting on the chloride measurements. The powder samples from each hole at a given depth from the uncoated face were combined to provide a sufficient quantity (approximately 20 g) for chemical analyses (Figure 7.2f).



**a.** Bituminous paint applied on five faces except the 250 x 250 mm bottom face.



**b.** Samples fully immersed in 4 % NaCl by weight



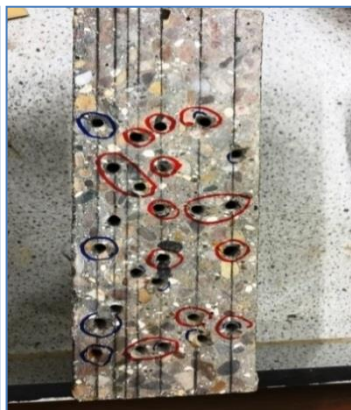
**c.** Samples wet-cut into two equal halves by a masonry saw.



**d.** Six depth locations marked before drilling powder



**e.** Sample drilled at 8, 15, 25, 35, 50 and 65 mm depth from the uncoated surface



**f.** The fine powder stored in self-sealing bags for chemical analyses

**Figure 7.2** Sample preparation for chemical analyses

### 7.2.5. Testing Procedures

The drilled powder was sieved through a 150 µm sieve, the fine powder was collected and stored in a self-sealing bags and later subjected to chemical analyses to determine the chemical bound chloride in the matrix (acid-soluble) and the physical bound (water-soluble) chloride at each depth.

#### 7.2.5.1. Acid-soluble Chloride Analyses

Volhard's titration method was used to determine the acid-soluble chloride concentration of concrete powder at each depth following the procedures described in BS EN14629 [9] standard. Five grams of the concrete powder was dissolved in 50 ml of distilled water then, 10 ml of 5 mol/l nitric acid was added followed by 50ml of hot water. The mixture was heated on a hot plate for 3 minutes with continuous stirring, and then the solution was filtered through a textured filter paper to be ready for titration to determine the chloride concentration in the solution. 5 ml of silver nitrate (AgNO<sub>3</sub>) solution was used to precipitate the mixture and ammonium thiocyanate solution was used as titrant while continually agitating the solution until the faint reddish-brown coloration no longer disappears. The volume  $V_1$  of solution used in the titration was recorded. To obtain  $V_2$ , a further 5 ml of AgNO<sub>3</sub> was added and the titration continued until the endpoint is reached a second time. The percent chloride, by weight of concrete powder, was calculated using the following equation:

$$C_{as} (\%) = 3.545 * f * \frac{(v_2 - v_1)}{m} \quad 7.1$$

where:  $v_1$  and  $v_2$  are the volumes of the ammonium thiocyanate solution used in the first and second titration (ml),  $f$  is the molarity of silver nitrate solution, and  $m$  is the mass of the concrete powder sample (g) [9].

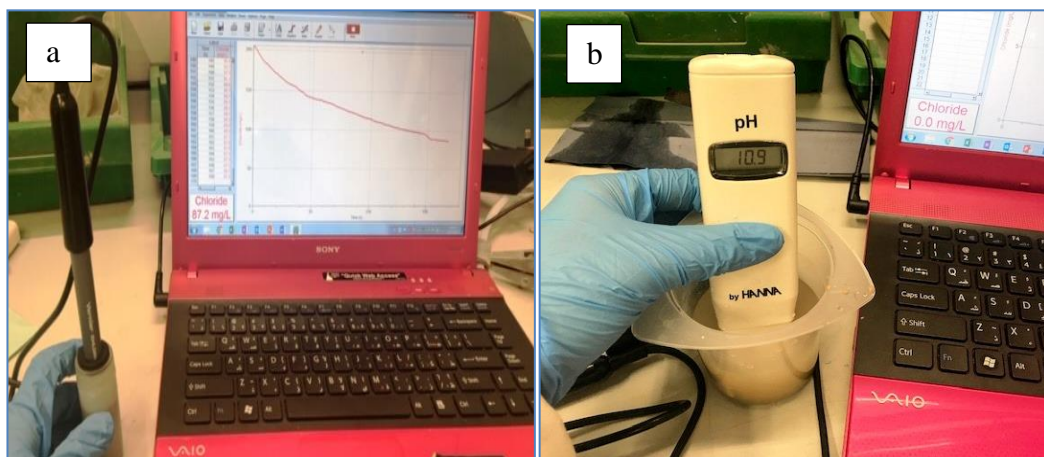
The obtained value was then converted to percent chloride by weight of the binder (cement + fly ash) using equation 7.2 after calculating the percentage of binder content in the concrete mix from the mix proportions information.

$$Cl \% (\text{ by mass of the binder}) = \frac{Cl\% (\text{ by mass of concrete sample})}{\% \text{ binder content}} \quad 7.2$$

### 7.2.5.2. Water-soluble Chloride Analyses

A chloride ion-selective electrode (ISE) was used to measure the water-soluble chloride concentrations of concrete powder at each depth. The electrode is designed for the detection of chloride ions ( $\text{Cl}^-$ ) in aqueous solutions. To achieve accuracy, the ISE was calibrated by using pre-prepared 1000 mg/l and 10 mg/l standard NaCl solution before and after each measurement. Five grams of the concrete powder was dissolved in 50 ml of distilled water and stirred manually. The ISE was soaked in the solution and held until the reading stabilized then; the reading was recorded as shown in Figure 7.3a. The ISE was rinsed by deionized water, dried by a laboratory tissue and recalibrated for the next measurement. The measurement for each powder sample was repeated twice for accuracy. The pH of the powder solution was recorded by using a digital pH meter as shown in Figure 7.3b.

The obtained value was then converted to percent chloride by weight of the binder using the same equation used in the last section (equation 7.2).



a. Electrode reading of powder

b. pH reading of powder solution

**Figure 7.3 Water-soluble chloride analyses**

## 7.3. Results and Discussion

### 7.3.1. Introduction

A wide range of results is presented in this section for the two fly ashes (CFA and EBA) and OPC concrete to determine the chloride diffusion characteristics including the chloride diffusion profiles, the equilibrium surface chloride concentration ( $C_0$ ), and diffusion coefficient ( $D_c$ ). The chloride diffusion equation derived from Fick's second law of diffusion was applied to the chloride experimental data at different depths from the concrete surface to determine the best-fit curves at different exposure periods. The diffusion equation is given in chapter 2 and rewritten in equation 7.3.

$$C_{(x,t)} = C_0 \left[ 1 - \operatorname{erf} \left( \frac{x}{2\sqrt{D_c t}} \right) \right] \quad 7.3$$

Where:  $C(x,t)$  is the chloride concentration (% by weight of binder) at distance  $x$  and exposure time  $t$ ;  $x$  is the distance from the concrete surface (m);  $t$  is the time (seconds);  $D_c$  is the chloride diffusion coefficient ( $\text{m}^2/\text{s}$ );  $C_0$  is the chloride concentration (% by weight of binder) on the concrete surface and erf is the error function.

The experimental data of acid and water-soluble chloride contents were plotted against each depth, a non-linear regression analysis of the experimental data was carried out by a computer programme (Microsoft Excel) to determine the best-fit curve together with the chloride diffusion parameters  $D_c$  and  $C_0$  at each test age. The experimental results show a good correlation (ranging from 0.90 to 0.99) with the chloride profiles provided by the regression analyses using Fick's second law of diffusion equation (equation 7.3).

Long term values of chloride diffusion coefficient  $D_c$  were calculated after determining the age factor ( $m$ ) which represents the change in diffusion coefficient ( $D_c$ ) with time.

### 7.3.2. Chloride Diffusion Profiles

Profiles of acid-soluble chloride concentrations with depth in the EBA, CFA, and OPC concrete specimens which were immersed in 4% NaCl solution for 90, 210, 300 and 400 days are presented in Figures 7.4 to 7.6. The corresponding water-soluble chloride profiles for EBA and CFA concrete are shown in Figures 7.8 and 7.9. The acid-soluble chloride profiles for OPC concrete were obtained at 90 and 300 days whereas the water-soluble profiles were obtained only at 210 days due to insufficient powder samples. The symbols in the figures represent the experimental data while the accompanying curves are the best-fit regression lines obtained by applying Fick's second law of diffusion (equation 7.3). The chloride concentrations are expressed as a percentage weight of the binder.

#### 7.3.2.1. Acid-soluble Chloride

The acid-soluble chlorides which are chemically bound to the EBA, CFA, and OPC concrete matrix for the ages 90, 210, 300 and 400 days are presented in Figures 7.4 to 7.6. The experimental data and regression profiles show high correlation factors ranging between 0.95 and 0.99.

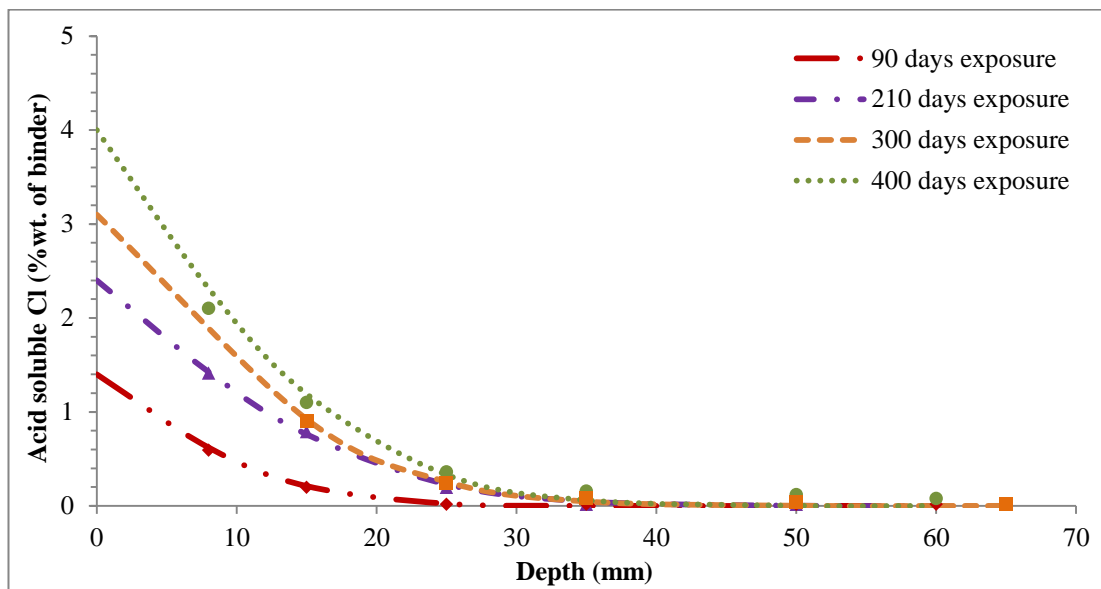


Figure 7.4 Acid-soluble chloride profiles of EBA concrete exposed to 4% NaCl solution at 90, 210, 300 and 400 days

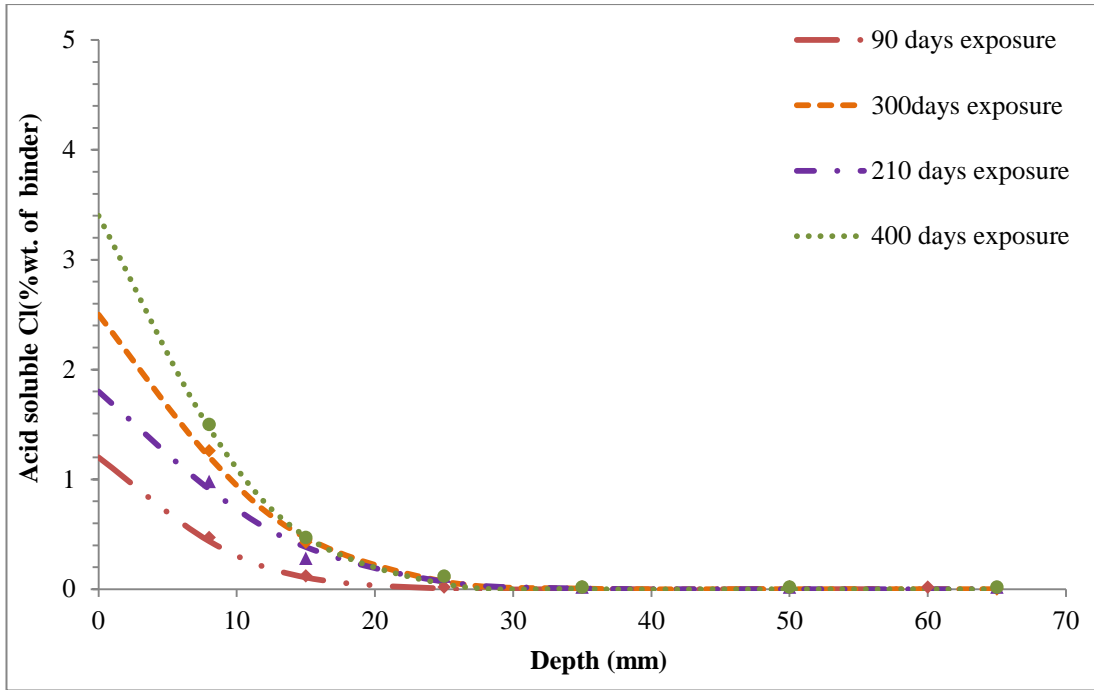


Figure 7.5 Acid-soluble chloride curves of CFA concrete exposed to 4% NaCl solution at 90, 210, 300 and 400 days

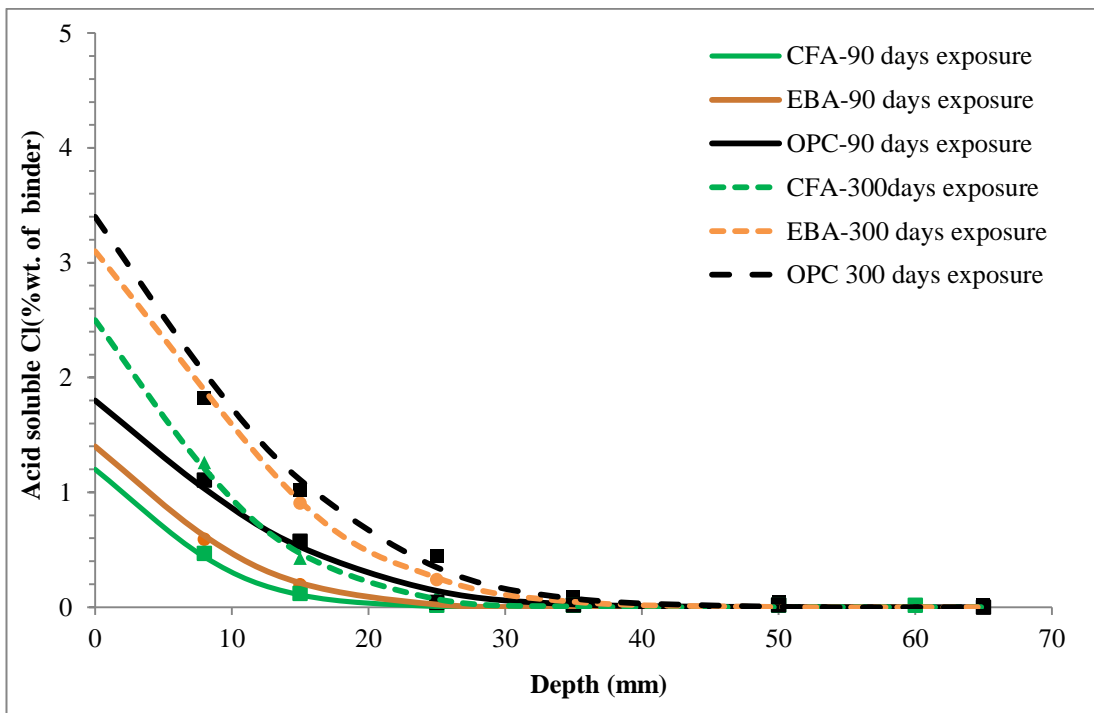


Figure 7.6 Acid-soluble chloride curves of OPC, EBA and CFA concrete exposed to 4% NaCl solution at 90 and 300 days

The acid-soluble chloride concentration increases with the exposure period at the concrete surface and all depths. A lower acid-soluble chloride concentration is shown by EBA and CFA concrete compared to OPC concrete at all ages (Figure 7.4 to 7.6) indicating higher chemical binding of chloride in OPC concrete. However, CFA concrete shows the lowest chloride content at each depth for all exposure periods. For instance, after 300 days of exposure, the chloride concentration of OPC concrete at the depth 25mm is 0.44% by weight of the binder while the chloride concentration of EBA and CFA at the same age is 0.29% and 0.1% respectively. The chloride concentration value of OPC concrete exceeds the corrosion threshold concentration value of 0.4%, which given in BS EN 206 standard [10] for reinforced concrete, whereas the values of EBA and CFA are lower than this limit. However, the accelerated diffusion test under 4% chloride concentration exposure is recommended for comparative purposes and determining the parameters  $D_C$  and  $C_0$ . It does not represent the time of corrosion initiation under in-service conditions, such as marine conditions, where the chloride concentration of exposure is lower than 4%.

The increase in acid-soluble chloride concentration with age is due to the formation of Friedel's salt and calcium chloroferrite produced by the reaction of chloride ion in the solution with un-hydrated  $C_3A$  and  $C_4AF$  of the binder [11]. Similar results have been reported by several researchers which confirms that the pozzolanic reaction of fly ash leads to lower chloride ingress than normal OPC concrete [12–14]. For instance, Chalee et al. [12] have investigated the performance of 7-years old coal fly ash concrete exposed to hot and high humidity climate in marine conditions compared to control OPC concrete. The specimens were tested for chloride penetration profiles and chloride concentration at different depths. After 7 years of exposure, the chloride concentration at depth of 25 mm from the surface was 4% for OPC concrete compared to 2.2% for 25% fly ash concrete.

Figure 7.7 shows the relationship between acid-soluble chloride and the exposure periods at depths 8, 15, 25 mm for EBA and CFA concretes. It shows a linear relationship with a strong correlation factor ranging between 0.91 - 0.99. At depth 25 mm for EBA concrete, the chloride concentrations are 0.017, 0.195, 0.239 and 0.36% by weight of binder at 90, 210, 300 and 400 days of exposure respectively.

The corresponding values for CFA concrete are 0.017, 0.078, 0.1 and 0.117 respectively.

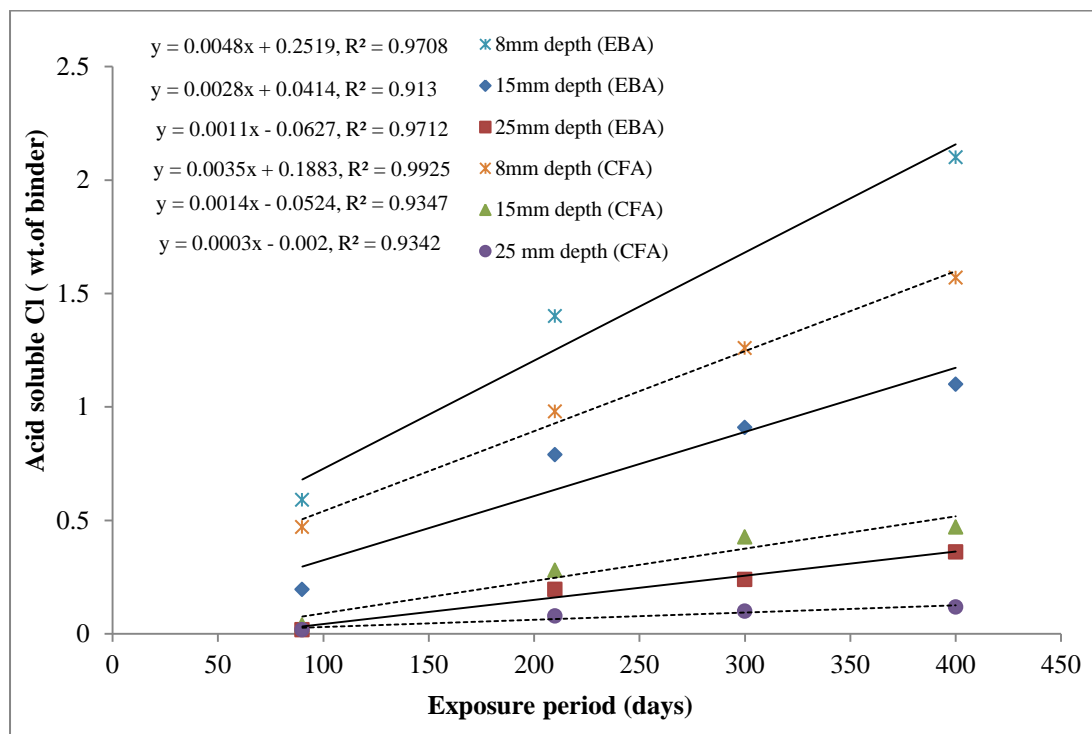


**Figure 7.7 Acid-soluble chloride concentration for EBA and CFA concrete at the depths 8, 15, 25 mm**

The chemical composition and physical properties of the two ashes are different, which results in a different effect on the chloride ingress. Generally, the amount of binding increases with the available alumina content of the pozzolanic materials to form Friedel's salt [2]. XRF results which were reported in chapter 3 reveal that both CFA and EBA have similar values of total alumina content ( $\text{Al}_2\text{O}_3$ ), 25.3% and 23.4% respectively which indicate their reaction with chloride ion should give similar quantity of Friedel's salt. However, the total alumina content determined by XRF does not give a reliable indication of how the fly ash will behave regarding chloride binding because some of the alumina in fly ash is present in a crystalline form such as mullite, which would not react with the chloride ion to form Friedel's salt. XRD results which are also reported in chapter 3 show the presence of mullite as a crystalline phase in CFA while it is not present in EBA. Therefore, the chemical binding in CFA is lower compared to EBA.

### 7.3.2.2. Water-soluble Chloride

Figures 7.8 and 7.9 show the water-soluble chloride profiles for the EBA and CFA concretes under the chloride exposure conditions used for the acid-soluble chloride tests. The water-soluble chloride refers to the chloride which is physically absorbed by the walls of the binder gel. The experimental results show good correlation with the profiles determined by regression analyses of the experimental data with Fick's second law of diffusion. The analysis also provides the constant values of parameters,  $D_c$  and  $C_0$  at each test age.

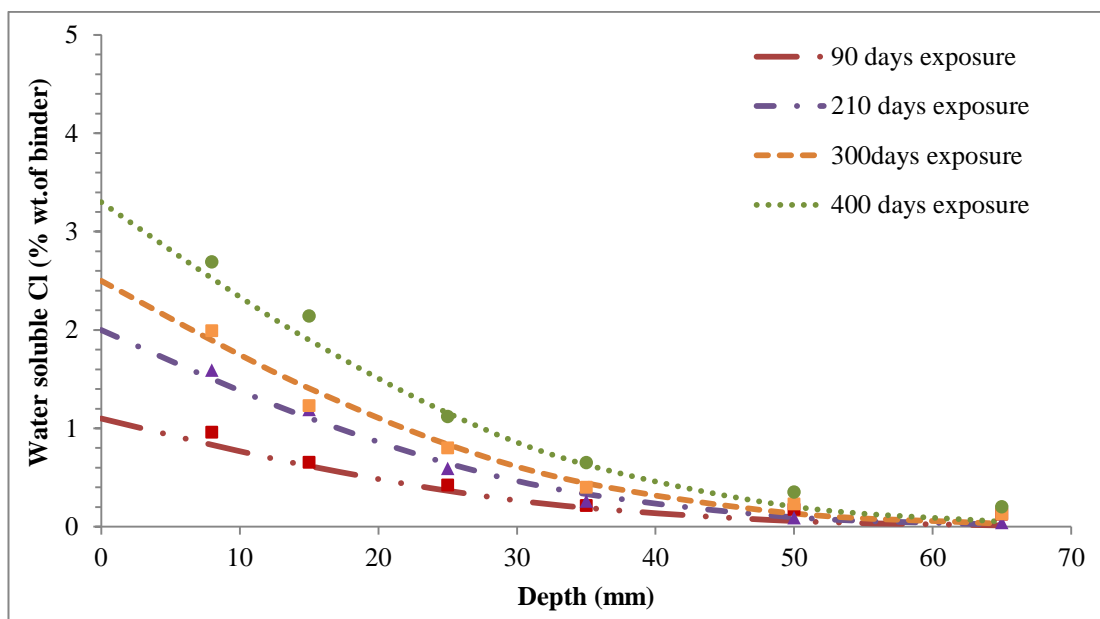


**Figure 7.8 Water-soluble chloride curves of EBA concrete at 90, 210, 300 and 400 days of exposure to 4% NaCl solution**

The water-soluble chloride concentration for EBA and CFA concrete shows an increase of chloride content with the exposure period. A higher water-soluble chloride concentration is observed by EBA compared to CFA concrete at all ages (Figure 7.8 and 7.9). For example, after 210 days of exposure, the chloride concentration of EBA concrete at the depths 15 and 25 mm are 1.19% and 0.59% by weight of the binder respectively. The corresponding values for CFA concrete at the same age are 0.66% and 0.39% respectively. However, the water-soluble chloride concentration for OPC concrete was the highest at 210 days of exposure (Figure 7.9).

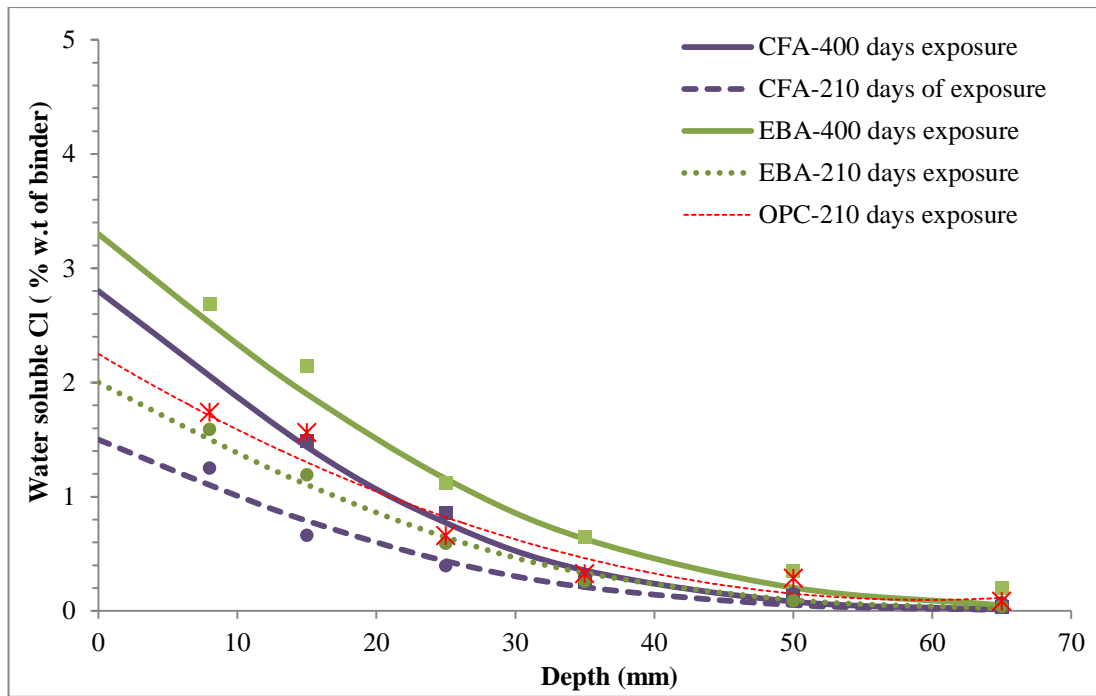


**Figure 7.9 Water-soluble chloride of EBA, CFA and OPC concretes at 210 and 400 days of exposure to 4% NaCl solution.**

The microstructure of EBA and CFA concrete investigated in chapter 4 (section 4.3.4) reveals differences in the porosity and pore structure between these two mixes, therefore, its effect on the chloride diffusion is considered. The porosity and the volume of large pores of EBA mix are 12.18% and 1.48% respectively at 90 days while the CFA mix had porosity and volume of large pores of 11.01% and 0.65% respectively which resulted in lower water-soluble chloride concentration at all ages. Therefore, the higher rate of water-soluble chloride for EBA compared to CFA is attributed to its higher porosity and higher percentage of large pores. This also indicates that porosity and pore structure have a greater influence on water-soluble chloride than acid-soluble chloride because the latter is dominated by chemical binding reactions.

Tina et al. [14] have conducted a comparative study of chloride penetration into fly ash concrete and OPC concrete under wetting-drying cycles. Two types of coal fly ashes (FA1 and FA2) with different chemical compositions (mainly the CaO content) were used at 20% and 50% cement replacement. They found that both coal fly ashes concrete exhibited lower water-soluble chloride concentration than traditional OPC. They attributed the higher resistance of fly ash concrete to chloride penetration to its

lower porosity and the high percentage of small pores (i.e. lower % of large pores). However, no results are available in the literature on biomass fly ashes.

### 7.3.3. Chloride Diffusion Parameters ( $C_0$ , $D_c$ )

The constant values of the parameters  $C_0$  and  $D_c$  were determined from the chloride profiles at each exposure periods for both acid-soluble and water-soluble chlorides by applying Fick's second law of diffusion to the experimental data and carrying out a regression analyses. Both, surface chloride concentration,  $C_0$ , and chloride diffusion coefficient,  $D_c$ , for EBA, CFA and OPC concrete are presented in Table 7.2 and discussed in the following sections.

**Table 7.2 Acid and water -soluble chloride concentration parameters ( $C_0$ ,  $D_c$ )**

Chloride exposure (days)	Acid-soluble chloride			Water-soluble chloride			MIX
	$C_0$ (%)	$D_c \times 10^{-12}$ (m <sup>2</sup> /s)	$R^2$	$C_0$ (%)	$D_c \times 10^{-19}$ (m <sup>2</sup> /s)	$R^2$	
90	1.4	7	0.98	1.1	13	0.93	EBA
210	2.40	6.2	0.98	2.0	9.7	0.97	
300	3.1	4	0.98	2.5	5	0.97	
400	4	3	0.95	3.3	3	0.96	
90	1.2	5	0.96	-	-	-	CFA
210	1.8	4	0.96	1.5	8.5	0.90	
300	2.5	2.5	0.96	-	-	-	
400	3.4	1.5	0.96	2.8	2.2	0.99	
90	1.8	9.5	0.99	-	-	-	OPC
210	-	-	-	2.16	11.2	0.95	
300	3.4	4.5	0.97	-	-	-	

### 7.3.3.1. Surface Chloride Concentration ( $C_0$ )

The surface chloride concentrations ( $C_0$ ) for both acid-soluble and water-soluble chlorides presented in Table 7.2 show an increase of chloride concentration at the surface with the increasing chloride exposure period for all mixes. OPC concrete has the highest surface acid-soluble concentration ( $C_0$ )<sub>as</sub> values among all mixes of 1.8 % and 3.4% by weight of binder at 90 and 300 days exposure. The corresponding values for EBA and CFA at the same ages are 1.4%, 3.1% and 1.2% and 2.5% respectively. This indicates a lower ingress of acid-soluble chloride in both EBA and CFA concrete compared to OPC mix.

The ( $C_0$ )<sub>as</sub> values of OPC, EBA and CFA concrete are in a similar range of 1.1-7.5% by weight of the binder (OPC and fly ash) given in literature from other researchers [12, 15–19]. The significantly higher surface chloride concentration of 7.5% by weight of the binder has been reported by Chalee et al. [17] for concrete exposed to 7-years to hot and high humidity marine conditions. However, existing literature lacks data for biomass fly ash and co-combustion fly ash concrete; only limited data are available which are based on rapid chloride permeability (RCPT) tests [20, 21] which do not determine chloride diffusion parameters  $C_0$  and  $D_c$ .

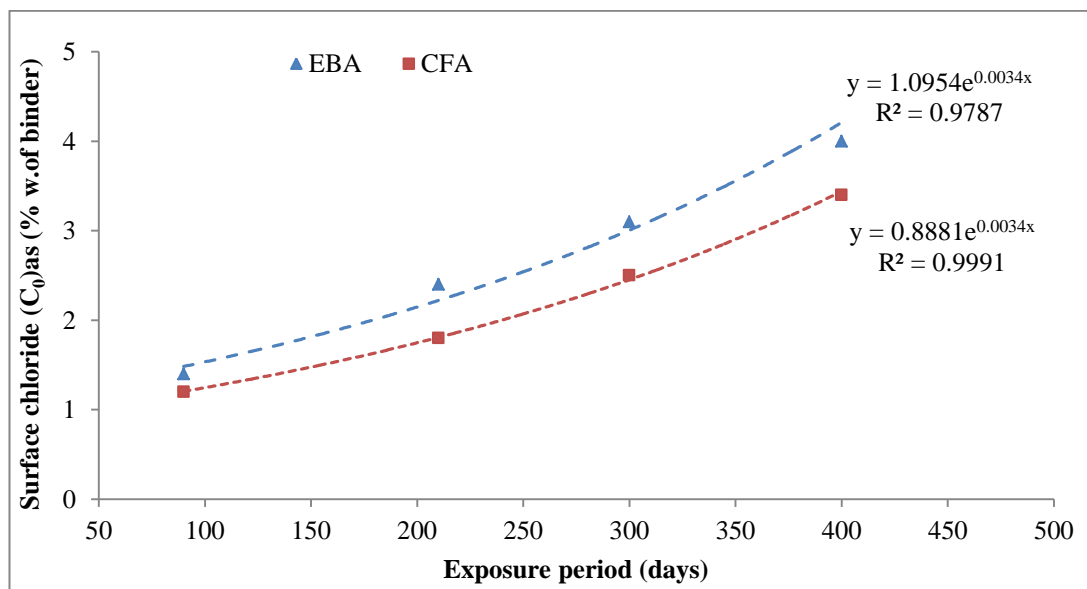
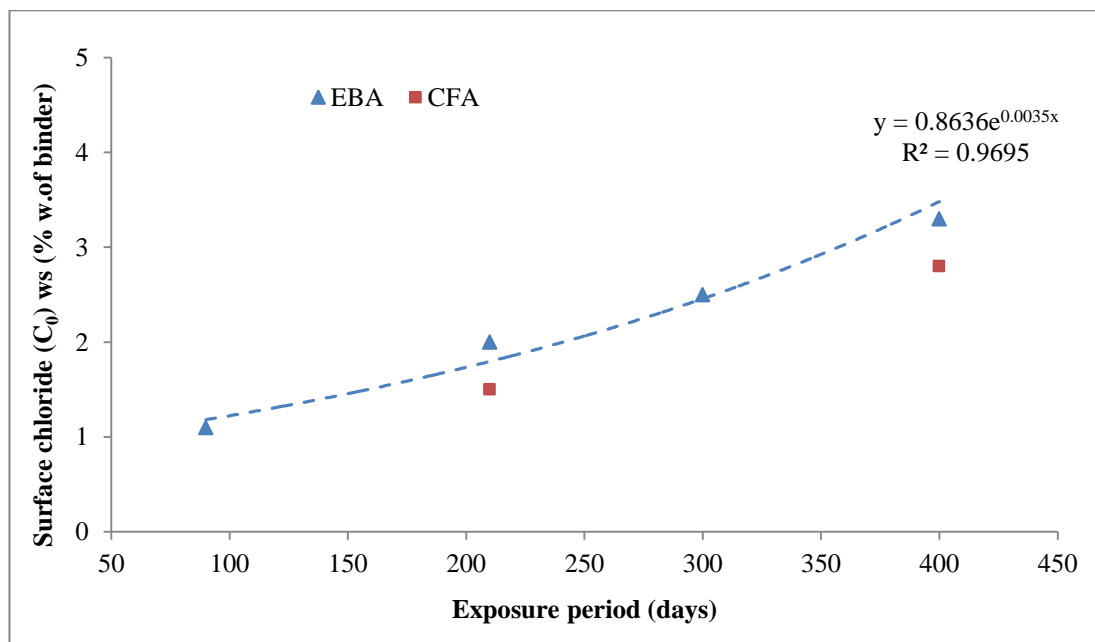


Figure 7.10 Relationship between the acid-soluble surface chloride concentration, ( $C_0$ )<sub>as</sub> , and chloride exposure period.

Figure 7.10 shows the relationship between the acid-soluble surface chloride concentration,  $(C_0)_{as}$ , and the exposure period for both EBA and CFA concretes. A nonlinear relationship is evident with a strong correlation factor ranging between 0.97 - 0.99.

The surface water-soluble concentration,  $(C_0)_{ws}$ , values for EBA concrete are plotted against their exposure periods in Figure 7.11. It shows similar trend in its relationship with exposure period to that of acid-soluble surface chloride concentration  $(C_0)_{as}$ . A nonlinear relationship with a correlation factor of 0.969 is evident. The surface water-soluble concentration,  $(C_0)_{ws}$ , for CFA was also plotted in the figure at two ages (210 and 400 days).

The chloride concentration at the surface increases with the exposure period for both EBA and CFA. CFA concrete has lower  $(C_0)_{ws}$  values of 1.5% and 2.8% by weight of binder at 210 and 400 days respectively compared to 2% and 3.3% for EBA at the same ages respectively.



**Figure 7.11 Relationship between the water-soluble surface chloride concentration,  $(C_0)_{as}$ , and exposure period.**

The acid-soluble chloride concentration at the surface  $(C_0)_{as}$  is greater than the corresponding water-soluble chloride concentration at the surface  $(C_0)_{ws}$  for all

mixes. For example,  $(C_0)_{as}$  values at 400 days of exposure are 4% and 3.4% by weight of binder for EBA and CFA concrete respectively whereas the  $(C_0)_{ws}$  values at the same age are 3.3% and 2.8% respectively. This shows that a higher proportion of chloride is chemically rather than physically bound to the walls of binder gel. Similar results have been reported for OPC concrete which shows higher chemically bound chloride (acid-soluble chloride) than physically bound chloride (water-soluble chloride). Figure 7.12 shows a comparison between the results of EBA, CFA concrete and the results reported in literature [19] for OPC concrete at a similar w/c ratio of 0.486 exposed to 5% NaCl solution up to 180 days.

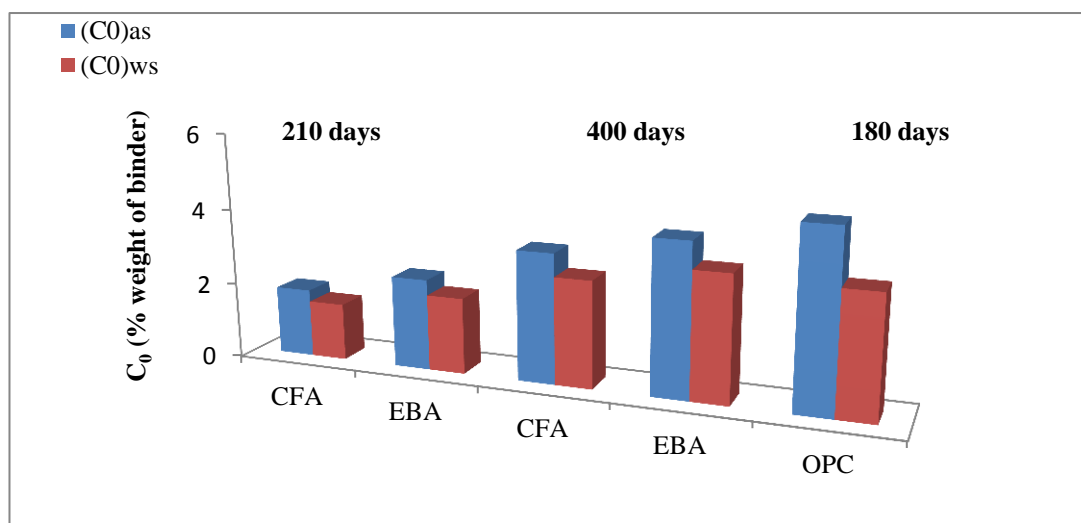


Figure 7.12 Acid-soluble and water-soluble surface chloride concentration of EBA and CFA concrete at 210 and 400 days of exposure and 180 days for OPC concrete [19].

### 7.3.3.2. Chloride Diffusion Coefficient ( $D_c$ )

The chloride diffusion coefficient ( $D_c$ ) is an indicator of the rate of chloride transport within the concrete matrix. It is used in durability analyses for design to prevent reinforcement corrosion in concrete. Unlike surface chloride concentration ( $C_0$ ) which increases with exposure period, the chloride diffusion coefficient  $D_c$  values presented in Table 7.2 (section 7.3.3) show that they decrease with time for all mixes. This is due to the change in properties such as the porosity and pore structure of concrete with time which reduces the permeability of concrete with age [12, 18]. The decrease of  $D_c$  with time has been shown by various researchers [17, 18, 22]. The results in Table 7.2 (section 7.3.3) also show that the highest values of

$D_c$  were produced by OPC followed by EBA and the lowest values were observed for CFA concrete. For example, between 90 to 300 days chloride exposure, the diffusion coefficient for acid-soluble chloride ( $D_c$ )<sub>as</sub> for OPC concrete decreases from  $9.5 \times 10^{-12} \text{ m}^2/\text{s}$  to  $4.5 \times 10^{-12} \text{ m}^2/\text{s}$ , for EBA decreases from  $7 \times 10^{-12} \text{ m}^2/\text{s}$  to  $4 \times 10^{-12} \text{ m}^2/\text{s}$  and for CFA decreases from  $5 \times 10^{-12} \text{ m}^2/\text{s}$  to  $2.5 \times 10^{-12} \text{ m}^2/\text{s}$ .

The chloride diffusion coefficient for water-soluble chloride ( $D_c$ )<sub>ws</sub> follows a similar trend to acid-soluble chloride ( $D_c$ )<sub>as</sub>. For example, between 210 to 400 days chloride exposure, ( $D_c$ )<sub>ws</sub>, for EBA concrete decreases from  $9.7 \times 10^{-19} \text{ m}^2/\text{s}$  to  $3 \times 10^{-19} \text{ m}^2/\text{s}$  whereas in CFA concrete it decreases from  $8.5 \times 10^{-19} \text{ m}^2/\text{s}$  to  $2.2 \times 10^{-19} \text{ m}^2/\text{s}$ .

The refined pore structure of CFA and EBA concrete as revealed by MIP results which are reported in chapter 4 is the reason for their lower chloride ingress compared to OPC concrete and corresponding lower  $D_c$  values. The volume of large pores in CFA concrete is 0.65% compared to 1.48% in EBA and 1.56% in OPC concrete. The pore-blocking effect caused by pozzolanic reactions in EBA and CFA concrete reduces the permeability of fly ash concrete and prevents chloride ions from diffusing into the concrete [18]. There is no clear relationship between the total porosity (obtained in chapter 4) and the chloride diffusion parameters values ( $C_0$ ,  $D_c$ ), however, a linear relationship is observed between these two parameters and the volume of large pores as shown in figures 7.13 and 7.14.

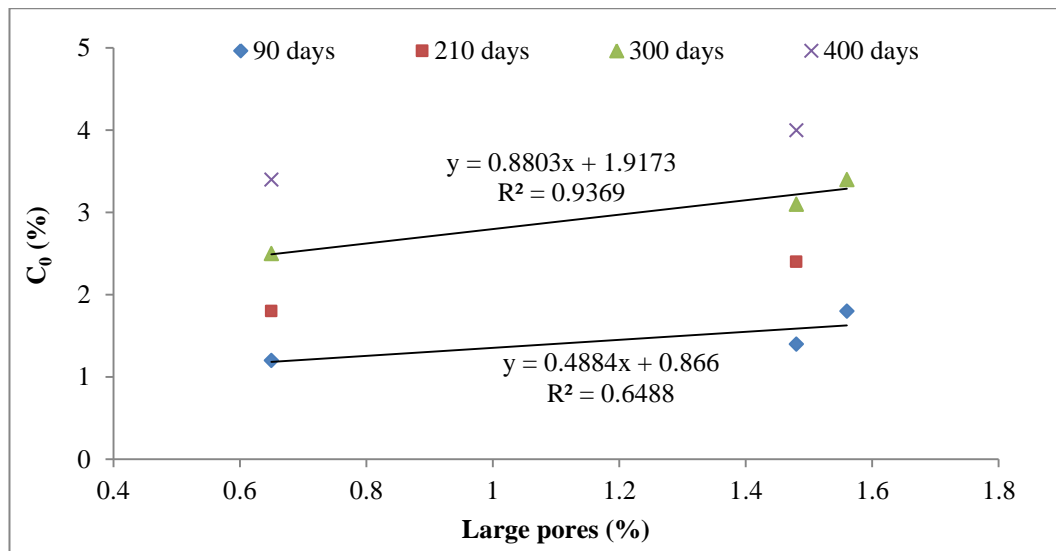


**Figure 7.13 Relationship between the surface chloride concentration and the volume of large pores**

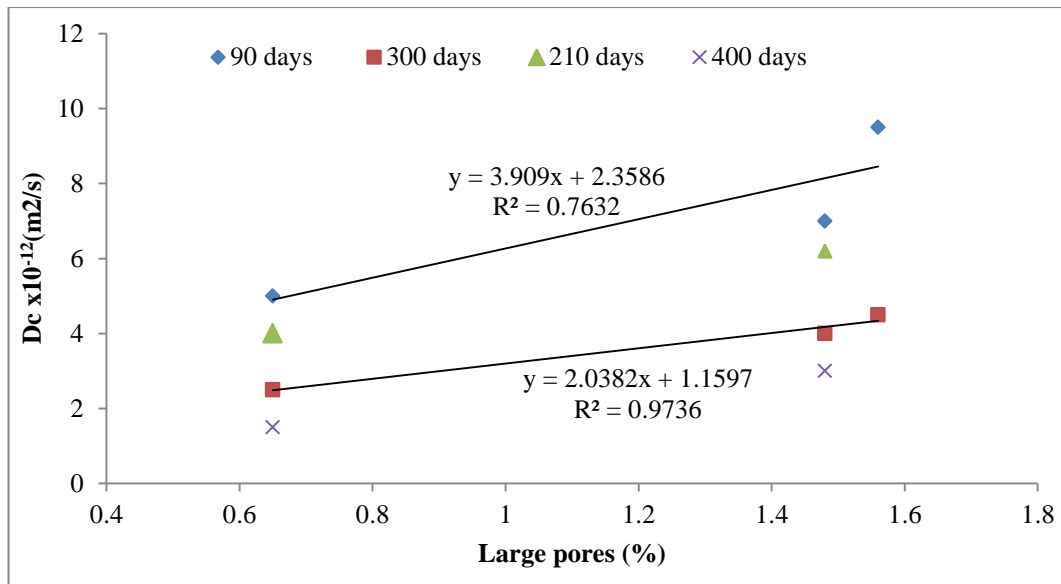


**Figure 7.14 Relationship between the chloride diffusion coefficient and the volume of large pores**

The current practice for determining chloride ingress in concrete uses the acid-soluble chloride diffusion coefficient,  $(Dc)_{as}$ , values in long-term prediction models [9, 17, 19, 23]. Diffusion coefficients given in the literature are usually determined from acid-soluble chloride diffusion data, which is assumed to represent the total bound chloride, without taking the water-soluble chloride into account. Table 7.2 shows that the water-soluble chloride  $(Dc)_{ws}$  values of all mixes are in the  $(10^{-19})$  order of magnitude compared to  $(10^{-12})$  in  $(Dc)_{as}$ . This supports the assumption of considering the acid-soluble chloride as a total chloride. Therefore, the diffusion coefficients  $(Dc)_{as}$  for EBA, CFA and OPC are considered as total diffusion coefficients  $Dc$ .

Table 7.3 shows a wide range of  $Dc$  values ( $1 \times 10^{-12}$  to  $52.3 \times 10^{-12} \text{ m}^2/\text{s}$ ) determined by various methods for several concrete mixes. The table covers a wide range of mixes with w/c ratio varying from 0.4 to 0.65 and different concentrations of salt exposure. For example, the higher chloride diffusion coefficient of  $52.3 \times 10^{-12} \text{ m}^2/\text{s}$ , which is determined in fibre reinforced concrete after 28 days of exposure to wet/dry cycles in the laboratory with high salt concentration, is due to the high w/c ratio of 0.58 which makes the concrete more permeable. However, the diffusion coefficient decreased to  $10 \times 10^{-12} \text{ m}^2/\text{s}$  after 270 days exposure period [18]. The experimental results of chloride diffusion coefficient  $Dc$  for EBA, CFA and OPC concrete

presented in Table 7.2 are within most of the limits published in the literature and summarised in Table 7.3.

**Table 7.3 Chloride diffusion coefficient  $D_c$  values as Published in literature**

<b><math>D_c</math> (<math>10^{-12} \text{ m}^2/\text{s}</math>)</b>	<b>W/C ratio</b>	<b>Curing age</b>	<b>Author</b>	<b>Concrete type &amp; Environment</b>
1.1 -4	0.4 - 0.54	1-14 weeks	R.B.Polder [24]	Fly ash concrete exposed to salt/dry cycle
2.5	0.43	1.5 year		
15.3-0.42	0.44 - 0.68	2-10 years	Thomas & Matthews [22]	Fly ash concrete exposed to tidal zone of BRE marine site
3.65-1.19	0.5	2 Months	Zhang & Gjørsv [25]	Theoretical analysis of concrete under RCPT test
52.3-10	0.58	28-270 days	Mangat& Molloy [18]	Steel fibre reinforced concrete exposed to wet/dry cycle
2.27 -0.36	-	28-180 days	Mangat & Limbachiya [26]	Concrete repair materials immersed in 175g of NaCl per 1L of water solution in laboratory
6.13-2.81	0.4	154-1250 days	Mangat& Gurusamy [4]	Steel fibre reinforced concrete under marine exposure
7.1-0.8	0.45-0.65	7 years	W.Chalee et.al [12]	Reinforced fly ash concrete exposed to hot and high humidity climate in marine condition
7.3-2.5	0.486	55-270 days	Mangat & Ojedokun [19]	Concrete under bulk diffusion test immersed in 5% NaCl solution in laboratory
17.32-0.3	0.45	28-365 days	Mangat & Khatib [27]	Concrete containing cement replacement materials under high-temperature and low-humidity curing then immersed in 175 g/l NaCl solution in laboratory

### 7.3.4. Long-term Prediction of Chloride Diffusion Coefficient

The Fick's second law of diffusion assumes constant values for the parameters  $C_0$  and  $D_c$ . However, previous studies have indicated that these parameters are time-dependent [17–19, 28–30]. The decrease in diffusion factor with time is represented by the age factor ( $m$ ) [31]. Mangat & Molloy[18] have proposed an empirical relationship between the diffusion coefficient and time by a power function as follows:

$$D_c = D_i \cdot t^{-m} \quad 7.4$$

Where:  $D_c$  is the diffusion coefficient at time  $t$ ;  $D_i$  is diffusion coefficient at reference time  $t$  (1 second) and  $m$  is the age factor.

The experimental data of  $D_c$  for EBA and CFA concrete are plotted against the exposure time up to 400 days in Figure 7.15. The age factor  $m$  and  $D_i$  were derived by regression analysis of the experimental data. The regression equations and their correlation coefficient are presented in Figure 7.15. It is clear that the relationship is a power function as previously proposed by Mangat & Molloy [18]. The age factor,  $m$ , is 0.596 for EBA and 0.751 for CFA. These values lie within the ranges of some values published in the literature [18, 19] and summarised in Table 7.4.

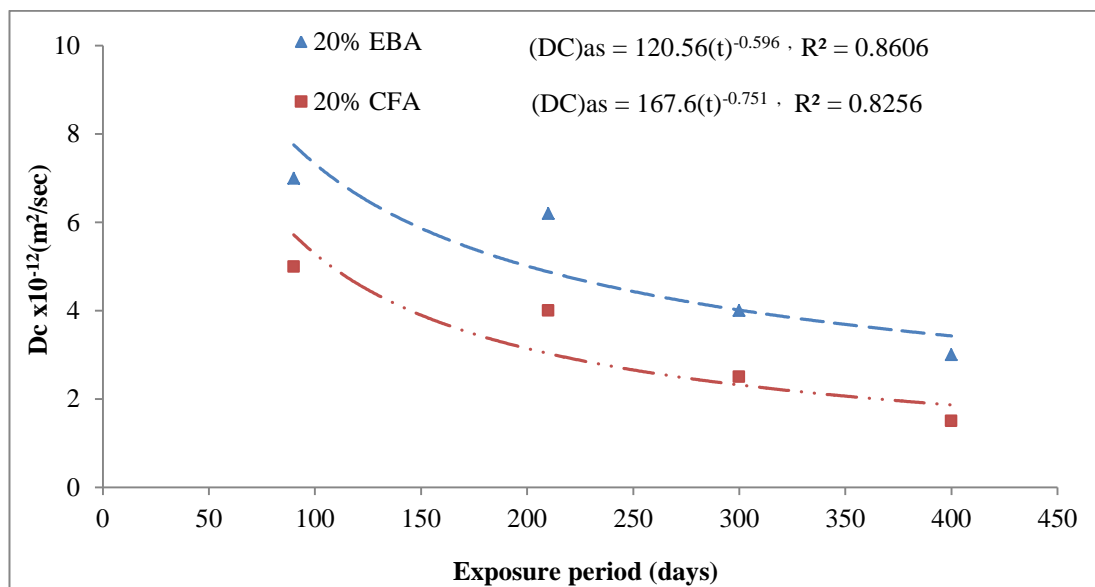


**Figure 7.15 Relationship of acid-soluble chloride diffusion coefficient with chloride exposure period for EBA and CFA concrete.**

The higher pozzolanic reactivity of CFA leads to higher value of the age factor,  $m$ , and lower diffusion coefficient ( $D_c$ ).

**Table 7.4  $m$  values as Published in literature**

Author	$m$	Curing time	Concrete type & Environment
Mangat & Molloy [18]	0.44 - 0.74 0.86- 1.34	28- 270 days	Steel fibre reinforced concrete exposed to wet/dry cycles
Mangat & Ojedokun [19]	0.588	55- 270 days	Concrete under bulk diffusion test immersed in 5 % NaCl solution in laboratory

Long-term chloride diffusion coefficients for 10 and 20 years of chloride exposure periods were calculated after determining the age factor ( $m$ ), which represents the change in diffusion coefficient with time, and  $D_i$  by using regression equations as shown in Table 7.5.

**Table 7.5 Predicted chloride diffusion coefficient at 10 and 20 years of exposure**

Mix	Regression Equation	$R^2$	$D_c(10 \text{ years})$ $m^2/s$	$D_c(20 \text{ years})$ $m^2/s$
EBA	$D_c=120.56 (t)^{-0.596}$	0.8606	$0.9 \times 10^{-12}$	$0.6 \times 10^{-12}$
CFA	$D_c=167.6 (t)^{-0.751}$	0.8256	$0.35 \times 10^{-12}$	$0.21 \times 10^{-12}$

## 7.4. Conclusions

The influence of EBA and CFA fly ashes on the chloride diffusion characteristics in terms of chloride diffusion profile, diffusion coefficient ( $D_c$ ) and surface chloride concentration ( $C_0$ ) was investigated. EBA, CFA and OPC concrete mixes were exposed to 4% NaCl solution in laboratory up to 400 days. The water and acid-soluble chlorides were determined at 90, 210, 300 and 400 days exposure. The following conclusions can be drawn based on the results of this investigation.

1. The acid and water-soluble chloride profiles for OPC, EBA, and CFA concrete show a good correlation with Fick's second law of diffusion.
2. Both, the chloride diffusion coefficient and the surface chloride concentration are time-dependent.
3. The acid and water-soluble chloride concentration at the concrete surface and all depths increase with the exposure period. The trend of increasing the surface chloride concentration,  $C_0$  is accompanying by a decrease in chloride diffusion coefficient,  $D_c$ . For example, the acid-soluble chloride concentration at the concrete surface,  $C_0$ , for EBA increased from 1.4% to 4% by weight of the binder whereas the chloride diffusion coefficient,  $D_c$ , decreased from  $7 \times 10^{-12}$  to  $3 \times 10^{-12}$   $m^2/s$  between 90 to 400 days of chloride exposure. On the other hand, the water-soluble chloride concentration at the concrete surface,  $C_0$ , for the same mix increased from 1.1% to 3.3% by weight of the binder while the chloride diffusion coefficient,  $D_c$ , decreased from  $13 \times 10^{-19}$  to  $3 \times 10^{-19}$   $m^2/s$  during the same period (between 90- 400 days).
4. The acid and water chloride concentration at the concrete surface  $(C_0)_{as}$ ,  $(C_0)_{ws}$  increase with exposure periods for OPC, EBA, and CFA concrete. However, all mixes revealed more acid-soluble surface chloride concentration  $(C_0)_{as}$  compared with water-soluble surface chloride concentration  $(C_0)_{ws}$ .
5. The chloride diffusion coefficient  $D_c$  decreases with exposure periods for OPC, EBA, and CFA concrete; however, the highest rate of chloride ingress is exhibited by OPC whereas CFA concrete has the lowest rate. For example, the chloride diffusion coefficient at 90 days exposure for OPC, EBA and

CFA are  $9.5 \times 10^{-12} \text{ m}^2/\text{s}$ ,  $7 \times 10^{-12} \text{ m}^2/\text{s}$ ,  $5 \times 10^{-12} \text{ m}^2/\text{s}$  respectively while it is  $4.5 \times 10^{-12} \text{ m}^2/\text{s}$ ,  $4 \times 10^{-12} \text{ m}^2/\text{s}$  and  $2.5 \times 10^{-12} \text{ m}^2/\text{s}$  at 300 days exposure.

6. The  $D_c$  values for all mixes are in the range  $13 \times 10^{-12}$  to  $1.5 \times 10^{-12} \text{ m}^2/\text{s}$ . These values lie within the limits  $D_c$  values for marine concretes ( $2 \times 10^{-12}$  to  $22 \times 10^{-12} \text{ m}^2/\text{s}$ ).
7. The use of both CFA and EBA reduces the rate of chloride ingress in concrete however; CFA is more effective than EBA in resisting chloride penetration. For example, the chloride diffusion coefficient for EBA was  $7 \times 10^{-12} \text{ m}^2/\text{s}$  compared to  $5 \times 10^{-12} \text{ m}^2/\text{s}$  for CFA at 90 days exposure. This reduction can be attributed to the refined pore structure (discontinuous pore) of fly ash concrete.
8. The chloride diffusion coefficient  $D_c$  for EBA and CFA decreases with longer exposure period following the relationship  $D_c = D_i (t)^{-m}$ , where  $D_c$  is the diffusion coefficient at time  $t$ ;  $D_i$  is diffusion coefficient at reference time  $t$  and  $m$  is the age factor. The age factor,  $m$ , is 0.596 for EBA and 0.751 for CFA.
9. Long- term chloride diffusion coefficient for EBA and CFA concrete can be predicted after determining the age factor ( $m$ ) by regression analysis of the experimental data. The Long-term chloride diffusion coefficient is determined by using the following equations respectively  $D_c = 120.56(t)^{-0.596}$  for EBA and  $D_c = 167.6 (t)^{-0.751}$  for CFA.

## 7.5. References

1. Florea MVA, Brouwers HJH (2011) Chloride binding related to hydration products. *Cem Concr Res* 42:282–290 . doi: 10.1016/j.cemconres.2011.09.016
2. Thomas MDA, Hooton RD, Scott A, Zibara H (2012) The effect of supplementary cementitious materials on chloride binding in hardened cement paste. *Cem Concr Res* 42:1–7 . doi: 10.1016/j.cemconres.2011.01.001
3. Justnes H (1996) A Review of Chloride Binding in Cementitious Systems, Cement and concrete. *Nord Concr Res* 21:1–6
4. Mangat PS, Gurusamy K (1987) Chloride Diffusion in Steel Fiber Reinforced Concrete Containig PFA. *Cem Concr Res* 1987:1–49
5. Yuan Q, Shi C, De Schutter G, Audenaert K, Deng D (2009) Chloride binding of cement-based materials subjected to external chloride environment - A review. *Constr Build Mater* 23:1–13 . doi: 10.1016/j.conbuildmat.2008.02.004
6. NT Build 443 (1995) Accelerated Chloride Penetration. Nordtest. doi: www.nordtest.org
7. CEN/TS 12390-11:2010 (2010) Testing hardened concrete ,Part 11: Determination of the chloride resistance of concrete, unidirectional diffusion. NSAI stanards
8. Kosalram R, Vijayabhaskara G.S AM. (2015) Mix Design of Fly Ash based concrete using DOE Method. *Int J Eng Technol* 10:7–12
9. BS EN 14629 (2007) Products and systems for the protection and repair of concrete structures - Test methods - Determination of chloride content in hardened concrete. Br Stand
10. BS EN 206 (2013) Concrete — Specification , performance , production and conformity. Br Stand
11. Sumranwanich T, Tangtermsirikul S (2004) A model for predicting time-dependent chloride binding capacity of cement-fly ash cementitious system. *Mater Struct Constr* 37:387–396 . doi: 10.1617/13930
12. Chalee W, Ausapanit P, Jaturapitakkul C (2010) Utilization of fly ash concrete in marine environment for long term design life analysis. *Mater Des* 31:1242–1249 . doi: 10.1016/j.matdes.2009.09.024
13. Papadakis VG (2000) Effect of supplementary cementing materials on

- concrete resistance against carbonation and chloride ingress. *Cem Concr Res* 30:291–299 . doi: 10.1016/S0008-8846(99)00249-5
14. Simčič T, Pejovnik S, De Schutter G, Bosiljkov VB (2015) Chloride ion penetration into fly ash modified concrete during wetting-drying cycles. *Constr Build Mater* 93:1216–1223 . doi: 10.1016/j.conbuildmat.2015.04.033
  15. Petcherdchoo A (2013) Time dependent models of apparent diffusion coefficient and surface chloride for chloride transport in fly ash concrete. *Constr Build Mater* 38:497–507 . doi: 10.1016/j.conbuildmat.2012.08.041
  16. Chen HJ, Huang SS, Tang CW, Malek MA, Ean LW (2012) Effect of curing environments on strength, porosity and chloride ingress resistance of blast furnace slag cement concretes: A construction site study. *Constr Build Mater* 35:1063–1070 . doi: 10.1016/j.conbuildmat.2012.06.052
  17. Chalee W, Jaturapitakkul C (2009) Effects of W/B ratios and fly ash finenesses on chloride diffusion coefficient of concrete in marine environment. *Mater Struct Constr* 42:505–514 . doi: 10.1617/s11527-008-9398-2
  18. Mangat PS& M (1994) Prediction of long term chloride concentration in concrete. *Mater Struct* 27:338–346
  19. Mangat PS, Ojedokun OO (2019) Bound chloride ingress in alkali activated concrete. *Constr Build Mater* 212:375–387 . doi: 10.1016/j.conbuildmat.2019.03.302
  20. Wang S, Llamazos E, Baxter L, Fonseca F (2008) Durability of biomass fly ash concrete : Freezing and thawing and rapid chloride permeability tests. *Fuel* 87:359–364 . doi: 10.1016/j.fuel.2007.05.027
  21. Cheah Chee Ban MRS (2011) The incorporation of wood waste ash as a partial cement replacement material for making structural grade concrete: An overview. *Resour Conserv Recycl* 55:669–685 . doi: 10.1016/j.asej.2014.11.005
  22. Thomas MDA, Matthews JD (2004) Performance of pfa concrete in a marine environment - 10-year results. *Cem Concr Compos* 26:5–20 . doi: 10.1016/S0958-9465(02)00117-8
  23. Drilled T, Statements B (2006) Standard Test Method for Acid-Soluble Chloride in Mortar and Concrete 1 ASTM. 15:5–8 . doi: 10.1520/C1152
  24. Polder R.P (1997) Chloride diffusion and resistivity testing of five concrete

- mixes for marine environment. RILEM Int Work Chloride Penetration into Concr 225–233
25. Zang T, Gjørv O (1994) An electrochemical method for accelerated testing of chloride diffusivity in concrete. *Cem Concr Res* 24:1534–1548
  26. Mangat PS, Limbachiya MC (1999) Effect of initial curing on chloride diffusion in concrete repair materials. *Cem Concr Res* 29:1475–1485 . doi: 10.1016/S0008-8846(99)00130-1
  27. Khatib JM, Mangat PS (2002) Influence of high-temperature and low-humidity curing on chloride penetration in blended cement concrete. *Cem Concr Res* 32:1743–1753
  28. Mangat PS, Gurusamy K (1987) Long-term properties of steel fibre reinforced marine concrete. *Mater Struct* 20:173–282 . doi: <https://doi.org/10.1007/BF02485924>.
  29. Mangat PS, Ojedokun OO (2018) Influence of curing on pore properties and strength of alkali activated mortars. *Constr Build Mater* 188:337–348 . doi: 10.1016/j.conbuildmat.2018.07.180
  30. Costa A, Appleton J (1999) Chloride penetration into concrete in marine environment—Part I: Main parameters affecting chloride penetration. *Mater Struct* 32:252–259 . doi: 10.1007/bf02479594
  31. Appleton AC (1999) Chloride penetration into concrete in marine environment - Part II : Prediction of long term chloride penetration. 32:354–359

## CHAPTER 8 CONCLUSIONS AND FUTURE WORK

### 8.1 Conclusions

This research project investigated the suitability of two types of biomass fly ashes, an enhanced biomass fly ash (EBA) and virgin wood biomass ash (WBA), as supplementary cementitious materials (SCMs) in concrete production. The ashes were first characterized in terms of their chemical, mineralogical compositions and physical properties. Then, partial replacement of Portland cement by both ashes was investigated and compared in terms of their impact on the fresh and hardened properties. Finally, the durability properties of biomass fly ashes concrete were investigated by exposing to long-term sulphate, chloride and carbon dioxide environments under laboratory conditions over a period of one year. The effect of biomass fly ashes on the expansion caused by alkali-silica reaction was also examined by using the accelerated mortar bar test. Control samples of ordinary OPC concrete and Class F coal fly ash concrete were produced for comparison purpose. Specific conclusions pertaining to each chapter are given at the end of that chapter. The overall conclusions from this investigation are given in this chapter.

The enhanced biomass fly ash (EBA) tested in this work has a composition similar to coal fly ash (CFA). The main components are  $\text{SiO}_2$ ,  $\text{Al}_2\text{O}_3$  and  $\text{Fe}_2\text{O}_3$  and to a lower extent  $\text{MgO}$ ,  $\text{Na}_2\text{O}$ ,  $\text{P}_2\text{O}_5$  and  $\text{SO}_3$  in addition to the presence of trace elements such as  $\text{BaO}$ ,  $\text{MnO}$  and  $\text{ZnO}$ . Some fibrous particles were observed intermixed with mostly spherical particles which are the typical morphology of coal fly ash. According to ASTM C618-12, EBA is classified as low calcium fly ashes class F and satisfy the strength activity requirements of ASTM C618-12 and BS EN 450-1 standards. The results demonstrated that EBA had similar overall properties to CFA when it is used as SCMs in mortar or concrete production. This is due to the similarity in their chemical composition despite their potential differences. For example, the incorporation of EBA reduces the water demand, improves the workability and increases the total porosity of cement pastes similar to the effect of coal fly ash. In addition, the use of EBA improves the sulphate resistance, reduces the expansion caused by ASR and reduces the rate of chloride ingress in concrete

compared to control OPC but its efficiency is still less than coal fly ash. Therefore, it is suitable for use as a pozzolanic material to partially replace cement to provide long-term strength and enhanced durability.

The composition and behaviour in mortar and concrete of the virgin wood biomass ash (WBA) are different from coal fly ash and enhanced biomass ash used in this investigation. CaO is its main component whereas the main oxides SiO<sub>2</sub>, Al<sub>2</sub>O<sub>3</sub> and Fe<sub>2</sub>O<sub>3</sub> are present in lower quantities than EBA and CFA. It failed to meet strength activity requirements of ASTM C618-12 and BS EN 450-1 standards mainly due to its lower content of silica and alumina, which are the important components in the cementitious and pozzolanic reactions. In addition to its lower reactivity, this ash has high alkali and high carbon contents which have impacted some properties. For example, this ash increased the water demand, reduced the workability and reduced the strength compared to EBA, CFA and the control OPC cement. The incorporation of WBA does not control the expansion caused by ASR due to its higher alkali and calcium contents. Therefore, additional technologies are required to remove excess carbon and improve its pozzolanic reactivity before it can be used as a SCM.

The composition of biomass ashes is highly variable. This study represents only two sources, however, their results are discussed in the context of the state-of-the-art which represents other types of biomass ashes.

## **8.2 Future Work**

The following areas have been identified for further research based on the outcomes of this research:

1. The present study investigated the use of each type of biomass fly ash in concrete as a single supplementary cementitious material (SCM). The work needs to be extended to the use of multiple SCMs in concrete in order to enhance its mechanical and durability properties.
2. Further research is required to study other properties not addressed in this study (e.g., mechanical properties, durability and field testing).
3. The accelerated mortar bar test, ASTM C1567, used for ASR investigation may not be suitable since it puts the test samples in aggressive conditions to

accelerate the rate of chemical reaction compared to the rate under ambient conditions. In addition, the effect of pozzolanic reaction on the time-dependent properties and all possible mechanisms of ASR mitigation such as permeability and alkali binding capacity may not be adequately considered due to short curing time in this method. The ASTM C1293 can be used as it is more realistic, less aggressive than ASTM C1567 and it performs on concrete specimens which are more representative of field conditions.

4. The suitability of biomass fly ashes as precursors for forming alkali-activated geopolymers is still relatively unknown and could be investigated. Preliminary tests on using both EBA and WBA with alkali-activated cementitious materials (AACM) are in progress.
5. The investigation indicates that EBA performs similar to CFA in terms of strength and durability properties of concrete, therefore, ASTM C 618 and BS EN 450 may need to be amended to include additional limits for biomass fly ash.
6. WBA used in this investigation needs additional processing to remove unburned carbon and improve its fineness in order to improve its pozzolanic reactivity. Further research on this aspect is needed.

## **APPENDIX I LIST OF PUBLICATION**

- Eman H. Elbuaishi and P.S.Mangat, Characterization of Enhanced Pozzolanic Biomass Ash, Fifth International Conference on Sustainable Construction Materials and Technologies, Kingston University, London, UK, 14-17 July 2019.
- Eman H. Elbuaishi and P.S.Mangat, Characterization and Pozzolanic Activity Index of a Biomass Fly Ash, 20th International Conference on High-Performance Construction Materials and Systems, Rome, Italy, 23-24 July 2018.
- Eman H. Elbuaishi and P.S.Mangat, Chemical Shrinkage of Cementitious Materials, Proceeding of the 2017annual Materials and Engineering Research Institute (MERI) Symposium, Sheffield Hallam University.